THE DESIGN AND CONSTRUCTION OF A HELIUM GAS GUN

AND A NUMERICAL SOLUTION OF THE HYPERVELOCITY

IMPACT OF A THIN PLATE

By

BOB ADRAIN HARDAGE

Bachelor of Science

Oklahoma State University

1961

Submitted to the Faculty of the Graduate College
of the Oklahoma State University
in partial fulfillment of the requirements
for the degree of
MASTER OF SCIENCE
May, 1967

THE DESIGN AND CONSTRUCTION OF A HELIUM GAS GUN

AND A NUMERICAL SOLUTION OF THE HYPERVELOCITY

IMPACT OF A THIN PLATE

Thesis Approved:

_____
Thesis Adviser

_____

_____
Dean of the Graduate College

558803

ii

PREFACE

This work was undertaken at the suggestion of Dr. F. C. Todd who acted as my adviser and project supervisor. The purpose of the work was to construct a helium gas gun capable of launching high velocity projectiles and to obtain a one-dimensional numerical solution of a porous plate impacting at high velocity onto an aluminum target. These two distinct areas of the study are to be used to investigate, both experimentally and analytically, the mechanism of hypervelocity impact.

The work could not have been completed without the assistance, the guidance, and the patience of Dr. Todd. Mr. H. Gurney designed many parts of the light gas gun and supervised the construction and installation of the gun. The suggestions of Mr. B. A. Sodek were invaluable in formulating and constructing the digital computer program. Marylynn Luther of Continental Oil Company, Ponca City, Oklahoma, helped in "debugging" the program.

Computer time was made available by Mr. W. M. Alexander of Goddard Space Flight Center, and Mr. William Cahill and his staff arranged for the scheduling of computer time.

TABLE OF CONTENTS

LIST OF TABLES

LIST OF FIGURES

LIST OF FIGURES (Continued)

LIST OF FIGURES (Continued)

LIST OF FIGURES (Continued)

CHAPTER I

INTRODUCTION AND STATEMENT OF THE PROBLEM

The two problems that are presented in this thesis are a continuation of the NASA project at Oklahoma State on the hypervelocity impact of microparticles. This project started as an analytical study of hypervelocity impact but has grown to include a significant experimental program. The most active studies on hypervelocity impact are confined to particles with the same ranges of mass, density and velocity which micrometeoroids are estimated to have. The mass range is arbitrarily defined as less than 10^{-4} grams. The radiation pressure of the sun will gradually force particles with a mass of 10^{-11} to 10^{-12} grams into orbits around the sun which are outside of the orbit of the earth. Micrometeoroids have a possible range of specific densities between 8.0 grams per cubic centimeter for an iron-nickel eutectic to densities as low as 0.05 grams per cubic centimeter for an aggregation of "micro-microdust" particles which collide and cohere in space. The theoretical range of velocities for these particles range from 30,000 to 240,000 feet per second. Most micrometeoroids appear to be in the lower velocity range which indicates an origin in our solar system. Although these particles are very small, they may produce a crater of significant size. This is a consequence of their large momentum and kinetic energy although their mass is rather small.

This thesis consists of two parts, an experimental phase and an

analytical phase. The first, experimental part describes the design and construction of a helium gas gun which is to be used to launch a small aluminum projectile. Although the gun was successful, it could not be employed for tests that would be meaningful for this project. The surface of the hemispherical target is eventually displaced by an impact of the projectile at the geometric center of the hemisphere. The devices for measuring and recording the surface displacements were not entirely completed.

The second part of this thesis is an analytical study and presents a computer solution for a one-dimensional, hypervelocity impact; i.e. a solution for the impact of a thin plate of infinite width and length onto a very thick plate of infinite extent. This solution investigates the changes in the phenomena of impact when the porosity of the impacting projectile is varied. This study is a necessary step in obtaining a general analytical solution for a hypervelocity impact. The subject of my next thesis for a still higher degree is based on the information from this analytical study, on three theses by former students on this project and on the published literature. A computer solution is sought to predict the phenomena that occur in hypervelocity impact and their variation with velocity and with the diameter of the impacting sphere. The solutions will be made for a wide range of velocities and will include the velocity of impact that is obtained with the helium gas gun.

<div align="center">

PART I - DESIGN AND CONSTRUCTION
OF THE HYPERVELOCITY GAS GUN

</div>

For experimental studies of hypervelocity impact, a launcher is required to accelerate a small projectile to a high velocity. The

shock waves from the impact of the projectile onto an aluminum target can then be subjected to quantitative measurements. These measurements will be employed to evaluate the correctness of the hydrodynamic model and the equations for plastic flow that are employed to obtain the computer solution for hypervelocity impact. It is also known that a flash of light accompanies a hypervelocity impact (9). This flash can not be studied with a light gas gun since the hot, light gas follows the projectile into the vicinity of the impact and will absorb some of the radiation (probably all of it).

Several groups have built hypervelocity launchers, and the characteristics of several of these are presented in the following publications (4), (5), (8), (12), (14), (15), (16), (17), (24), (25), (28), (30). These launchers were employed to study the free flights of aerodynamic bodies and the parameters of craters that are formed by a hypervelocity impact. Representative parameters are the diameter, the depth and shape as a function of the velocity of impact. The launcher that is described in this paper is not for studies of the preceding type, but will be used to collect data on the shock waves from hypervelocity impact which propagate into the elastic portion of the target and reach the free surface. Experiments are being formulated to study the shock-produced fluid portion of the target and the shock-produced plastic regions and to follow the movement of the interfaces between these regions and the portion of the target that the shock does not change from the elastic state. The experiments will measure the transmission of shock waves through these interfaces by observation of the motion of the elastic surface that surrounds the point of impact. These same features are being examined in the proposed analytical thesis

problem which is a computer solution for hypervelocity impact, with nearly all, presently known corrections.

The work in this thesis on this part of the project may be summarized as follows:

(1) Various types of hypervelocity launchers are discussed.

(2) The basic theory of the light gas gun is presented.

(3) The design procedures for the light gas gun are outlined.

(4) The design parameters and the equations are programmed for a computer in the FORTRAN IV language. The solution is presented and yields the loading conditions for the gun.

(5) With the computer solutions as a guide, the details for construction of the gun are given.

(6) Preliminary results are given that were obtained by firing the gun.

PART II - A DIGITAL COMPUTER SOLUTION OF A HYPERVELOCITY, POROUS-PLATE IMPACT

When micrometeoroids collide at low velocities in the vacuum of outer space, their surfaces will be completely outgassed and the particles will often weld together, as a consequence of the intermolecular forces. An aggregate of several of these particles, which are welded together, would constitute a porous body. Particle collectors on satellites have verified the existence of these porous micrometeoroids (13). For this reason, it is necessary to investigate the effect of porosity on hypervelocity impact.

A simplified computer solution can yield important information about the effect of projectile porosity on hypervelocity impact. The

problem assumes that a thin plate, which extends an infinite distance

in the lateral directions, impacts on a thick slab of infinite lateral

dimensions. This assumption has the effect of reducing the mathematical

statement of the problem to a solution in one dimension. The analytical

part of this thesis considers this problem and presents a computer

solution when the thin plate is of iron with reciprocal porosities of

1.0, 1.33, 2.0 and 4.0; and when it is of stone with reciprocal porosi-

ties of 1.0, 1.33 and 2.0. By reciprocal porosity of 2.0, it is to be

understood that the true pore volume is 50 per cent of the total volume.

The work on this part of the project may be summarized as follows:

(7) The hydrodynamic flow equations and some equations of state

for the hypervelocity impact of a plate are presented and

discussed.

(8) The flow equations and the equation of state are written in

finite difference form for a computer solution.

(9) The solutions of the various cases for hypervelocity impact

of the thin porous plate are presented.

PART I

CHAPTER II

TYPES OF HYPERVELOCITY LAUNCHERS

In order to better understand the mechanics of the hypervelocity impact of particles, it is necessary to perform experiments. This requires devices that are capable of accelerating small particles to a high velocity. Some methods are discussed which have been successfully employed. They are:

(1) Electrostatic accelerators

(2) Drag force from high velocity gases

    (a) High velocity from electrical energy that is stored
    in a condenser

    (b) High velocity from shaped explosives

(3) Light gas guns

    (a) Light, isentropically-compressed, gas gun

    (b) Light, accelerated-reservoir, gas gun

    (c) Light, shock-compressed, gas gun

ELECTROSTATIC ACCELERATORS

A common and very successful method to accelerate very small particles is to charge the particles, usually with a negative charge, and to accelerate them by a large difference in potential. Excellent sources for the large potential difference are the accelerators that

6
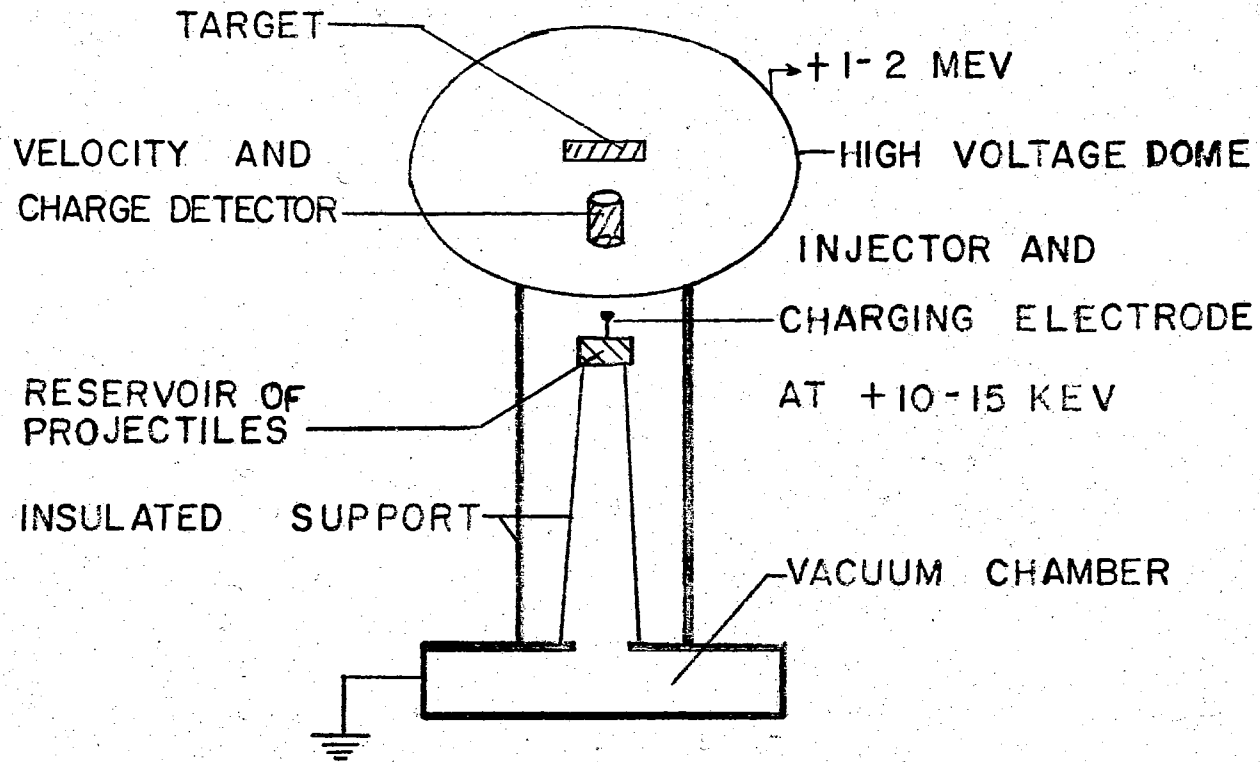
FIGURE I - ELECTROSTATIC ACCELERATOR

are available from High Voltage Engineering. The design of a typical

accelerator of this type is shown in Figure 1. The projectiles are

usually very small, of the order of microns. A supply of the pro-

jectiles are placed in a small box, near the injector and charging

electrode in many of the accelerators. A few accelerators employ a

pulse of electrostatic force to inject groups of particles into the

region in which the particles are charged. Later designs employ

techniques which inject one particle at a time. After the particle is

charged, it leaves the negative electrode and enters the gradient of

the electrostatic field where it is accelerated toward the electrode

of opposite potential. Velocities of the order of 10,000 to 25,000

feet per second are reached in this electrostatic field. Even higher

velocities have been reported. In a field-free space in the opposite

electrode, the charge and the velocity of the particle are measured.

With this information, the mass, m, of the particle is known from the

relation $\frac{1}{2} mv^2 = qV$, where v is the velocity, q is the charge on the

particle and V is the potential difference in the accelerator. If

the particles are known to be spherical, then their radii are easily

calculated from their mass.

A deficiency of the electrostatic accelerators, which fire

showers of particles, is the difficulty in controlling the number of

projectiles which leave the reservoir when a voltage pulse is applied

to the injector electrode. If a shower of particles accelerate toward

the target, it is impossible to identify a particle crater with a

projectile of measured velocity and mass. For useful data, a crater

must be identified with the mass, radius and velocity of the pro-

jectile that produced it. Simultaneous measurement of these variables

for a number of particles is extremely difficult. An ideal device would accelerate a single particle through a known difference of potential. Recent designs of some electrostatic accelerators have succeeded in injecting single particles into the field. The very latest design for these guns inject one particle at a time and reject this particle when it does not have the desired narrow range of velocities.

An electrostatic accelerator has two advantages which make it a valuable tool.

(1) It accelerates microscopic projectiles which are in the same range of sizes as the typical micrometeoroid.

(2) It can accelerate brittle particles without the particles breaking up.

DRAG FORCE FROM HIGH VELOCITY GASES

There are two, much used methods for obtaining a dense, high velocity gas. In one method, a metal wire, or ribbon, is exploded to supply the dense gas, or to supply energy to a medium in which the wire is embedded. In the other method, a shaped charge of explosive is detonated and the particle is driven by the gaseous products from this mixture.

High Velocity from Electrical Energy Stored in a Condenser.

Quantities of gases at high temperatures and high velocities may be obtained from the energy that is stored in a charged condenser. A possible arrangement for a device to employ this energy is illustrated in Figure 2. If extremely high, gas-flow velocities are desired, the
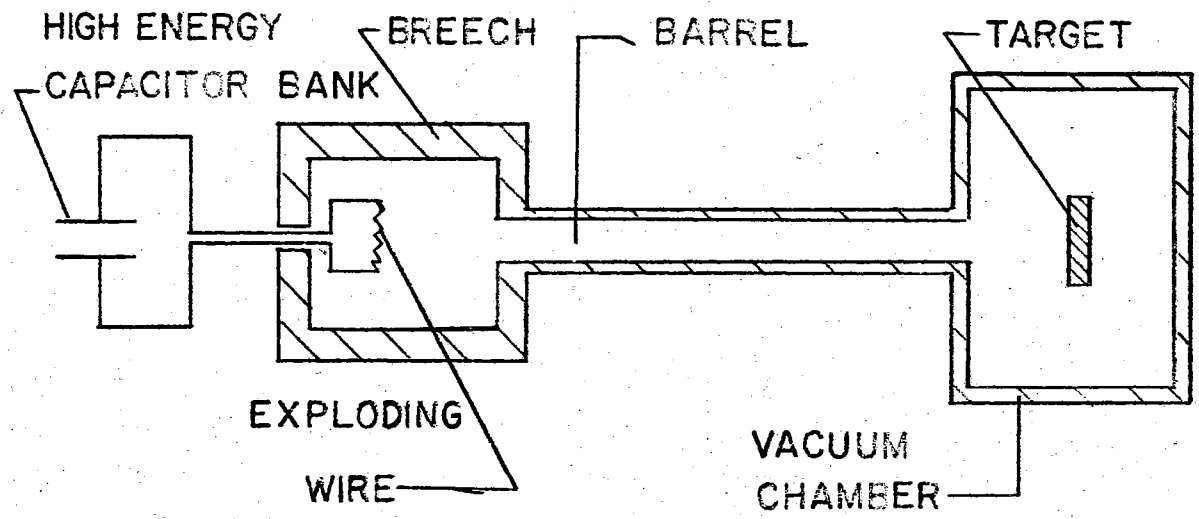
FIGURE 2 - DRAG-FORCE ACCELERATOR

gas must have a low molecular weight and a high temperature. The high temperature may be obtained by the injection of a considerable quantity of energy into a propellant mass in a very short time interval, such as is obtained by discharging a bank of fast, high-energy capacitors through a small wire that is embedded in the propellant. A possible arrangement is indicated in the figure. Stable gases at room temperature are not the best propellants because their densities are too low for significant drag forces, even when they are highly compressed. One propellant, which has been employed successfully, is a massive, electrically-exploded wire (24). Another propellant that has been used is ordinary water which has received energy from a small exploding wire (25). With each propellant, the gaseous products expand from the breech and travel down the barrel toward the target in an evacuated chamber. The projectiles, whose diameters are of the order of 1/20 th of the diameter of the barrel, attain a velocity almost equal in magnitude to the velocity of the gas stream. Particles 10 to 100 microns in size have reached velocities of 30,000 feet per second in this type of accelerator.

Shaped Charge of Explosive

Particles with the highest velocities are obtained with shaped charges, or explosives. Commonly used explosives are TNT, pentolite and composition B. A booster explosive may, or may not, be placed between the igniter and the main explosive charge. A typical arrangement of the explosive in a shaped charge is illustrated in Figure 3. When the main charge is ignited at the opposite end to the shaped portion, a plane, explosive wave travels parallel to the longitudinal
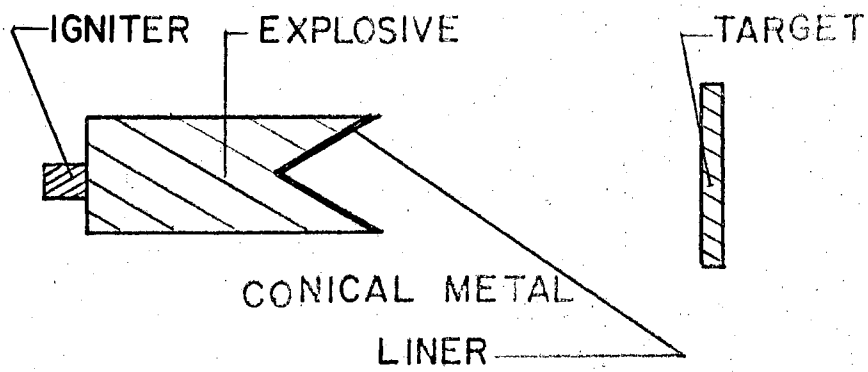
FIGURE 3 - SHAPED-CHARGE ACCELERATOR

axis of the charge. This explosive wave collapses the metal cone when it reaches the apex of the shaped portion. The walls of the cone approach each other at a high velocity and produce a long, thin jet of metal particles which travel toward the target at tremendous velocity. The pressures which are produced during the collapse of the metal liner may be of the order of a few tenths of a megabar, and jet velocities of 30,000 to 50,000 feet per second are possible. More complete discussions of shaped charges are given in references 6 and 23.

With the preceding arrangement, it is usual for a large number of particles to strike the target, and it is impossible to separate them according to either their sizes or their velocities. Neither is it possible to ascertain which craters were created by which projectiles. As a consequence, it is difficult to determine the correspondence between crater size and depth in relation to projectile size and velocity.

Single projectiles of a definite geometry may be accelerated by shaped charges only if the type, quantity, and geometry of the explosive is carefully controlled. Pressures and acceleration forces must be held below the ultimate strength of the projectile. One popular way to accomplish this objective is by the "air cavity" explosive charge that is illustrated in Figure 4. As in the preceding arrangement, a plane, explosive wave travels along the longitudinal axis of the main charge. With this arrangement, the size and the geometry of the air cavity cause the projectile to remain intact and to accelerate as a single fragment. Projectiles having a mass of several grams have been accelerated to velocities of 10,000 to 16,000 feet per second by this method (17).

Multistage, hollow-core, shaped-charge accelerators such as shown
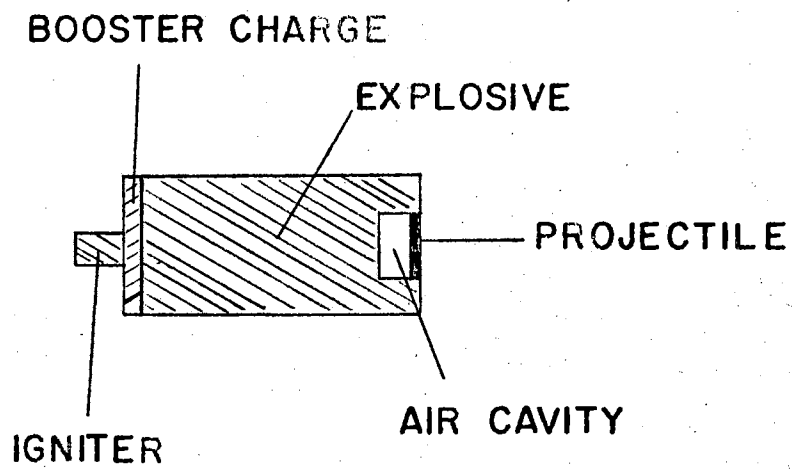
FIGURE 4 — AIR-CAVITY ACCELERATOR

in Figure 5 have been constructed (14). As the projectile passes the apex of the conical recess of each charge, the explosive ignites and forms a jet which accelerates the projectile so that its velocity is increased by a value, Δv. There are considerable difficulties involved in the operation of such an accelerator. For example, it is difficult to precisely time and control the ignition of the explosives, to preserve the axial alignment of the charges and projectile trajectory, and to reduce the amplitude of the pressure impulse to a safe, manageable level.

LIGHT-GAS GUNS

Light-gas guns are common devices for accelerating small projectiles to high velocities and will be described in detail. The first practical light-gas gun was made by a group at the New Mexico School of Mines during the period 1948-1952 (1). This group used hydrogen as the light gas and was able to fire light projectiles at muzzle velocities of 13,000 feet per second.

Following the success of the NMSM gun, other people began to investigate the possibilities of light-gas guns so that today there exist several satisfactory designs for light-gas guns. The basic design of a light gas gun is shown in Figure 6. All light-gas guns have two barrels of different sizes. The larger barrel is called the pump tube, and the smaller barrel is called the launch tube. The pump tube is sealed at one end by a piston and at the other end by the projectile. A light gas, such as hydrogen or helium, is introduced at low pressure into the volume between the piston and the projectile. Both the piston and the projectile must be held rigidly in position by any convenient
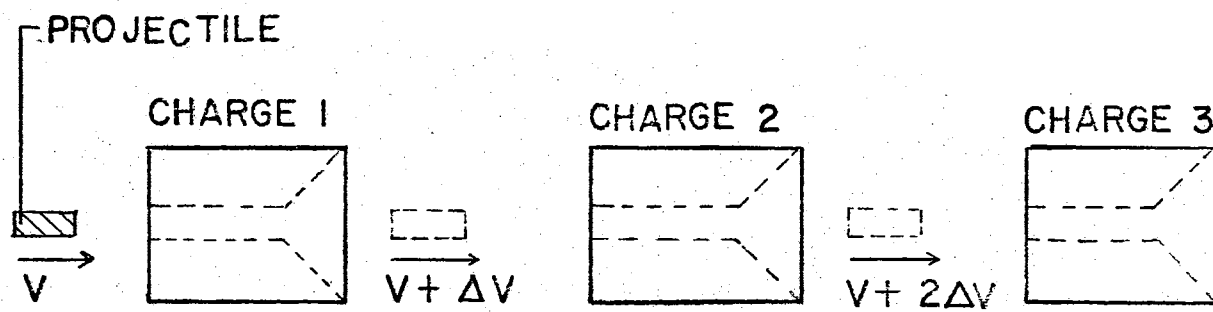
FIGURE 5 - MULTISTAGE SHAPED-CHARGE ACCELERATOR

BREECH

PUMP TUBE

LAUNCH TUBE

GUN —
POWDER

LIGHT GAS

PISTON

PROJECTILE
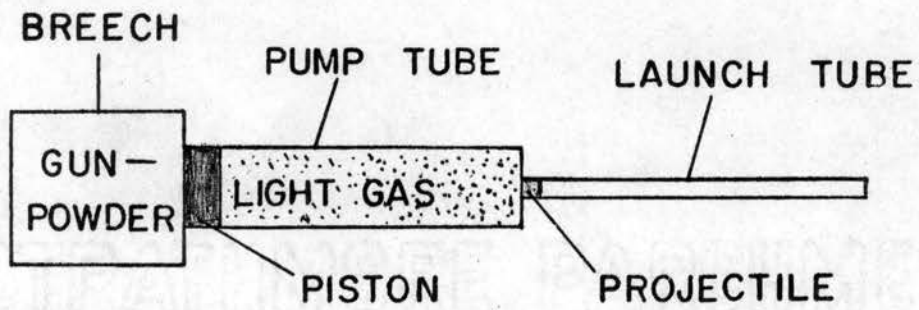
FIGURE 6 — LIGHT-GAS GUN

means; usually this is accomplished by machining a retaining flange on both of them.

When the gunpowder is ignited, it decomposes into a gas that is characterized by high pressure and high temperature. When the gunpowder gas pressure reaches about 2000 p.s.i., the flange holding the piston in place should rupture and release the piston. The pressure of the gunpowder gas continues to rise and forces the piston down the pump tube. As the piston progresses down the pump tube, it compresses the light gas and converts it into a high temperature, high pressure gas. When the pressure of the light gas reaches a desired value, the flange or restraint on the projectile should rupture and release the projectile. The pressure at which the projectile restraint releases depends upon the muzzle velocity that is desired, but it is usually between 20,000 and 100,000 p.s.i. The high pressure, light gas forces the projectile down the launch tube at a high acceleration.

The motion of the piston, after it has been rammed down the pump tube, constitutes the basic difference between the light, isentropically-compressed gas gun (8) and the light, accelerated-reservoir gas gun (12).

Light, Isentropically-Compressed Gas Gun

In the light, isentropically-compressed gas gun, the effect of the shock wave that forms in front of the rapidly moving piston is ignored. The gun is designed so the piston stops and reverses direction before it reaches the end of the launch tube. This leaves a small reservoir of high pressure gas which drives the projectile down the launch tube during the piston slow down, stop and reverse. With this

design, the piston does not reach the end of its travel and neither piston nor pump tube wall are damaged.

The distance that the piston travels between the time that the projectile first begins its motion and the time that the projectile leaves the end of the launch tube is small, usually of the order of an inch, or so. For all practical purposes, the flow of gas out of the pump tube may be represented as the flow from a small stationary reservoir of high temperature, high pressure gas. For this reason, the orientation of the launch tube with respect to the axis of the pump tube is not important. It is certainly not necessary to have the axes parallel as shown in Figure 6. For the intended use of the helium gas gun which is described in this thesis, it was more convenient to turn the axis of the launch tube 90° away from the axis of the pump tube.

As the projectile travels down the launch tube, acceleration results from the continuous push of the high pressure gas from the pump tube. It is impossible for this pressure to be maintained if the projectile travels faster than the speed of sound in the reservoir of confined gas. As the projectile travels down the launch tube, two factors arise which limit the muzzle velocity. First, the pressure at the base of the projectile decreases in magnitude as the projectile moves away from the high pressure reservoir. As a consequence, a reservoir at a very high pressure will not accelerate the projectile significantly after it has traveled a few feet away from the reservoir. Second, the projectile velocity increases as the projectile moves down the barrel, and whenever the projectile velocity equals the local speed of sound, it will be impossible for a pressure of any magnitude to continue to accelerate the projectile. It is, therefore, possible

for the last few inches of travel of the projectile within the launch
tube to be a hindrance rather than a help because the high pressure
reservoir will not be accelerating the projectile; whereas, the
friction forces will be decreasing the speed.

Light, Accelerated-Reservoir Gas Gun

The velocity of the projectile from a light, isentropically-
compressed, gas gun is limited by several factors. These may be over-
come to some degree with the light, accelerated-reservoir, gas gun.
In the latter gun, the piston is made of nylon, or polystyrene, and
the union between the launch tube and the pump tube consists of a
gentle taper which is illustrated in Figure 7, rather than as an abrupt
change in diameter as is indicated in Figure 6. In the design of
this gun, no attempt is made to leave a buffer of gas in front of the
piston in order to stop its forward motion. Instead, the piston is
allowed to ram forcibily into the tapered coupling. The nylon, or
polyethylene deforms easily so the end of the piston enters the smaller
diameter launch tube. The deformation of the piston from the diameter
of the pump tube to the diameter of the launch tube causes the for-
ward face of the piston to accelerate tremendously. As a consequence,
the reservoir of gas trapped between the piston and the projectile
is compressed to an even higher pressure and is also accelerated down
the barrel.

The projectile in the accelerated-reservoir gun attains its veloci-
ty as a result of the pressure from the high pressure reservoir follow-
ing and pushing on the base of the projectile. The pressure decreases
in magnitude as the projectile travels away from the reservoir. Since

PUMP TUBE   LAUNCH TUBE
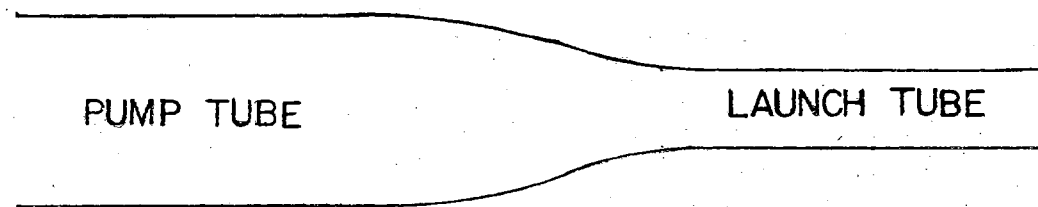
FIGURE 7 - UNION OF BARRELS IN ACCELERATED
RESERVOIR LIGHT-GAS GUN

the pressure of the reservoir is increased and since the reservoir is

forced down the launch tube and remains closer to the projectile, the

magnitude of the pressure on the projectile is several times larger

than in the preceding type of gun. In the accelerated reservoir gun,

the velocity of the reservoir must be added to the local speed of sound

in order to obtain the velocity that the projectile must attain in

order than the pressure decrease significantly. Since the velocity of

the reservoir can be quite large, it is generally true that the pressure

is maintained on the projectile.

Higher muzzle velocities are obtained from the accelerated-reser-

voir gun since it maintains a higher pressure on the base of the pro-

jectile. A respectable projectile velocity from the light, isentropi-

cally-compressed, gas gun would be 15,000 feet per second in contrast

to velocities of 30,000 feet per second, or higher, with the acceler-

ated-reservoir gun (8), (12).

Light, Shock-Compressed, Gas Gun

Another type of light-gas gun, which has recently been developed

is the light, shock-compressed, gas gun (5). This gun is quite similar

to the previously described guns except for the addition of a first

shock tube. When the gunpowder is ignited, a shock wave forms in the

light gas in the first shock tube. This shock wave travels down the

tube, is reflected at the opposite end, and creates a reservoir of

compressed and heated helium within the tube. This shock wave reflects

from the end of the tube and creates a second reservoir of hot, high

pressure gas. This latter reservoir of gas accelerates the projectile

down the launch tube. The general design of this type of gun is
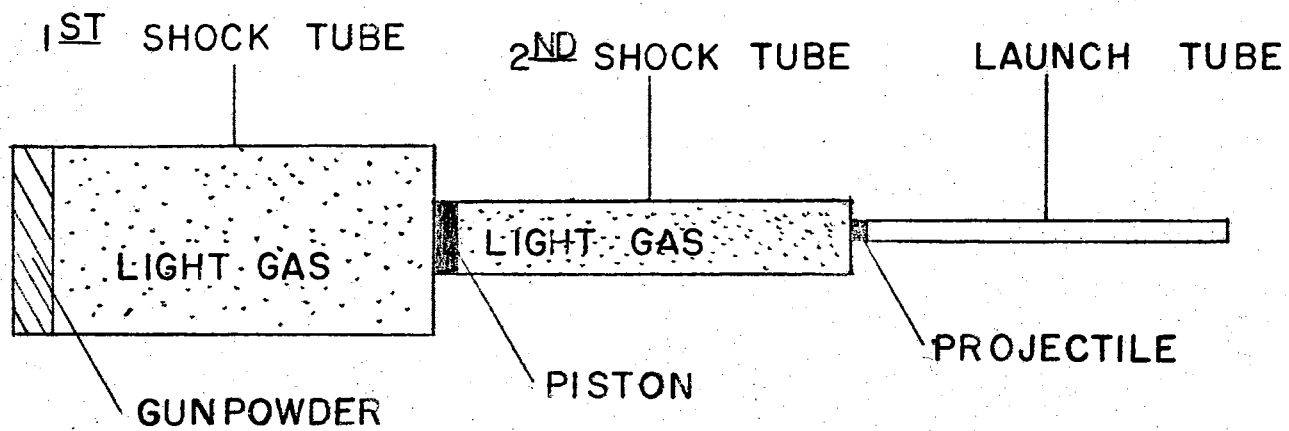
FIGURE 8 — SHOCK COMPRESSED LIGHT—GAS GUN

illustrated in Figure 8. The shock wave in the second tube will reflect several times between the front face of the piston and the end of the shock tube. Each time the shock wave passes through the light gas, it raises the temperature and pressure of the gas and provides a reservoir of light gas of rising pressure and temperature to flow into the launch tube and keep the pressure at the base of the projectile at a high value. The union between the second shock tube and the launch tube may be a tapered coupling and make this stage of the gun into an accelerated-reservoir gun, if desired.

CHAPTER III

THEORY OF LIGHT GAS GUNS

Importance of The Molecular Weight of The Propelling Gas

The gas which propels the projectile down the launch tube must

contain a large amount of potential energy at the instant that the

projectile begins its motion. This potential energy is converted into

the kinetic energy of the projectile and the kinetic energy of the ex-

panding gas. The division of energy between the projectile and the gas

depends upon the molecular weight of the gas, the weight of the pro-

jectile, and the length of time that the gas and the projectile remain

in contact.

If the barrel, down which the projectile travels, is infinite in

length, and such factors as heat loss to the barrel and bore friction

are negligible, then the projectile will accelerate until the gas

pressure at its base is equal to the pressure in front of it. A shock

wave will precede the projectile down the barrel if the bore in front

of the projectile is filled with air. The projectile will accelerate

until the base pressure is just balanced by the pressure behind the

shock wave. If the barrel is evacuated, no shock wave can be created

in front of the projectile, and the projectile will accelerate until

its velocity equals the velocity of efflux of the propelling gas into

a vacuum. This efflux velocity for air is about 28,000 feet per second;

while the limiting velocity, when the bore ahead of the projectile

is filled with air, is only 10,000 feet per second (8).

Two factors limit the velocity of the projectile to less than these theoretical maxima. First, the barrel must have a finite length so the length of time that the propelling gas acts upon the projectile is limited. Second, the barrel has a finite strength, so the maximum internal pressure and, hence, the allowable potential energy of the gas is limited.

The highest muzzle velocities will be obtained by reducing the weight of the projectile to a minimum and by bringing the gas to the maximum pressure that is permitted by the strength of the barrel. The maximum muzzle velocity will be determined by the manner in which the potential energy of the gas divides between the kinetic energy of the projectile and the kinetic energy of the gas. If the projectile is made as light as possible so that its weight is a fixed quantity, then the muzzle velocity will be determined solely by the molecular weight of the gas. The lighter the gas, the faster the gas will expand, and the higher will be the muzzle velocity.

The combustion products of ordinary gunpowder have a molecular weight of approximately 28. The molecular weight of these gases is an inescapable result simply because of the chemistry of nitrocellulose. No gun powder will decompose into gases of any significantly smaller molecular weight. It is evident that the molecular weight of the gases from the combustion of ordinary gun powders is quite heavy when compared to the molecular weight of 2 for hydrogen or 4 for helium. Firings in laboratories indicate that the practical limit of the muzzle velocity for a gun with a charge of nitrocellulose powder is around 10,000 feet per second, even if the barrel is evacuated. If the barrel is not

evacuated the limit is about 8,000 feet per second (8). For this reason, it is essential that a light gas, either hydrogen or helium, be used as the propelling gas behind the projectile if a high muzzle velocity is required.

The performance of any light-gas gun may be improved provided the temperature of the light gas may be increased during the time that the projectile is traveling down the launch tube. A higher temperature will increase the speed of sound in the light gas and permit a higher pressure on the projectile before it leaves the launch tube. A method of obtaining a high temperature gas that has been suggested by some investigations is to have an electrical discharge dissipate a large amount of energy in the gas volume behind the projectile in the manner that is illustrated in Figure 9, (4), (28), (30). Several of these discharges, spaced along the length of the launch tube, will further enhance the performance of the light-gas gun.

REQUIREMENTS IMPOSED UPON LAUNCHER

In the experimental work, two requirements dictated the type of launcher to build. These requirements were:

(1) The projectile must have a definite geometry and must strike the target at a specific orientation; i.e., the projectile cannot tumble, or yaw excessively, while in flight.

(2) The projectile must have a velocity of 10,000 feet per second, or higher.

Any of the particle accelerators that are described in Chapter II could satisfy requirement (2) above, if they were properly constructed.
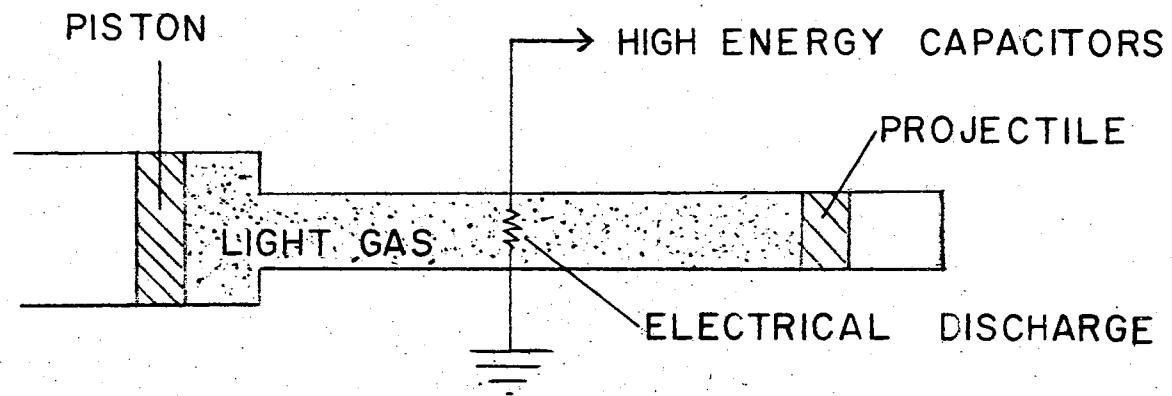
FIGURE 9 — METHOD TO INCREASE THE LIGHT–GAS

TEMPERATURE

Requirement (1) is more stringent, and it is impossible for some launchers to satisfy it. Since the projectiles must have a definite geometry, they must necessarily be large enough to be machined, or shaped, in some manner. Aluminum projectiles were desired, so this required that the size of the projectiles be consistent with masses of the order of 0.1 or 0.2 gram. It is difficult for an electrostatic accelerator, or an accelerator which utilizes the drag forces of rapidly moving gases, to accelerate a projectile of this size to a velocity of 10,000 feet per second. The projectiles must travel in a straight line without tumbling, or yawing excessively, so shaped charge accelerators are also eliminated. Electrostatic and drag-force accelerators could not satisfy this tumbling restriction.

The launcher which best satisfies requirements (1) and (2) is a light-gas gun. After careful consideration, it was decided to construct a helium, isentropically-compressed, gun. Preliminary calculations indicated that such a gun would accelerate the desired projectiles to velocities of 10,000 to 16,000 feet per second.

CHAPTER IV

DESIGN OF THE GUN

Basic Requirements and Assumptions

The general design procedure for the design of the light-gas gun

which is described in this thesis is similar to that followed by

Charters, Denardo and Rossow in the design of their gun (8). Charters,

et. al., began their analysis by considering the basic factors which

control the behavior of the projectile's velocity. The gun should be

designed so that the gas pressure at the projectile's base is held at

the highest possible value throughout the launching cycle. The launch-

ing cycle is defined as the interval of time between the initiation

of the projectile's motion and the exit of the projectile from the end

of the muzzle. As the projectile travels down the launch tube, the

gas pressure at its base decreases. A pressure drop is required to

accelerate the light gas from a low velocity im the pump tube to the

velocity of the projectile. This pressure drop is directly proportional

to the amount of kinetic energy which is required to accelerate the

light gas to the projectile's velocity. The pressure drop is minimized

if the density of the light gas is minimized, and the density is

minimized if the amount of helium originally loaded into the pump tube

is kept at the minimum that is required to launch the projectile.

These two requirements, of keeping the total amount of light gas

to a minimum and of holding the pump tube pressure to a maximum,

demand a careful adjustment of the loading conditions in order to obtain the highest muzzle velocity from the gun. The loading conditions are the initial light gas pressure in the pump tube, the mass of the piston which compresses the light gas, the quantity of gunpowder, and the rupture pressure of the restraint which holds the projectile in place. The dimensions of the pump tube, of the launch tube and of the weight of the projectile are assumed to be fixed, and therefore, are not considered to be loading conditions.

The assumptions on which the design by Charters, et. al., is based are:

(1) The light gas must be compressed to a specified pressure, p_2.

(2) The pump piston must move the correct distance $(x_2 - x_3)$, so that a constant pump tube pressure, p_2, is maintained during the time that the projectile is accelerated down the launch tube.

(3) The pump piston shall complete its forward motion and shall come to rest at a short distance from the end of the pump tube; just as the projectile leaves the end of the muzzle.

(4) A small buffer of gas shall remain between the front face of the piston and the end of the pump tube at the end of the compression stroke of the piston.

(5) The velocity of the light gas, which flows from the pump tube into the launch tube, jumps to the local speed of sound at the entrance to the launch tube and remains at this value throughout the entire launching cycle.

(6) The equations of state are assumed to be those of perfect gases.

(7) All thermodynamic processes are assumed to take place adia-
batically and isentropically.

(8) The pressures of the gunpowder gas and the light gas are
assumed to be constant throughout their respective volumes at
any instant of time. These pressures may, however, vary with
time.

(9) The friction between the projectile and the launch tube is
neglected.

(10) The launch tube is assumed to be evacuated ahead of the pro-
jectile.

Condition (3) insures that the kinetic energy of the piston is
completely used up in compressing the light gas. Condition (4) is a
safety factor to prevent the end of the launch tube from being damaged
by the piston. The position at which the piston comes to rest is set
arbitrarily at 0.2 of a foot from the end of the pump tube.

Conditions (6) and (7) are certainly only approximations to the
true physical picture. The shock waves in the compression stroke of
the piston, the heat loss to the pump tube and to the launch tube, and
the skin friction of the light gas are all ignored. The shock waves
are not overly important, since the maximum velocity of the piston
(about 1300 ft/sec) is low compared to the local speed of sound in
helium (about 10,000 ft/sec). The decrease in energy from heat loss
to the tubes and skin friction are small when compared to the changes
in potential energy and kinetic energy that occur during the launching
of the projectile. From these considerations, all of the approximations
are believed to be sufficiently accurate.

COMPUTATIONAL PROCEDURE

In order to determine the values of the loading conditions, the following computational procedure was developed. This procedure was suggested by Charters, et. al., and the development of all of the equations except those for P_1 and P_2 in steps (18) and (19) are found in their report. The equations for P_1 and P_2 were altered. The breech design and the method of escape of the gunpowder gases out of the breech are considerably different for the gun in this paper from the gun that is described in reference (8). The derivation of the equations for P_1 and P_2 is given in Appendix A. Table I and Table II contain a full explanation of all symbols and subscripts.

(1) Assume a value, a_o, for the speed of sound in the light gas in the pump tube. If helium is used, a good first approximation is a_o = 10,000 ft/sec.

(2) Compute the quantity, α_o , from

$$\alpha_o = \frac{2}{\gamma - 1} a_o$$

where γ is the ratio of specific heats and has a value of 1.667 for helium.

(3) Compute the dimensionless projectile velocity, $\overline{u}_s$, from

$$\overline{u}_s = \frac{u_s}{\alpha_o}$$

where u_s is the projectile velocity.

(4) Compute the dimensionless projectile travel, $\overline{z}$, from

$$\overline{z} = \frac{\gamma-1}{2}\left\{\left[\frac{\left(\frac{2}{\gamma+1}\right) - \left(1-\overline{u}_s\right)}{\left(1-\overline{u}_s\right)^{\frac{\gamma+1}{\gamma-1}}}\right] + \frac{\gamma-1}{\gamma+1}\right\}$$

TABLE I

LIST OF SYMBOLS USED IN COMPUTATIONAL PROCEDURE

a   - speed of sound

A_p - cross-sectional area of pump tube

d   - diameter

L   - length of launch tube

L_p - length of pump tube

p   - light gas (helium) pressure

P   - gunpowder-gas pressure

R   - perfect gas constant

S   - cross-sectional area of launch tube

t   - time

$\bar{t}$ - dimensionless time

T   - temperature

u   - velocity

$\bar{u}$ - u/α_0

U   - volume of gunpowder chamber

v   - volume of gunpowder-gas which escapes out blowout hole in breech
      plug

V   - volume of gunpowder-gas at a given time

w   - mass

x   - distance from end of pump tube to front face of pump piston

z   - distance traveled by the projectile

$\bar{z}$ - $p_0 Sz/W_s \alpha_0^2$

α_0 - $2a_0/(\gamma - 1)$

γ - ratio of specific heats of the light gas

Γ - ratio of specific heats of the gunpowder gas

TABLE II

SUBSCRIPTS USED IN COMPUTATIONAL PROCEDURE

---

0 – conditions in the reservoir of light gas

1 – conditions at the start of the pump cycle

2 – conditions at the start of the launch cycle

3 – conditions at the end of the launch cycle

c – charge of gunpowder

L – conditions at the muzzle of the launch tube

p – pump piston or pump tube

s – projectile or launch tube

---

(5) Compute the dimensionless time of projectile travel, $\tilde{t}$, from

$$\tilde{t} = \frac{\gamma-1}{\gamma+1}\left[\left(1-\bar{u}_s\right)^{-\frac{\gamma+1}{\gamma-1}} - 1\right]$$

(6) Compute the pressure of the light gas, p_2, from

$$P_2 = \frac{\tilde{z}\,W\alpha_o^2}{SL}$$

where W is the mass of the projectile, S is the cross sectional area of the launch tube, and L is the length of the launch tube.

(7) Compute the time, t_L, for the projectile to travel the length of the launch tube from

$$t_L = \frac{W\alpha_o\,\tilde{t}}{Sp_2}$$

(8) Compute the position x_2 of the piston at the time the projectile begins its motion from

$$X_2 = X_3 + a_2 t_L\,\frac{S}{A_p}\left(\frac{2}{\gamma+1}\right)^{\frac{\gamma+1}{2(\gamma-1)}}$$

where x_3 is the final rest position of the piston and is set equal to 0.2 foot, and A_p is the cross sectional area of the pump tube.

(9) Compute the local speed of sound, a_2, at the time that the projectile begins its motion from

$$a_2 = a_1\left(\frac{x_1}{x_2}\right)^{\frac{\gamma-1}{2}}$$

where x_1 is the total length of the pump tube, and a_1 is the value of the speed of sound assumed in step (1).

(10) Replace a_o in step (1) by a_2 of step (9) and repeat steps (1) through (9) until the values of a_2 in step (1) and step (9) agree to within 1%.

(11) Compute $\bar{u}_s$ using the final value of a_2.

(12) Compute $\bar{z}$ and $\bar{t}$ from this value of $\bar{u}_s$.

(13) Compute p_2 from this value of $\bar{z}$. This final value of p_2 determines the rupture pressure of the restraint on the projectile.

(14) Compute the initial light gas pressure, p_1, from

$$p_1 = p_2 \left(\frac{x_2}{x_1} \right)^{\gamma}$$

(15) Compute t_L from $\bar{t}$ of step (12).

(16) Compute the mass of the pump piston, W_p, from

$$W_p = \frac{A_p (p_2 - P_2) t_L^2}{2 (x_2 - x_3)}$$

where P_2 is the pressure of the gunpowder gases and is set equal to zero since P_2 is an order of magnitude smaller than P_2.

(17) Compute the velocity, u_{p_2}, of the pump piston at the instant when the projectile begins its motion from

$$u_{p_2} = \frac{A_p (p_2 - P_2) t_L}{W_p}$$

(18) Compute the pressure of the gunpowder gas at the time when

the piston begins its motion from

$$P_1 = \frac{(\Gamma-1)\left[\frac{1}{2}W_p U_{p_2}^2 + \frac{A_p P_1 x_1}{\gamma-1}\left(\left(\frac{x_1}{x_2}\right)^{\gamma-1}-1\right)\right]\left(A_p + \frac{20.8}{x_1-x_2}\right)}{A_p U\left[1 - \left(1 + \frac{A_p}{U}(x_1-x_2) + \frac{20.8}{U}\right)^{1-\Gamma}\right]}$$

where U is the volume of the gunpowder chamber, and Γ is

the ratio of specific heats of the gunpowder gas. A value

of 1.3 for Γ was selected from reference (21).

(19) Compute P_2 the pressure of the gunpowder gas at the time the

projectile begins its motion from

$$P_2 = \frac{P_1}{\left(1 + \frac{A_p}{U}(x_1-x_2) + \frac{20.8}{U}\right)^{\Gamma}}$$

(20) Repeat steps (16) through (19), by using the value of P_2 from

(19) and continue the iteration until the values of P_2 from

successive iterations agree to within 1%.

(21) Compute W_p, U_{p_2}, and P_1 by using this final value of P_2.

(22) Compute W_c, the mass of gunpowder needed, from

$$W_c = \frac{P_1 U}{RT}$$

RT is called the force constant of the gunpowder, and a

typical value is 70 (long tons) $(Cm^3)/in^2)$ (gram) (22)

The preceding computational method was written in FORTRAN language

for the IBM 650 computer. Table III contains the fixed, geometrical

and physical quantities of the helium gun. These numerical values

were needed as input data for the computer program.

In the computer solution, the projectile's mass was increased from

0.02 gram to 0.40 gram in steps of 0.02 gram, and the projectile's

TABLE III

FIXED QUANTITIES FOR THE LIGHT GAS GUN

Ratio of specific heats

    Gunpowder gas, Γ ---------------------------------   1.3

    Helium, γ --------------------------------- 1.667

Gunpowder chamber

    Volume, U --------------------------------- 100.5 inch

Pump tube

    Length, L_p , --------------------------------- 9.23 feet

    Diameter, d_p --------------------------------- 0.786 inch

    Pump piston stop position, x_3 ------------------- 0.2 foot

Launch tube

    Length, L --------------------------------- 2.67 feet

    Diameter, d_s --------------------------------- 0.200 inch

velocity was allowed to vary from 5,000 feet per second to 20,000 feet per second in steps of 1,000 feet per second. For each value of projectile mass and velocity, the values of the loading conditions were calculated which would cause a projectile of that mass to leave the muzzle with the specified velocity. These loading conditions are summarized in Figures 10 to 13. Careful study of these loading conditions resulted in the construction of the helium gun which is described in the following chapter.
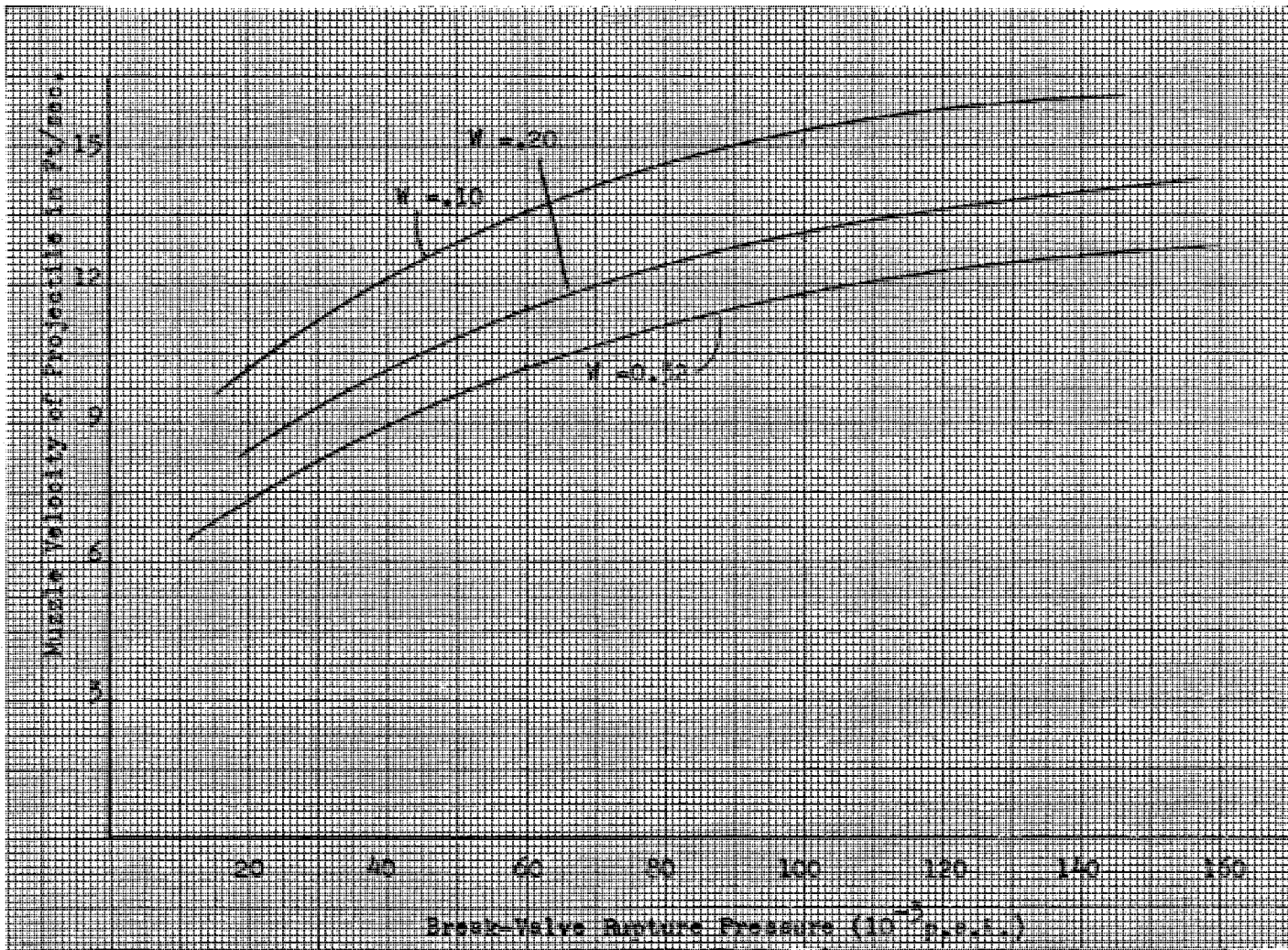
Figure 10. Perfromance Chart. Muzzle Velocity of Projectile of Mass W
Grams as a Function of Break-Valve Rupture Pressure.
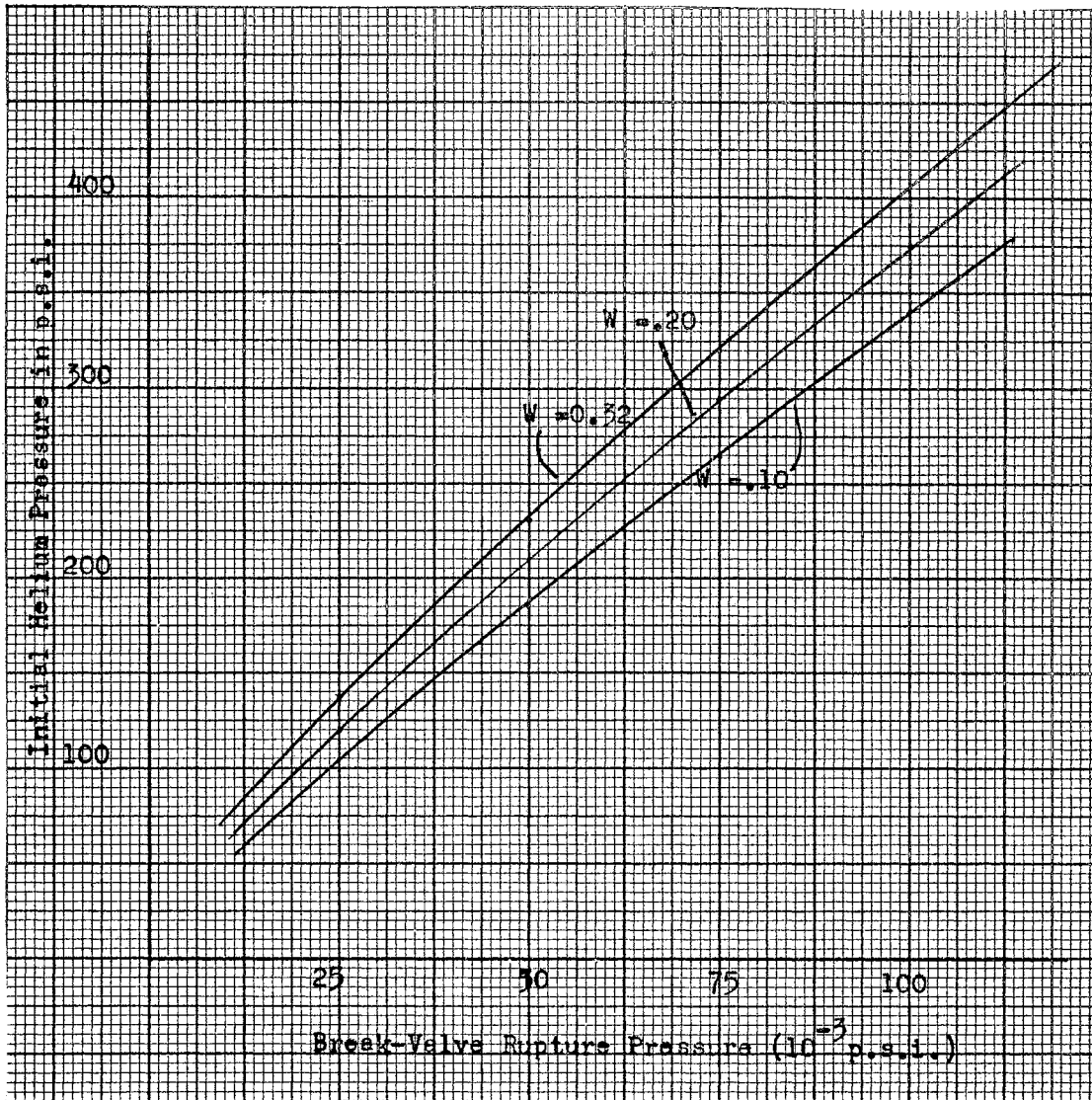
Figure 11. Loading Conditions. Helium Pressure That is
Needed in Pump Tube with Break-Valve. W is
Mass of Projectile in Grams.
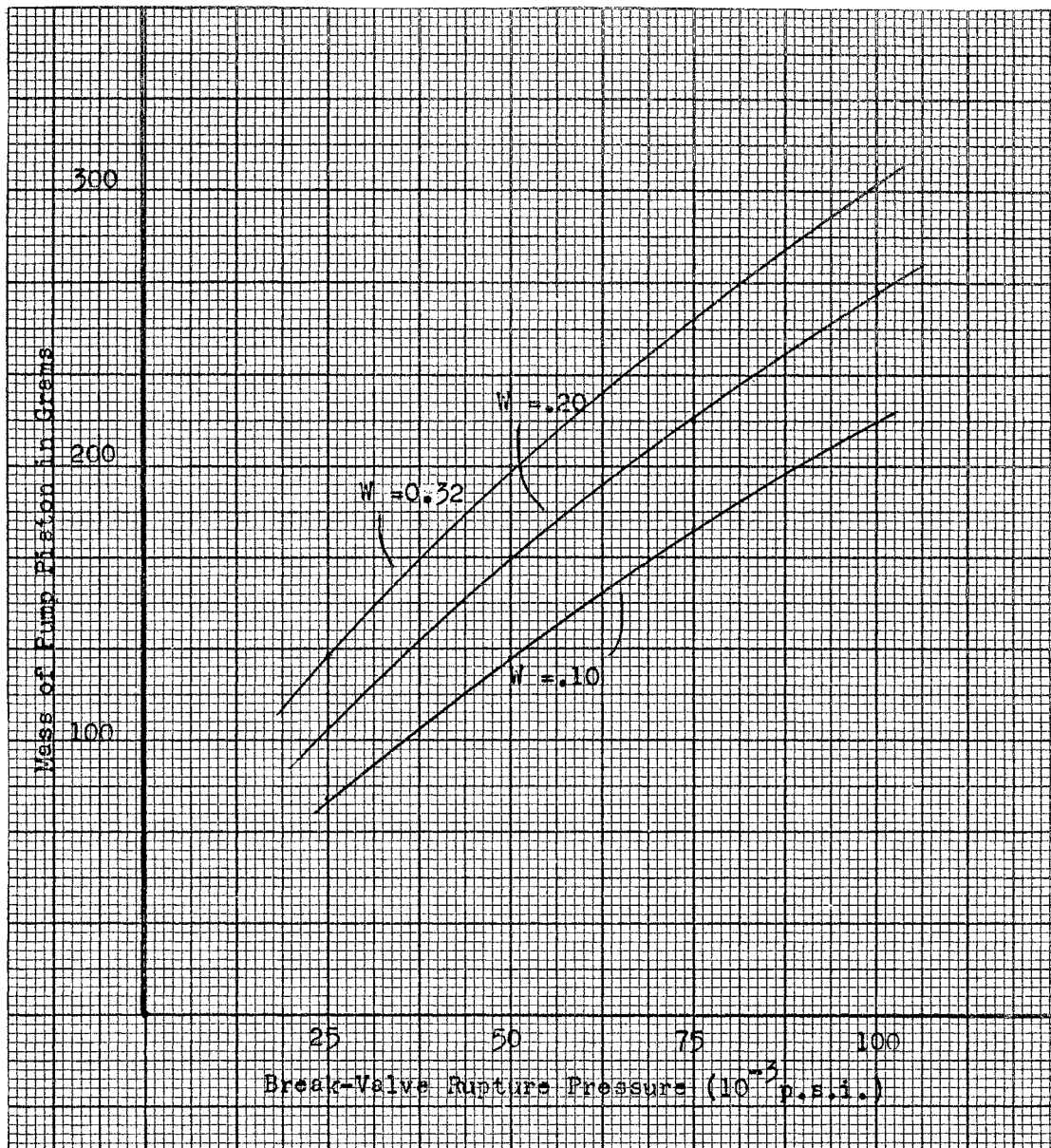
Figure 12. Loading Conditions. Mass of Pump Piston That
is Needed with Break-Valve. W is Mass of
Projectile in Grams.
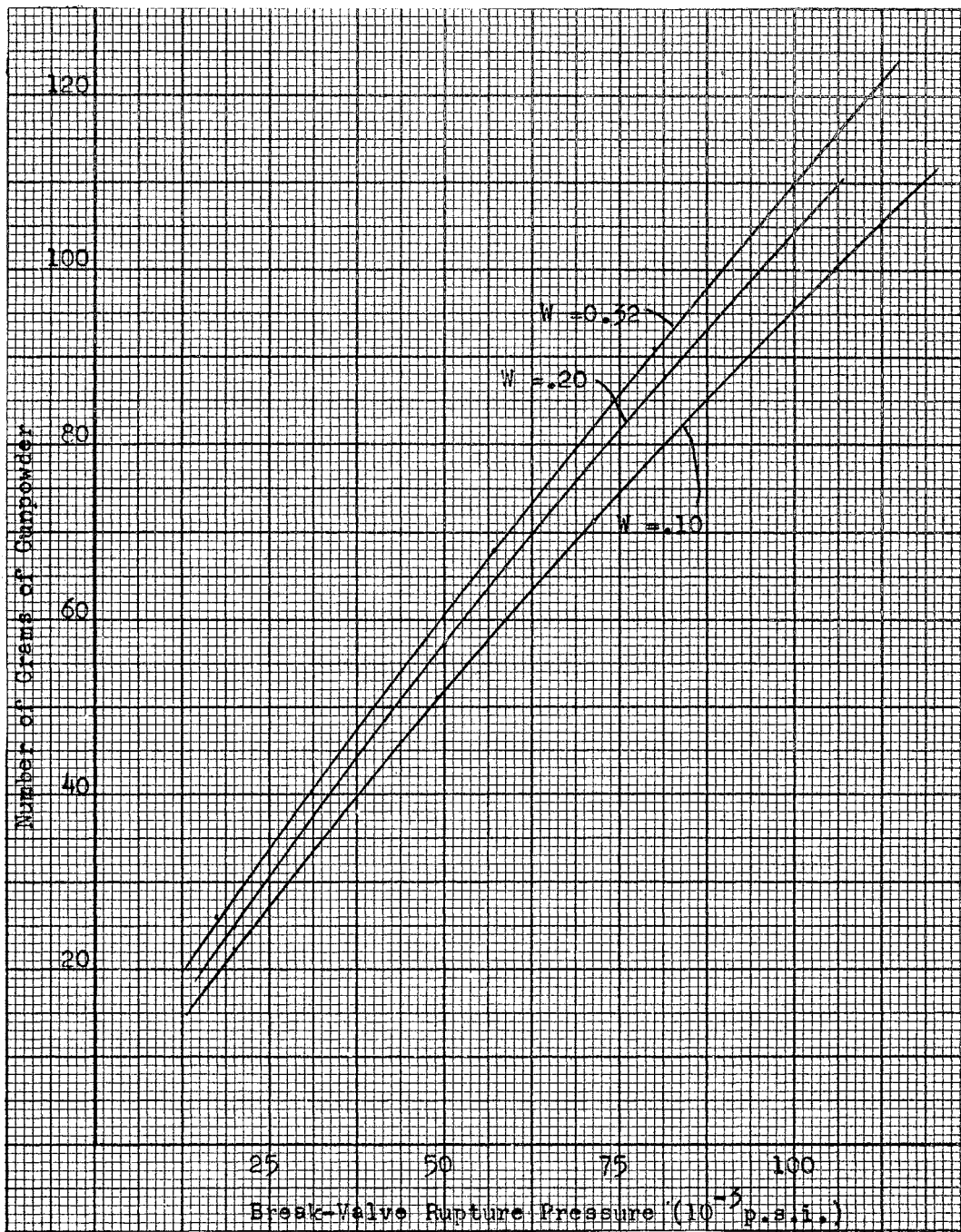
Figure 13. Loading Conditions. Amount of Gunpowder That
              is Needed with Break-Valve. W is Mass of
              Projectile in Grams.

CHAPTER V

DESCRIPTION OF THE GUN

Entire Assembly

The feature which distinguishes this gun from those in the refer-
ences is the fact that the launch tube is mounted so that its axis is
at a right angle to the longitudinal axis of the pump tube. Since
this gun is a stationary reservoir gun, it is not necessary for the
launch tube and pump tube to be axially aligned; the helium will rush
into the launch tube at the local speed of sound, regardless of the
orientation between the pump tube and launch tube. This feature and
the entire gun assembly are illustrated in Figure 14.

The gun rests on a sturdy wooden table, and on top of this table
are fastened three wobbly stands made of lightweight angle iron. Two
H-beams are bolted across the tops of these stands. The gunpowder
chamber, muzzle breech, and pump tube supports are bolted to the top
flanges of these H-beams. These supports align the muzzle breech,
the pump tube and the gunpowder chamber to the same center line and
hold them rigidly in place.

The gun is made gas tight by the use of o-ring seals at the joints
between the mated pieces. Although high, internal-gas pressures,
sometimes greater than 100,000 pounds per square inch, occur in the
gun, these seals are quite satisfactory. If pressures of this magnitude
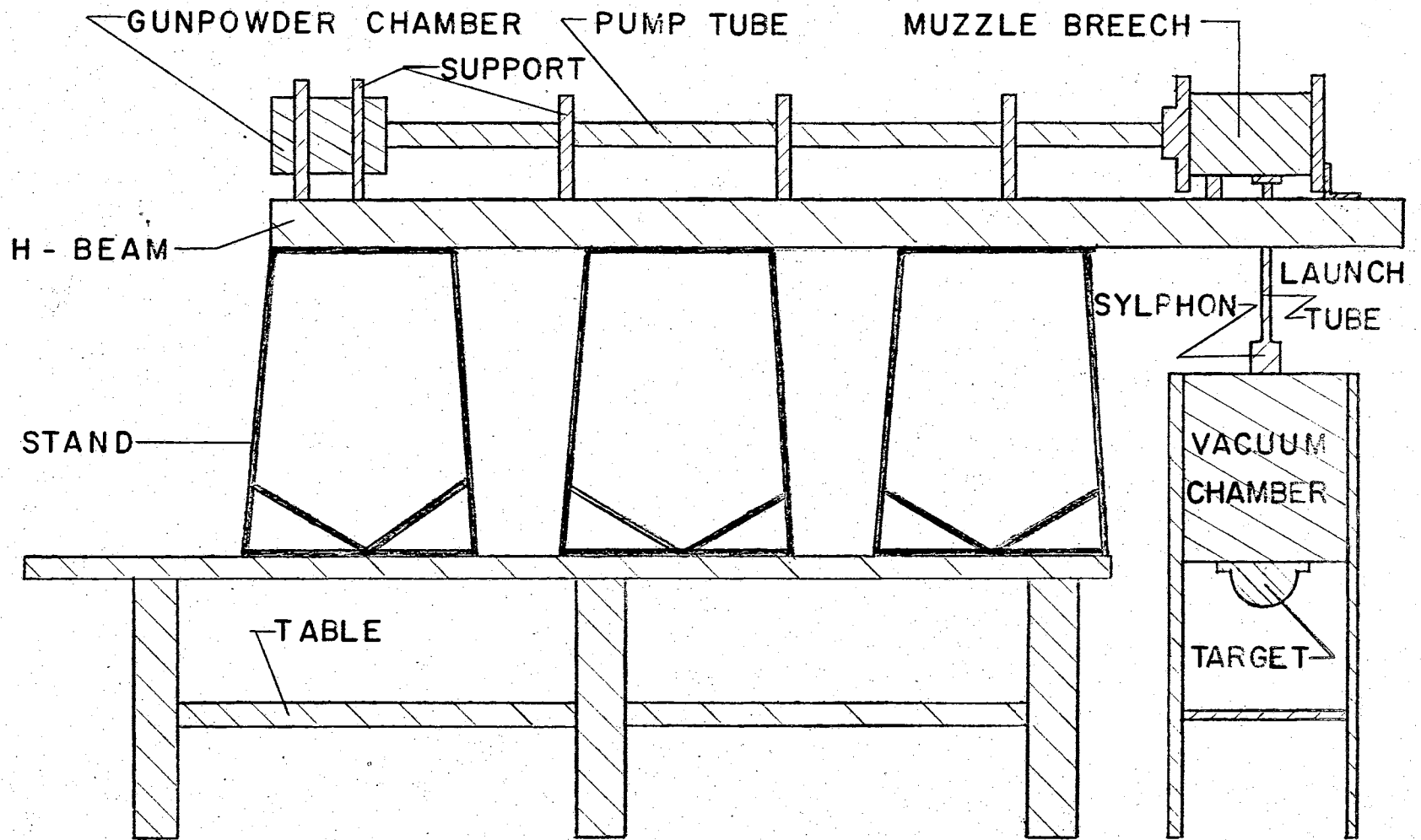
FIGURE 14 · COMPLETE GUN ASSEMBLY

existed within the gun for very long periods of time, no doubt the
o-ring seals would fail, and perhaps structural damage would occur to
the gun. Since the launch cycle requires only about ½ millisecond,
these pressures are highly transient and cause little o-ring damage.

PUMP TUBE AND LAUNCH TUBE

The pump tube is a 20 mm cannon barrel which is made of chrome-
moly vanadium steel. It is 100 inches long and 2½ inches in outside
diameter. The large wall thickness of the barrel was desired since
large internal pressures exist inside the pump tube. Two of these
20 mm barrels were made for this gun by the Springfield Arsenal in
Springfield, Massachusetts. In order to avoid excessive friction,
so assumption (7) of Chapter IV is satisfied, these barrels were left
with a smooth bore and were not rifled.

A smooth bore launch tube is also used on account of the as-
sumptions (7) and (9). One tube is a 0.20 caliber barrel, 32 inches
long; and the other tube is a 0.17 caliber barrel, 27 inches long.
Thick walls were desired so the barrel would not rupture when a large
internal pressure was applied.

VACUUM CHAMBER

The vacuum chamber permits the evacuation of the launch tube in
front of the projectile and this satisfies assumption (10) of Chapter
IV. The vacuum chamber is a cube of reinforced steel plate. This box
is supported separately from the gun assembly, and the union between
the launch tube and vacuum chamber is made vacuum tight by means of a
flexible syphon. As a consequence, no mechanical motion of the gun

is transferred to the vacuum chamber and interfere with the measurement
of the projectile's velocity, or other desired measurements. Openings
were made on opposite sides of the vacuum chamber. These openings per-
mit the insertion of glass windows so that the projectile's motion
may be observed, and its velocity measured. They also allow tools to
be inserted inside of the vacuum chamber to make necessary adjustments.
A large circular opening in the bottom of the box allows the projectile
to strike a target which is bolted tightly to the bottom of the vacuum
chamber.

The dimensions of the vacuum chamber were selected after a study
of Figure 11. It was assumed that all of the helium in the pump tube
flowed through the launch tube and entered the vacuum chamber. It
was desired that the volume, V, of the vacuum chamber be large enough
so this amount of helium, at the pressures indicated in Figure 11, when
expanded into the volume, V, would not raise the pressure above 15
pounds per square inch. If this condition is satisfied, the glass
windows of the vacuum chamber will not be shattered by a pressure
pulse.

POWDER CHAMBER

The powder chamber, or breech, is constructed from a 10 inch
round of 4340 steel which is heat treated to a hardness of Rockwell 40.
The cavity in which the gunpowder is ignited is 4 inches in diameter
and 8 inches long. These thick, strong walls are capable of with-
standing the large pressures generated by the explosion of the gun-
powder. The cavity was designed with a large diameter so that a person
could reach his hand into the cavity and insert the piston and piston

plug into their respective positions. The details of the powder chamber are shown in Figure 15.

The breech plug has a small diameter hole, the blowout hole, drilled through it. This hole permits the lead wires of the electric squib to pass through and go to the voltage source which ignites the squib, and also allows the gunpowder gases to escape out of the chamber after the projectile has been launched. A small recess is machined in the front face of the breech plug to serve as a receptacle for the cardboard tube with the gunpowder.

The piston plug squeezes the shear ring of the piston tightly between itself and the end of the pump tube. The shear ring serves as a gasket which seals the breech end of the pump tube so that no helium can leak out. The main purpose of the shear ring; however, is to hold the piston rigidly in place until the gunpowder gas pressure reaches a pressure of about 2000 pounds per square inch. Holding the volume of the gunpowder gas constant until the gas reaches a pressure of this magnitude insures that the gunpowder is completely ignited. Partial, or incomplete burning of the gunpowder may result if this practice is not followed.

MUZZLE BLOCK

The muzzle block is made from a 10 inch round of 4340 steel which is heat treated to Rockwell 40. The union allows the pump tube to be rigidly bolted to the coupling. A hole through the union to the pump tube serves as an entry to admit helium into the pump tube.

A hole of the same diameter as the bore of the 20 mm cannon barrel is drilled through the union and part way into the muzzle block.
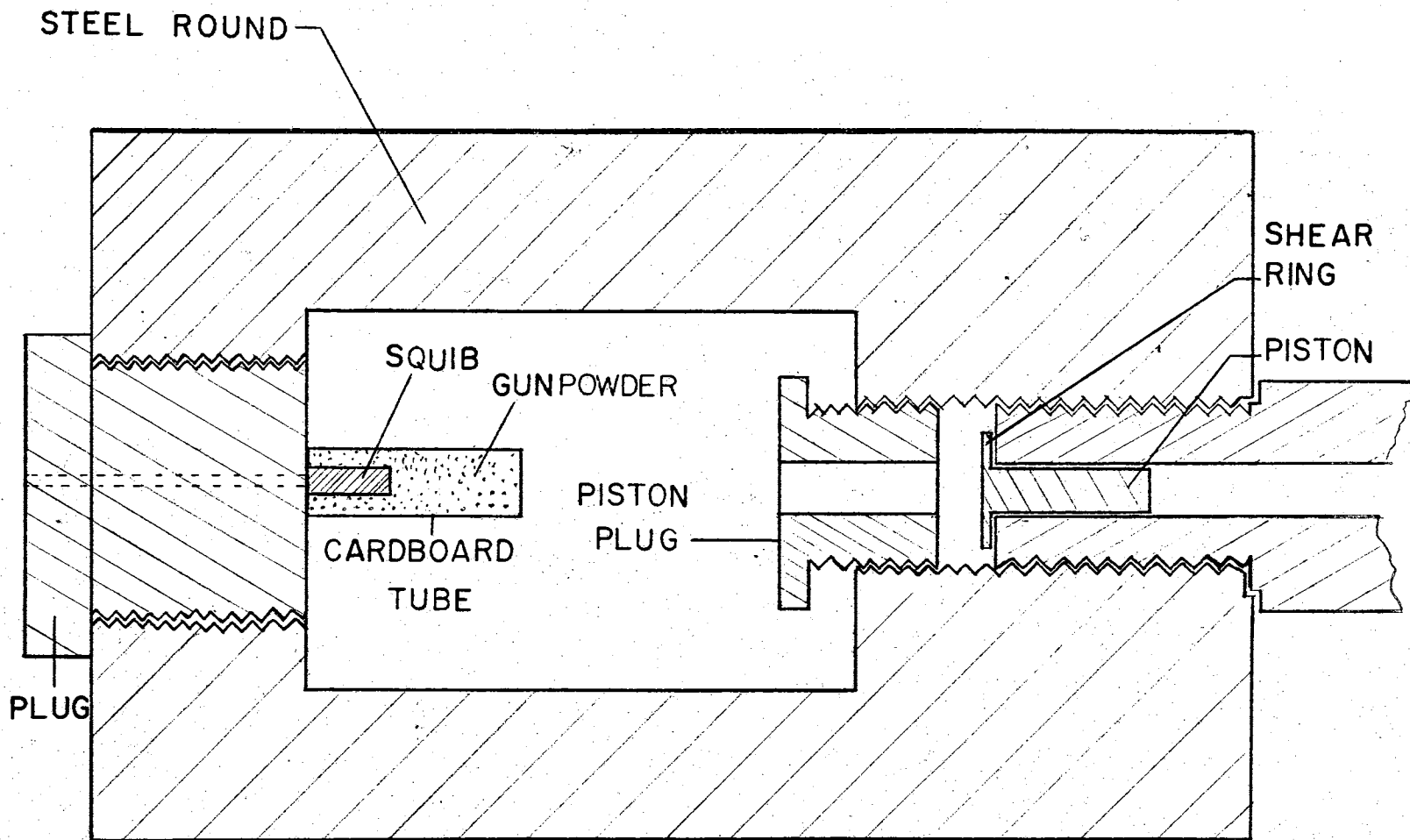
STEEL ROUND

SHEAR
RING

PISTON

SQUIB
GUNPOWDER

PISTON
PLUG

CARDBOARD
TUBE

PLUG

FIGURE *15* · GUNPOWDER CHAMBER

This is illustrated in Figure 16 and it provides an addition to the
length of the pump tube. The last few inches of the pump tube is the
region in which the tremendous, internal pressures occur. In the
design of this gun, this high pressure region is surrounded by the
thickest walls, about 4 inches of steel, of anywhere along the pump
piston's travel.

BREAK VALVE

The coupling plug has a recess in its top which serves as a
receptacle for a break valve. This break valve is a piece of aluminum
with a V-slot cut across its upper side and a small kerf on its bottom
side. It is illustrated in Figure 17. The kerf lies directly below
the apex of the V-slot and is cut completely across the piece so it
creates a stress riser which will make the break valve split clean.
The break valve is installed in its receptacle with the V-slot up.
The pressure of the helium exerts a force whose direction is normal
to the surfaces of the slot. The lateral component of this force
causes the break valve to split along the vertical plane between the
kerf and the apex of the slot. This separates the valve into two
pieces. The high pressure helium rushes through the break and strikes
the projectile which lies immediately below the break valve. By
changing the depth of the slot, the rupture pressure of the break
valve may be changed; and, as a result, the muzzle velocity of the
projectile changes.

PISTON

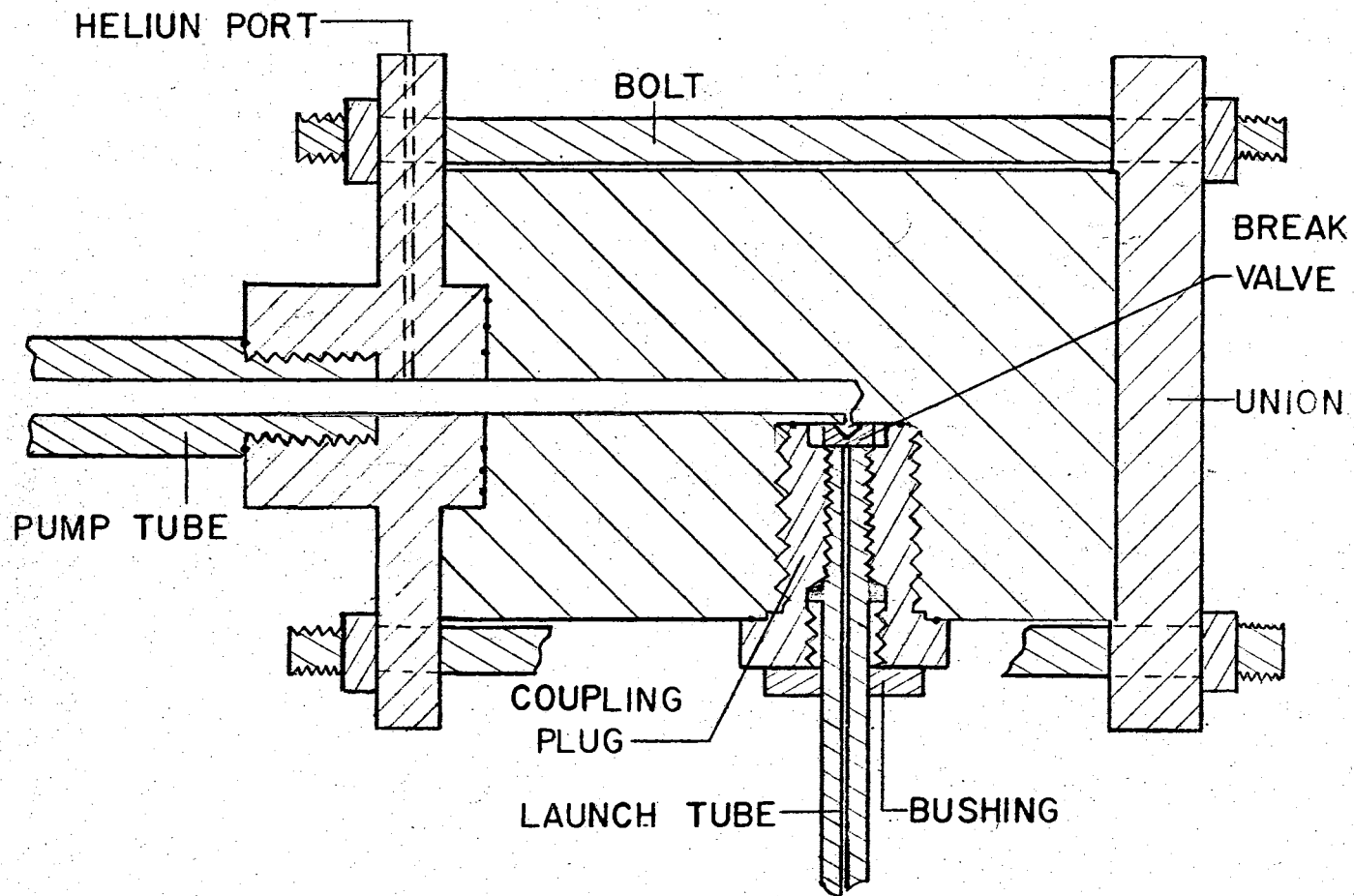The body of the piston is made of 1020 steel. The body diameter
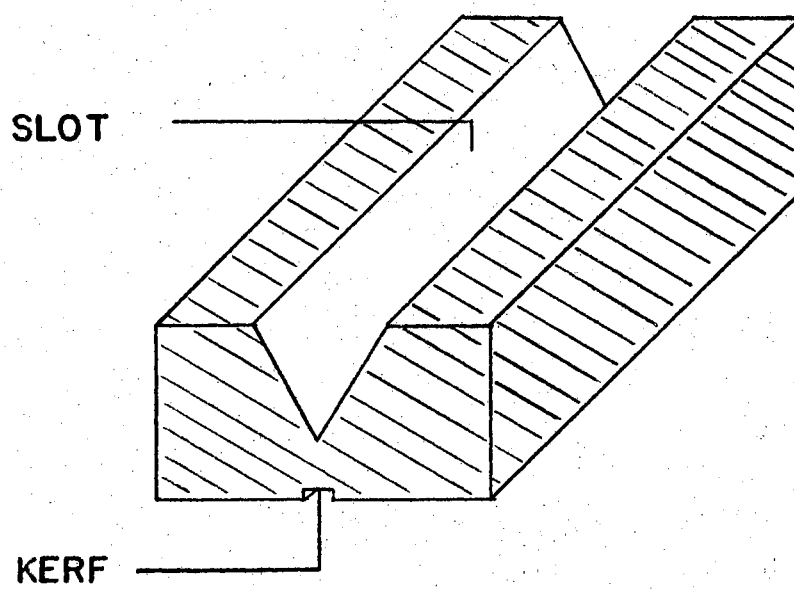
FIGURE 16 · MUZZLE BREECH

FIGURE 17 — BREAK VALVE

is smaller than the bore of the pump tube so there will be no seizure between the piston and the barrel. Two aluminum rings fit the bore tightly and form a gas tight seal which prevents helium from escaping past the piston. These are illustrated in Figure 18. There is very little friction between these rings and the sides of the pump tube. The shear disk is made of brass shim stock. The thickness of this disk is selected so the disk ruptures at a pressure of 2000 pounds per square inch. A teflon head is placed at the front of the piston to serve as a bumper in case the piston accidentally fails to stop its forward motion and rams into the end of the pump tube.

It is impossible to predict the rest position of the piston after its forward motion is stopped, and it "bounces" back toward the breech. In order to retrieve the piston in case it comes to rest in the pump tube, a female receptacle is machined into the rear of the piston. To retrive the piston, a ramrod may be inserted into the pump tube, and engage the piston and remove it.

VACUUM SYSTEM

The vacuum pumping system consists of a 19 cfm mechanical pump in conjunction with a 80 cfm blower and a 6 inch diffusion pump. In order to prevent the high pressure helium in the pump tube from entering the vacuum pumps and causing serious damage to them, a needle valve which is capable of withstanding 10,000 pounds per square inch is placed in the helium port of the muzzle block as illustrated in Figure 16. Since helium will be forced into the pump tube at pressures of 50 to 300 pounds per square inch, a gate valve is placed between the helium tank and the high vacuum valves in order to prevent the
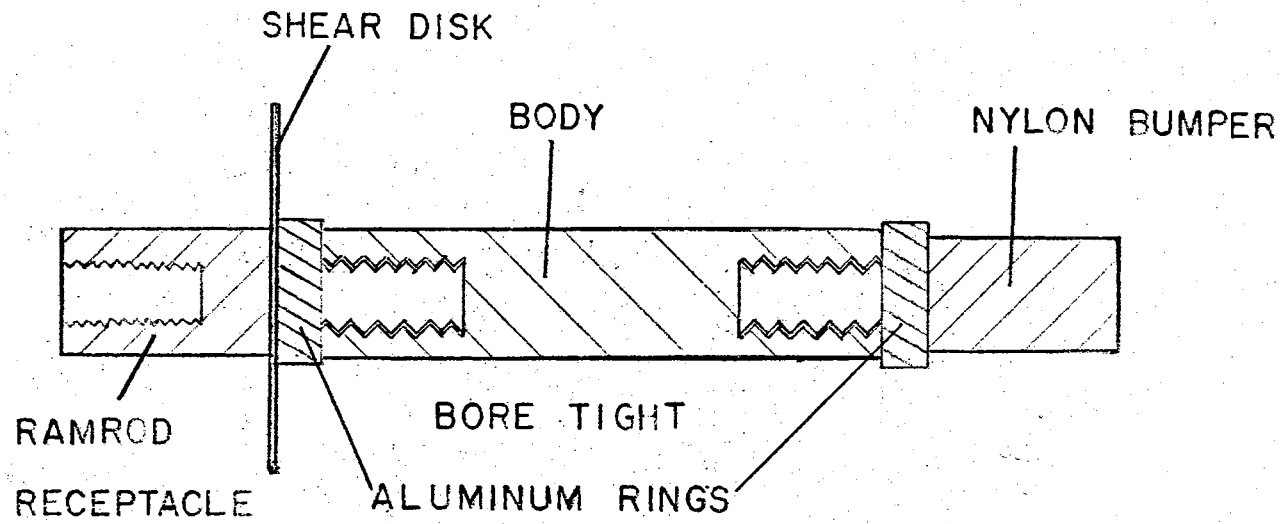
FIGURE 18 - PISTON

possibility of any damage occurring to these valves.

Evacuation of the vacuum chamber, of course, evacuates the launch tube. This prevents a shock wave from forming in front of the projectile and retarding its motion. The air in the pump tube is removed as completely as possible so only helium will be present in the pump tube when the gun is fired.

VELOCITY DETECTION SYSTEM

Various techniques have been employed to measure the velocity of hypervelocity projectiles. Principal among these methods are:

(1) Measuring the Doppler shift in microwaves, or radar waves, that are reflected from the moving projectile.

(2) Force the projectile to rupture two, or more, thin, conducting metal strips which are separated by a known distance and measure the time interval between these events.

(3) Pass the projectile through two, spaced light beams and measure the time interval between these passages.

The optical method was chosen from these possibilities. A framework was attached to the H-beams to hold the optical system. This framework was made quite rigid so that the lenses had no motion relative to each other and could not give a false intensity change on the detector. The detectors were Fairchild 1N3734 photodiodes. The outputs from these diodes are fed into a Hewlett-Packard Model 523 electronic counter. The distance between the two light beams is approximately 10 inches.

CHAPTER VI

OPERATION OF THE GUN

There have been four trial firings of the gun. The results of these tests are summarized in Table IV. From the known masses of the projectile and of the piston, as recorded for firing #1, the break valve should rupture at 30,000 p.s.i. This rupture point may be read from Figure 12. The initial helium pressure in the pump tube and the amount of gunpowder are determined from Figures 11 and 13, respectively, to be 160 p.s.i. and 40 grams. In the numerical calculations that are described in Chapter IV, the greatest uncertainty occurs in the calculation of the amount of gunpowder. For this reason and to test the structural strength of the gun, the amount of gunpowder in the first firing was only 25 grams. The initial, helium pressure in the pump tube was 95 p.s.i. for this amount of powder.

This amount of gunpowder did not generate enough pressure to rupture the piston restraint, so the amount of gunpowder was doubled for the second attempt. The powder and squib were loaded so that they were not in intimate contact; consequently, the gunpowder did not ignite in the second test.

The loading conditions were held constant for the next attempt, and the projectile was successfully launched. The projectile's velocity was not measured because of a failure in the velocity detection system. The framework to support the optical system for

TABLE IV

SUMMARY OF FIRING RESULTS

	m	p	t	n	M	v
Firing No. 1	0.323	95	0.070	25.0	152.4	*
Firing No. 2	0.323	95	0.070	51.4	152.4	**
Firing No. 3	0.323	95	0.070	50.6	152.4	***
Firing No. 4	0.336	275	0.150	75.2	232.7	****

m - mass of projectile in grams

p - initial helium pressure in pump tube in pounds per square inch

t - thickness of break valve in inches

n - number of grams of gunpowder

M - mass of piston in grams

v - measured velocity in feet per second

* - Piston was not released

** - Squib fired, but powder did not ignite

*** - Projectile was launched, but velocity measuring circuit failed

**** - Needle valve was not closed; break valve did not rupture

measuring the projectile velocity was not properly designed. The frame-
work was made of 3/4 inch round steel bar and was fastened to the
vacuum chamber. This support, although fastened as rigidly as possible,
permitted the vibrations of the vacuum chamber to displace the light
beams. The projectile broke the first beam but missed the second one,
so the electronic counter was not turned off. The optical support
system was redesigned and made of 4 inch channel iron and 2 inch angle
iron. The framework is attached to the H-beams which support the
pump tube assembly and is completely independent of the vacuum chamber.
This framework has such a large inertia that vibrations cause no
relative motions among the components of the optical system. The light
beams move in unison, if they move at all.

For these, preliminary test firings, a piece of steel was used as
a target. The crater that was formed in this steel plate by the pro-
jectile is indicated by the photograph in Figure 19. The projectile
was a cylinder of aluminum, 0.2 inches long and 0.2 inches in diameter.
The ring-shaped piece in the photograph is the retaining flange at
the rear of the projectile. This remained at the top of the launch
tube. The 0.2 inch diameter hole in the ring shows where the cy-
lindrical projectile was sheared away from the retaining flange. The
third object in the picture is the largest remnant of the projectile
that was found. A small, cylindrical nose, approximately 1/16 inch
long, was machined on the front of the projectile. The imprint of
this nose may be seen at the bottom of the crater, and the smashed nose
may be seen on the projectile remnant. This imprint implies that the
projectile does not tumble or yaw excessively in its flight. This
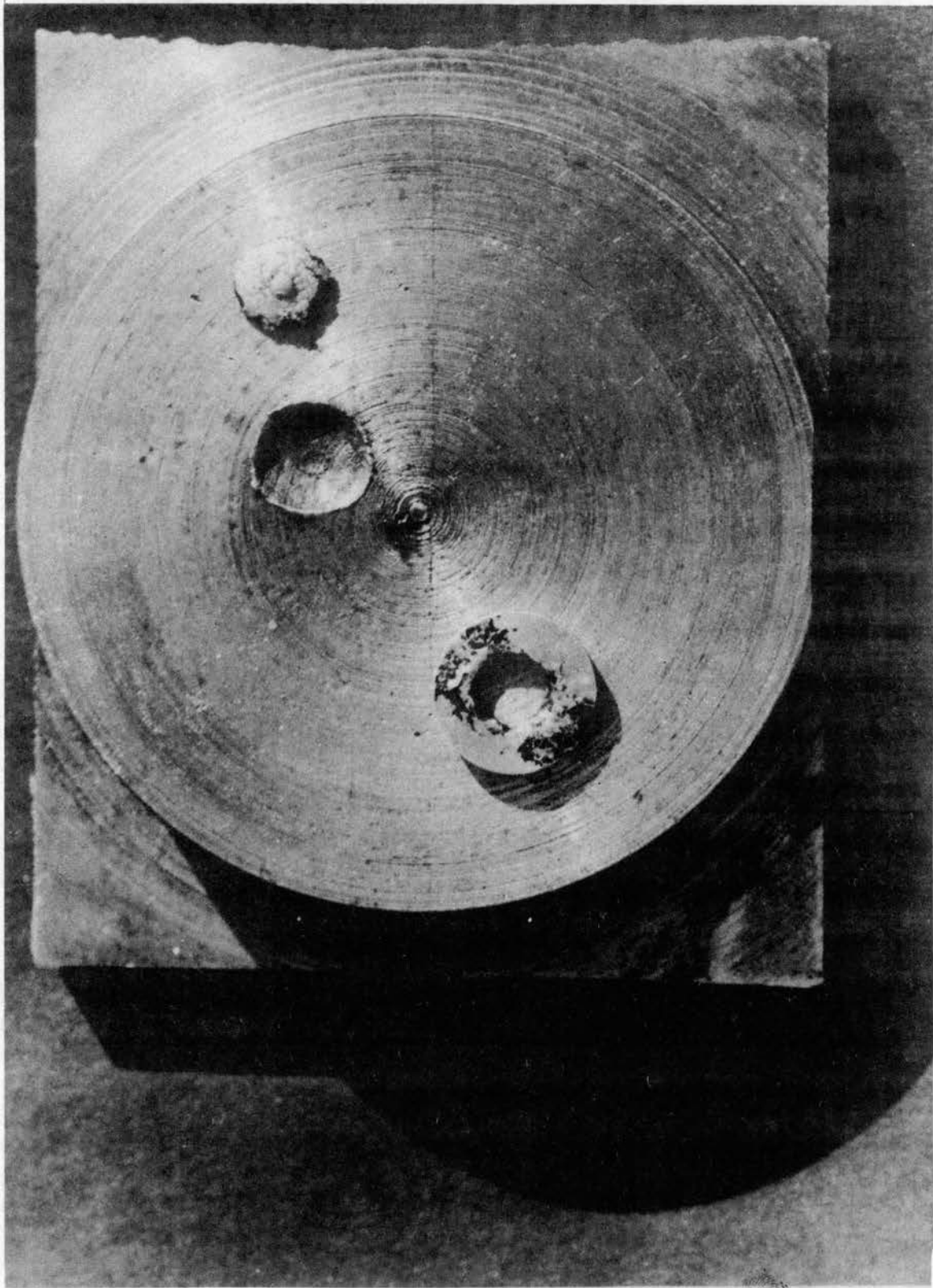knowledge will be invaluable in later work with the gun.

Figure 19.   Crater in Steel Target Plate, Remnant of Projectile,
and Projectile Flange

Although the projectile's velocity was not measured by the detection system, a quantitative estimate of the velocity may be obtained from measuring the crater depth. From their study of penetration parameters, Kinard and Collins (16) have suggested the equation

$$P = \frac{3797 \left(\rho_p V \ell - b \right)}{\left(\rho_p \right)^{0.278} \left(E + 2.8 \times 10^6 \right)^{0.78}}$$

for calculating the penetration depth. In this equation, P is the depth of the crater, 1 is the length of the projectile, E is the modulus of elasticity of the target, ρ_p is the density of the projectile, V is the speed of the impacting projectile, and b is the momentum per unit area which is necessary to cause a permanent deformation of the target. The measured depth of the crater is 0.068 inches, so the calculated velocity of the 0.20 caliber aluminum projectile is 5200 feet per second. The velocity, as estimated from the design charts, was 6000 feet per second.

The third firing revealed a design error in the piston that was corrected for the fourth firing. The two rings that form a boretight seal were originally made of teflon; however, the compressed gas became hot enough to melt the teflon. As a result, the gunpowder gases escaped past the piston and entered the launch tube and vacuum chamber. The heavy gunpowder gases ruined the effect of the light weight helium gas, and the velocity of the projectile would have been greater if this had not occurred. The teflon rings were replaced with the aluminum rings that are indicated in Figure 18.

The steel body of the piston was made longer so the mass of the piston was increased by 80 grams. Study of the design charts indicated

that the original piston mass was too small to attain the high pro-
jectile velocities which are desired. The ramrod receptacle which is
illustrated in Figure 18 was replaced with the boretight piece of alumi-
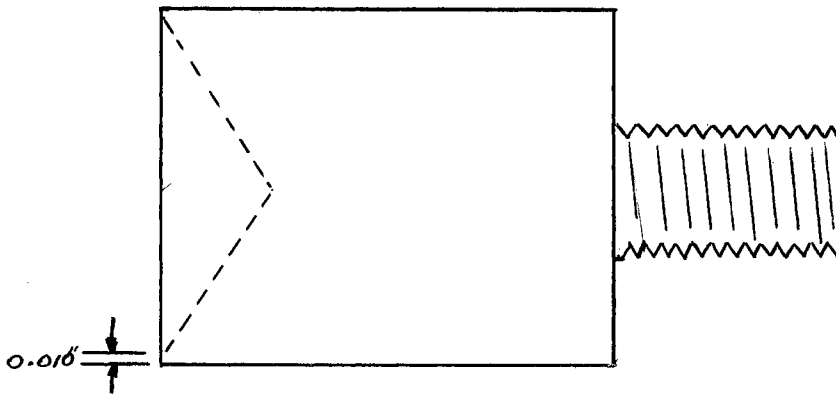num that is sketched below. The rear end of this piece is drilled out

Figure 20. Rear Portion of Piston

so there is a thin edged flange around the circumference. The gun-
powder-gas pressure causes this edge to flare out and to make a more
efficient seal against the barrel.

One more firing was made to test the piston design. The projectile
was not launched because the needle valve, which separates the pump
tube from the helium supply, was left open, but the test was successful
in demonstrating that no gunpowder gases escaped past the piston. The
existence of gunpowder gases in front of the piston is easily verified
by examining the face of the piston and the forward end of the pump
tube for carbon deposits.

These tests were successful since they revealed the features of the gun which were not adequately designed, and permitted them to be corrected. No structural damage to the gun results from the tests and the gun is now considered fully operational. Although the gun is operational, it will not be ready for meaningful experiments until the displacement of the surface of the target may be measured and recorded. This requires a considerable experimental program that includes the use of a c. w. laser to form interference fringes.

PART II

CHAPTER VII

A NUMERICAL SOLUTION FOR THE HYPERVELOCITY

IMPACT OF A THIN PLATE

The gun that is described in the first part of this thesis is to

be employed to collect data on the shock propagation away from a hyper-

velocity impact. Particular attention will be directed toward infor-

mation on the shock-induced formation of fluid and plastic regions in

an aluminum target. This experimental study is to include the movement

of the fluid-plastic and the plastic-elastic interfaces under the effect

of the shock. The propagation of shock waves through these interfaces,

as well as through the fluid, plastic and elastic regions in the target

is the basic study.

The experimental data from the gun can only be understood and

interpreted provided the results from the test firings are compared

with the predictions from an analytic solution for hypervelocity impact.

An analytical solution had just been obtained at the time that the pre-

ceding work in this thesis was completed. After a study of this so-

lution, the requirements for a much more complete solution became evi-

dent. The author of this thesis was more interested in extending and

completing this new solution than in completing the equipment for the

preceding experiments. The equipment that was not completed consisted

of techniques to measure and to follow displacements of the target sur-
face after the hypervelocity impact of the projectile.

There is much evidence that the majority of micrometeoroids are
porous particles of rock, or of an iron alloy (13). It cannot be
assumed that a porous projectile in the barrel of the above described
gun will remain porous up to the time of impact. As a consequence, a
complete solution requires that porous projectiles be included in the
computer solution for a hypervelocity impact. The target is always
taken as solid to simulate the shell of a space vehicle. Porosity must
be introduced into the equation of state that relates the thermodynamic
variables of the materials of the impacting plate, which may be either
porous stone, or porous iron. The second part of this thesis is con-
cerned with the analytical techniques for handling the impact of a thin,
porous plate.

In a complete, general, analytical solution for a hypervelocity
impact, a projectile of porous stone, or iron, is assumed to impact on
solid aluminum. The solution must show the inviscid flow of both
materials and it must record the position of the interface between these
materials at all times during the flow. Since the treatment of radial
shocks and of shocks from the hypervelocity impact of a sphere are
familiar to the group at Oklahoma State University, a simpler problem
could be employed as an introduction to a study of the effect of po-
rosity. The work on this second part of this thesis is concentrated on
a computer solution for a hypervelocity impact in one dimension. This
is accomplished by assuming that the target is semi-infinite (fills
half of all space) and the impacting body is a thin plate with infinite
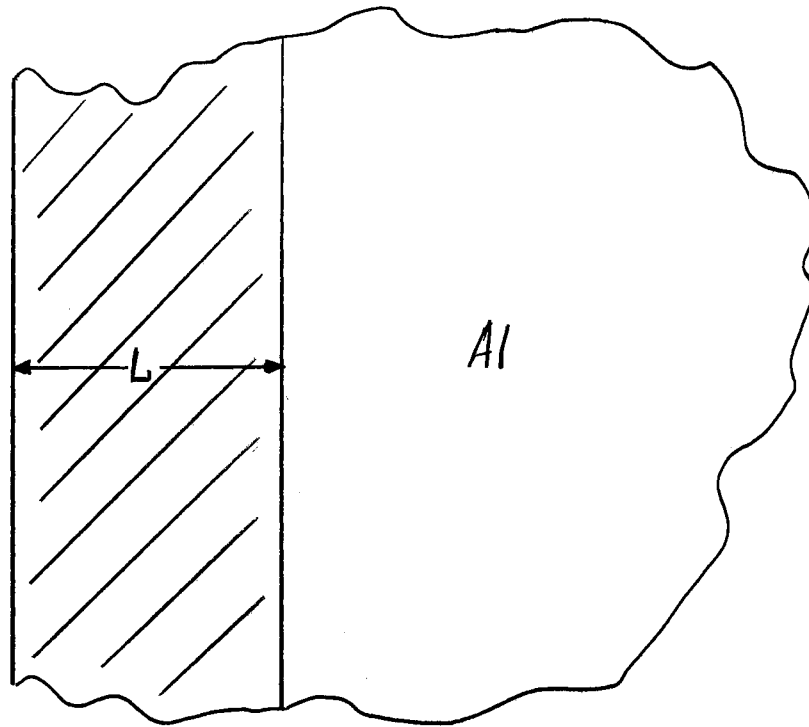extent in the two lateral directions. The plate is assumed to have just

Figure 21. Thin Infinite Plate Impacting on a Semi-
Infinite Aluminum Target

touched the target at time, t = 0. The physical situation at this instant of time is illustrated in Figure 21.

HYDRODYNAMIC EQUATIONS

The pressures from a hypervelocity impact are of the order of several megabars. At such pressures, metals behave as fluids, and their yield strengths and elastic limits may be ignored. A numerical solution of a hypervelocity impact problem is basically the solution of the hydrodynamic flow equations for inviscid flow with proper boundary conditions.

The equations of hydrodynamic flow will not be derived since excellent derivations may be found in many books. In their vector form, the equations are:

the conservation of mass

$$1) \quad \frac{\partial \rho}{\partial t} = -\vec{\nabla} \cdot (\rho \vec{V})$$

the conservation of momentum

$$2) \quad \rho \frac{d\vec{V}}{dt} = -\vec{\nabla} p$$

the conservation of energy

$$3) \quad \rho \frac{dE}{dt} = -\vec{\nabla} \cdot (p \vec{V})$$

In these equations, ρ is the density, $\vec{V}$ is material velocity vector, E is the total specific energy, t is the time, and $\vec{\nabla}$ is the space operator, $\vec{i} \frac{\partial}{\partial x} + \vec{j} \frac{\partial}{\partial y} + \vec{k} \frac{\partial}{\partial z}$.

In the simplified, semi-infinite plate impact problem, these equations take simple forms because the problem is one-dimensional. The

equations may be written:

the conservation of mass

4) $\dfrac{\partial \rho}{\partial t} = -\dfrac{\partial}{\partial x}(\rho u)$

the conservation of momentum

5) $\rho \dfrac{du}{dt} = -\dfrac{\partial p}{\partial x}$

the conservation of energy

6) $\rho \dfrac{dE}{dt} = -\dfrac{\partial}{\partial x}(p u)$

EQUATIONS OF STATE

An analytical solution for the propagation of a shock requires five equations and conditions. There are the three conservation equations that are given the the preceding section, an equation of state is the fourth relation and the condition that the entropy must increase across the shock front is the fifth. It is customary to combine the increase in entropy at the shock front with an equation of state into one equation. At the shock front, the Rankine-Hugoniot jump conditions include the increase in entropy and these may be combined into several equations of state. With this combination, four equations are obtained and they are sufficient to permit a solution for the four variables in the equations: P, U, E and D.

Two forms of the equation of state were used in the solution in this thesis. One form was suggested by Tillotson (29), and it is given

by

$$7) \quad P = \left(0.5 + \frac{C}{\frac{E}{E_o \eta^2} + 1} \right) E\rho + A\mu + B\mu^2$$

In this equation, P is the pressure, E is the specific internal energy, ρ is the density, η is the ratio ρ/ρ_o where ρ_o is the normal density, μ is the quantity $(\eta - 1)$, and A, B, C and E_o are constants. For aluminum, the values of the constants are A = 0.752 megabars, B = 0.65 megabars, C = 1.63 and E_o = 0.65 megabars cm^3/gm. For iron, the values of the constants are A = 1.279 megabars, B = 1.05 megabars, C = 1.5 and E_o = 0.095 megabars cm^3/gm. This equation is a best-fit extrapolation between the Thomas-Fermi-Dirac data at high pressures and experimental data at low pressures.

The second equation of state was developed in tabular form from analytical expressions first proposed in recent Soviet literature and modified and extended by McClosky (2), (3), (19), (22). A detailed description will not be given since it would be quite lengthy. Mc-Closky's paper gives a very adequate presentation of the mathematics and reasoning behind the development of the equations (22).

For this second equation of state, it is assumed that the pressure and specific internal energy may be represented as to the superposition of three effects.

$$8) \quad P(\eta, T) = P_c(\eta) + P_N(\eta, T) + P_e(\eta, T)$$

$$9) \quad E(\eta, T) = E_c(\eta) + E_N(\eta, T) + E_e(\eta, T)$$

In these equations, P is the pressure, E is the specific internal energy, η is the ratio ρ/ρ_0 where ρ is the density, and ρ_0 is the density at normal temperature and pressure, and T is the temperature.

The subscript c denotes the contribution due to "cold" compression; i.e., the effect of atomic lattice infractions at zero degrees Kelvin. The subscript N indicates the contribution of the thermal vibrations of the lattice ions; and the subscript e indicates the thermal excitation of the electrons.

These equations were developed by McClosky so the only input data to evaluate $P(\eta, T)$ and $E(\eta, T)$ in a computer code are: atomic number, atomic weight, density at normal conditions, Debye temperature, co-efficient of electronic specific heat, Gruneisen coefficient, and bulk modulus. The latter three quantities are for the material at zero absolute temperature and pressure; corresponding values at normal conditions can be estimated. A computer program was coded so the values of $P(\eta, T)$ and $E(\eta, T)$ were calculated over the range

$$\eta = exp(-3.0 + 0.1k) \qquad k = 1, 2, 3 \cdots 54$$

$$T = exp(5.3 + 0.2k) \qquad k = 1, 2, 3, \cdots 51$$

or

$$1/20 \leq \eta \leq 11$$

$$200 \leq T \leq 5.4 \times 10^{6} \, °K$$

These values were punched out as a table, and this table was then read in as input data for the impact program. The impact program

calculates η and E, and then P can be found by interpolation in the table.

DISSIPATIVE MECHANISM

Shock surfaces appear in the differential equations of hydrodynamics as regions where the density, energy, pressure, and flow velocity are discontinuous. In order to solve a problem which involves shock wave motion on a computer, it is necessary to change the shock front from an abrupt jump-discontinuity to a front having a finite width with large, but continuous, gradients for all of the flow variables. von Neuman and Richtmyer (31) proposed a method which forms desired shock front. Their method is based on the introduction of a viscous, or dissipative term, q, which is added to the pressure, p. Since the q term is artificially introduced to produce a desired mathematical effect, it is possible for it to be a function of any of the flow variables in the calculations as long as it is subject to the following three requirements which were set by von Neuman and Richtmyer:

(1) The three conservation equations must have solutions without discontinuities.

(2) The width of the shock front must be slightly less in magnitude than the finite difference mesh zoning.

(3) The effect of the q term must be negligible outside of the shock front.

These requirements on the q term can be satisfied by making q dependent upon the gradient of a variable. The expression chosen for q is based on the form given by Kolsky (18) and Landshoff (21) and

is

$$10) \quad q = - A_1^2 \, div \, \vec{V} \left(|div \, \vec{V}| + A_2 \right)$$

Here A_1 and A_2 are constants and $\vec{V}$ is the material flow velocity vector. In the one-dimensional, impact problem, this equation simplifies to

$$11) \quad q = - A_1^2 \frac{\partial u}{\partial x} \left(|\frac{\partial u}{\partial x}| + A_2 \right)$$

Everywhere that p appears in the conservation equations, it is replaced by the sum $(p + q)$, so the conservation equations become

$$12) \quad \frac{\partial \rho}{\partial t} = - \frac{\partial}{\partial x} (\rho u)$$

$$13) \quad \frac{du}{dt} = - \frac{\partial (p + q)}{\partial x}$$

$$14) \quad \rho \frac{dE}{dt} = - \frac{\partial [(p + q) u]}{\partial x}$$

CONVERSION TO FINITE DIFFERENCE EQUATIONS

For numerical solutions, the flow equations must be changed to finite difference equations. In Appendix B, it is shown that the flow equations may be written in the following forms.

conservation of mass

$$15) \quad \frac{\partial \rho}{\partial t} = - \frac{\partial}{\partial x} (\rho u)$$

conservation of momentum

$$16) \quad \frac{\partial}{\partial t} (\rho u) = - \frac{\partial p}{\partial x} - \frac{\partial}{\partial x} (\rho u^2)$$

conservation of energy

$$17) \quad \frac{\partial}{\partial t}(\rho E) = -\frac{\partial}{\partial x}(\rho u) - \frac{\partial}{\partial x}(\rho u E)$$

These equations may be easily converted to difference equations. In Appendix B, it is shown that the appropriate difference equations are:

$$18) \quad CD(L) = D(L) + \frac{DT}{DX}(D1 * U1 - D2 * U2)$$

$$19) \quad CD(L) * CU(L) = D(L) * U(L) + \frac{DT}{DX}(D1 * U1 * U1 - D2 * U2 * U2)$$

$$20) \quad CD(L) * CE(L) = D(L) * E(L) + \frac{DT}{DX}(P1 * U1 - P2 * U2 + D1 * U1 * E1 - D2 * U2 * E2)$$

In Appendix B, it is also shown that the dissipative equation is

$$21) \quad Q(L) = -A_1^2 \left(\frac{U2 - U1}{DX}\right) * \left(\left|\frac{U2 - U1}{DX}\right| + A_2\right)$$

In these equations, D is the density, U is the flow velocity, E is the total specific energy, P is the pressure, and Q is the dissipative term. $D(L)$, $E(L)$, and $U(L)$ are the values of D, E, and U at the center of cell L at time t; $CD(L)$, $CU(L)$, and $CE(L)$ are the values of D, U, and E at the center of cell L at time $t + \Delta t$. DX is the width of the cells, DT is the value of the time step Δt, D1, U1, E1, P1, and Q1 are the values of D, U, E, P, and Q at side L-½ of cell L, and D2, U2, E2, P2, and Q2 are the values of D, U, E, P, and Q at side L+½ of cell L. The finite difference cells are shown in Figure 22.
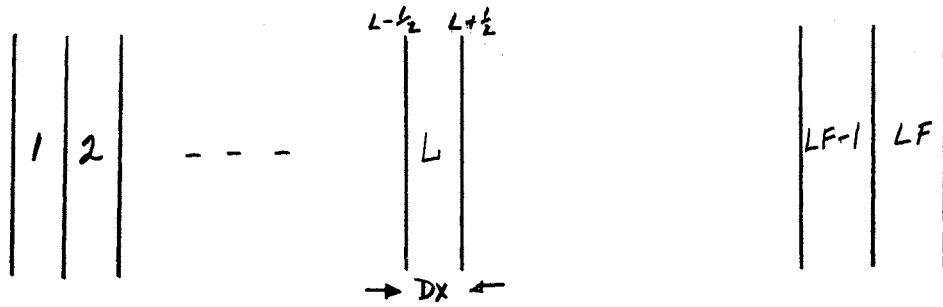
Figure 22. Finite Difference Cells

A step of major importance in obtaining a solution to these differ-
ence equations is the determination of the difference method to use to
evaluate the quantities D1, U1, . . . , D2, U2, . . . at the cell sides.
A good survey of appropriate differencing techniques is given by
Sodek (26). The difference equations suggested by Sodek and used in
this thesis are of three types:

$$\text{Type I} - X(L+\tfrac{1}{2}) = \tfrac{1}{2}(X(L) + X(L+1))$$

$$X(L-\tfrac{1}{2}) = \tfrac{1}{2}(X(L-1) + X(L))$$

Type II - $X(L+\tfrac{1}{2})$ = $X(L)$		$V > 0$
= 0		$V = 0$
= $-X(L+1)$		$V < 0$
$X(L-\tfrac{1}{2})$ = $X(L-1)$		$V > 0$
= 0		$V = 0$
= $X(L)$		$V < 0$

Type III - $X(L+\frac{1}{2}) = \frac{3}{4}X(L) + \frac{3}{8}X(L+1) - \frac{1}{8}X(L-1)$ $V > 0$

$= 0$ $V = 0$

$= \frac{3}{4}X(L+1) + \frac{3}{8}X(L) - \frac{1}{8}X(L+2)$ $V < 0$

$X(L-\frac{1}{2}) = \frac{3}{4}X(L-1) + \frac{3}{8}X(L) - \frac{1}{8}X(L-2)$ $V > 0$

$= 0$ $V = 0$

$= \frac{3}{4}X(L) + \frac{3}{8}X(L-1) - \frac{1}{8}X(L+1)$ $V < 0$

V is a test flow velocity which is given by

$$V = U(L) + U(L+1)$$

The methods used to evaluate the various cell side quantities are tabulated below:

D1 - Type III

U1 - Type III

D2 - Type III

U2 - Type III

E1 - Type II

E2 - Type II

P1 - Type I

P2 - Type I

Q1 - Type I

Q2 - Type I

INITIAL CONDITIONS

The initial conditions in the problem are:

1. A plate of thickness, X, and extending infinite distances
   in the lateral directions has just touched a semi-infinite
   piece of aluminum as shown in Figure 21.

2. The internal energy, pressure, and flow velocity of the alumi-

    num are all zero, and the aluminum density is normal.

3. The internal pressure in the plate is zero, and the plate

    has a porosity, n. The porosity, n, is defined as the ratio

    ρ_0/ρ_{oo} where ρ_0 is the density of a normal plate, and

    ρ_{oo} is the averaged density of the porous plate. Thus n=1

    if $\rho_0 = \rho_{oo}$ and n > 1 if $\rho_{oo} < \rho_0$.

4. The plate is moving toward the aluminum with a velocity of

    36 kilometers per second, 15.2 kilometers per second, or 60.6

    kilometers per second.
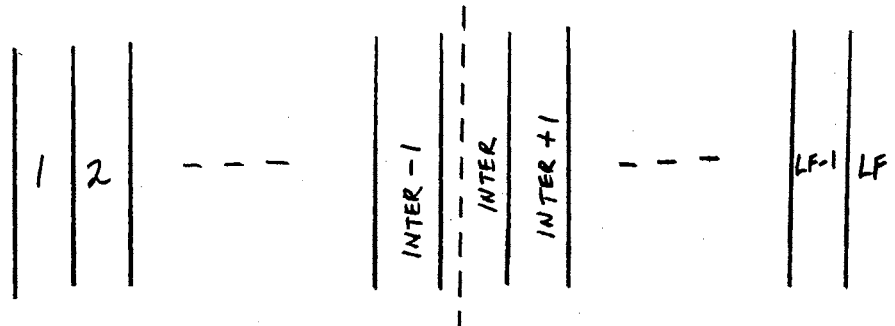
Figure 23.   Finite Difference Cells Representing Impact
of Figure 21

The physical situation which will satisfy these initial conditions

is shown in Figure 21, and the finite difference mesh is shown in

Figure 23. The interface between the iron and the aluminum is indi-

cated by the vertical dashed line in the cell which is labeled, INTER.

The initial density, velocity, internal energy and pressure of the iron

plate are placed in cells 1 to INTER-1, and the initial density values

of the aluminum are placed in cells INTER+1 to LF. The values placed

in cell INTER are weighted averages of the iron and aluminum values.

The steps in solving the hydrodynamic flow equations are:

1. The values of all the variables at time, t = 0, are read in as input data and placed in the appropriate cells of the finite difference mesh.

2. The values of the variables at each cell side are calculated by either Type I, Type II, or Type III differencing.

3. Equations 10, 11, and 12 are solved in each cell for the density, flow velocity, and total energy at the time $t + \Delta t$.

4. The specific internal energy in each cell is calculated from

$$EIN(L) = CE(L) - 0.5 * CU(L) * CU(L)$$

5. The pressure in each cell at time, $t + \Delta t$, is found from CD(L) and EIN(L) either by using equation 7 or interpolating in the pressure tables which are input data.

6. The artificial dissipation is calculated from equation 13.

7. The variables are "stepped" in time; i.e., the array D(L) is replaced by CD(L), the array U(L) by CU(L), and E(L) by CE(L).

8. The time is increased by an increment Δt.

9. Steps 2 through 8 are repeated as often as necessary to advance the solutions to time t_{final}.

CHAPTER VIII

NUMERICAL SOLUTIONS

Numerical solutions of the plate impact problem were obtained for impact velocities of 15.2, 36.0, and 60.6 kilometers per second. Each impact velocity was solved for different values of porosity of the impacting plate. The selected values of plate porosity were 1.0, 1.33, 2.0, and 4.0. These solutions were obtained for a porous iron plate for which the Tillotson equation of state was used, and the solutions were repeated for a porous stone plate by using the tabular equation of state. The solutions for porous iron are shown in graphical form in Figures 24 to 71, and the solutions for porous stone are shown in Figures 72 to 107.

In these figures, the abcissa represents the X dimension of the target and impacting plate. The vertical dashed line in cell 100 represents the position of the interface between the plate and the aluminum target at time, $t = 0$. The three shorter vertical dashed lines represent the position of this interface at the indicated time for each profile. The plate, either iron or stone, is always to the left of the interface, and the aluminum target is to the right. An arrow is shown in some profiles. This arrow indicates the position of the rear surface of the impacting plate. When the arrow is now shown, the rear surface is too far to the left of the interface to be shown on the graph. At time $t = 0$ the near surface of the plate is in cell 4.

78
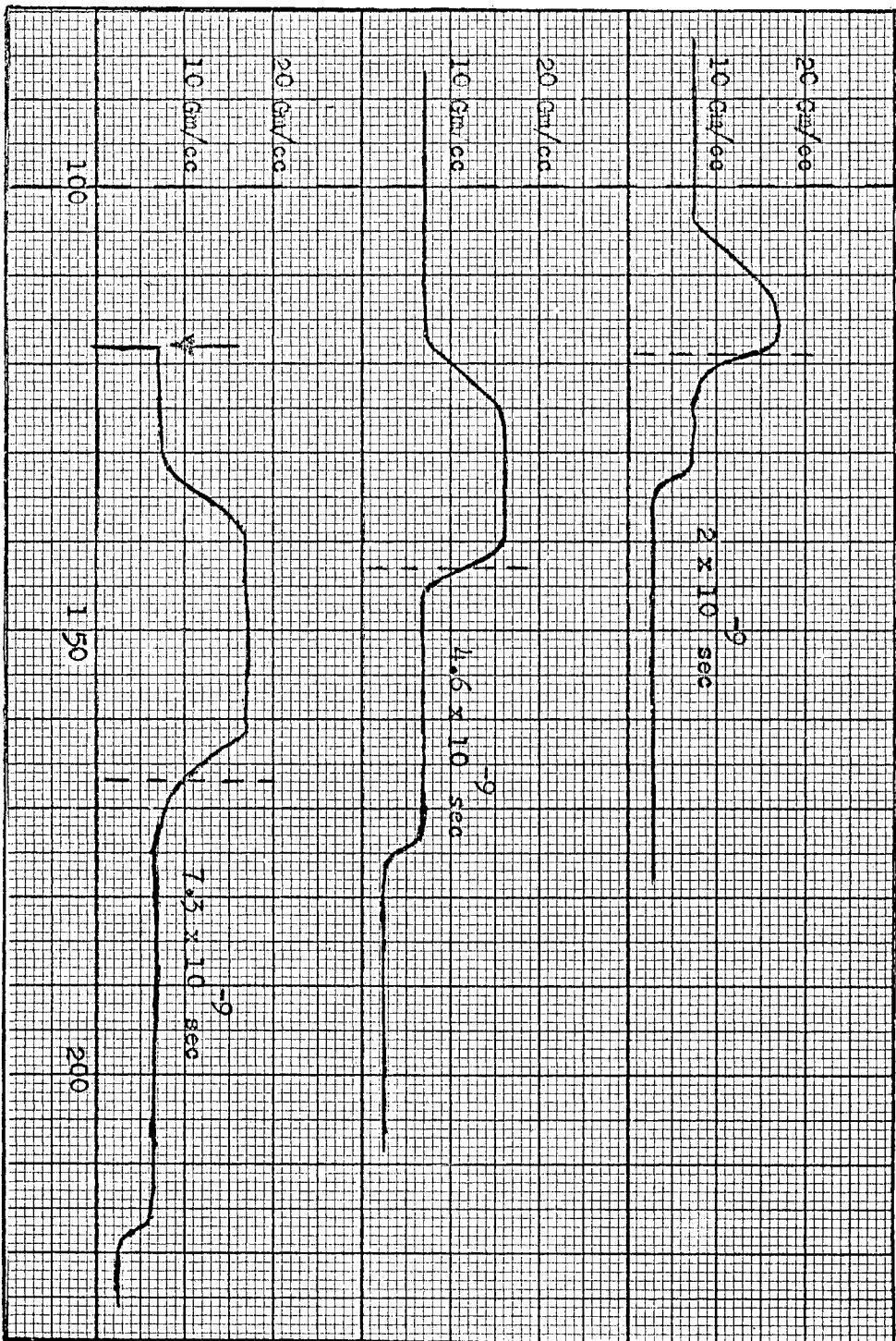
Figure 24. Density Profiles Resulting from Impact of Iron Plate of Porosity 1 Traveling at 15.2 Km/sec
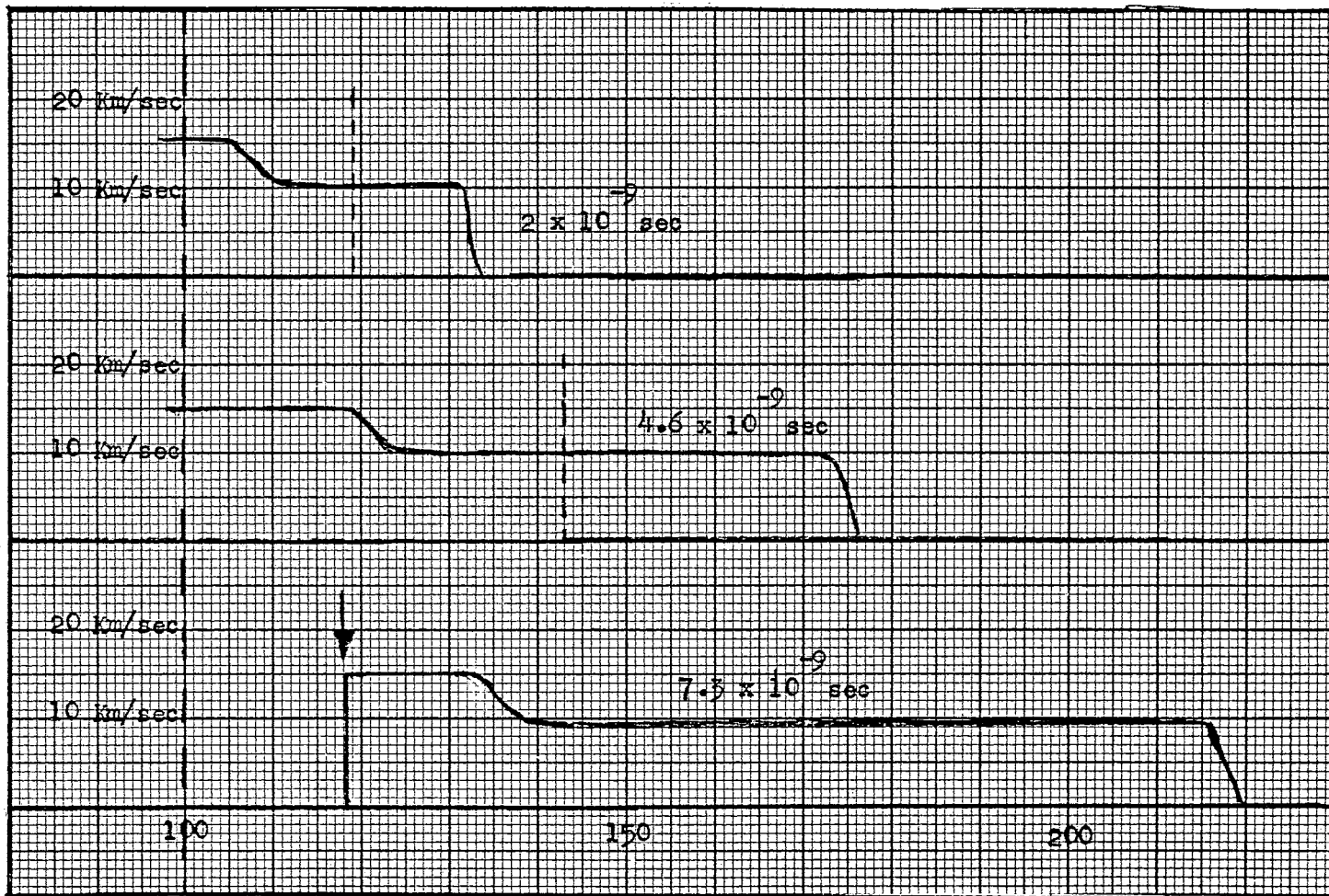
Figure 25. Velocity Profiles Resulting from Impact of Iron Plate of
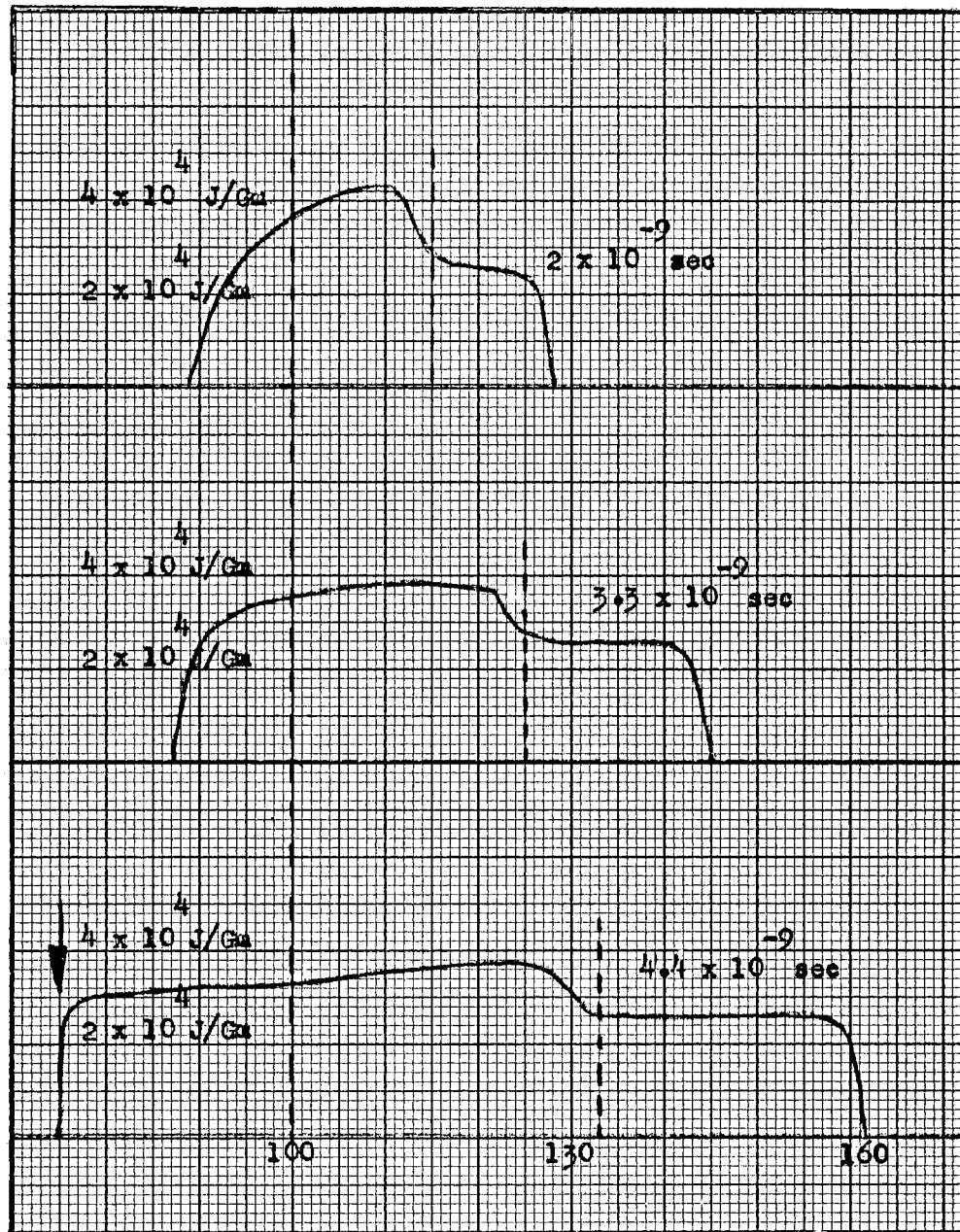Porosity 1 Traveling at 15.2 Km/sec
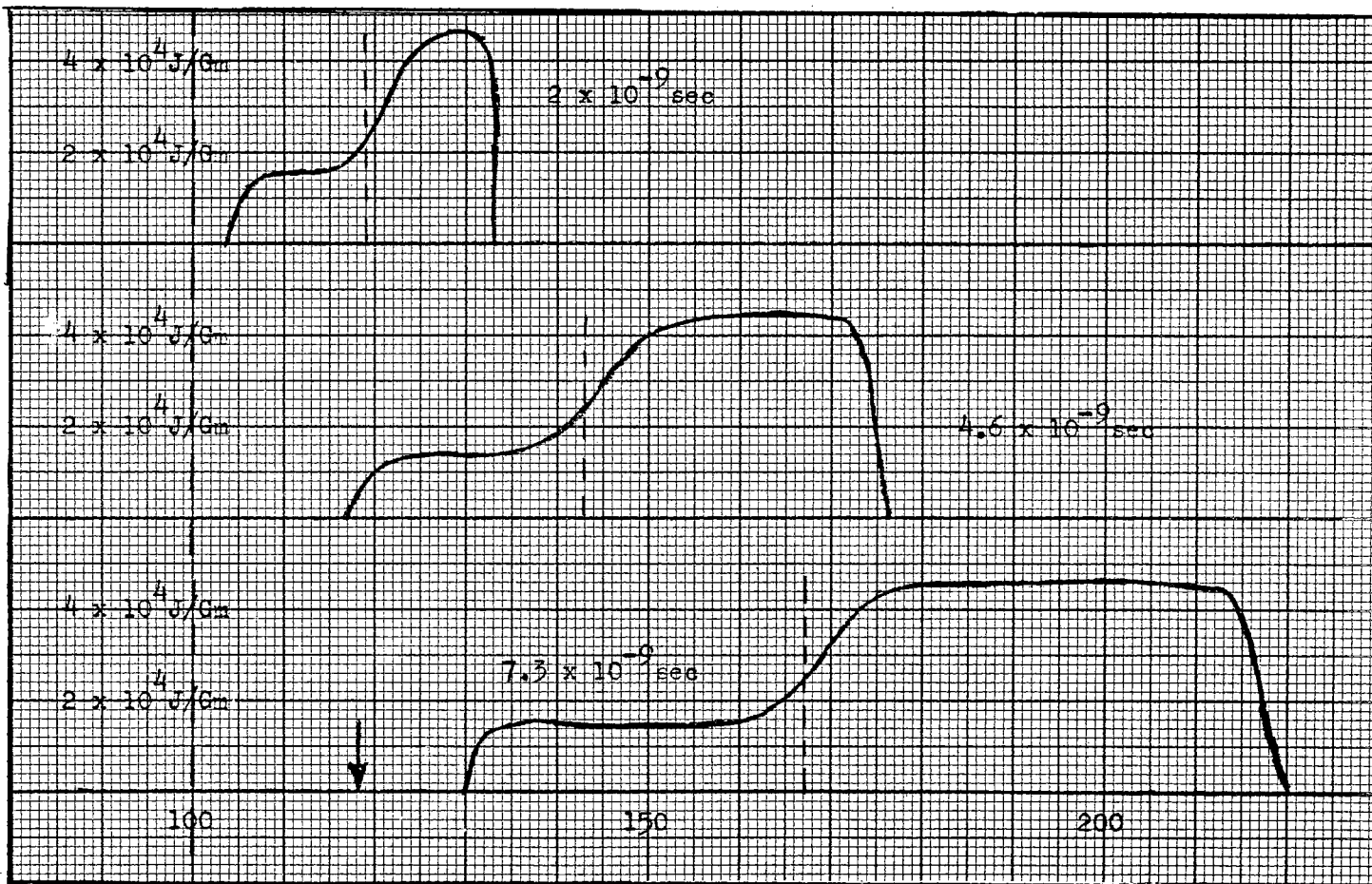
Figure 26. Internal Energy Profiles Resulting from Impact of Iron
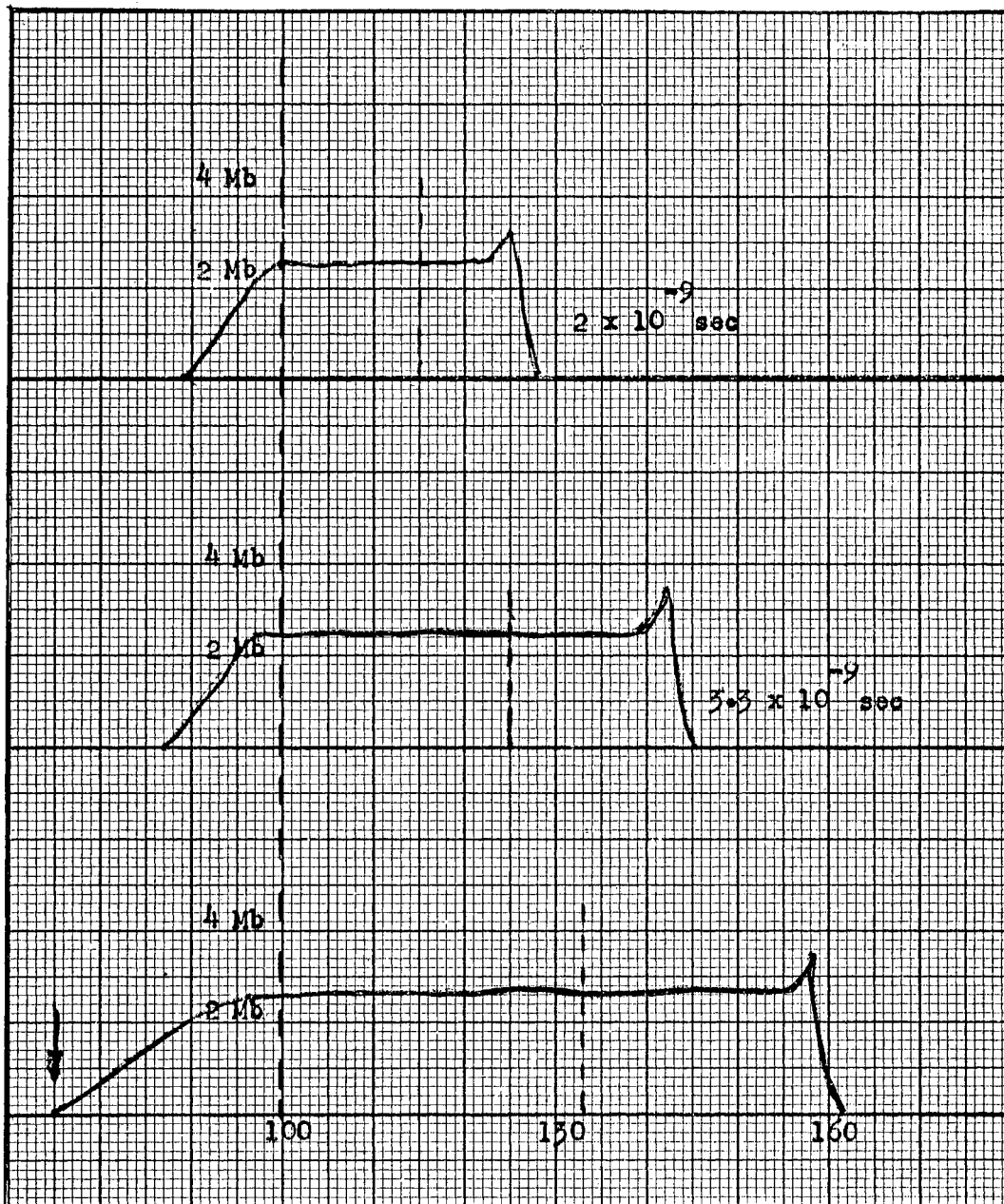Plate of Porosity 1 Traveling at 15.2 Km/sec
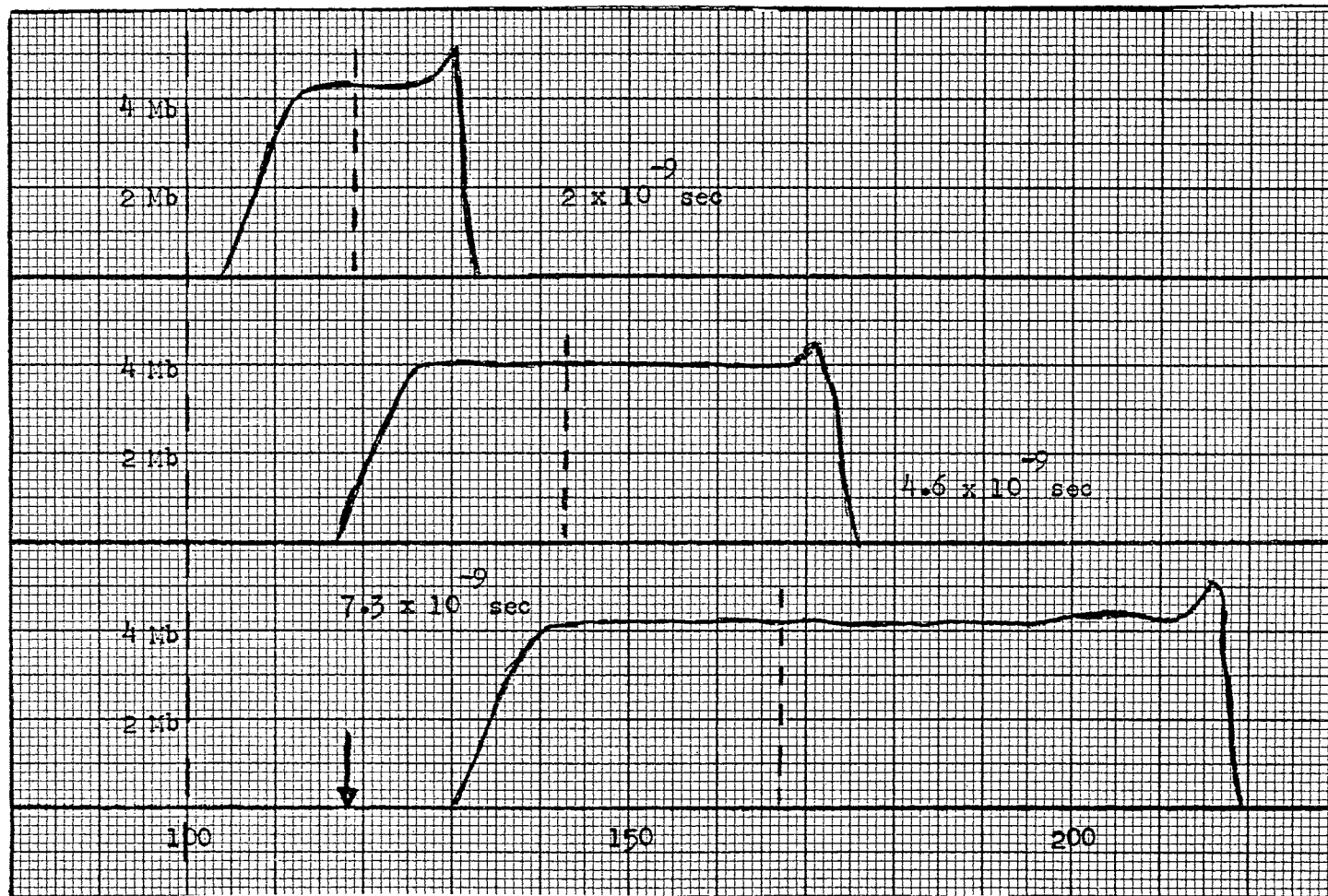
Figure 27.   Pressure Profiles Resulting from Impact of Iron Plate of
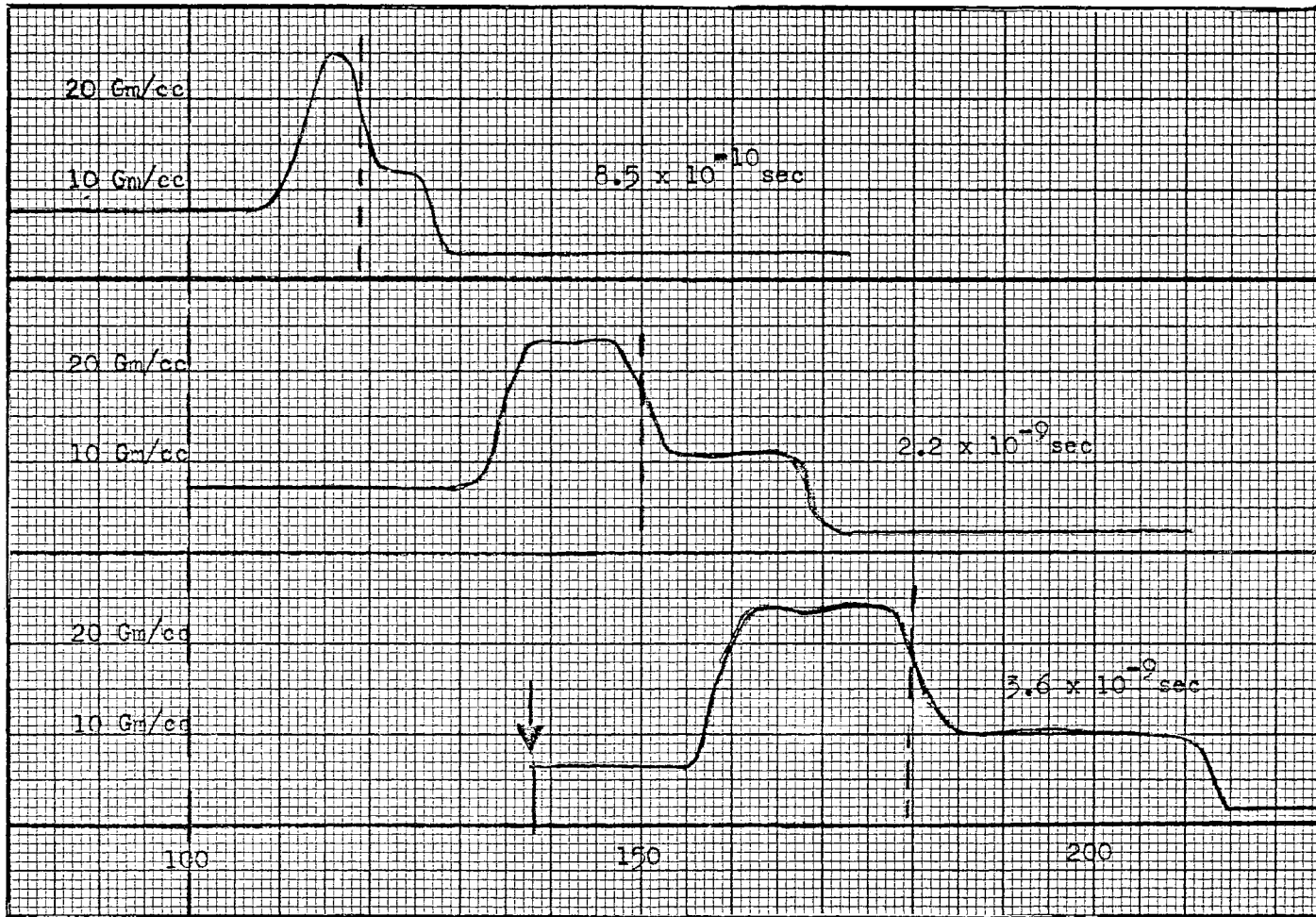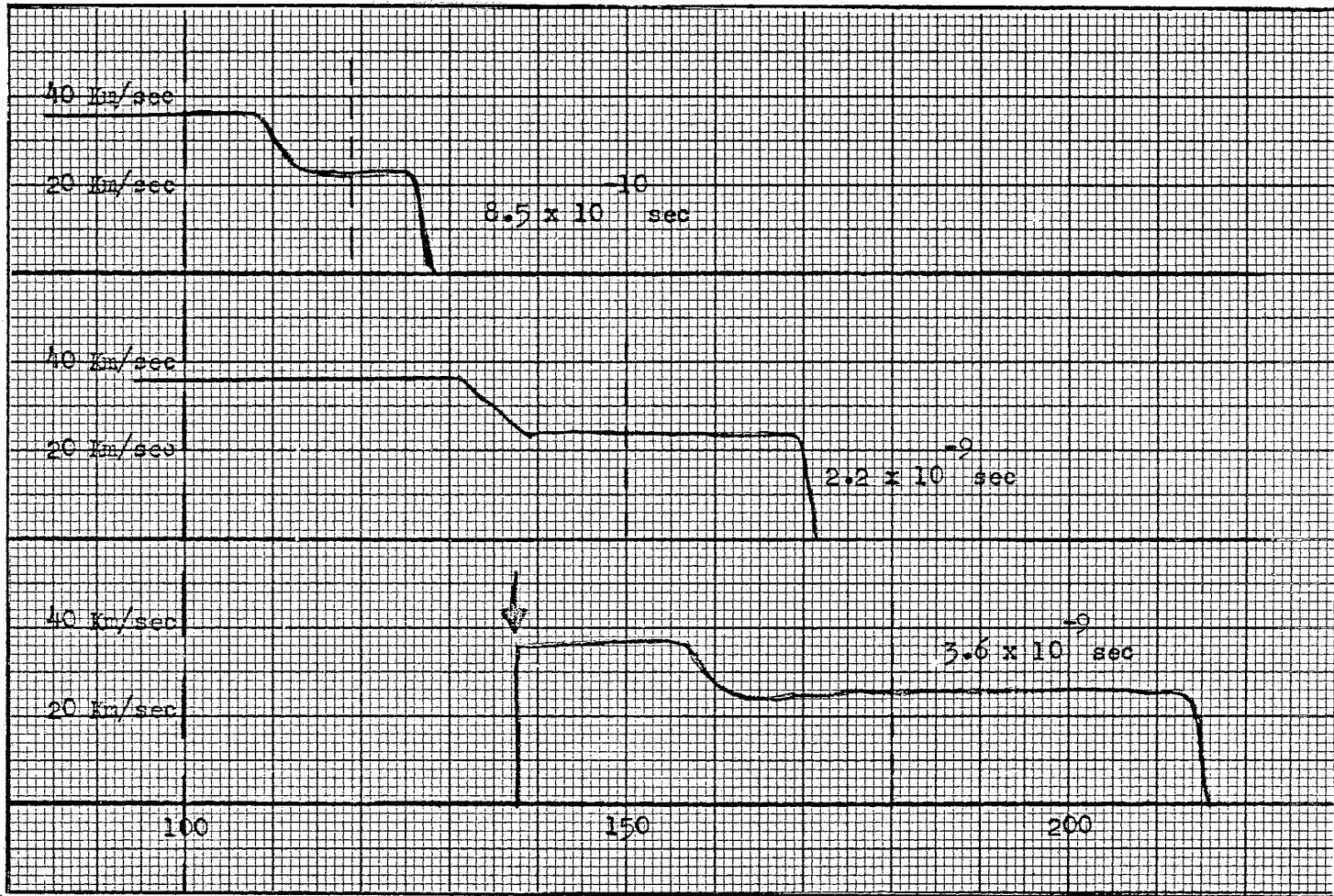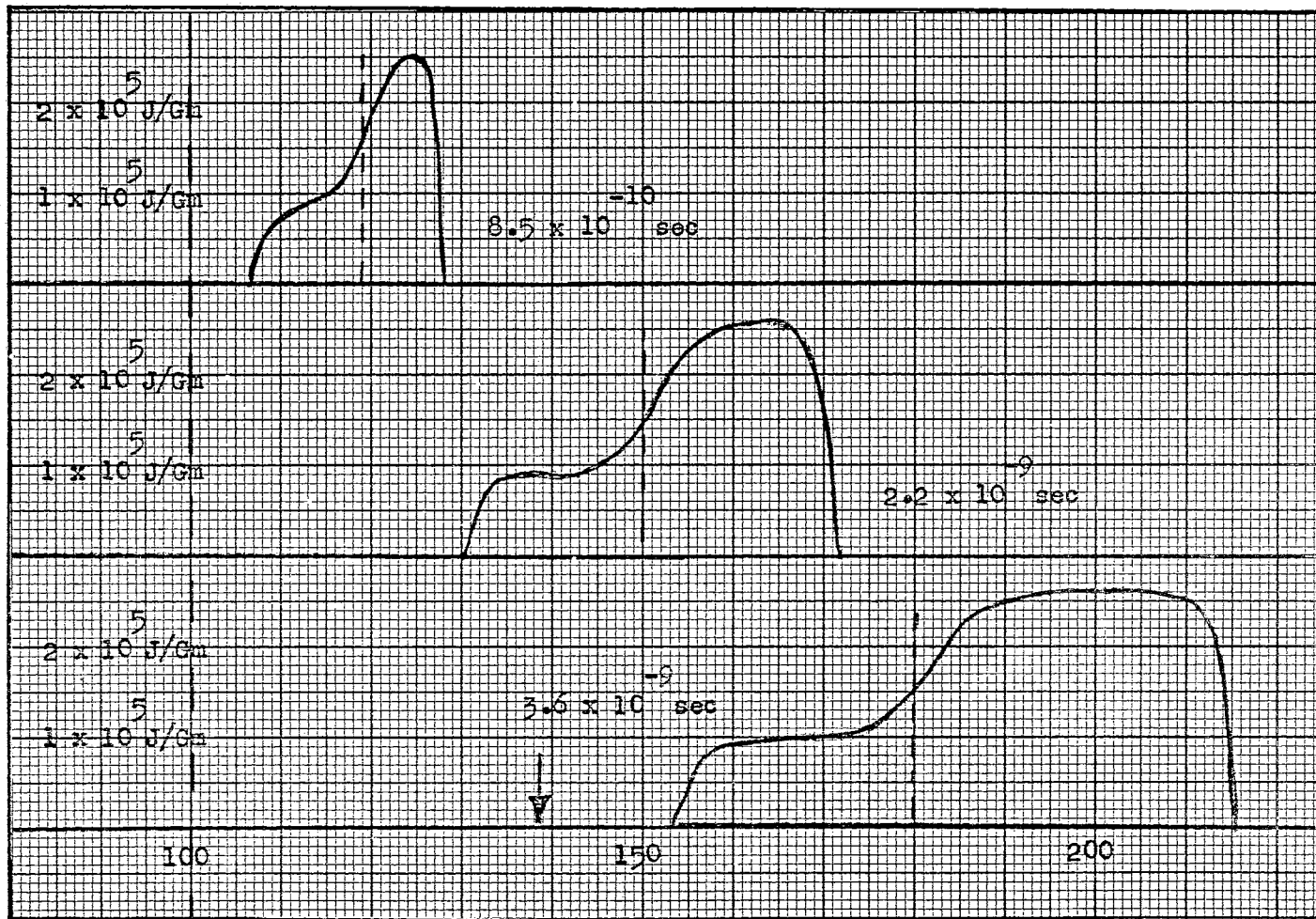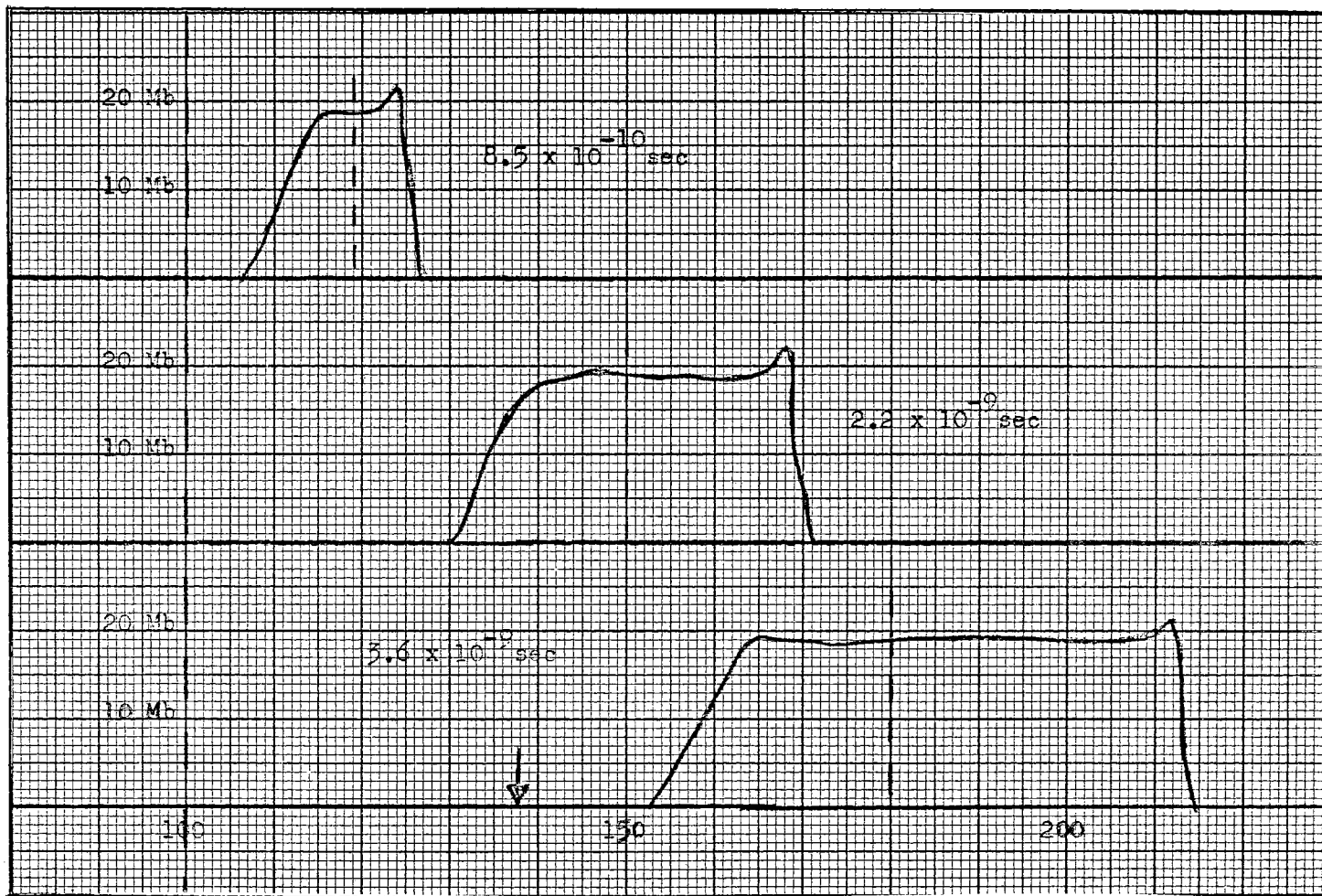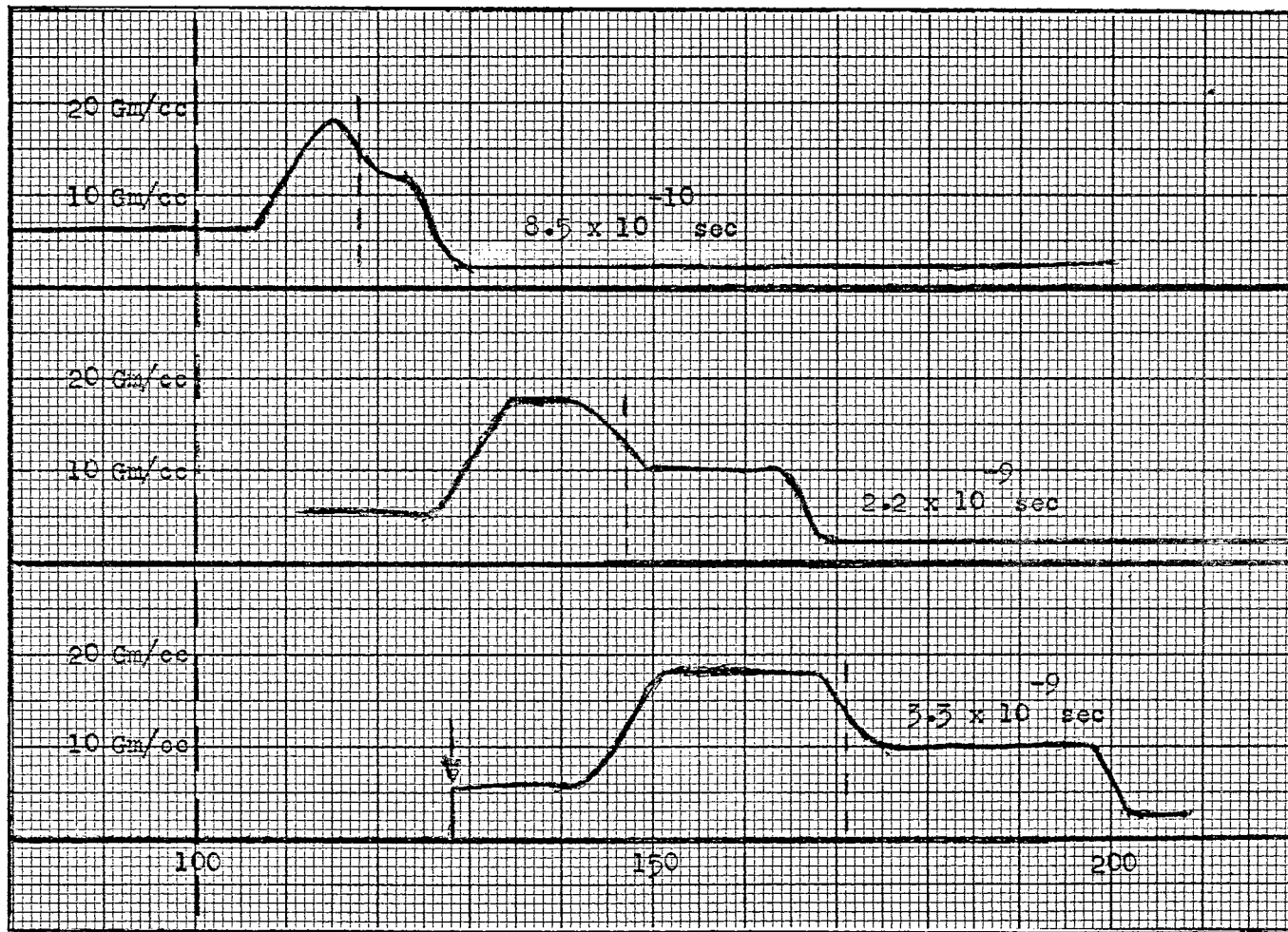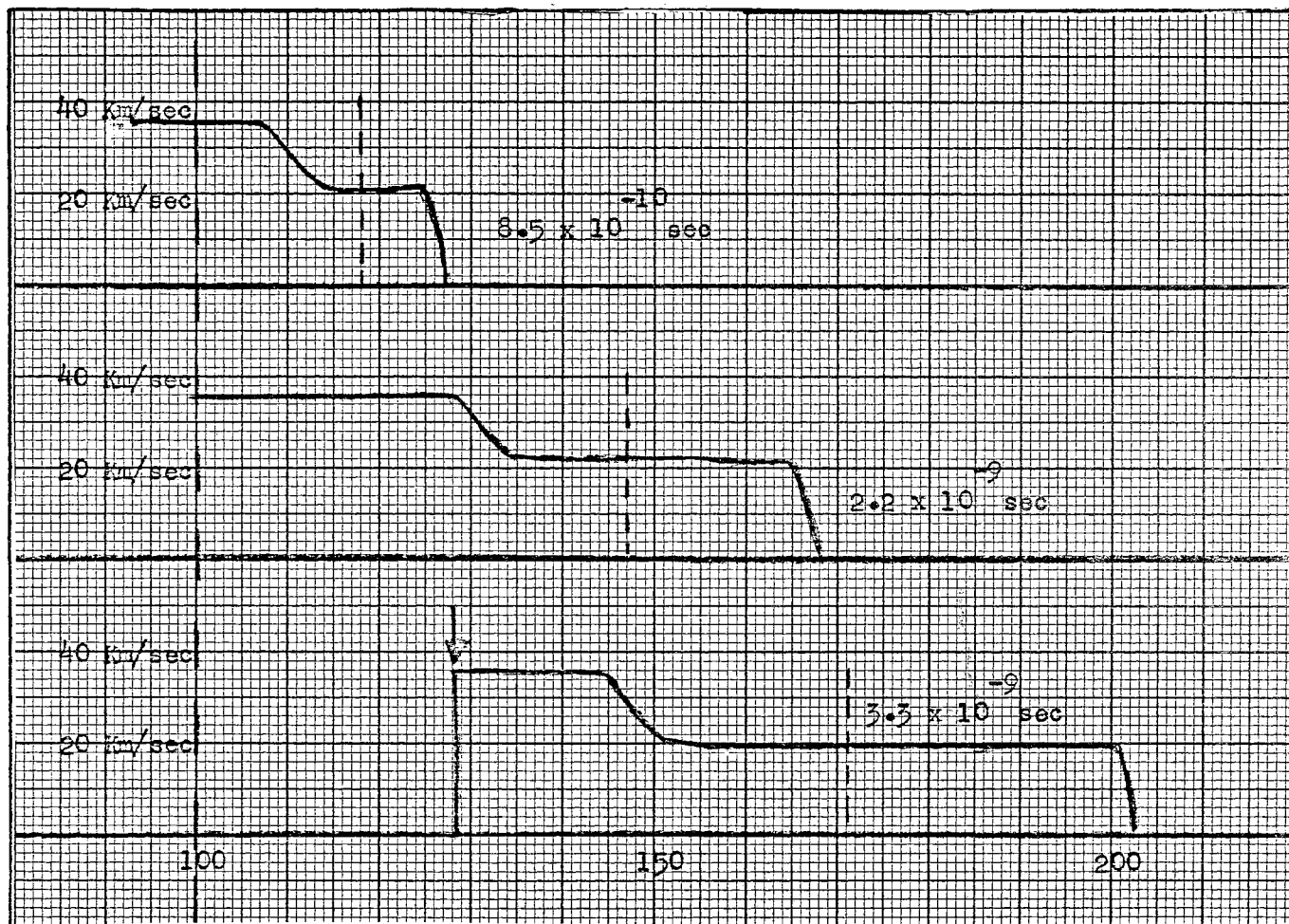Porosity 1 Traveling at 15.2 Km/sec
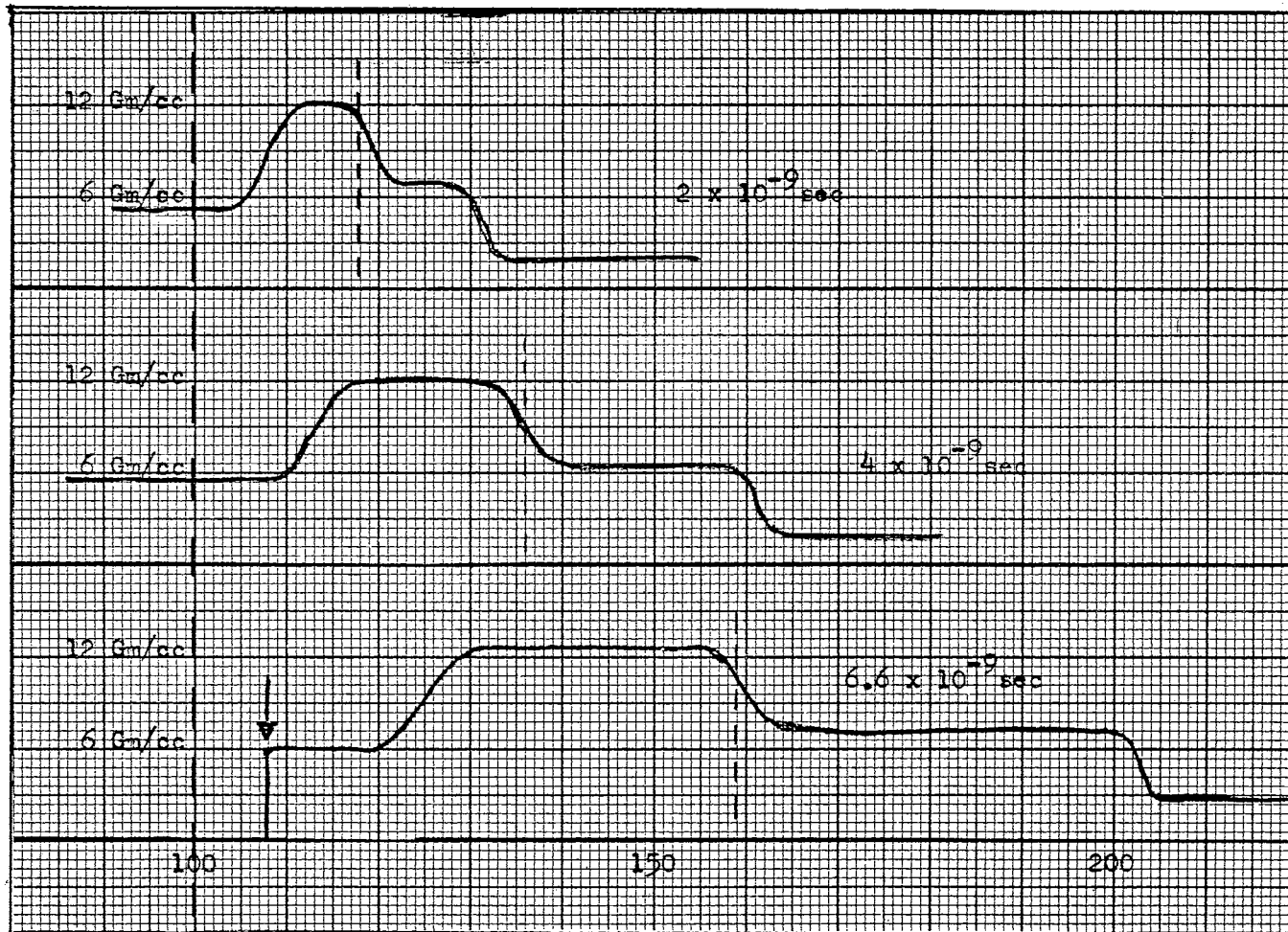
Figure 28.   Density Profiles Resulting from Impact of Iron Plate of
Porosity 1.33 Traveling at 15.2 Km/sec
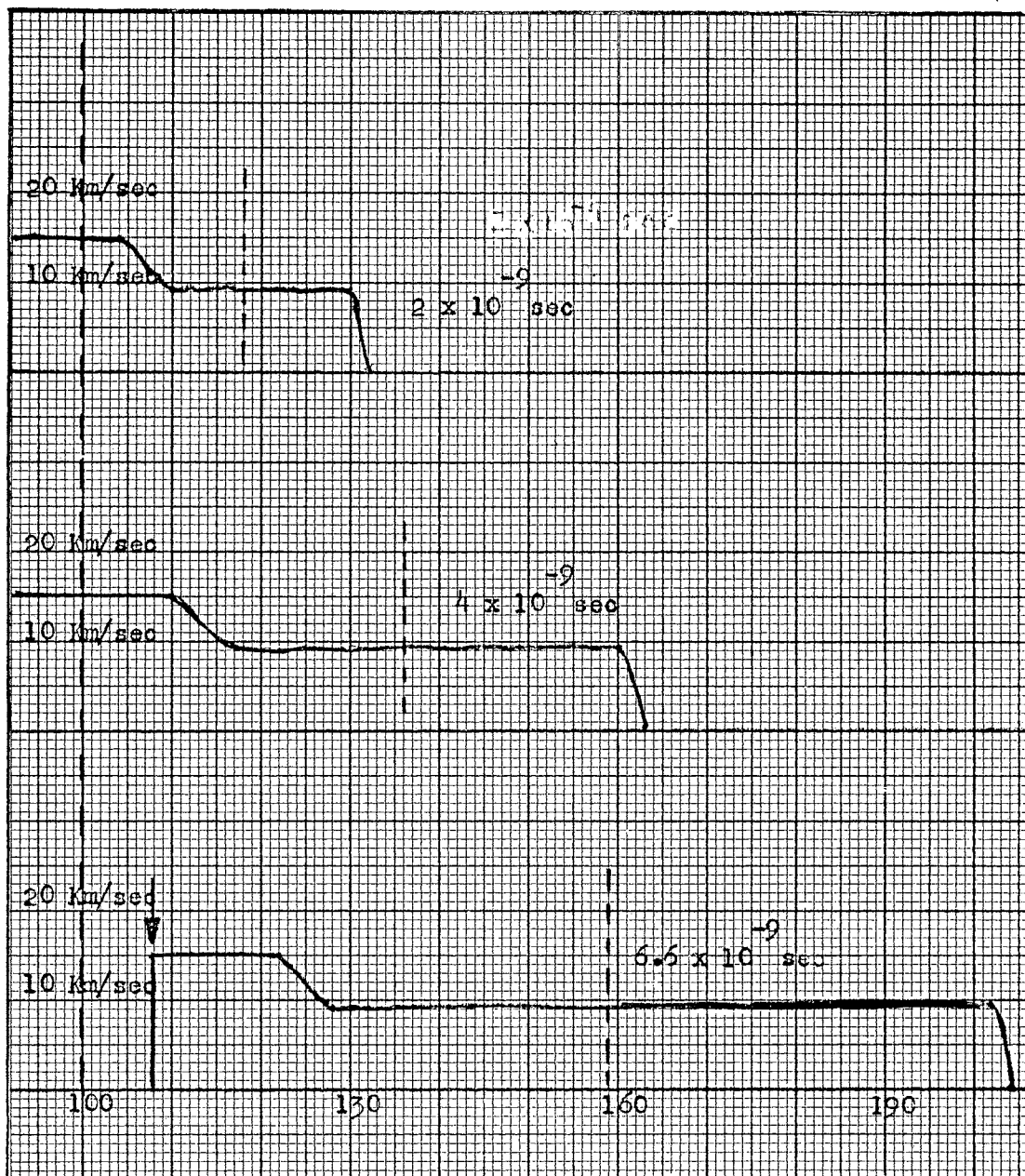
Figure 29. Velocity Profiles Resulting from
Impact of Iron Plate of
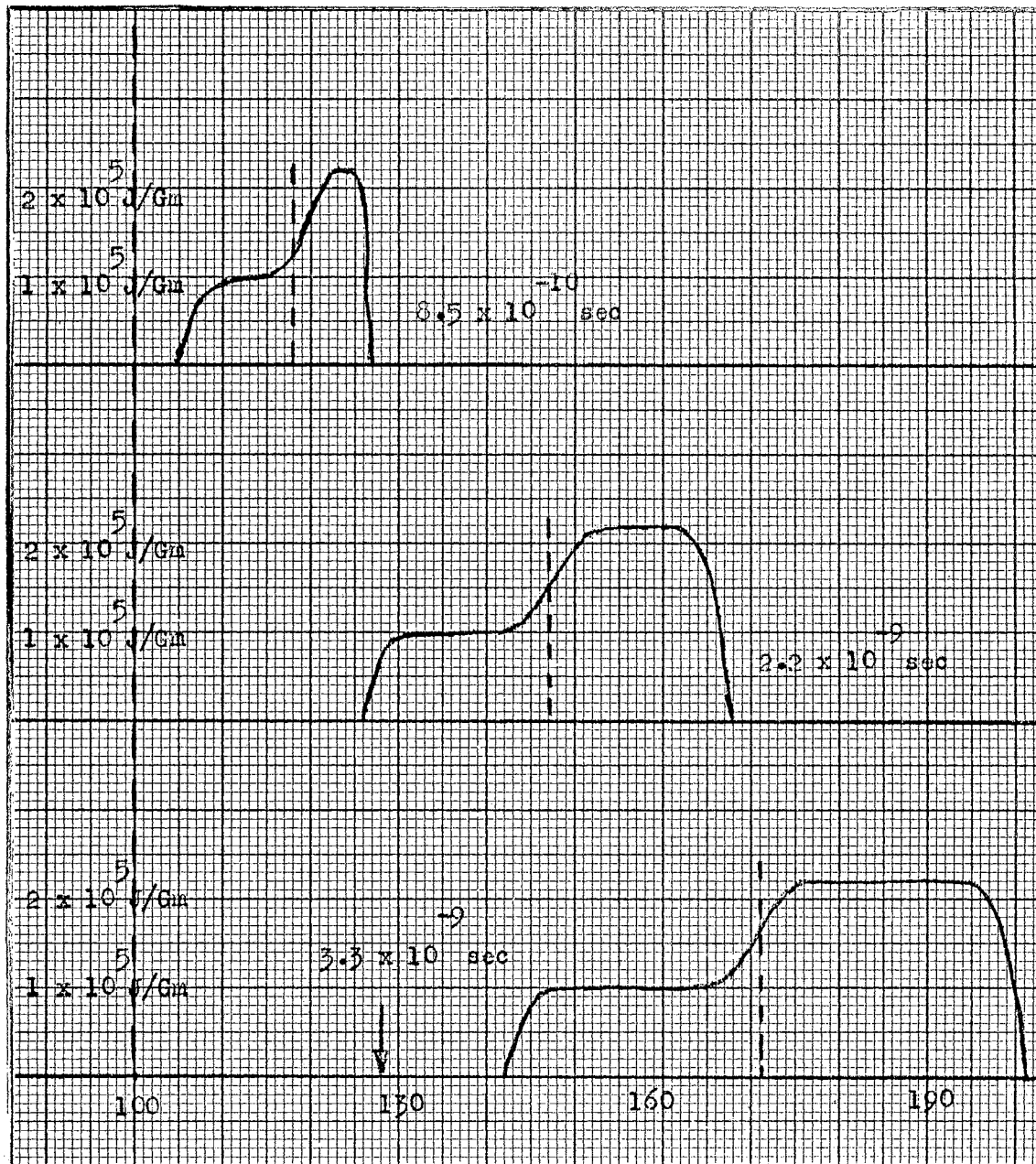Porosity 1.33 Traveling at
15.2 Km/sec
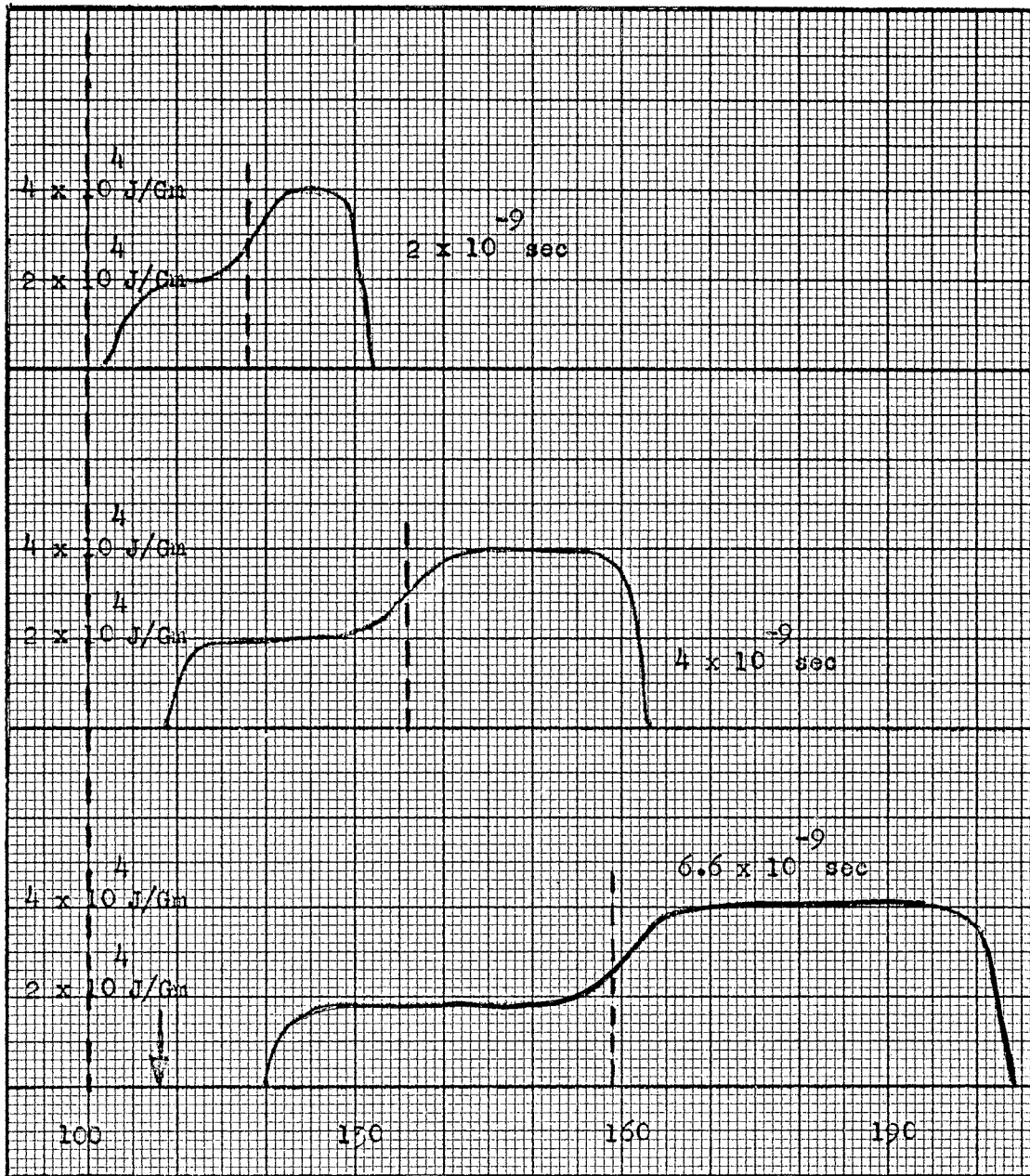
Figure 30. Internal Energy Profiles Resulting
from Impact of Iron Plate of
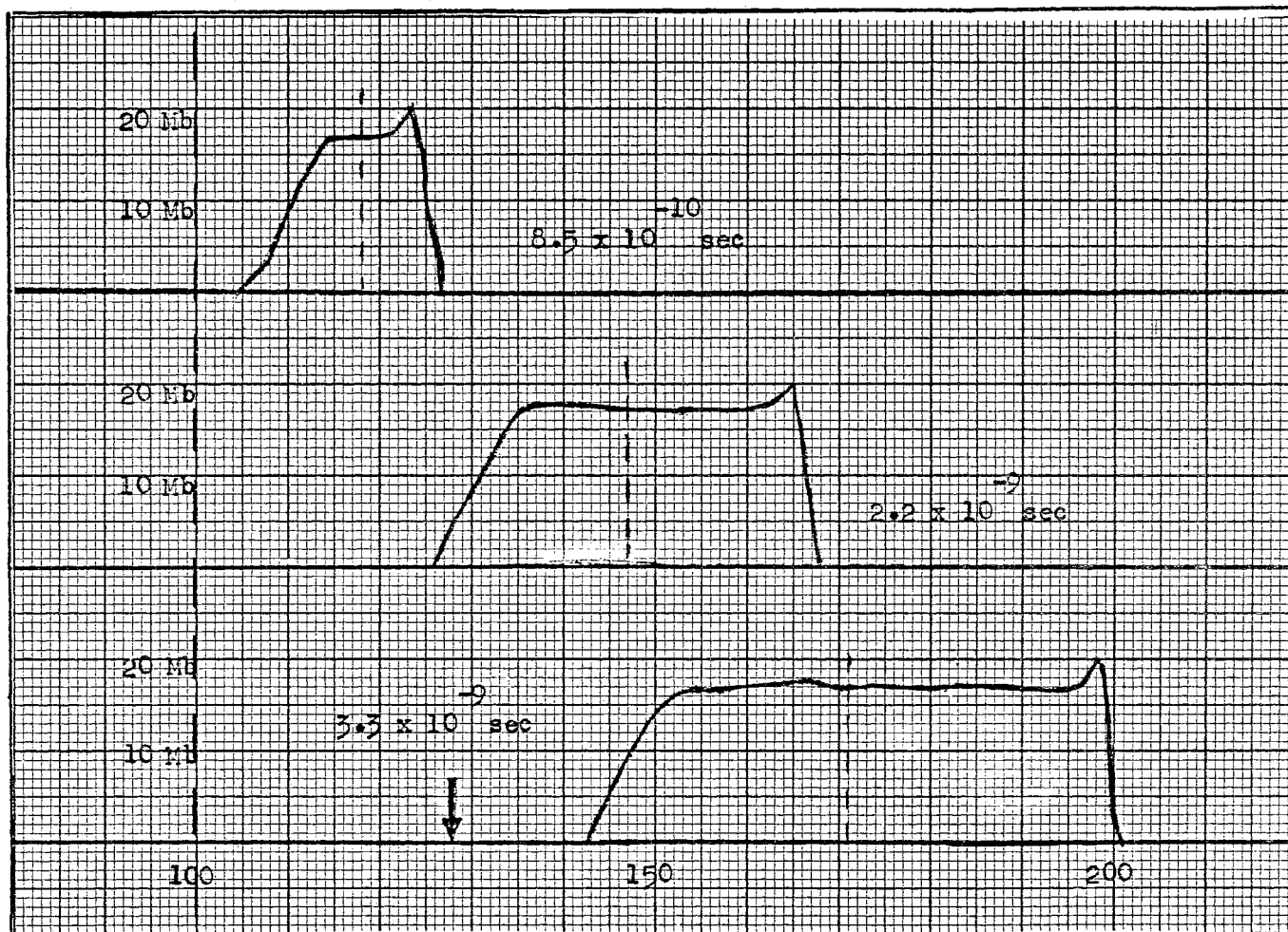Porosity 1.33 Traveling at 15.2
Km/sec

Figure 31. Pressure Profiles Resulting from Impact of Iron Plate of
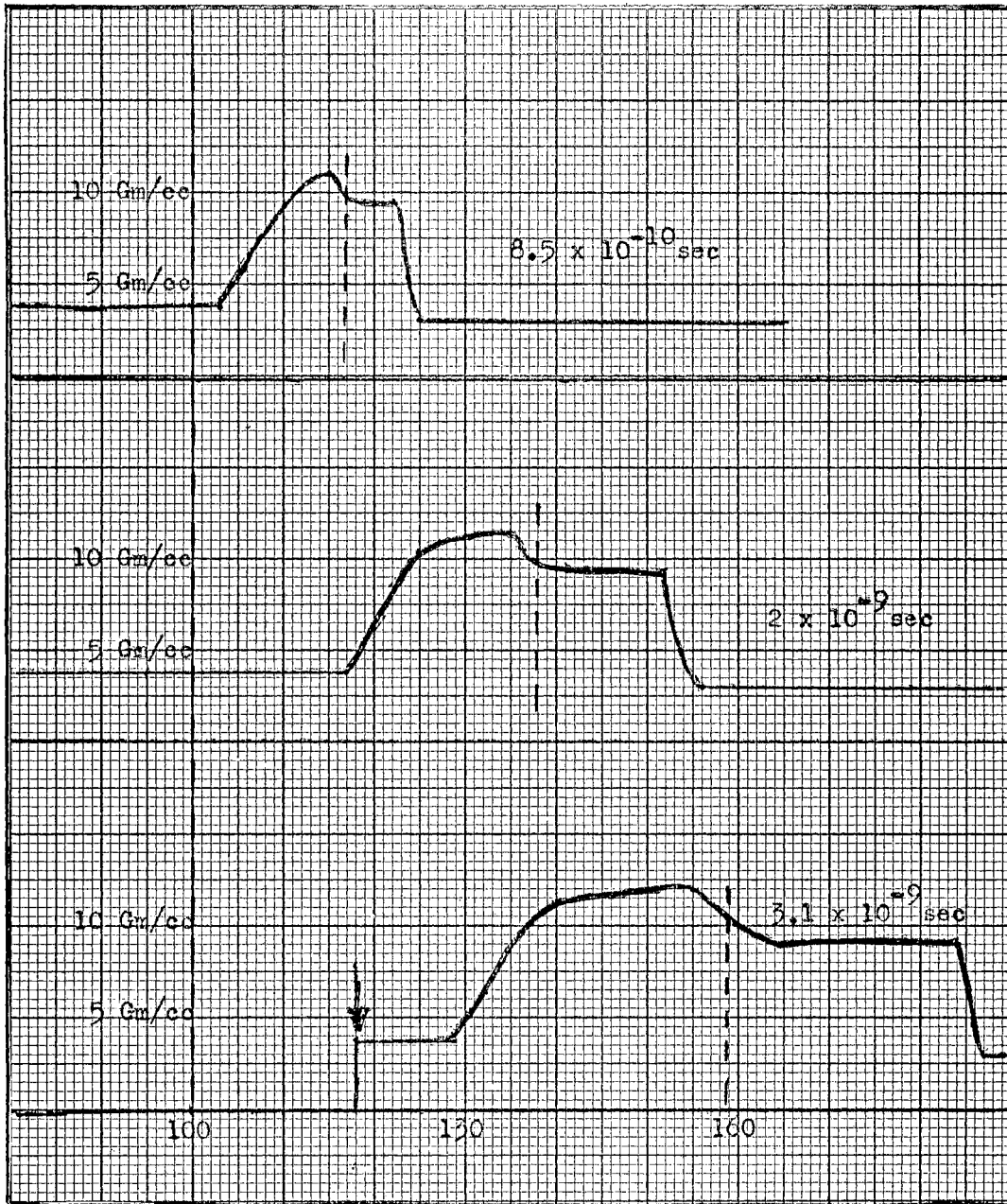Porosity 1.33 Traveling at 15.2 Km/sec
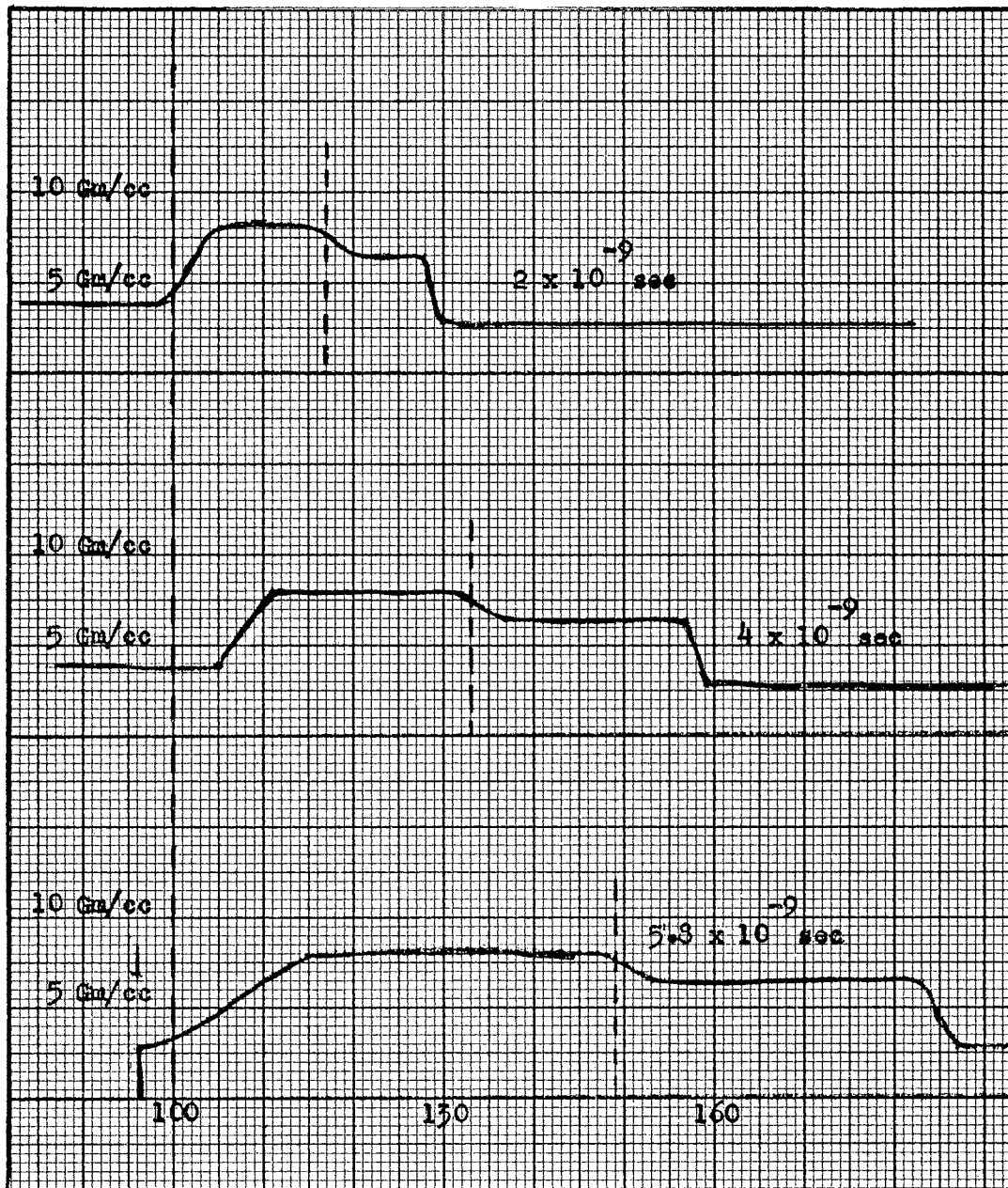
Figure 32. Density Profiles Resulting from
Impact of Iron Plate of
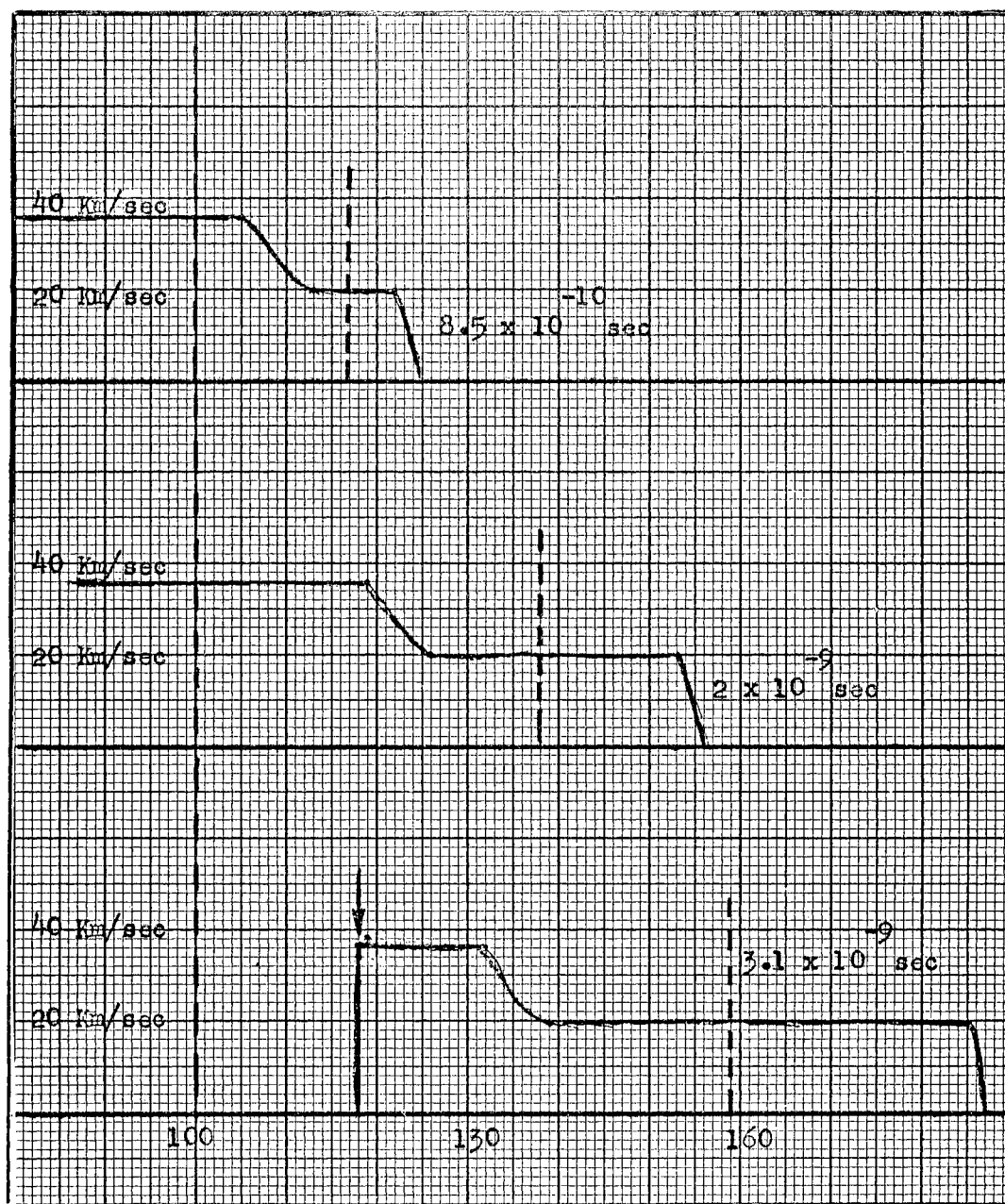Porosity 2 Traveling at 15.2
Km/sec
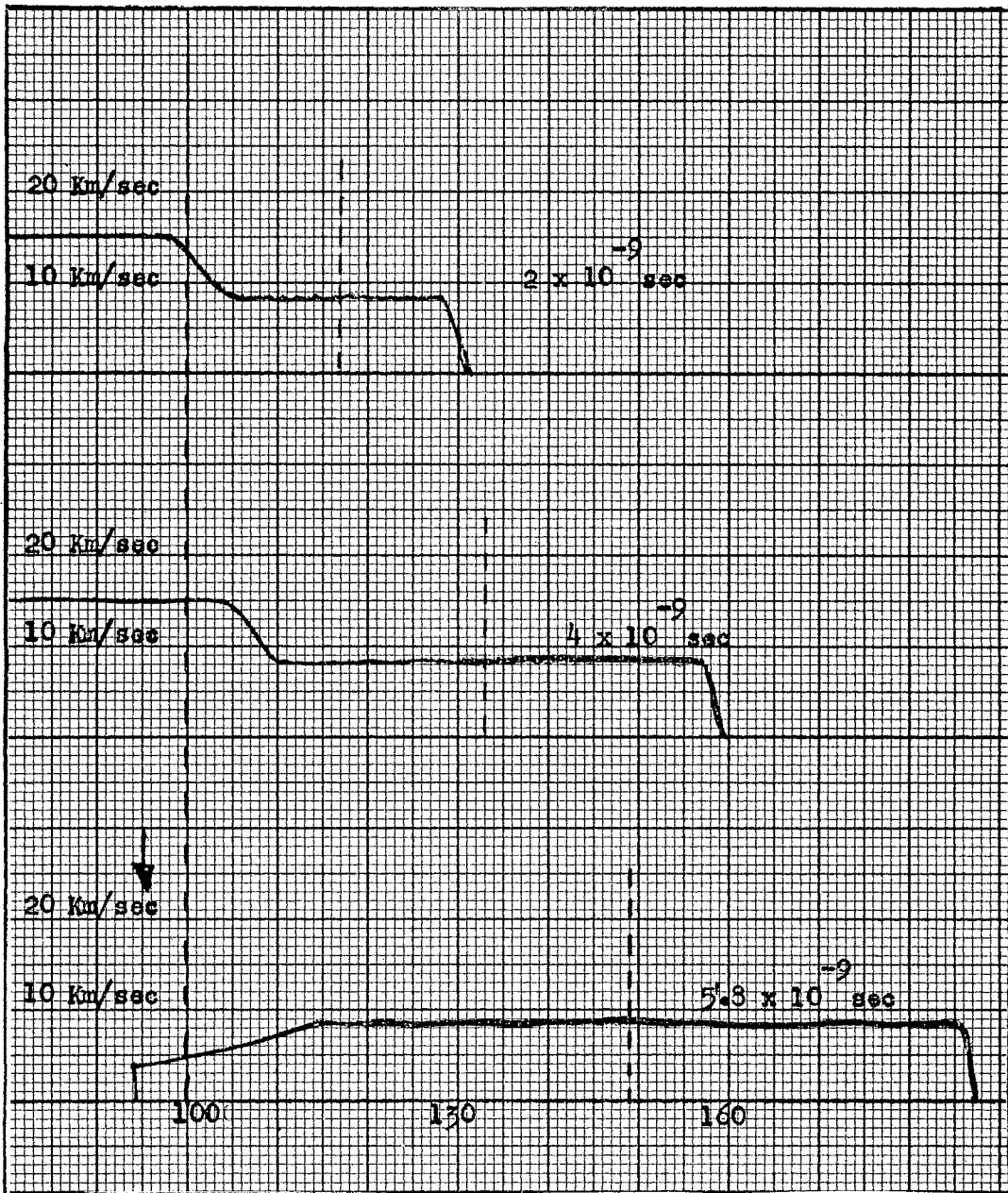
Figure 33. Velocity Profiles Resulting from
Impact of Iron Plate of
Porosity 2 Traveling at 15.2
Km/sec
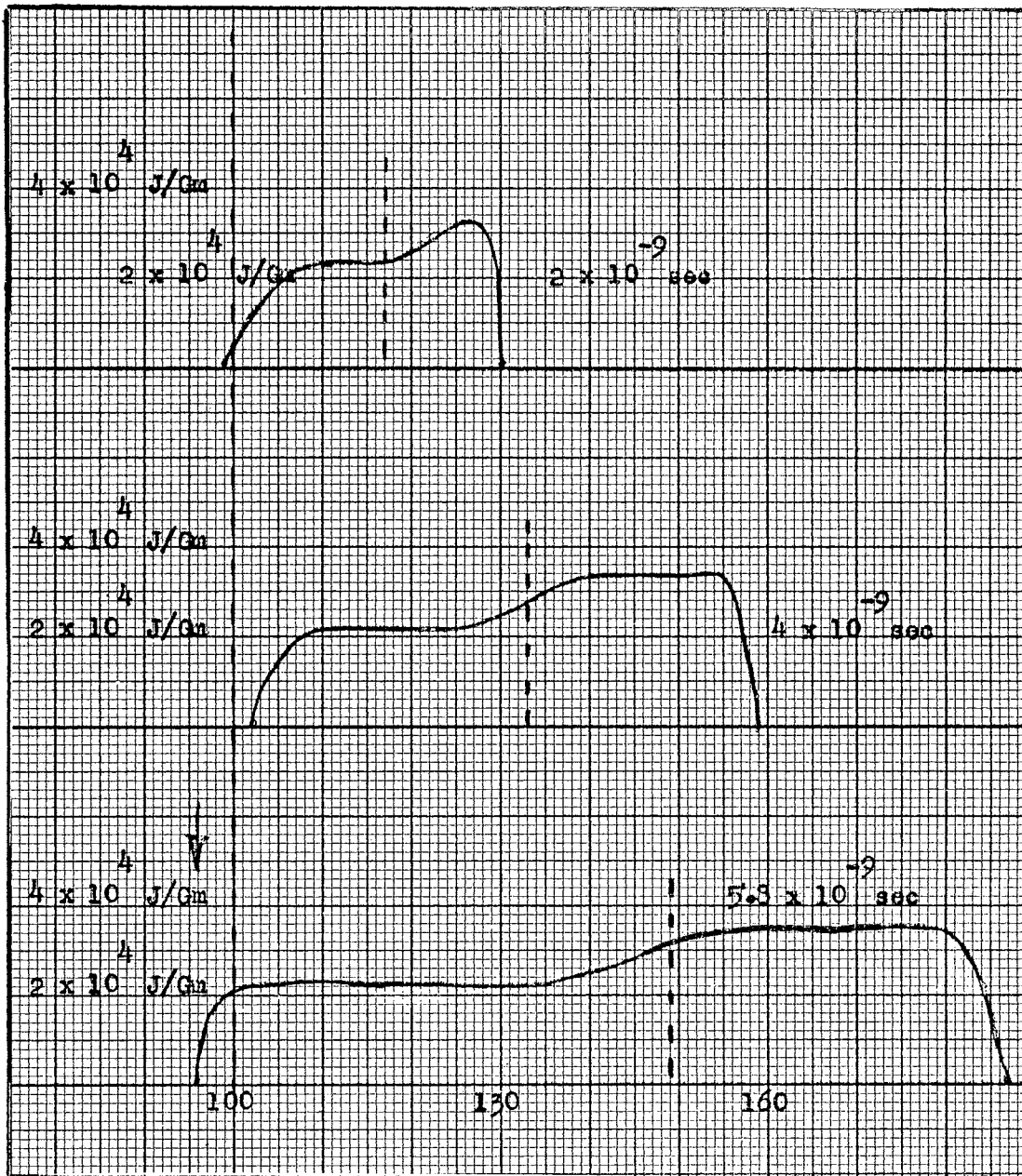
Figure 34. Internal Energy Profiles Resulting
from Impact of Iron Plate of
Porosity 2 Traveling at 15.2
Km/sec
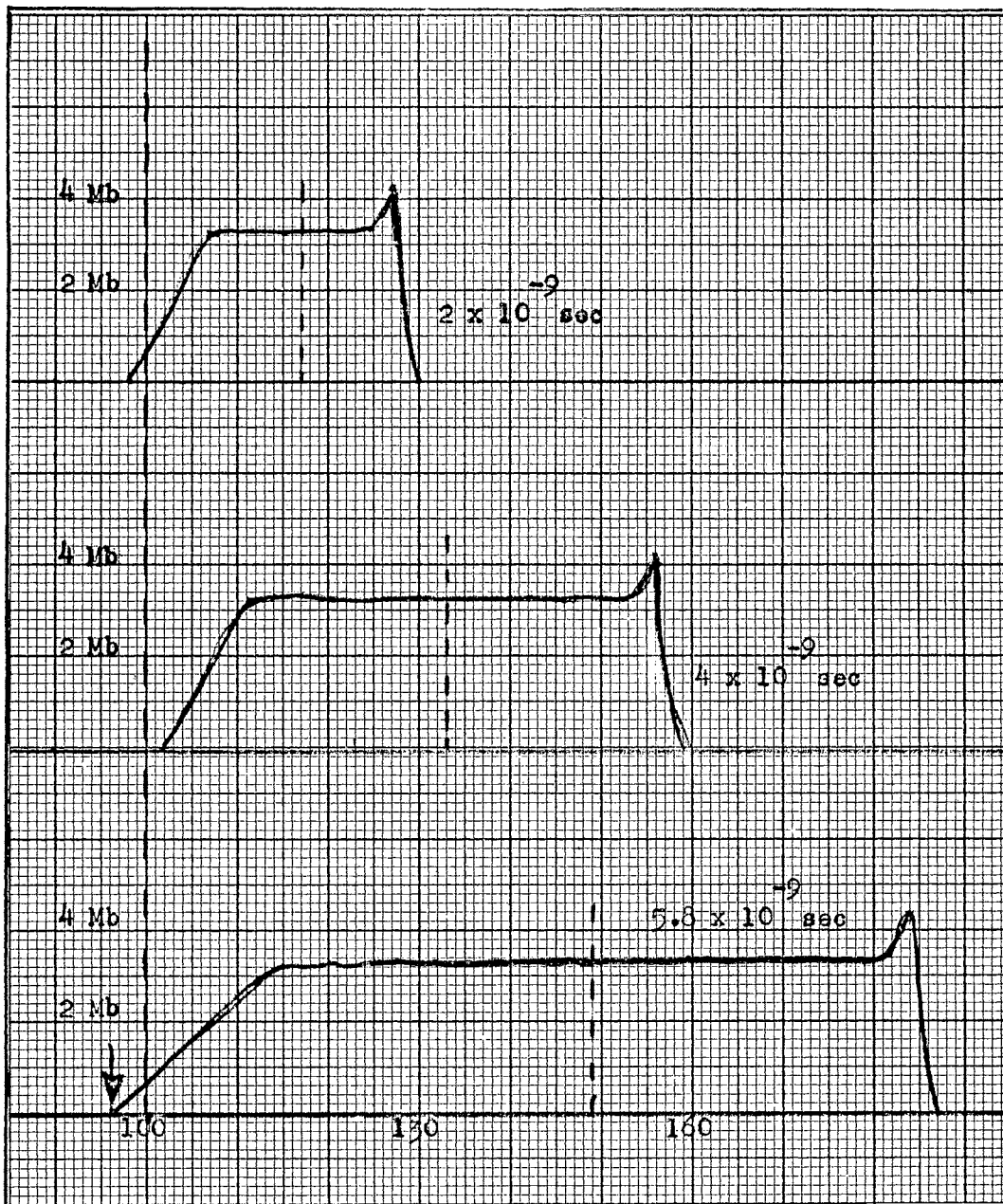
Figure 35. Pressure Profiles Resulting from
Impact of Iron Plate of
Porosity 2 Traveling at 15.2
Km/sec
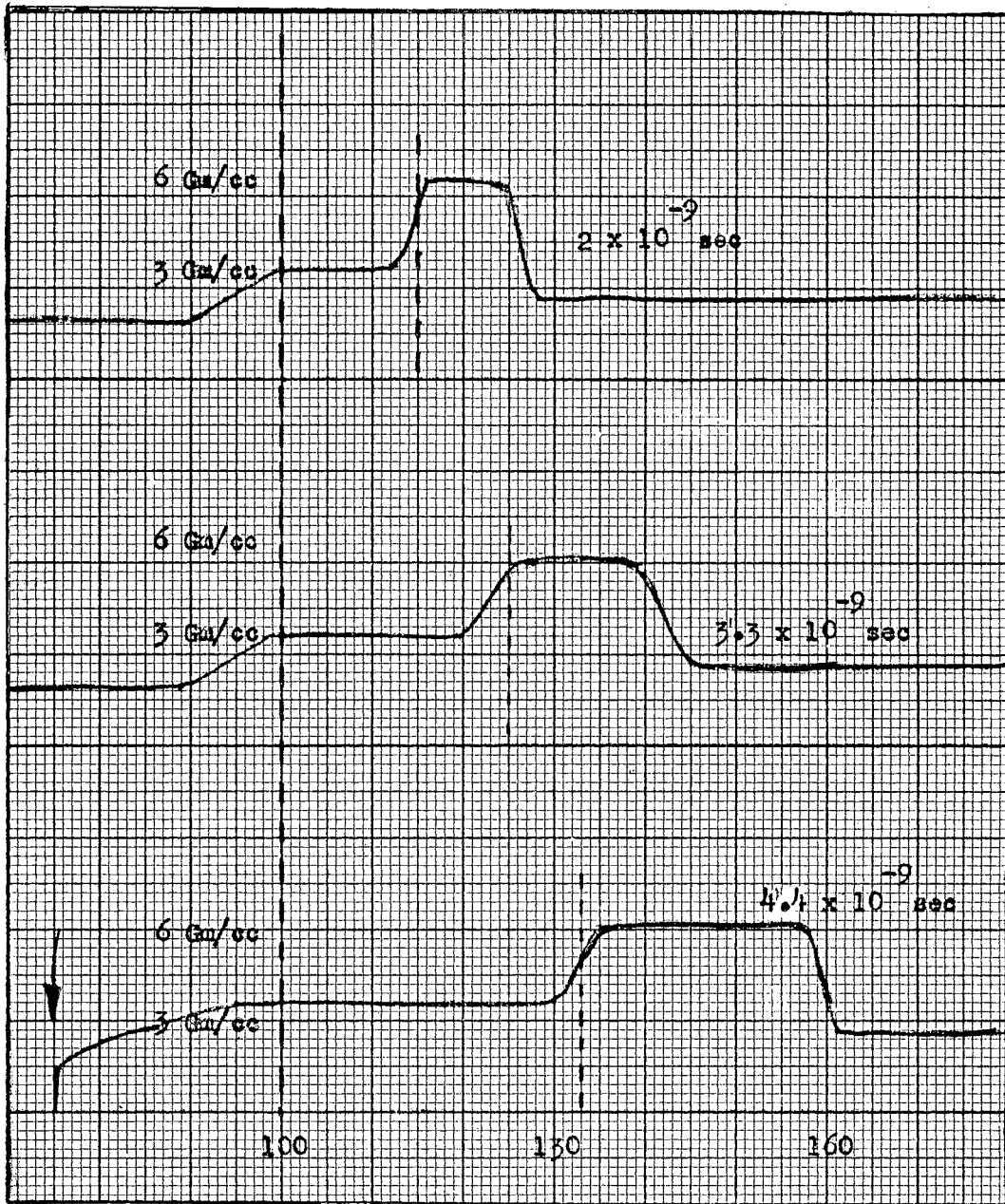
Figure 36. Density Profiles Resulting from
Impact of Iron Plate of
Porosity 4 Traveling at 15.2
Km/sec
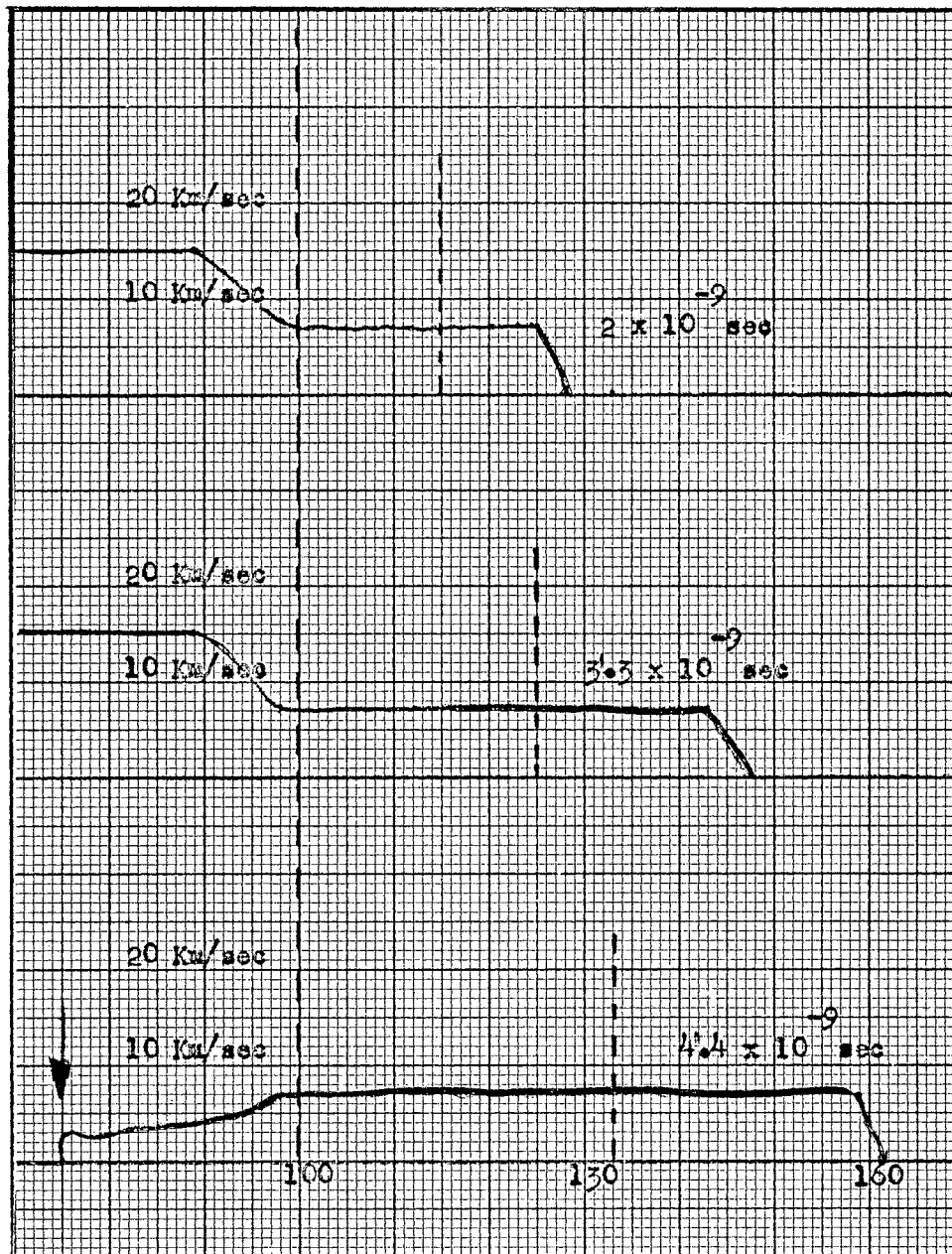
Figure 37. Velocity Profiles Resulting from
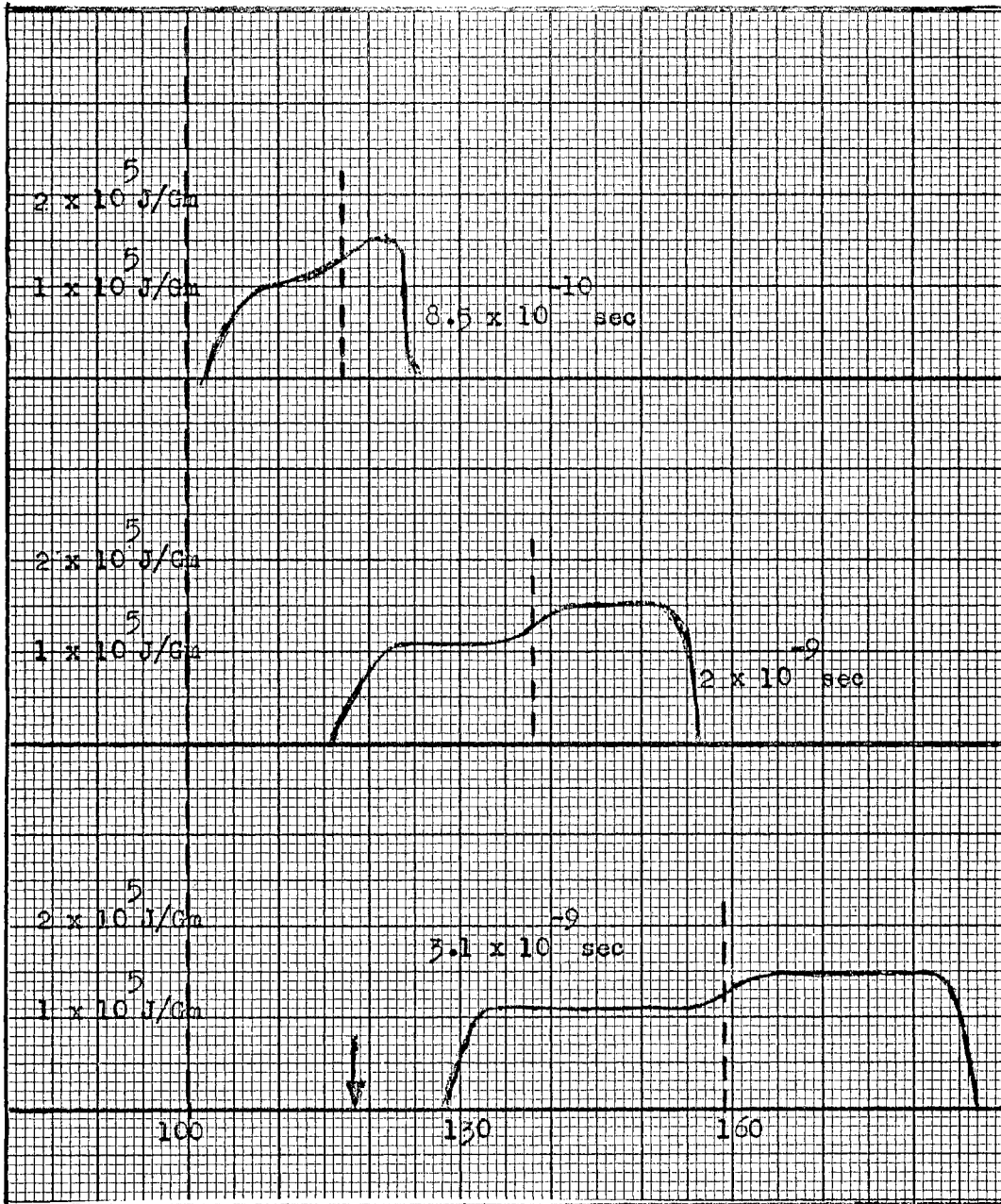Impact of Iron Plate of
Porosity 4 Traveling at 15.2
Km/sec

Figure 38.   Internal Energy Profiles Resulting
from Impact of Iron Plate of
Porosity 4 Traveling at 15.2
Km/sec

Figure 39. Pressure Profiles Resulting from
Impact of Iron Plate of
Porosity 4 Traveling at 15.2
Km/sec

Figure 40. Density Profiles Resulting from Impact of Iron Plate of
Porosity 1 Traveling at 36 Km/sec

Figure 41. Velocity Profiles Resulting from Impact of Iron Plate of
Porosity 1 Traveling at 36 Km/sec

Figure 42. Internal Energy Profiles Resulting from Impact of Iron Plate
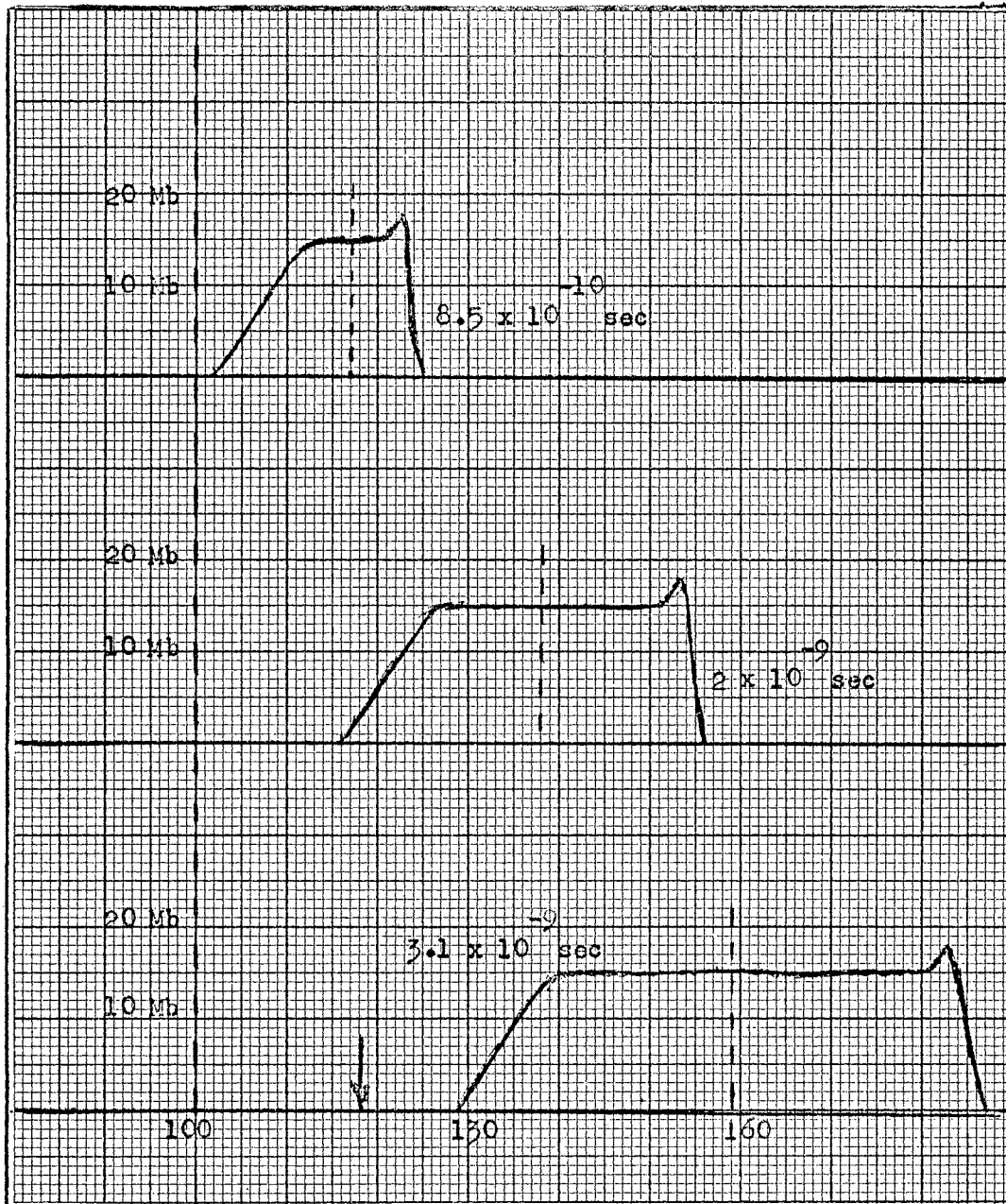of Porosity 1 Traveling at 36 Km/sec

Figure 43. Pressure Profiles Resulting from Impact of Iron Plate of
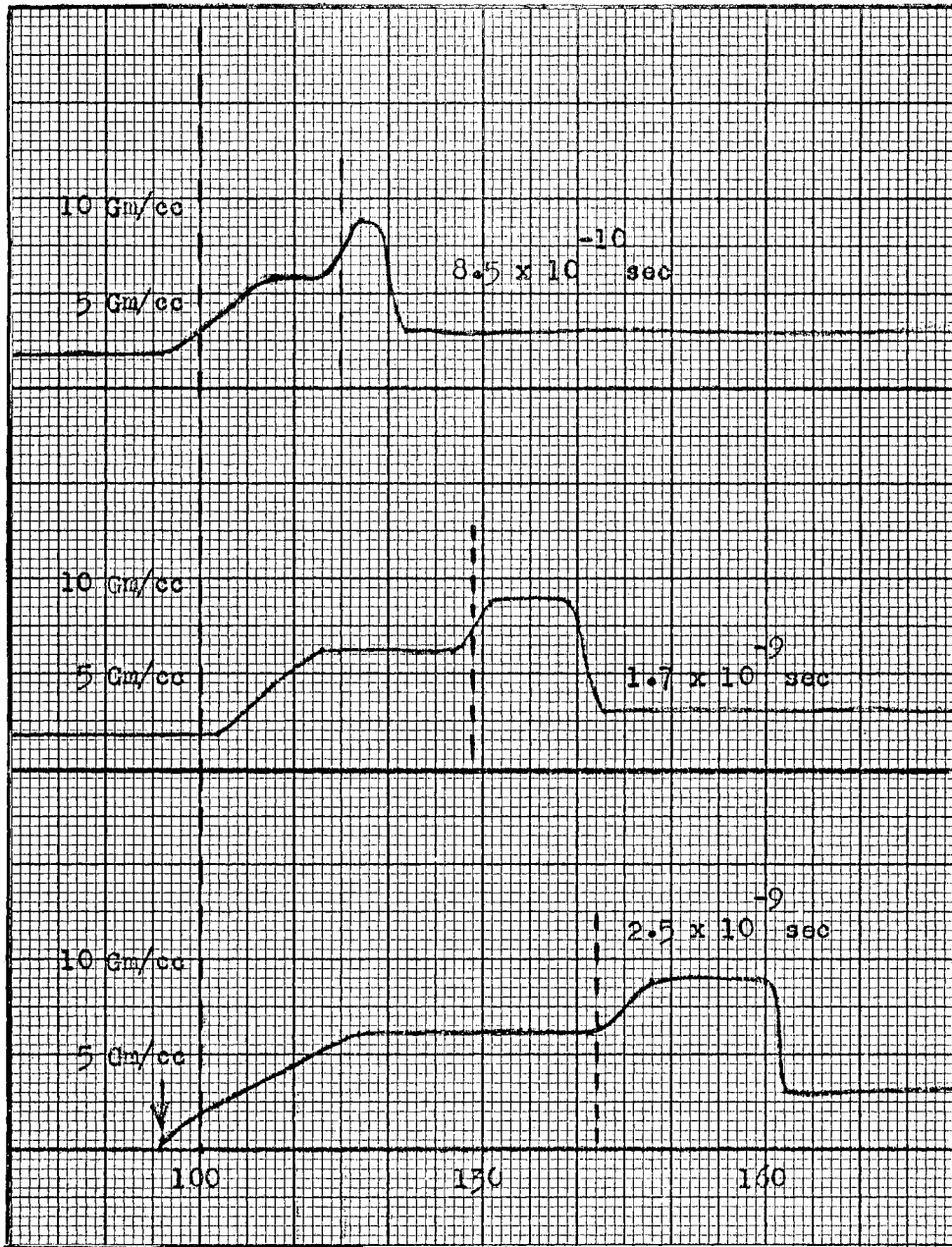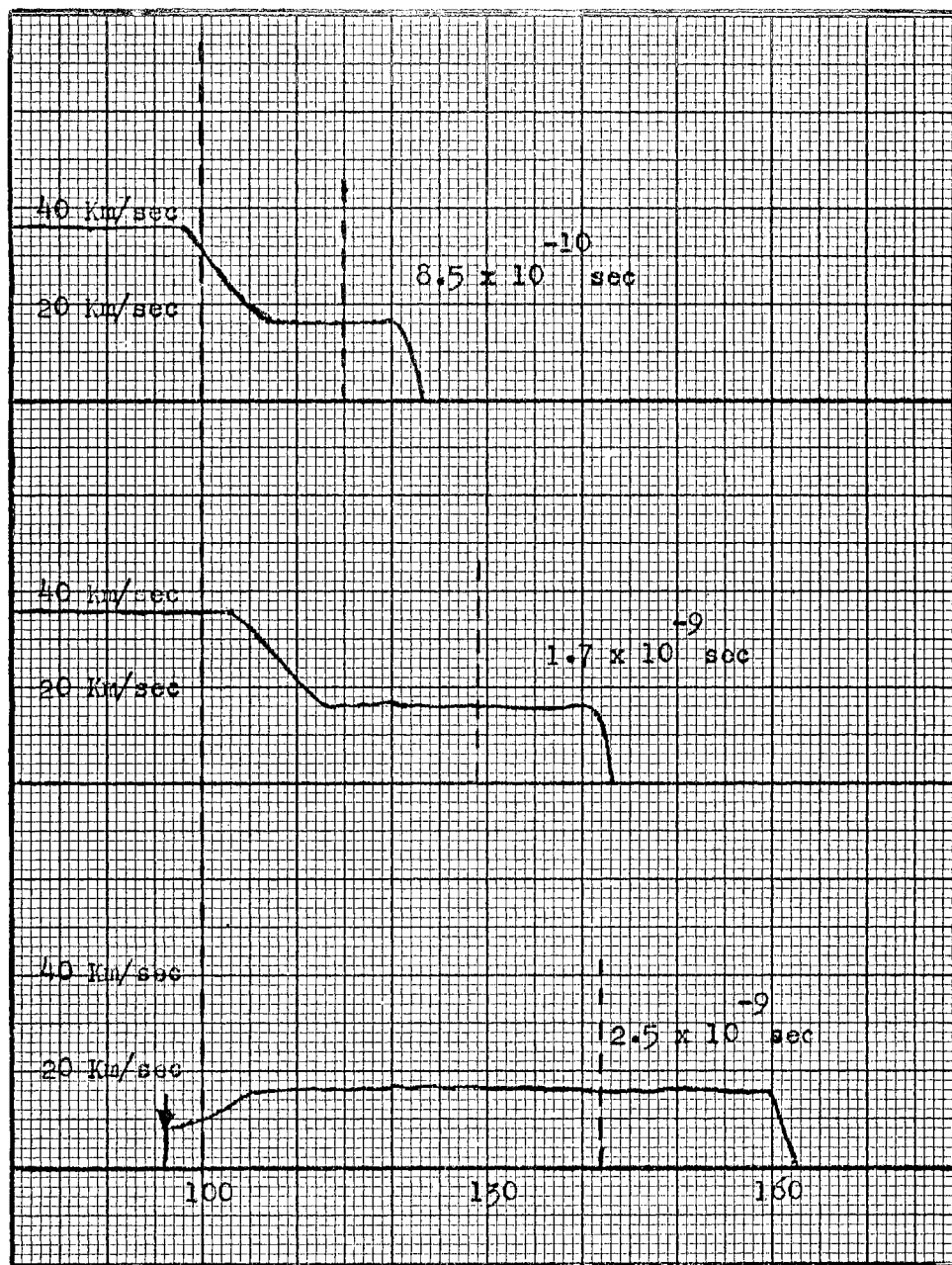Porosity 1 Traveling at 36 Km/sec

Figure 44. Density Profiles Resulting from Impact of Iron Plate of
Porosity 1.33 Traveling at 36 Km/sec

Figure 45. Velocity Profiles Resulting from Impact of Iron Plate of Porosity 1.33 Traveling at 36 Km/sec
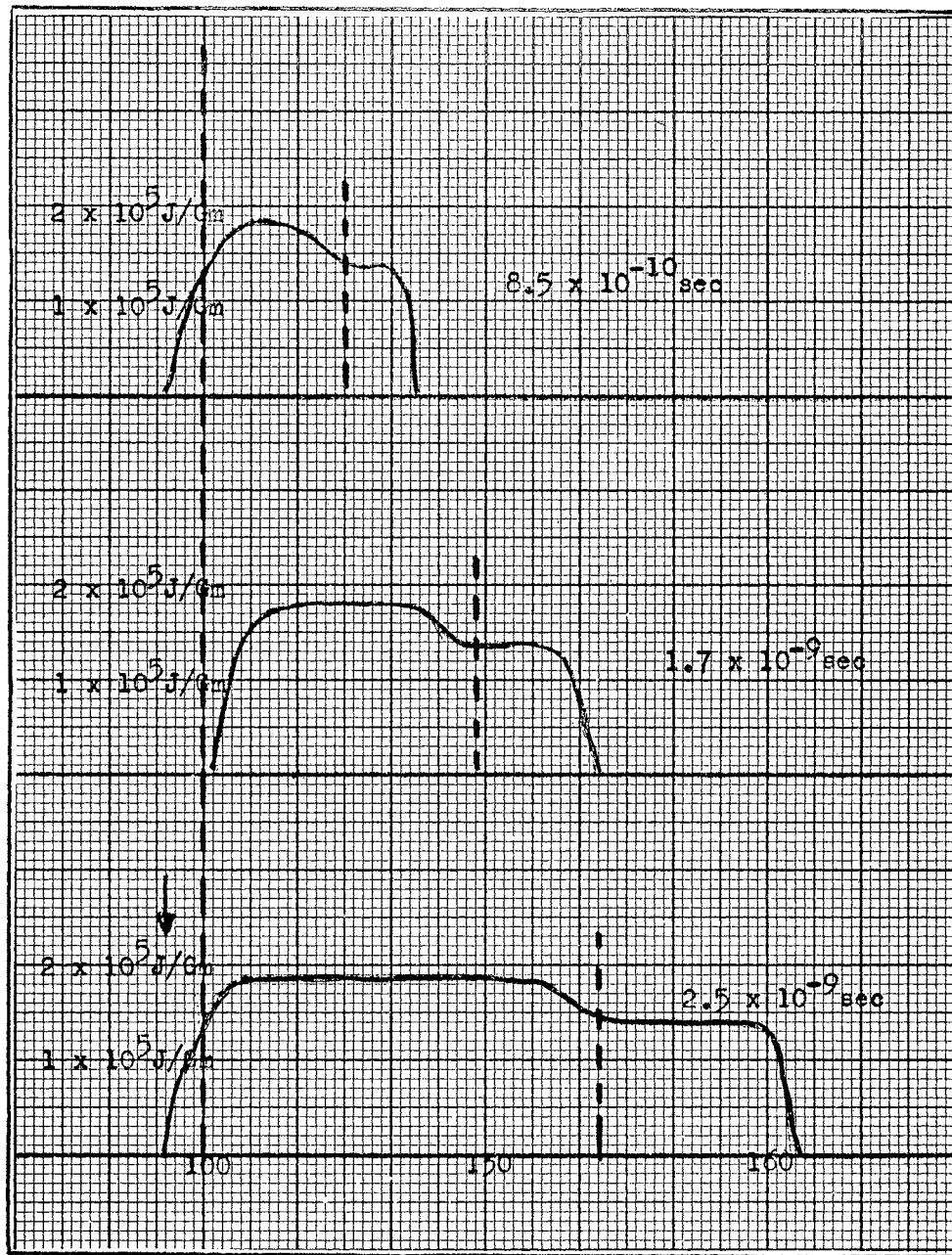
Figure 46. Internal Energy Profiles Resulting
from Impact of Iron Plate of
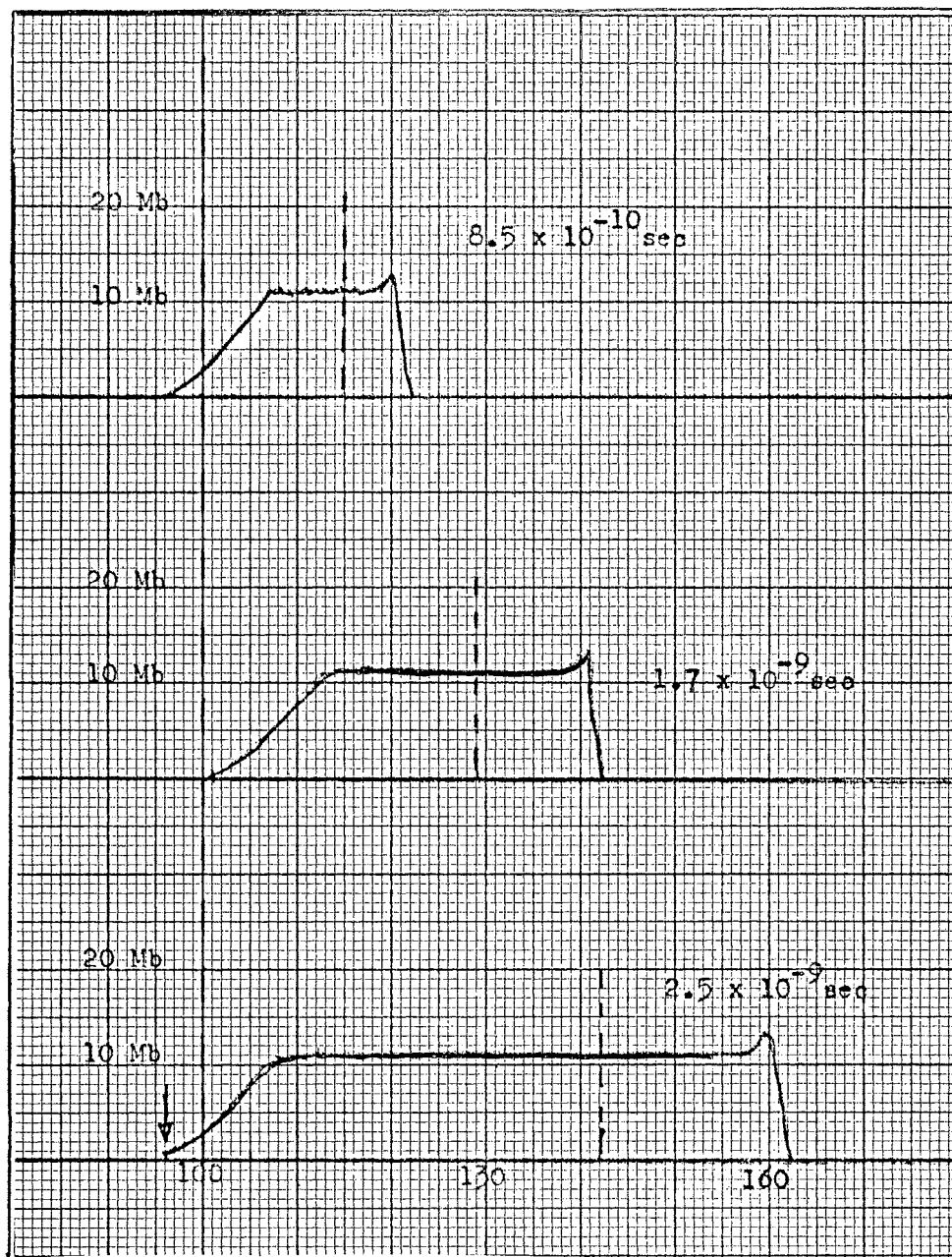Porosity 1.33 Traveling at 36
Km/sec

Figure 47. Pressure Profiles Resulting from Impact of Iron Plate of Porosity 1.33 Traveling at 36 Km/sec

Figure 48. Density Profiles Resulting from
Impact of Iron Plate of
Porosity 2 Traveling at 36
Km/sec

Figure 49.   Velocity Profiles Resulting from
Impact of Iron Plate of
Porosity 2 Traveling at 36
Km/sec

Figure 50. Internal Energy Profiles Resulting
from Impact of Iron Plate of
Porosity 2 Traveling at 36
Km/sec

Figure 51. Pressure Profiles Resulting from
Impact of Iron Plate of
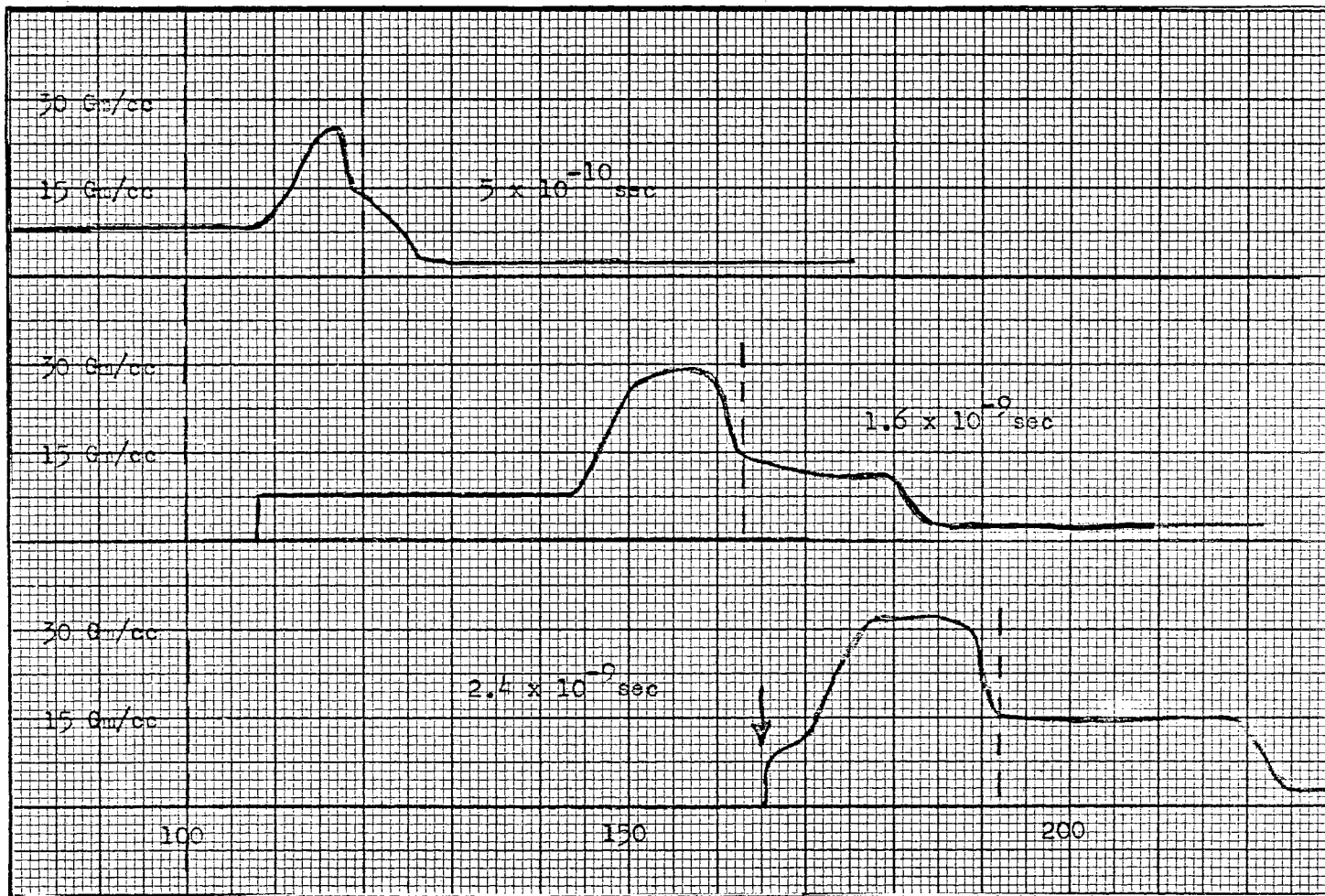Porosity 2 Traveling at 36
Km/sec

Figure 52. Density Profiles Resulting from
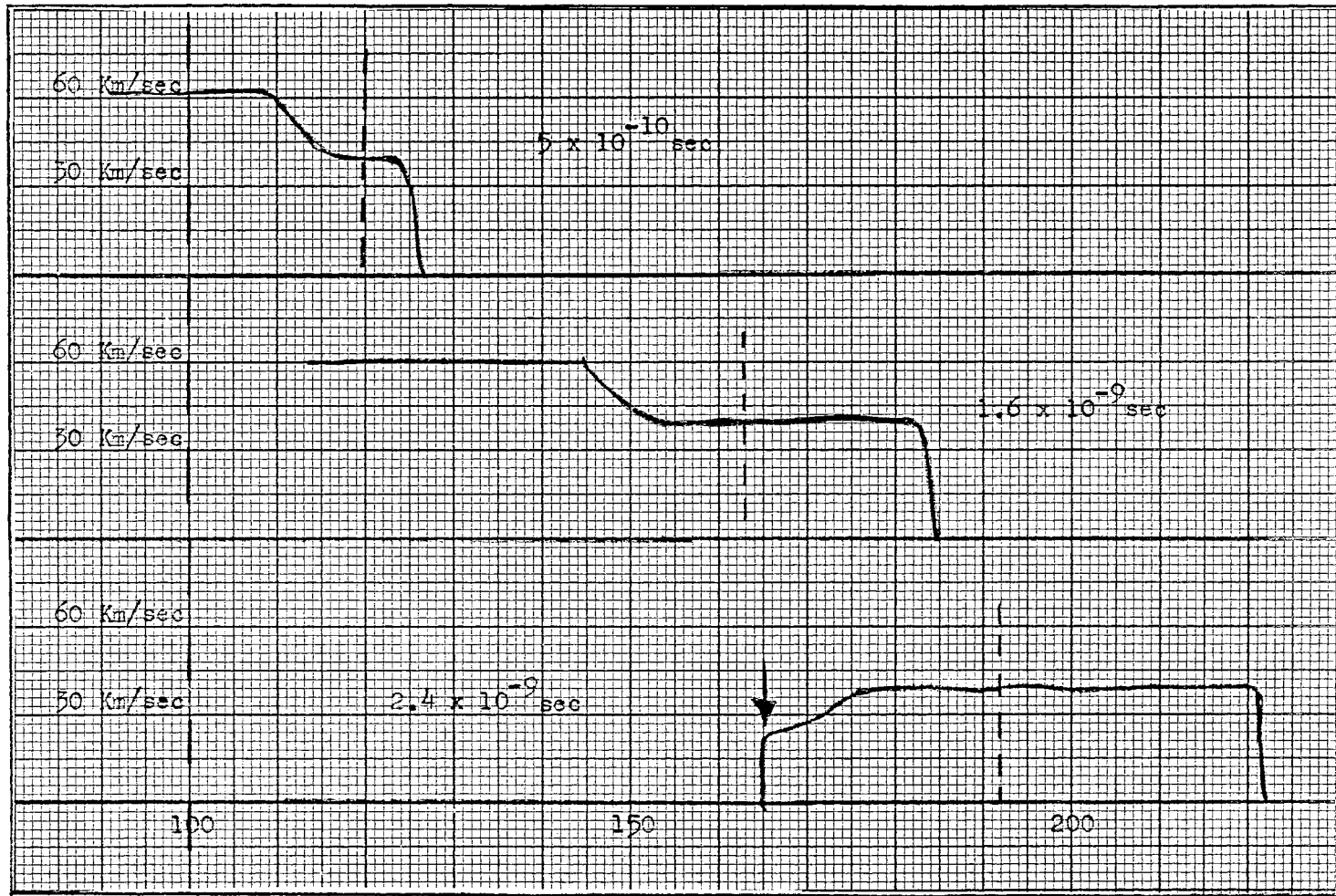Impact of Iron Plate of
Porosity 4 Traveling at 36
Km/sec

Figure 53. Velocity Profiles Resulting from
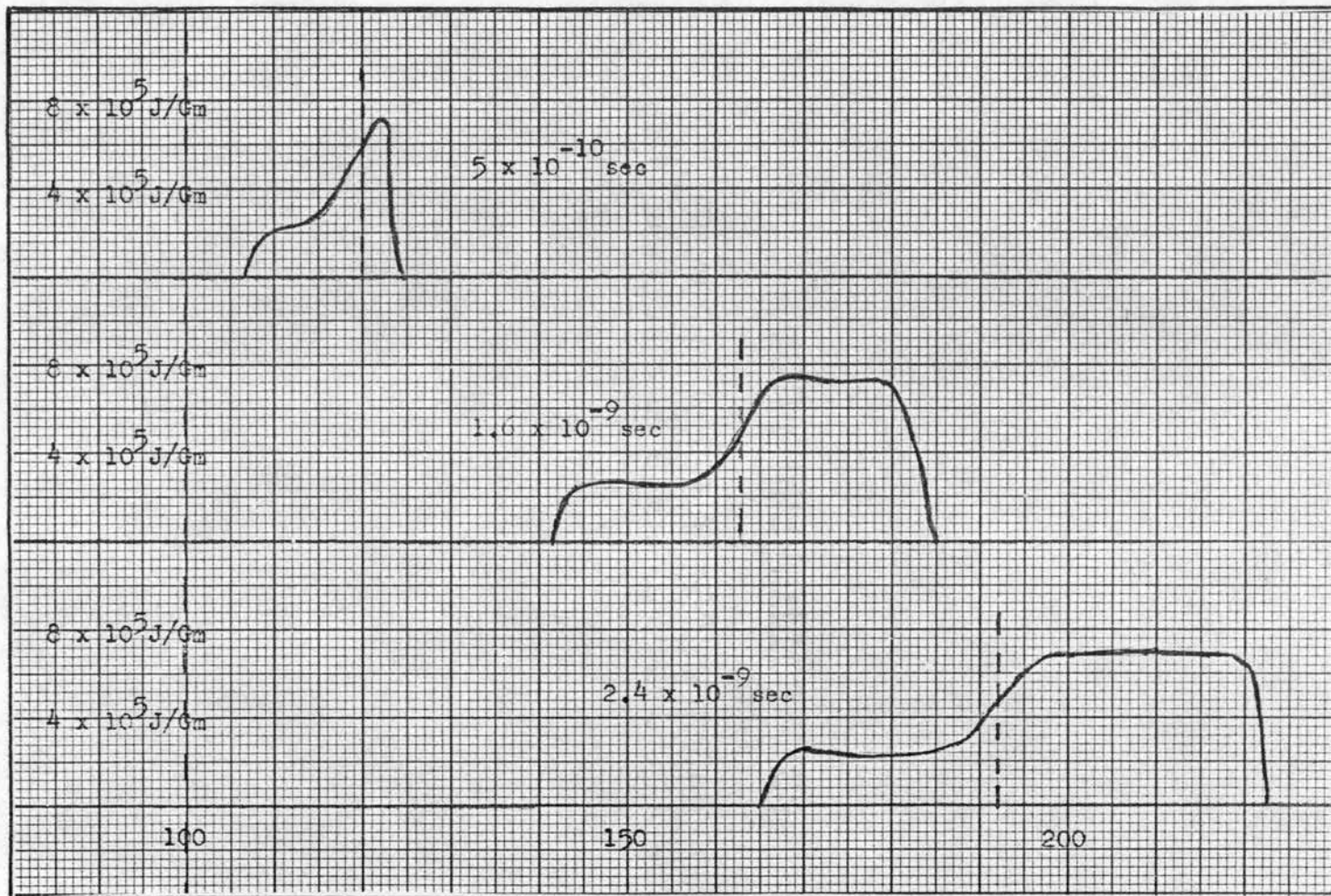Impact of Iron Plate of
Porosity 4 Traveling at 36
Km/sec

Figure 54. Internal Energy Profiles Resulting
from Impact of Iron Plate of
Porosity 4 Traveling at 36
Km/sec

Figure 55. Pressure Profiles Resulting from
Impact of Iron Plate of
Porosity 4 Traveling at 36
Km/sec

Figure 56. Density Profiles Resulting from Impact of Iron Plate of
Porosity 1 Traveling at 60.6 Km/sec

Figure 57. Velocity Profiles Resulting from Impact of Iron Plate of
Porosity 1 Traveling at 60.6 Km/sec

Figure 58. Internal Energy Profiles Resulting from Impact of Iron
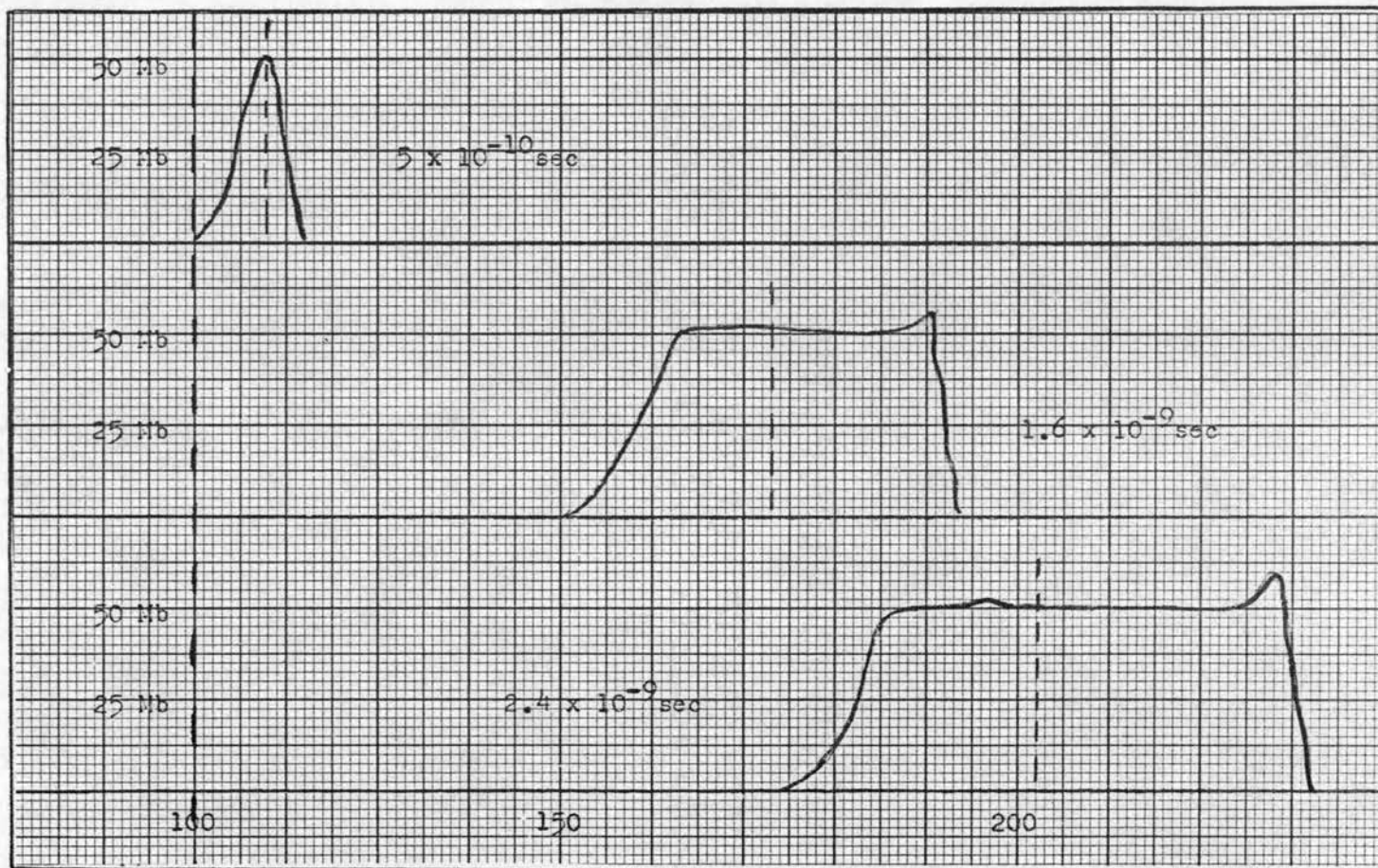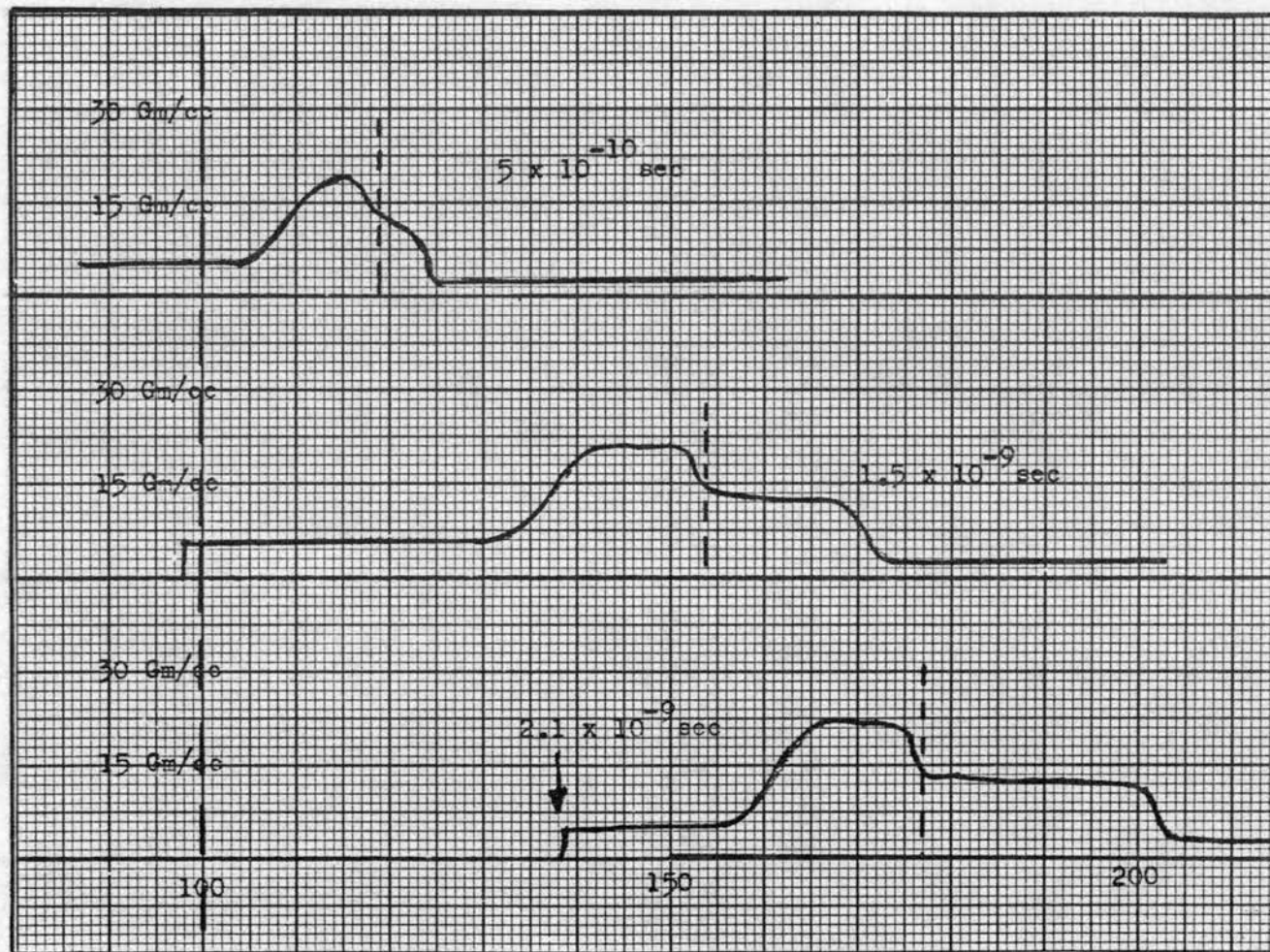Plate of Porosity 1 Traveling at 60.6 Km/sec

Figure 59. Pressure Profiles Resulting from Impact of Iron Plate of
Porosity 1 Traveling at 60.6 Km/sec

Figure 60. Density Profiles Resulting from Impact of Iron Plate of
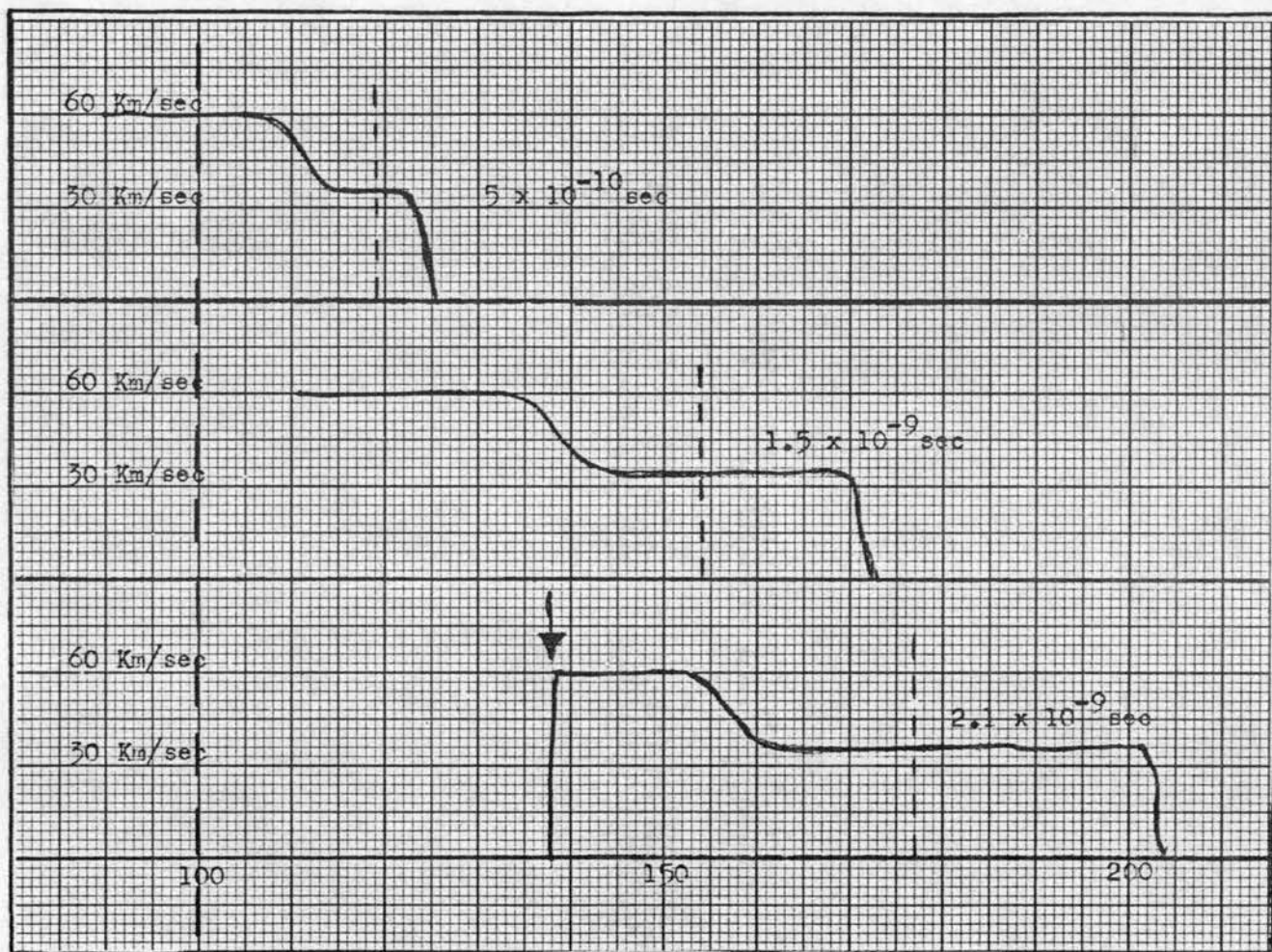Porosity 1.33 Traveling at 60.6 Km/sec

Figure 61. Velocity Profiles Resulting from Impact of Iron Plate of
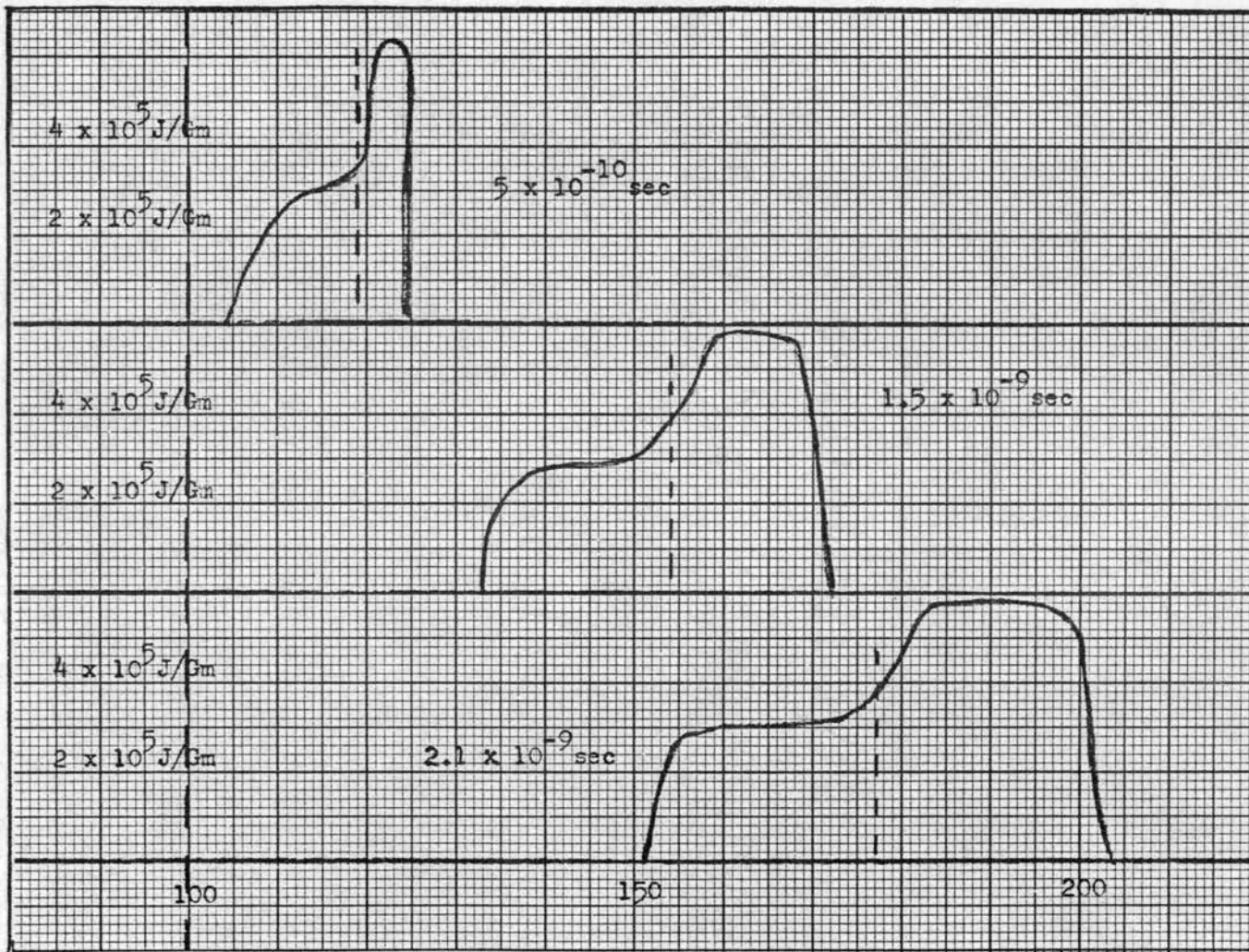Porosity 1.33 Traveling at 60.6 Km/sec

Figure 62. Internal Energy Profiles Resulting from Impact of Iron
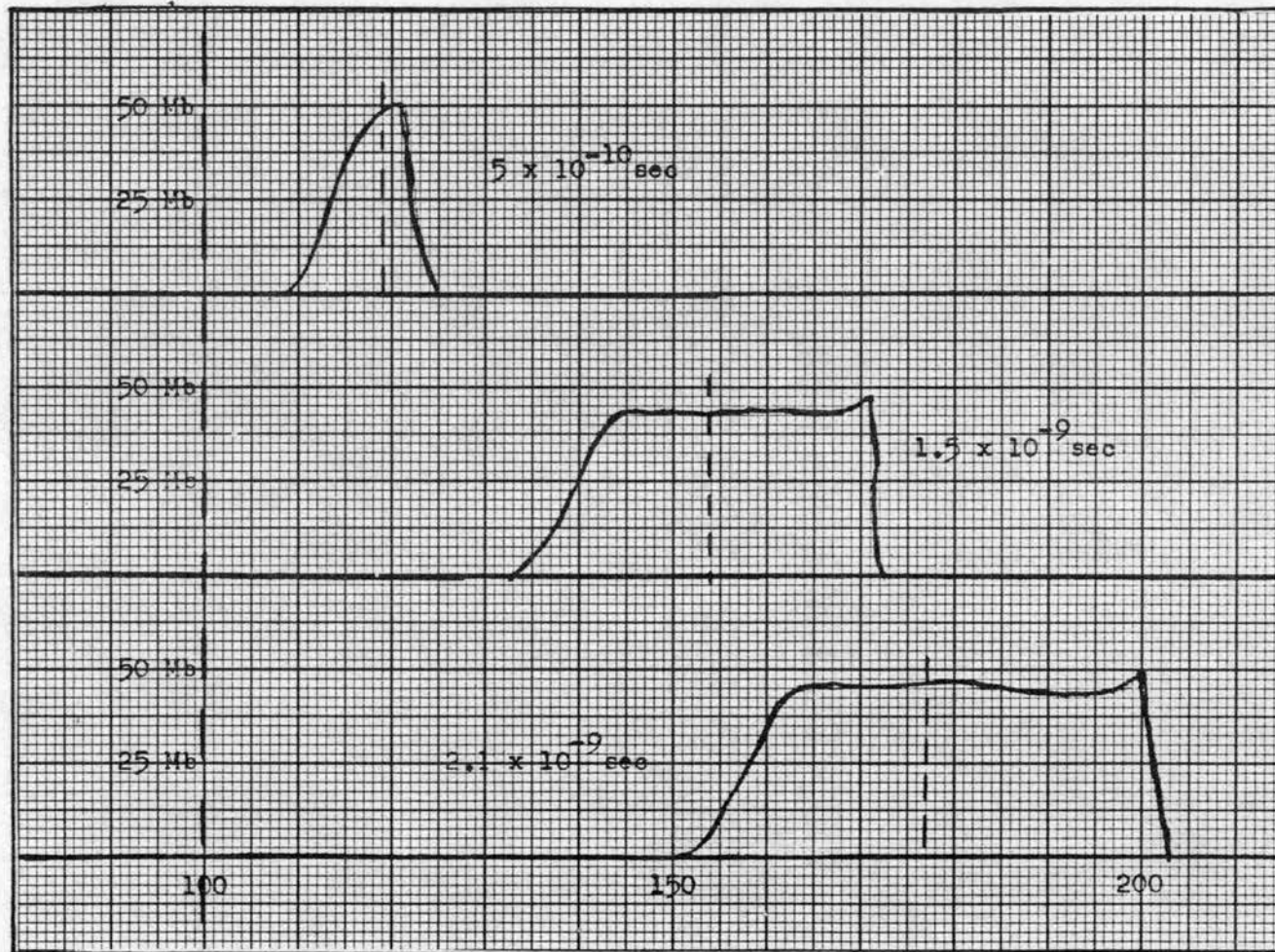Plate of Porosity 1.33 Traveling at 60.6 Km/sec

Figure 63. Pressure Profiles Resulting from Impact of Iron Plate of
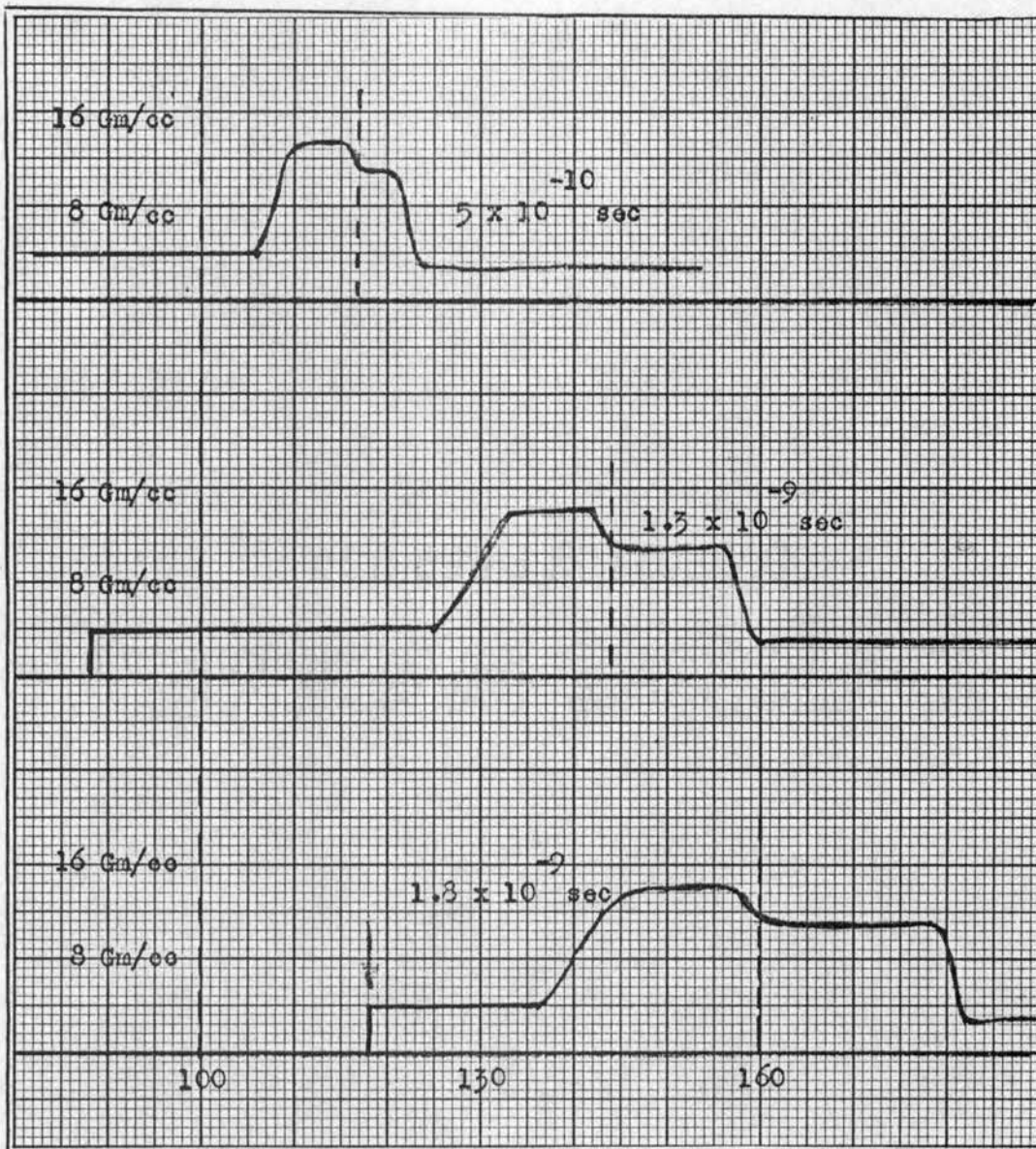Porosity 1.33 Traveling at 60.6 Km/sec

Figure 64. Density Profiles Resulting from
Impact of Iron Plate of
Porosity 2 Traveling at 60.6
Km/sec

Figure 65. Velocity Profiles Resulting from
Impact of Iron Plate of
Porosity 2 Traveling at 60.6
Km/sec

Figure 66. Internal Energy Profiles Resulting
from Impact of Iron Plate of
Porosity 2 Traveling at 60.6
Km/sec

Figure 67. Pressure Profiles Resulting from
Impact of Iron Plate of
Porosity 2 Traveling at 60.6
Km/sec

Figure 68.   Density Profiles Resulting from
Impact of Iron Plate of
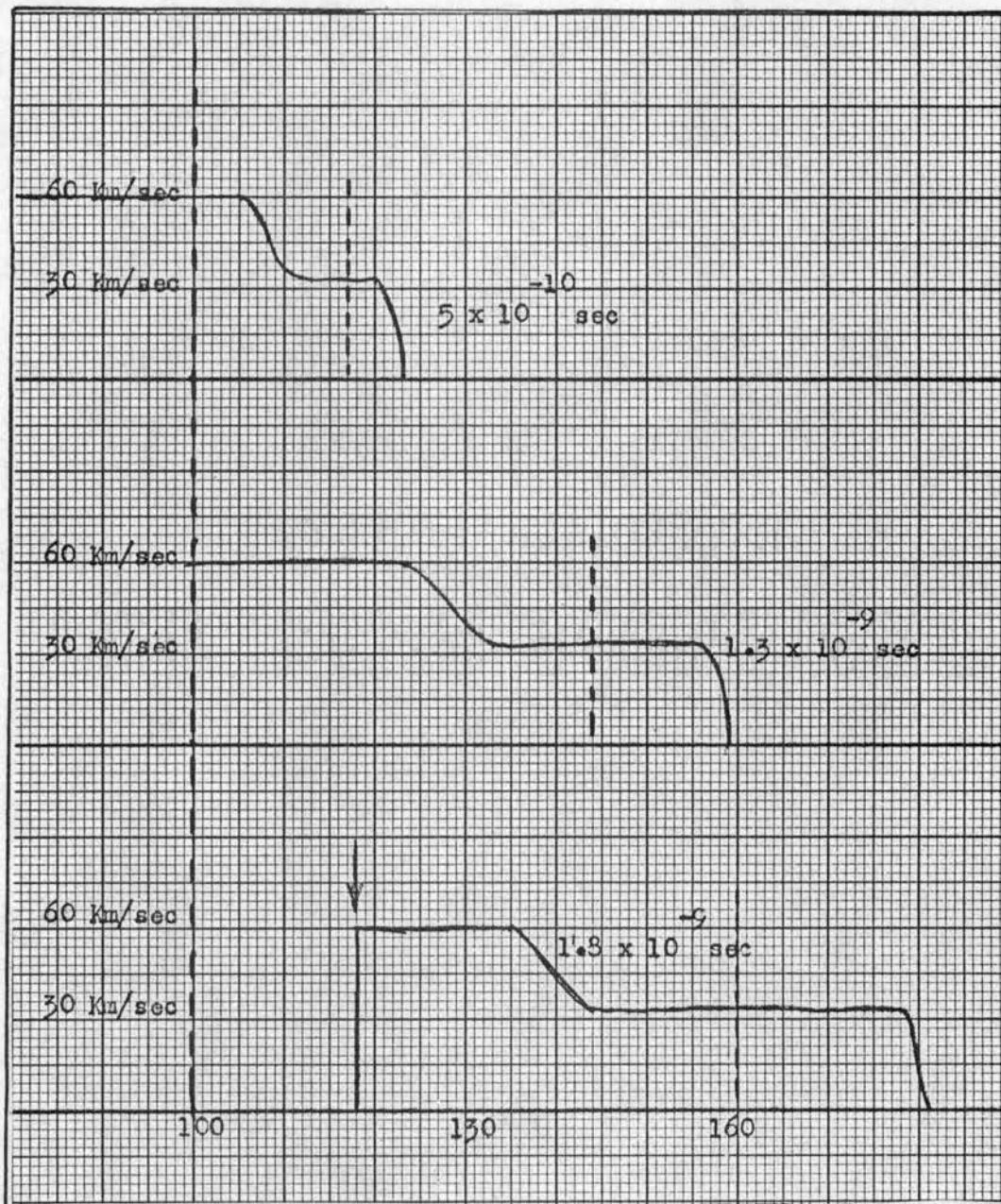Porosity 4 Traveling at 60.6
Km/sec

Figure 69. Velocity Profiles Resulting from
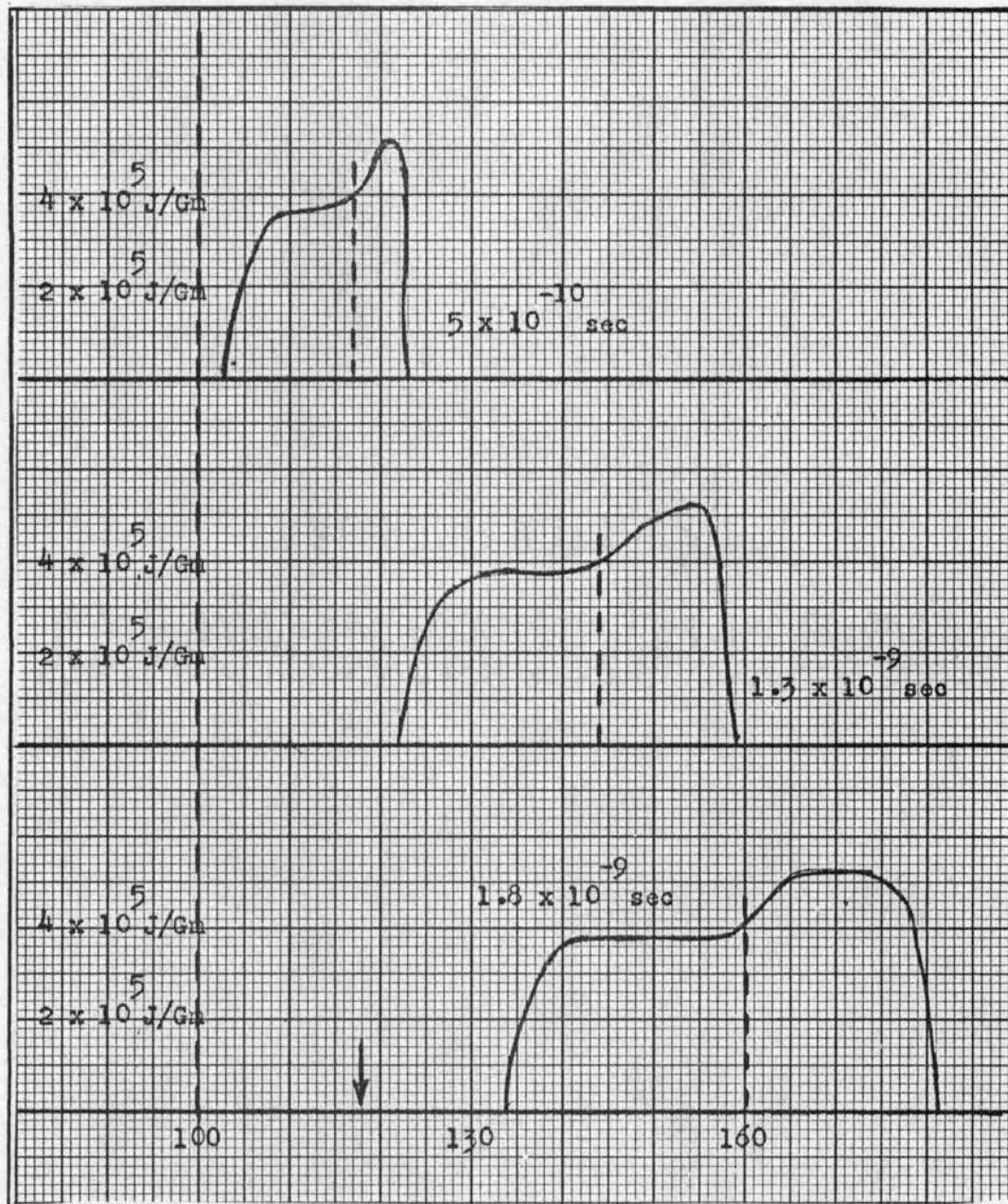Impact of Iron Plate of
Porosity 4 Traveling at 60.6
Km/sec

Figure 70. Internal Energy Profiles Resulting
from Impact of Iron Plate of
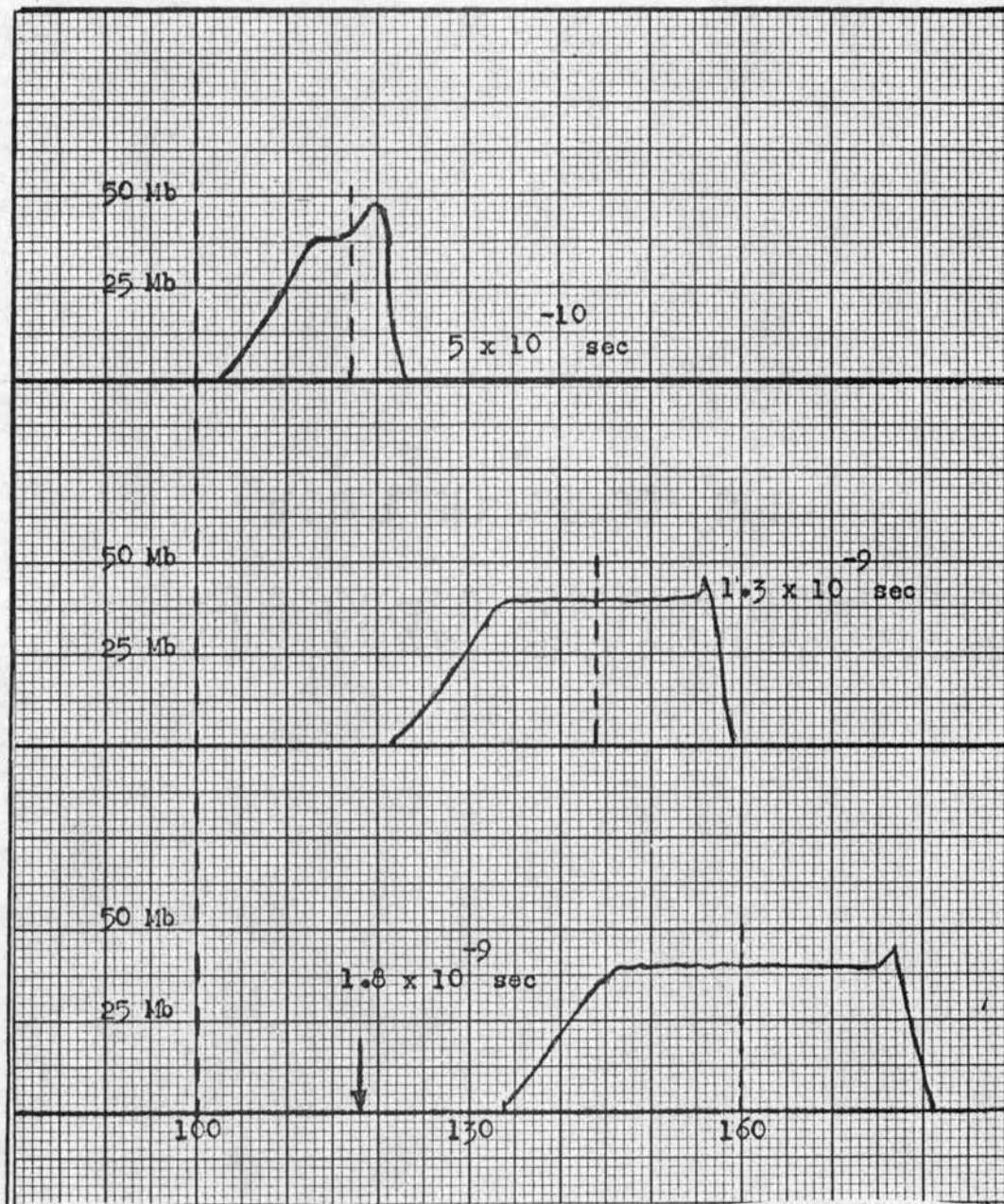Porosity 4 Traveling at 60.6
Km/sec

Figure 71. Pressure Profiles Resulting from
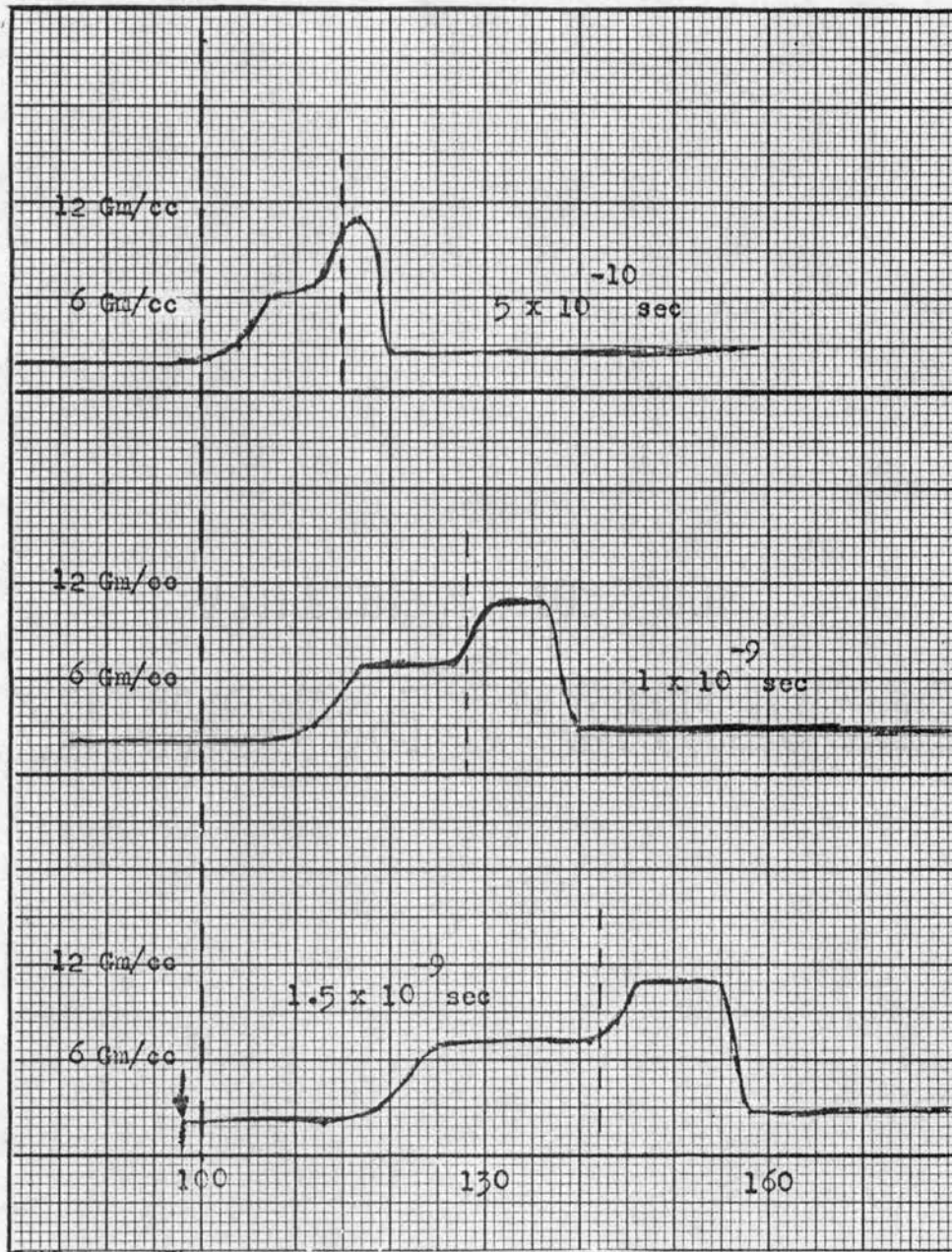Impact of Iron Plate of
Porosity 4 Traveling at 60.6
Km/sec

Figure 72. Density Profiles Resulting from
Impact of Stone Plate of
Porosity 1 Traveling at 15.2
Km/sec

Figure 73. Velocity Profiles Resulting from
Impact of Stone Plate of
Porosity 1 Traveling at 15.2
Km/sec

Figure 74. Internal Energy Profiles Resulting
from Impact of Stone Plate of
Porosity 1 Traveling at 15.2
Km/sec

Figure 75. Pressure Profiles Resulting from
Impact of Stone Plate of
Porosity 1 Traveling at 15.2
Km/sec

Figure 76. Density Profiles Resulting from
Impact of Stone Plate of
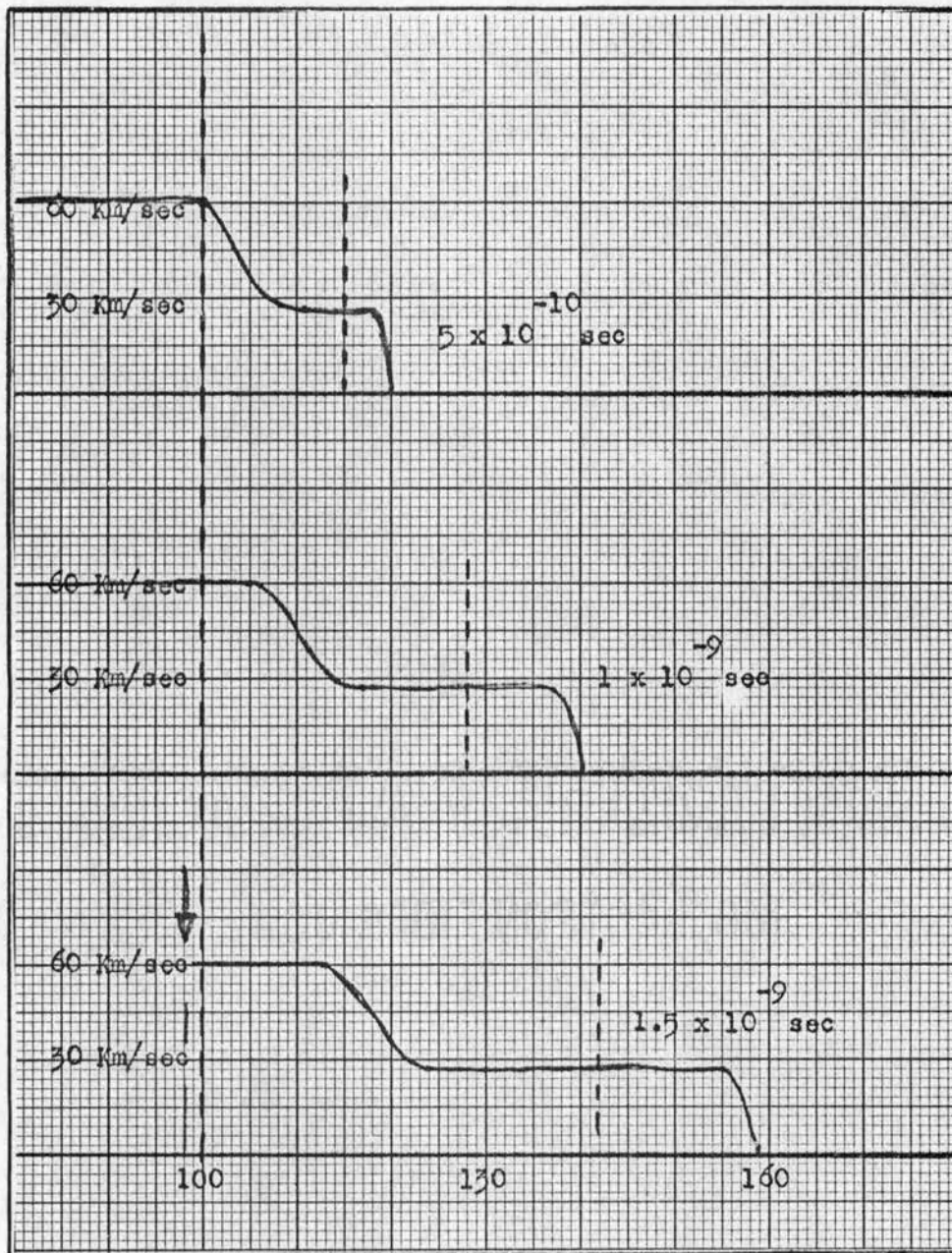Porosity 1.33 Traveling at
15.2 Km/sec

Figure 77. Velocity Profiles Resulting from
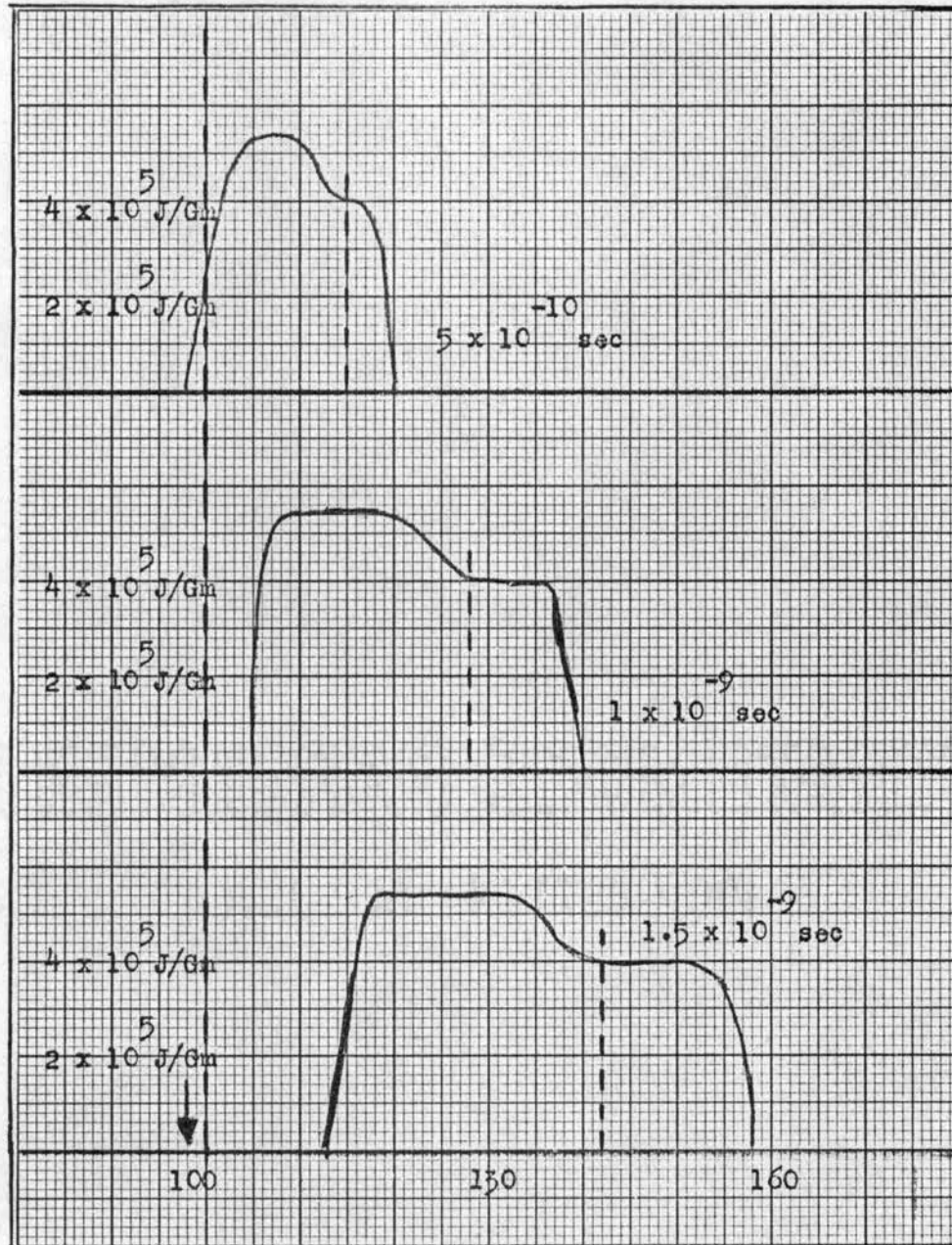Impact of Stone Plate of
Porosity 1.33 Traveling at
15.2 Km/sec

Figure 78. Internal Energy Profiles Resulting
from Impact of Stone Plate of
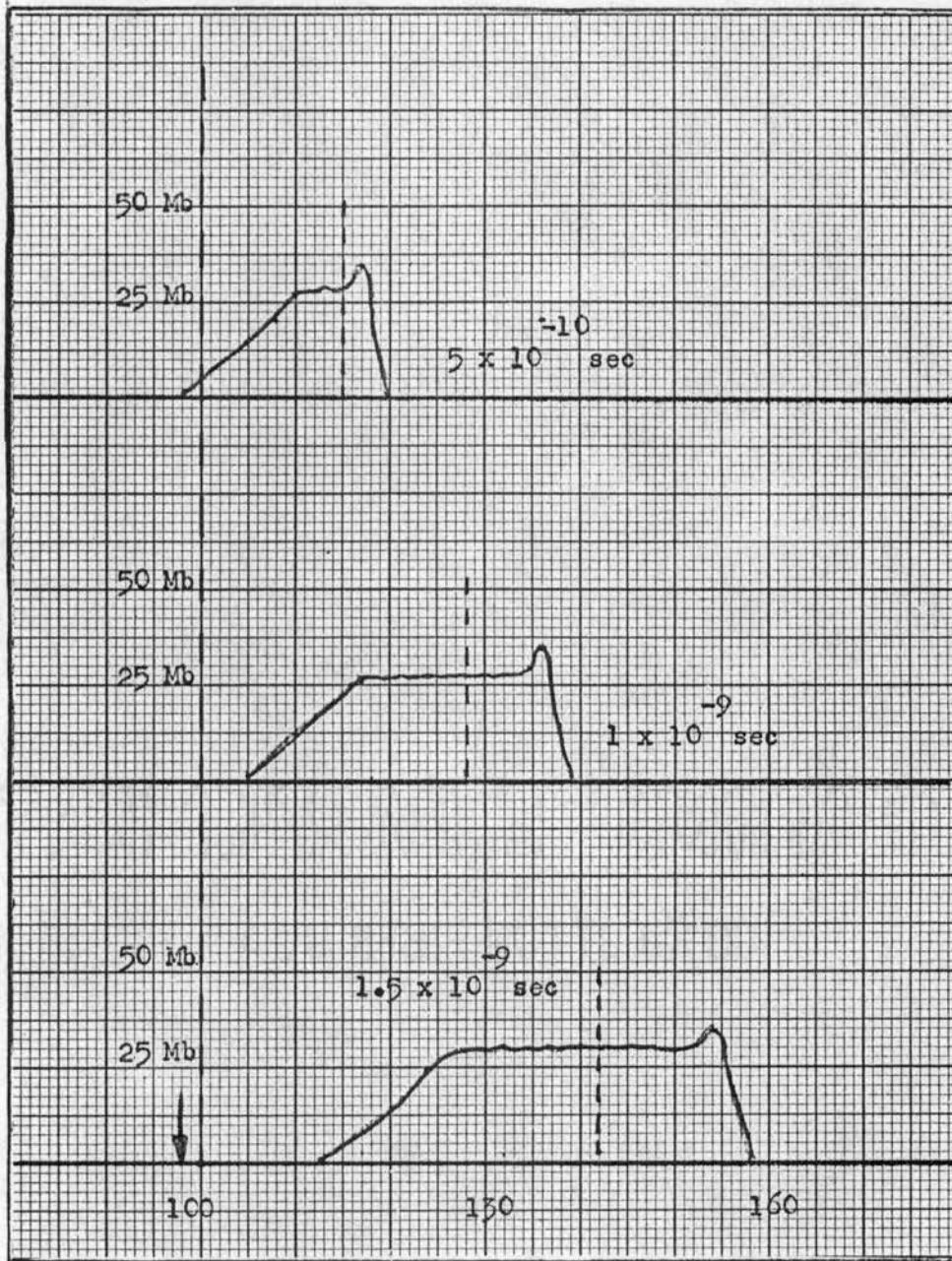Porosity 1.33 Traveling at
15.2 Km/sec

Figure 79. Pressure Profiles Resulting from
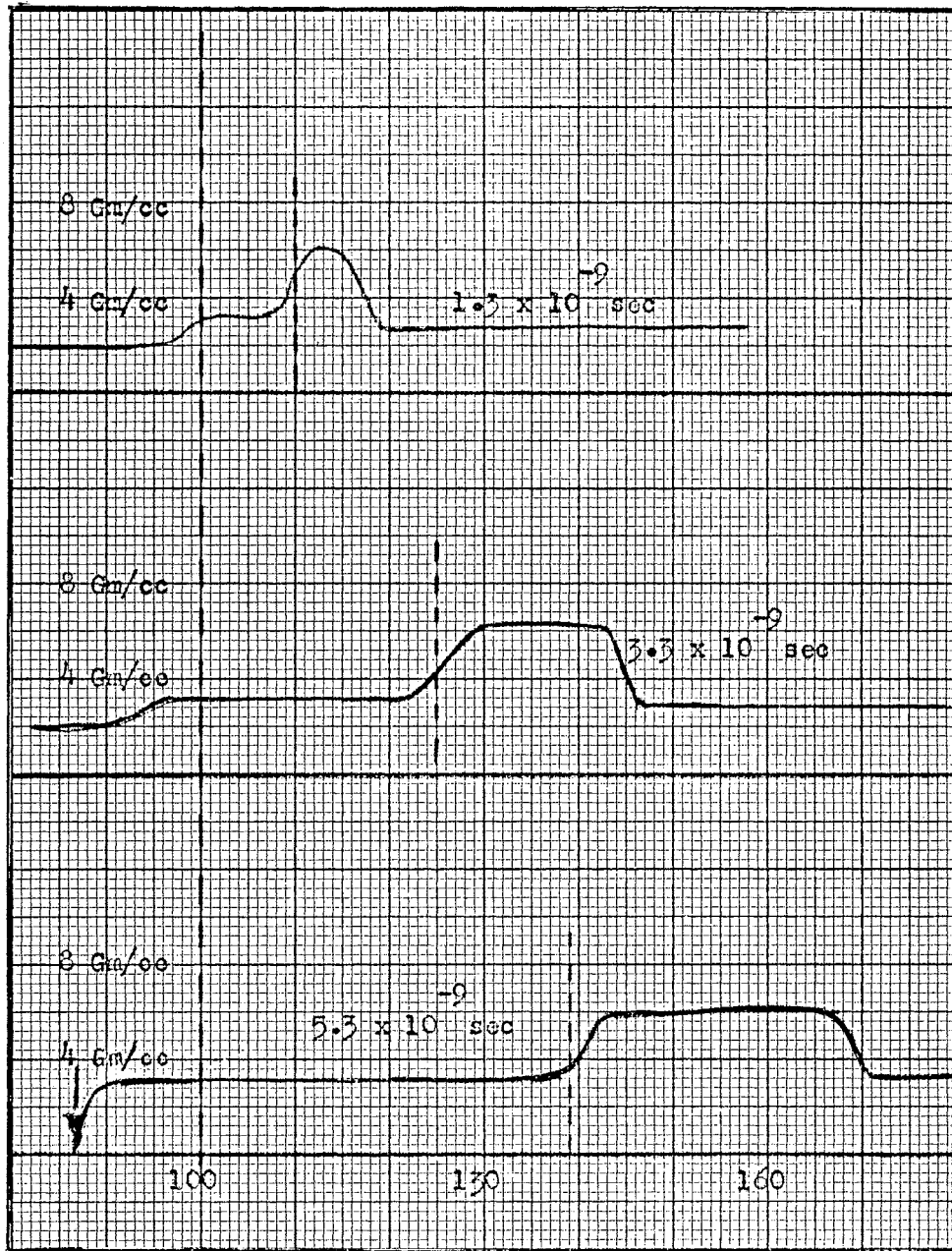Impact of Stone Plate of
Porosity 1.33 Traveling at
15.2 Km/sec

Figure 80. Density Profiles Resulting from
Impact of Stone Plate of
Porosity 2 Traveling at 15.2
Km/sec

Figure 81. Velocity Profiles Resulting from
Impact of Stone Plate of
Porosity 2 Traveling at 15.2
Km/sec

Figure 82. Internal Energy Profiles Resulting
from Impact of Stone Plate of
Porosity 2 Traveling at 15.2
Km/sec

Figure 83. Pressure Profiles Resulting from
Impact of Stone Plate of
Porosity 2 Traveling at 15.2
Km/sec

Figure 84. Density Profiles Resulting from
Impact of Stone Plate of
Porosity 1 Traveling at 36
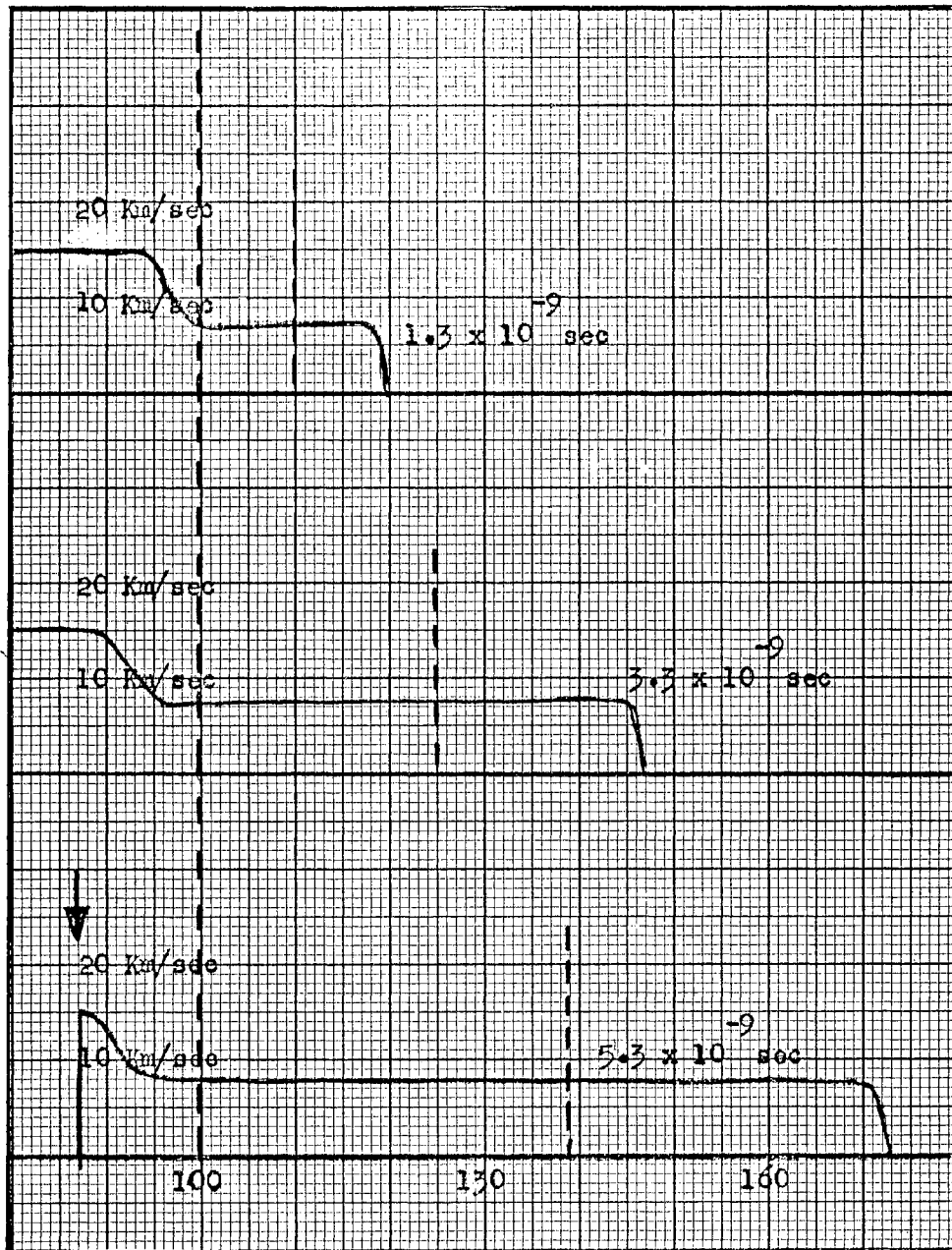Km/sec

Figure 85.   Velocity Profiles Resulting from
             Impact of Stone Plate of
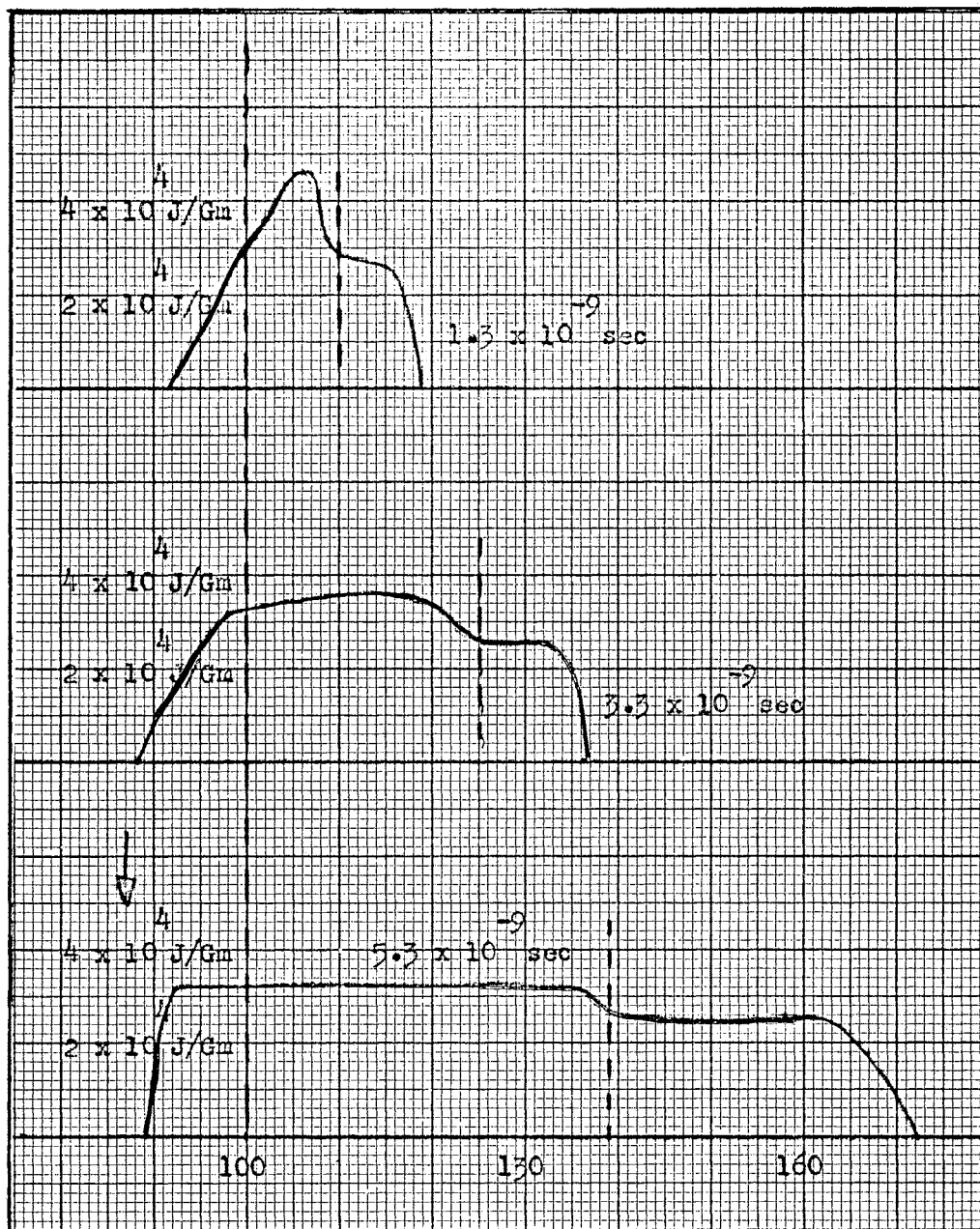   Porosity 1 Traveling at 36
             Km/sec

Figure 86. Internal Energy Profiles Resulting
Impact of Stone Plate of
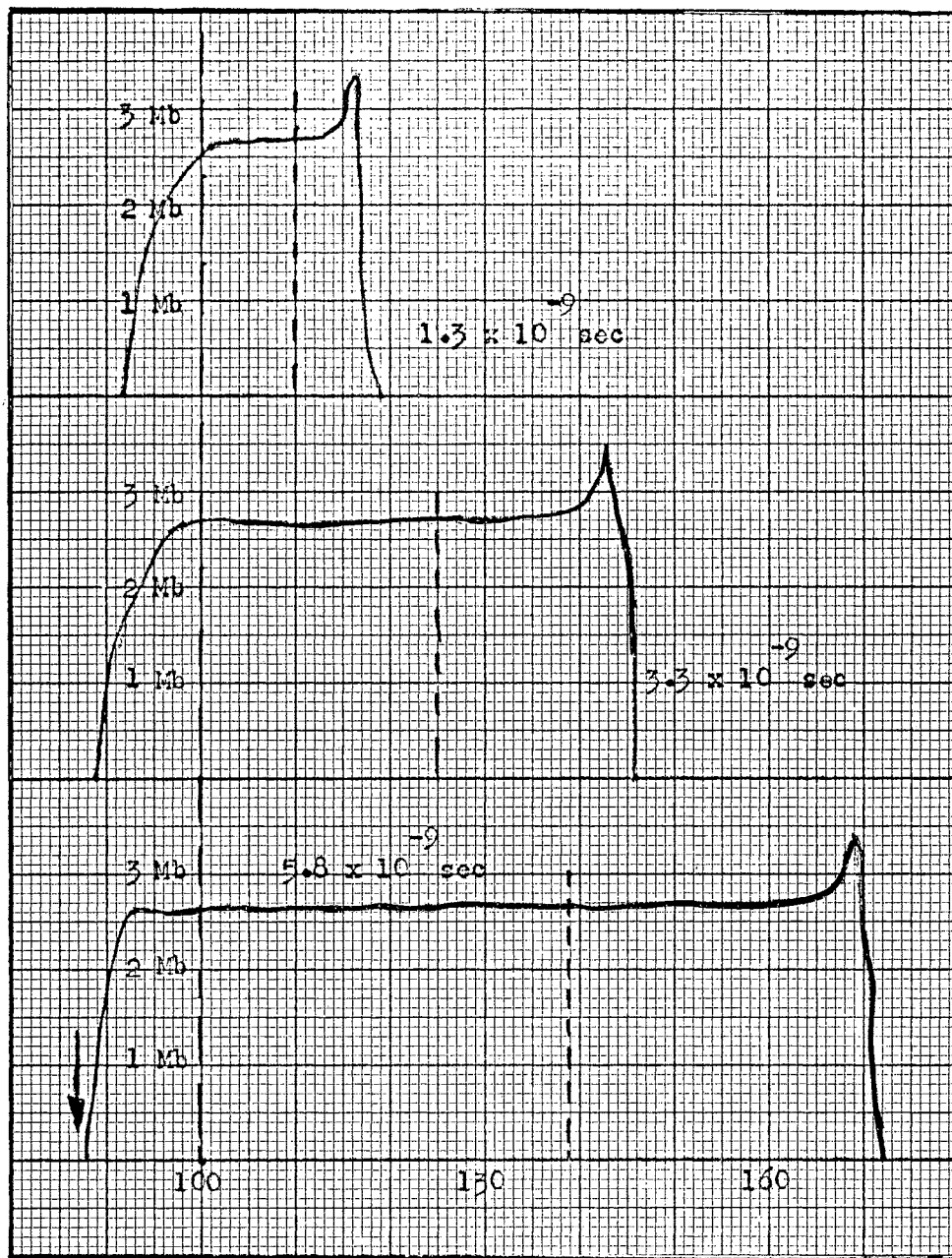Porosity 1 Traveling at 36
Km/sec

Figure 87. Pressure Profiles Resulting from
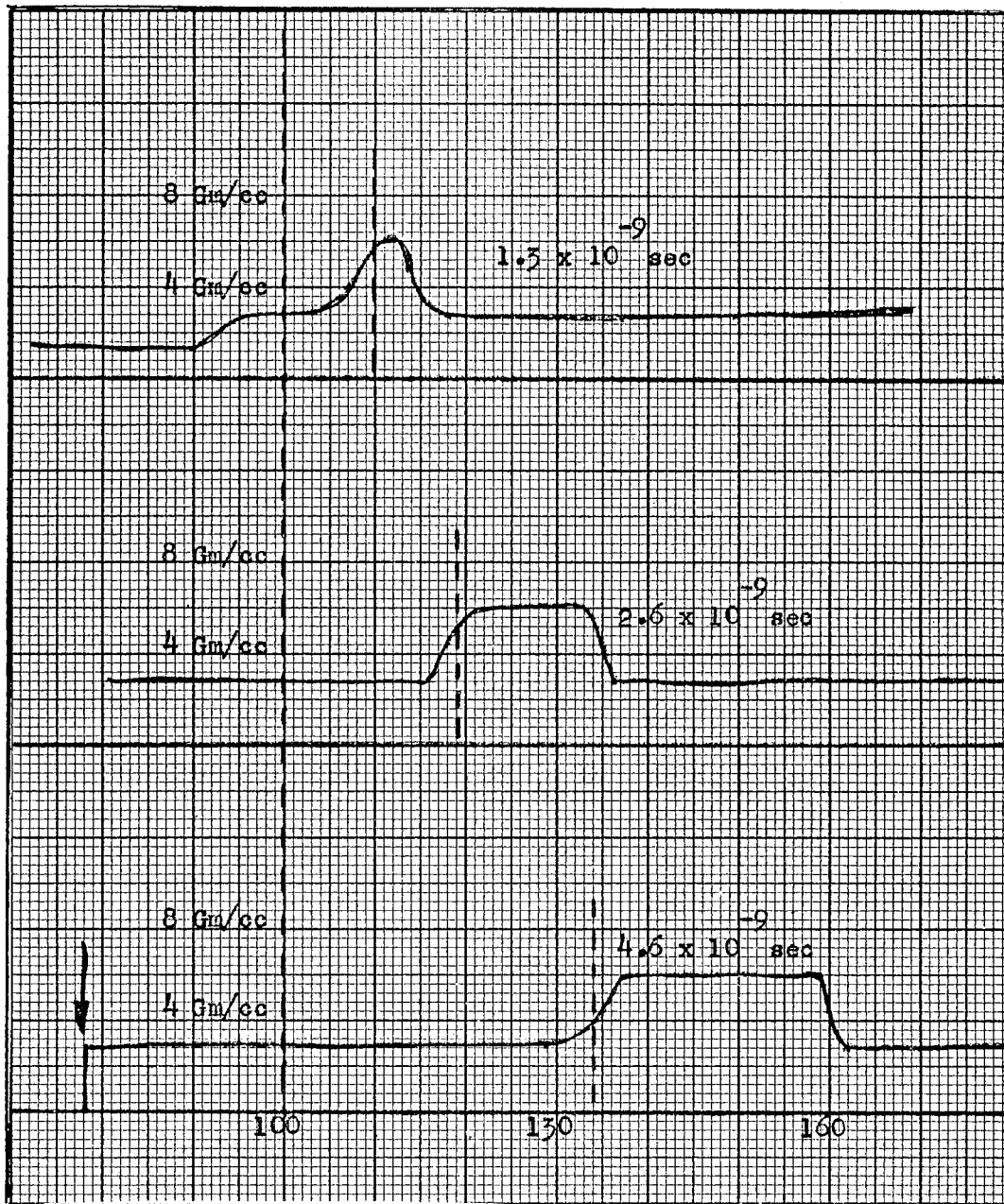Impact of Stone Plate of
Porosity 1 Traveling at 36
Km/sec

143

Figure 88. Density Profiles Resulting from
Impact of Stone Plate of
Porosity 1.33 Traveling at
36 Km/sec

Figure 89. Velocity Profiles Resulting from
Impact of Stone Plate of
Porosity 1.33 Traveling at
36 Km/sec

Figure 90. Internal Energy Profiles Resulting
from Impact of Stone Plate of
Porosity 1.33 Traveling at 36
Km/sec

Figure 91. Pressure Profiles Resulting from
Impact of Stone Plate of
Porosity 1.33 Traveling at
36 Km/sec

Figure 92. Density Profiles Resulting from
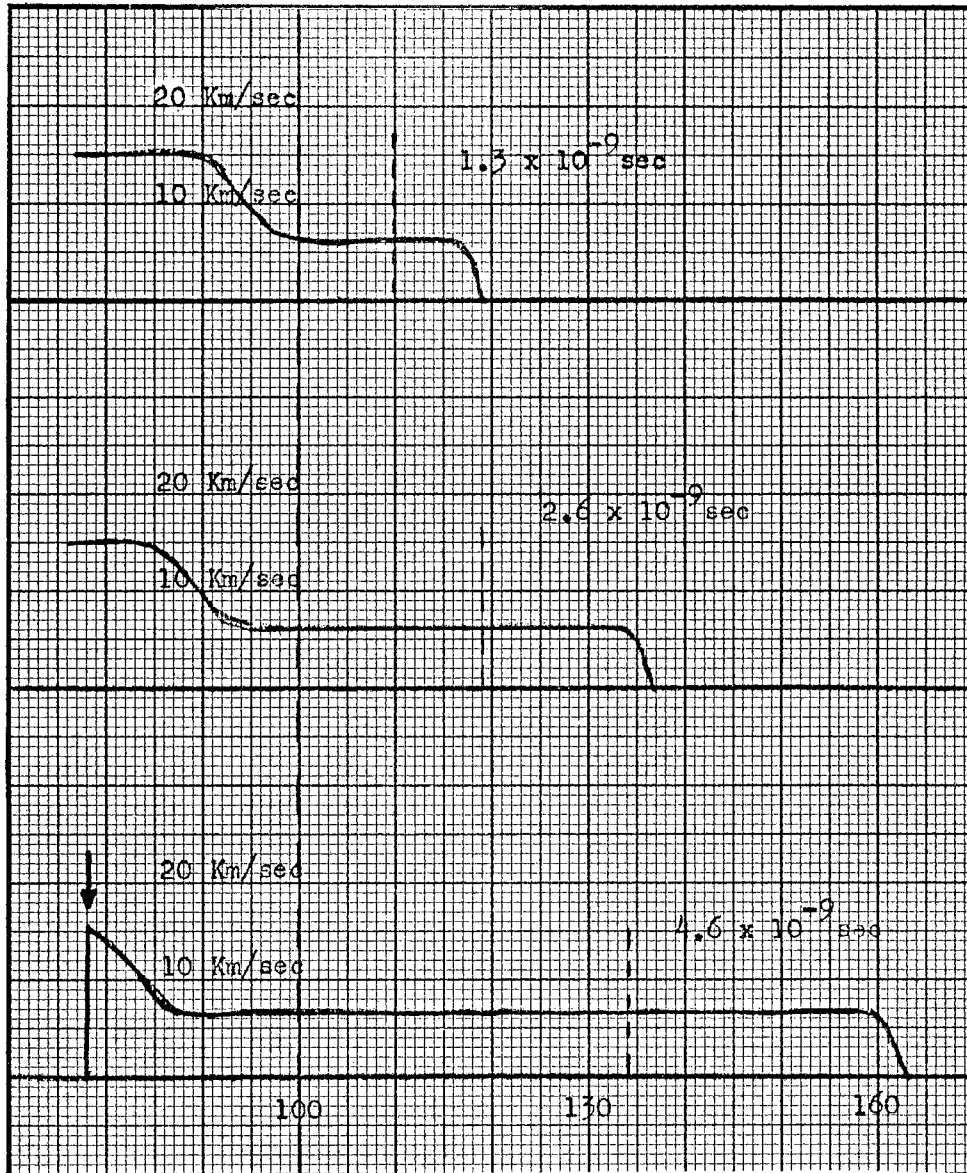Impact of Stone Plate of
Porosity 2 Traveling at 36
Km/sec
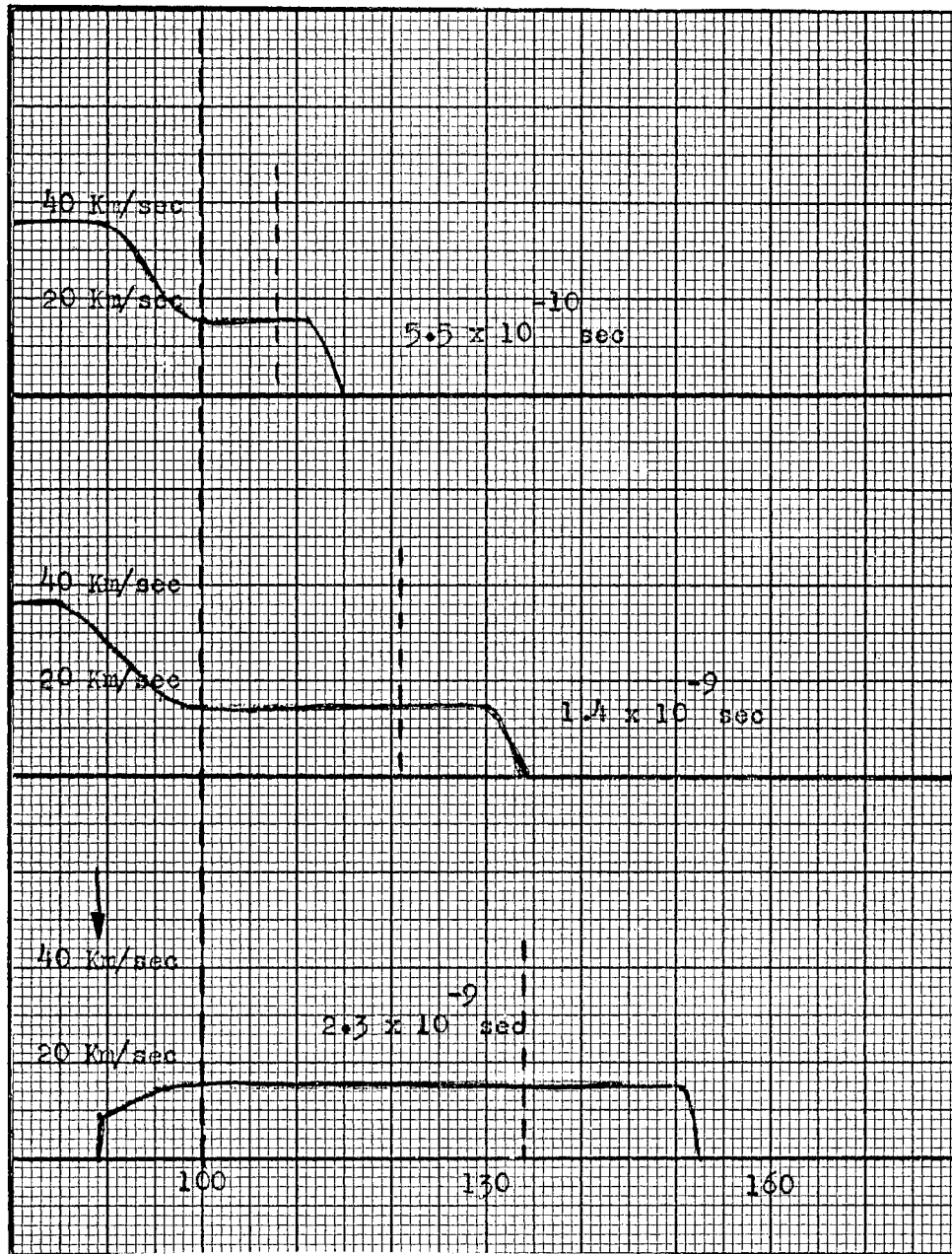
Figure 93. Velocity Profiles Resulting from
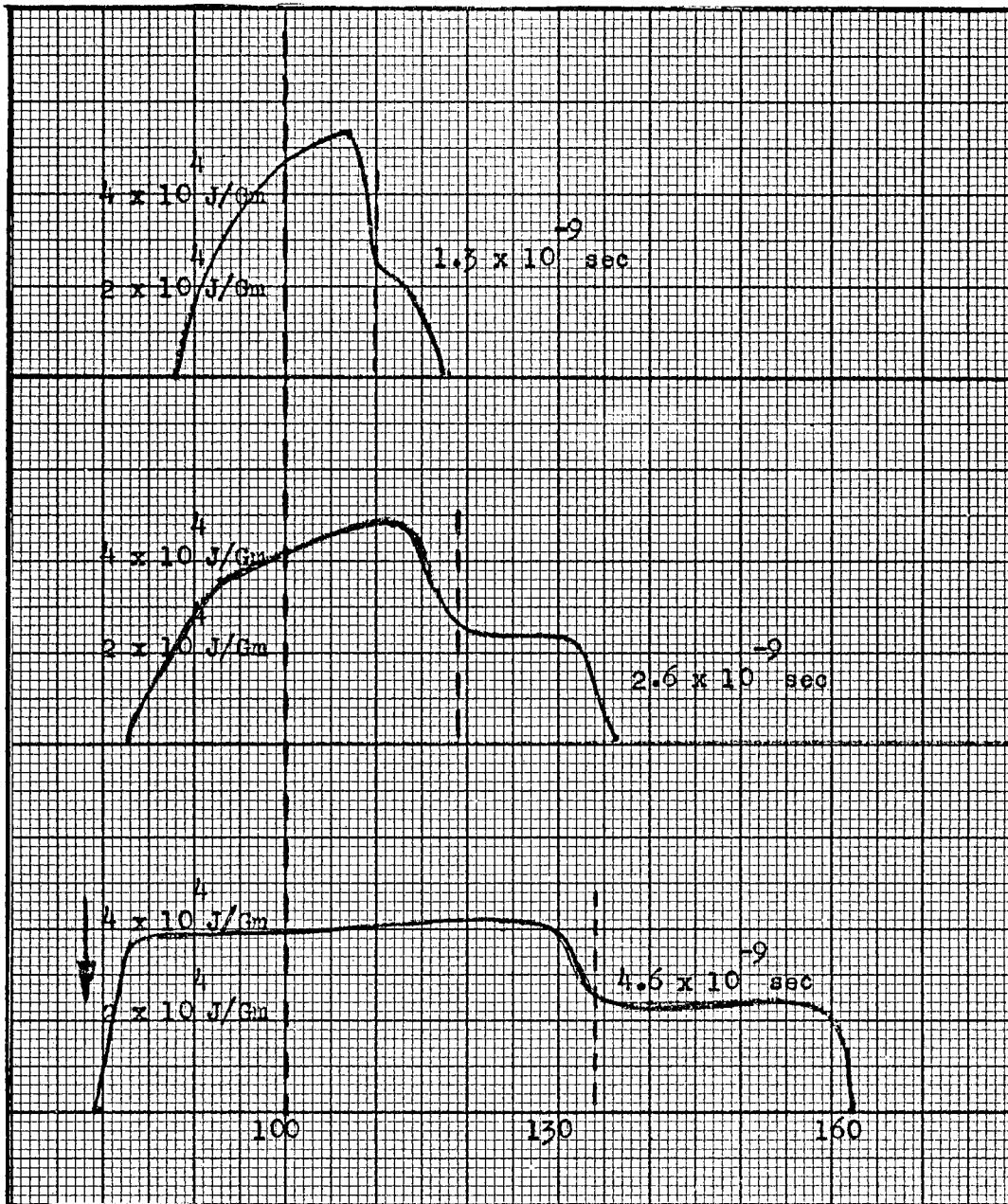Impact of Stone Plate of
Porosity 2 Traveling at 36
Km/sec
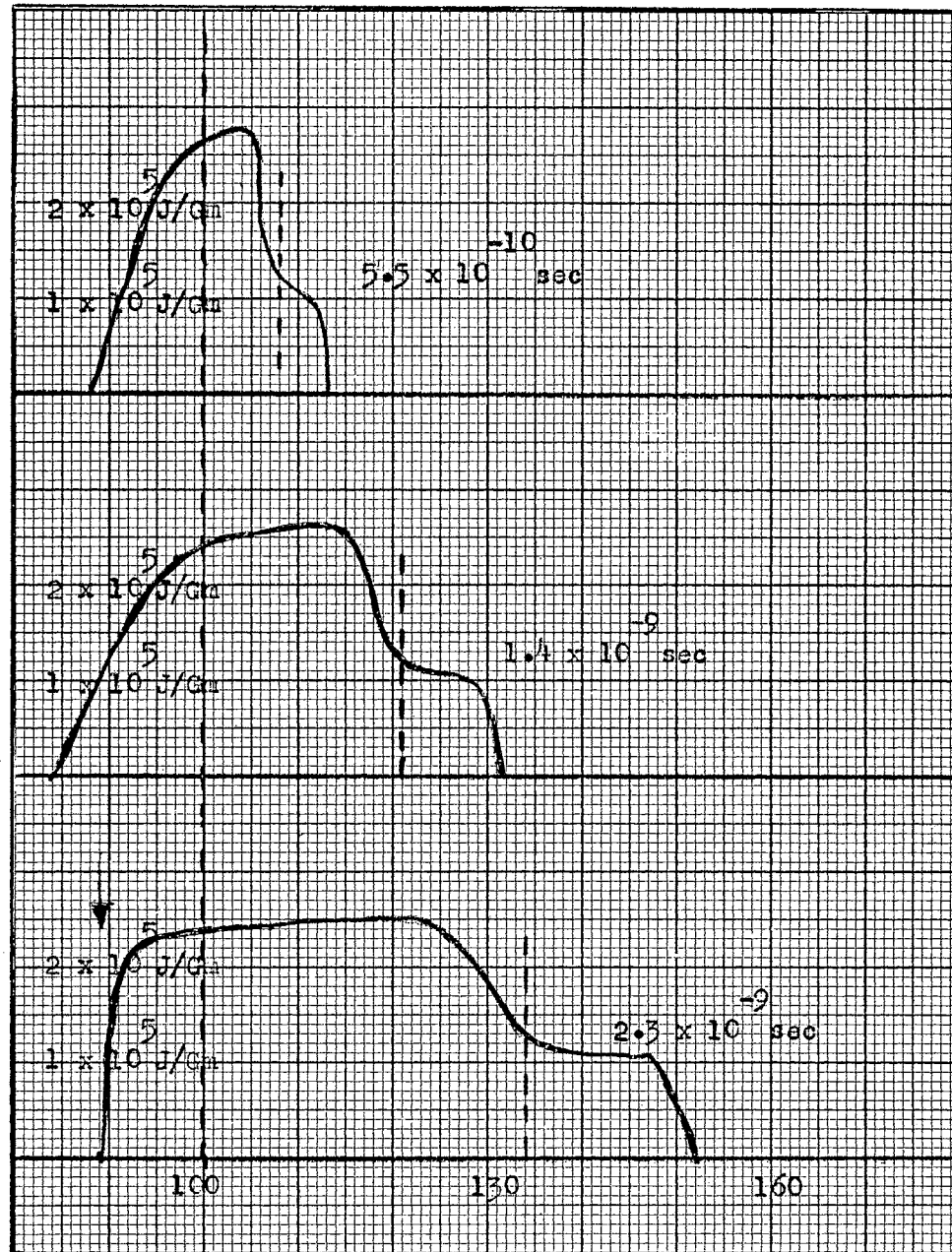
Figure 94. Internal Energy Profiles Resulting
from Impact of Stone Plate of
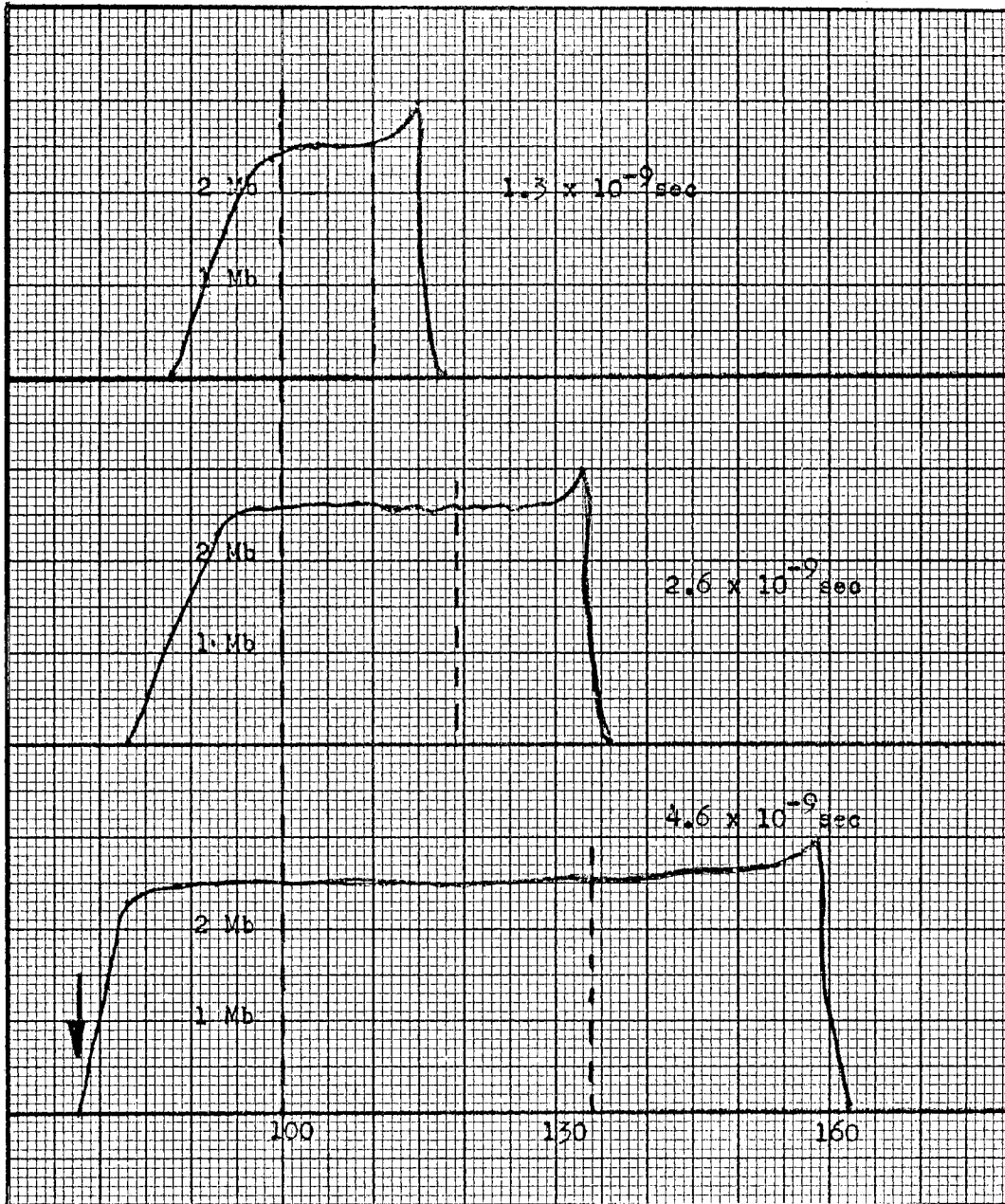Porosity 2 Traveling at 36
Km/sec
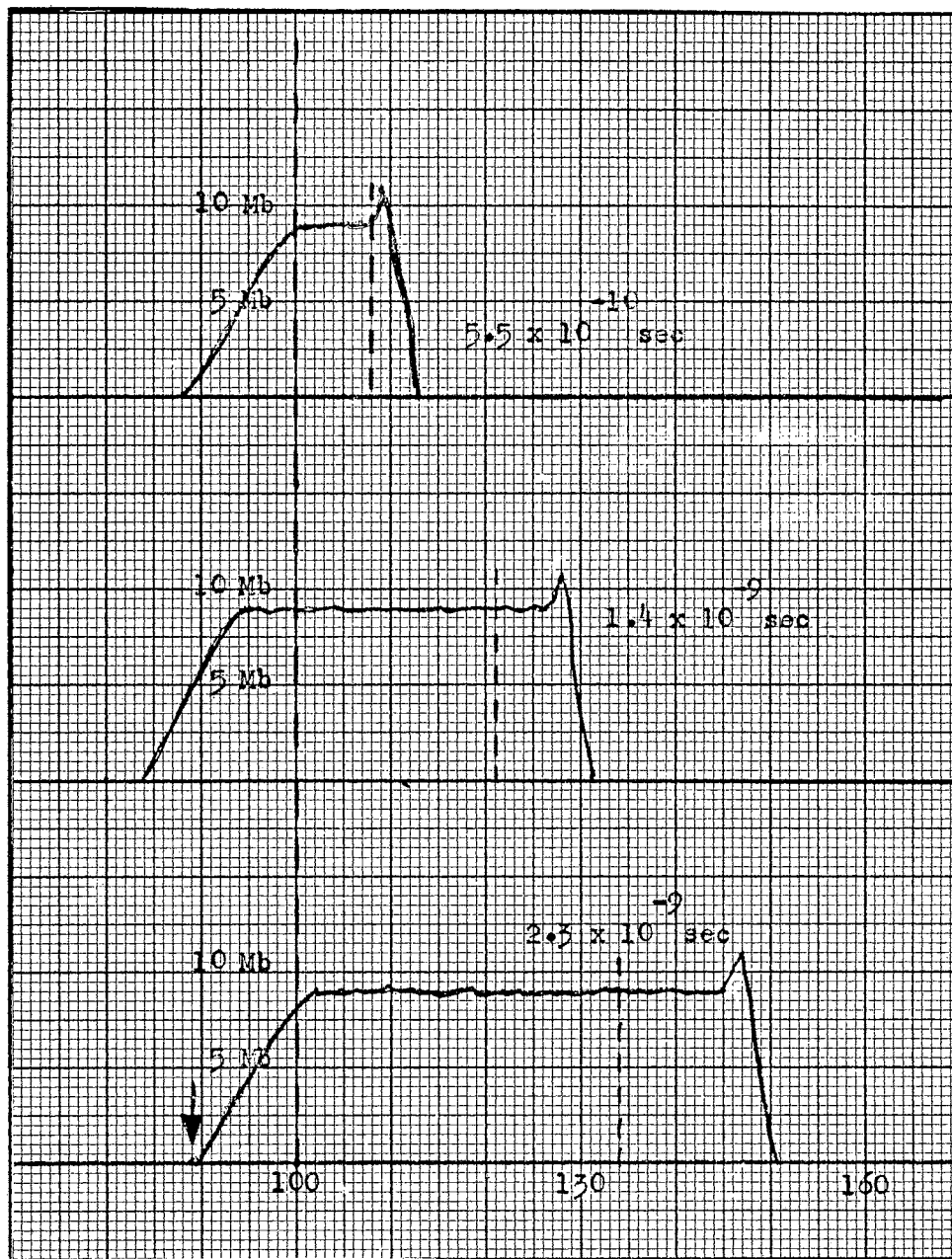
Figure 95. Pressure Profiles Resulting from
            Impact of Stone Plate of
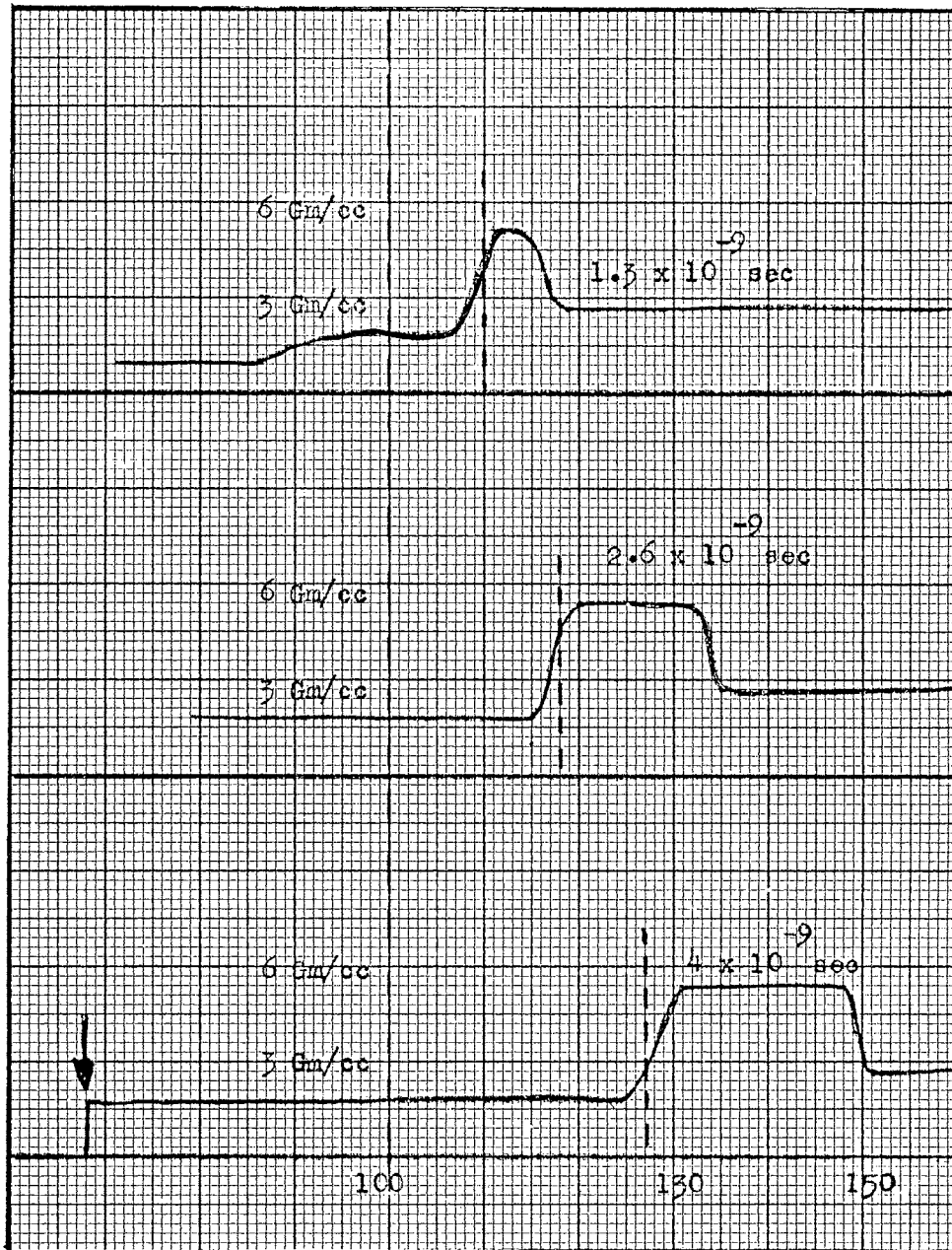   Porosity 2 Traveling at 36
            Km/sec
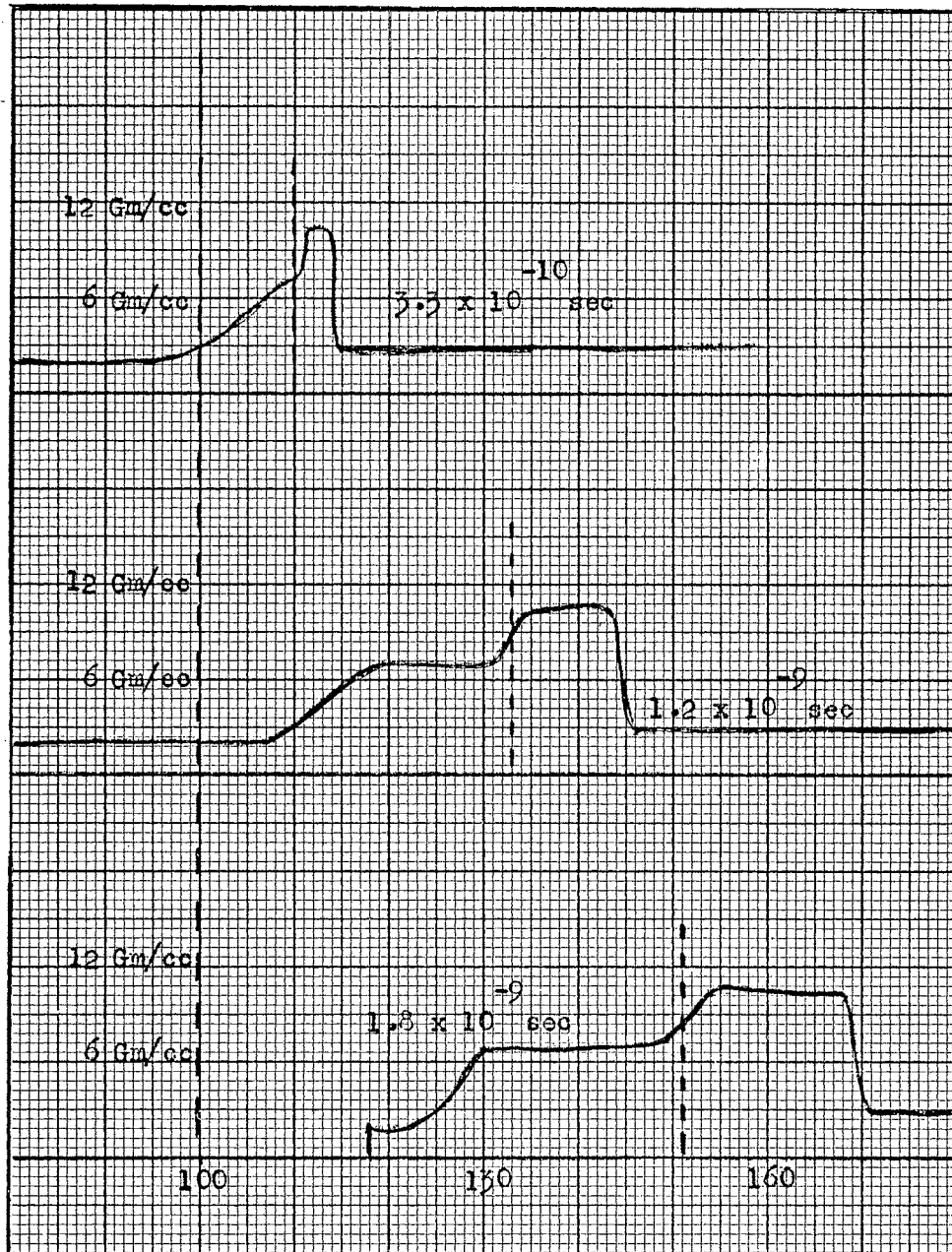
Figure 96. Density Profiles Resulting from
Impact of Stone Plate of
Porosity 1 Traveling at 60.6
Km/sec
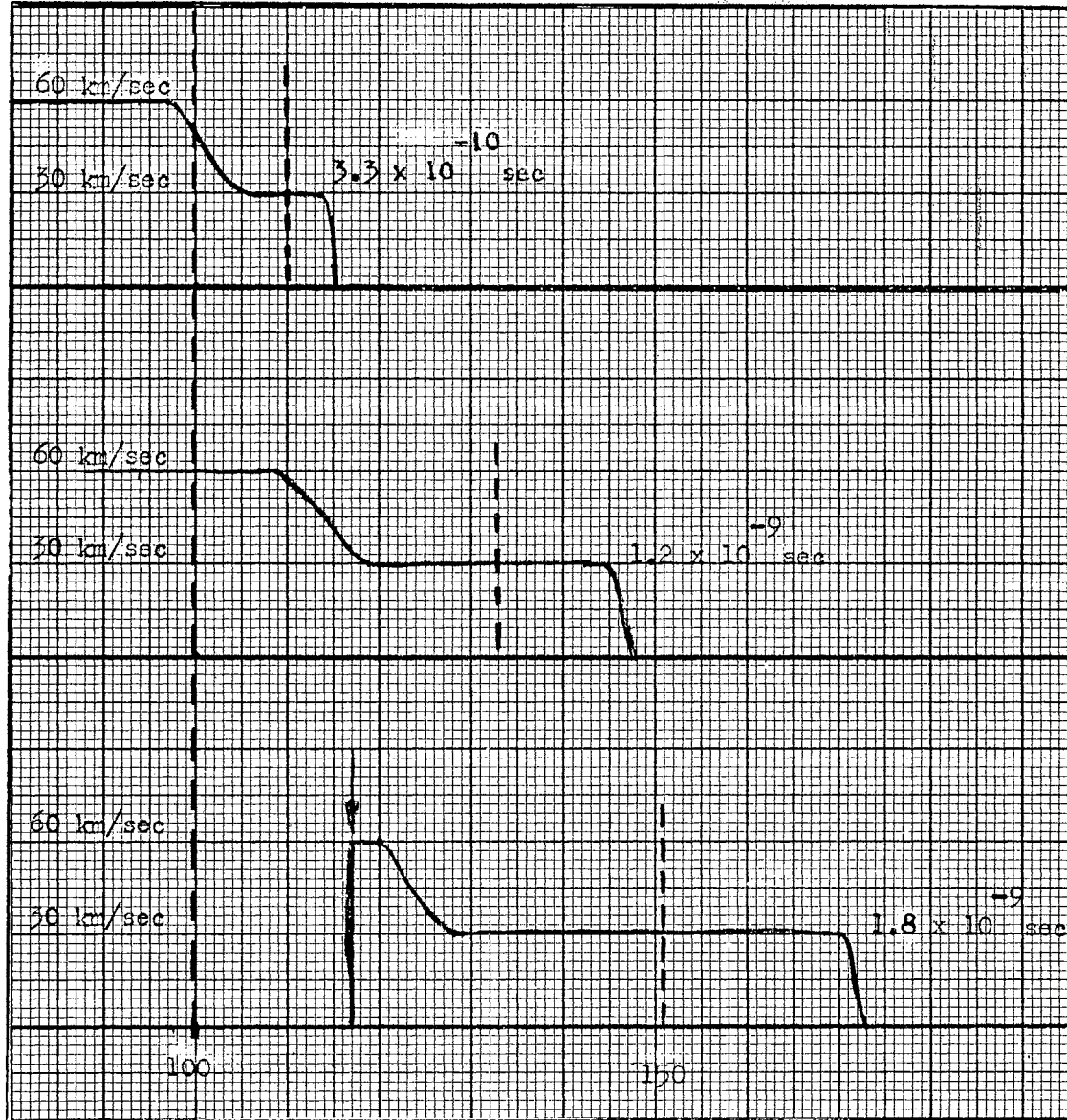
Figure 97. Velocity Profiles Resulting from
Impact of Stone Plate of
Porosity 1 Traveling at 60.6
Km/sec
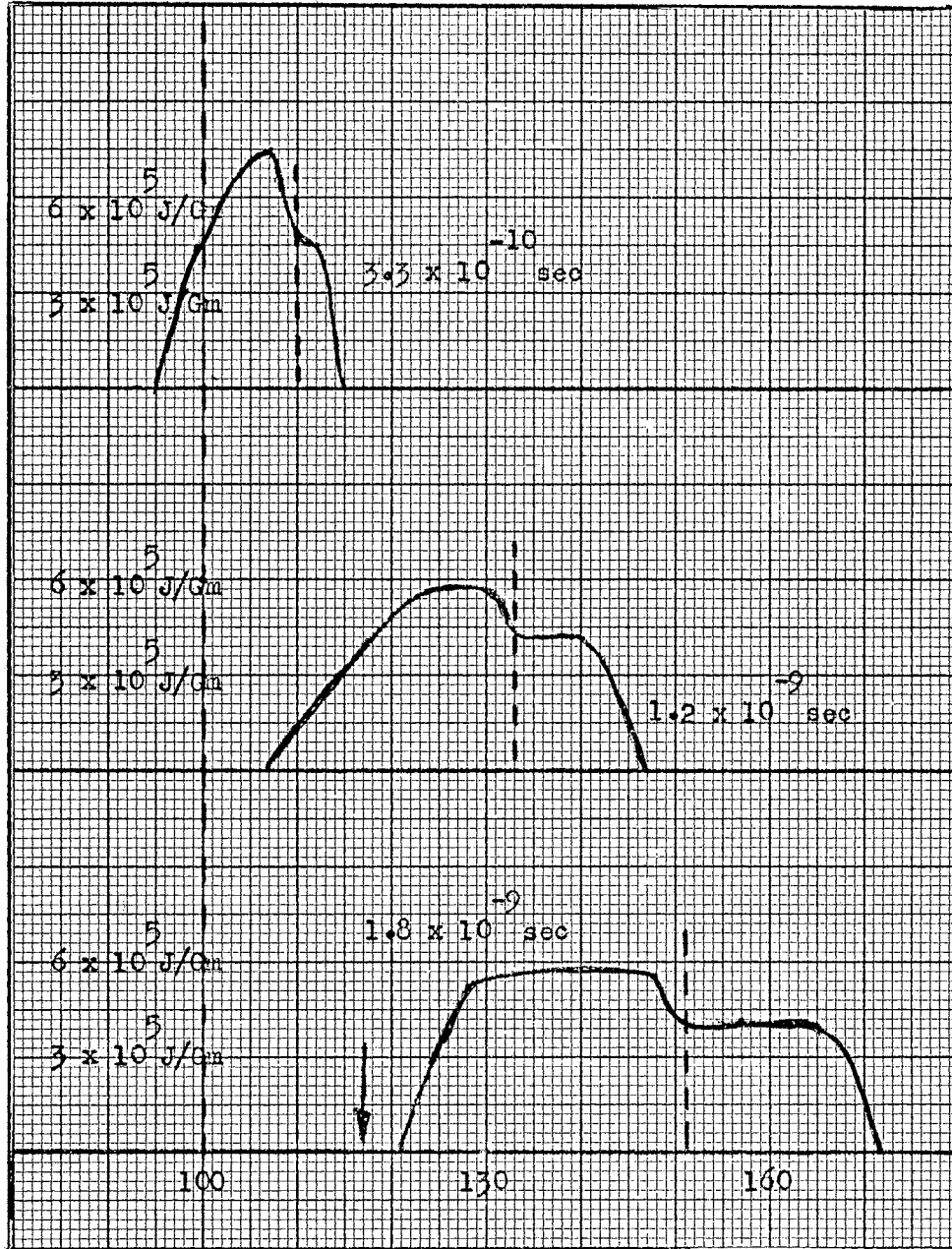
Figure 98. Internal Energy Profiles Resulting
from Impact of Stone Plate of
Porosity 1 Traveling at 60.6
Km/sec
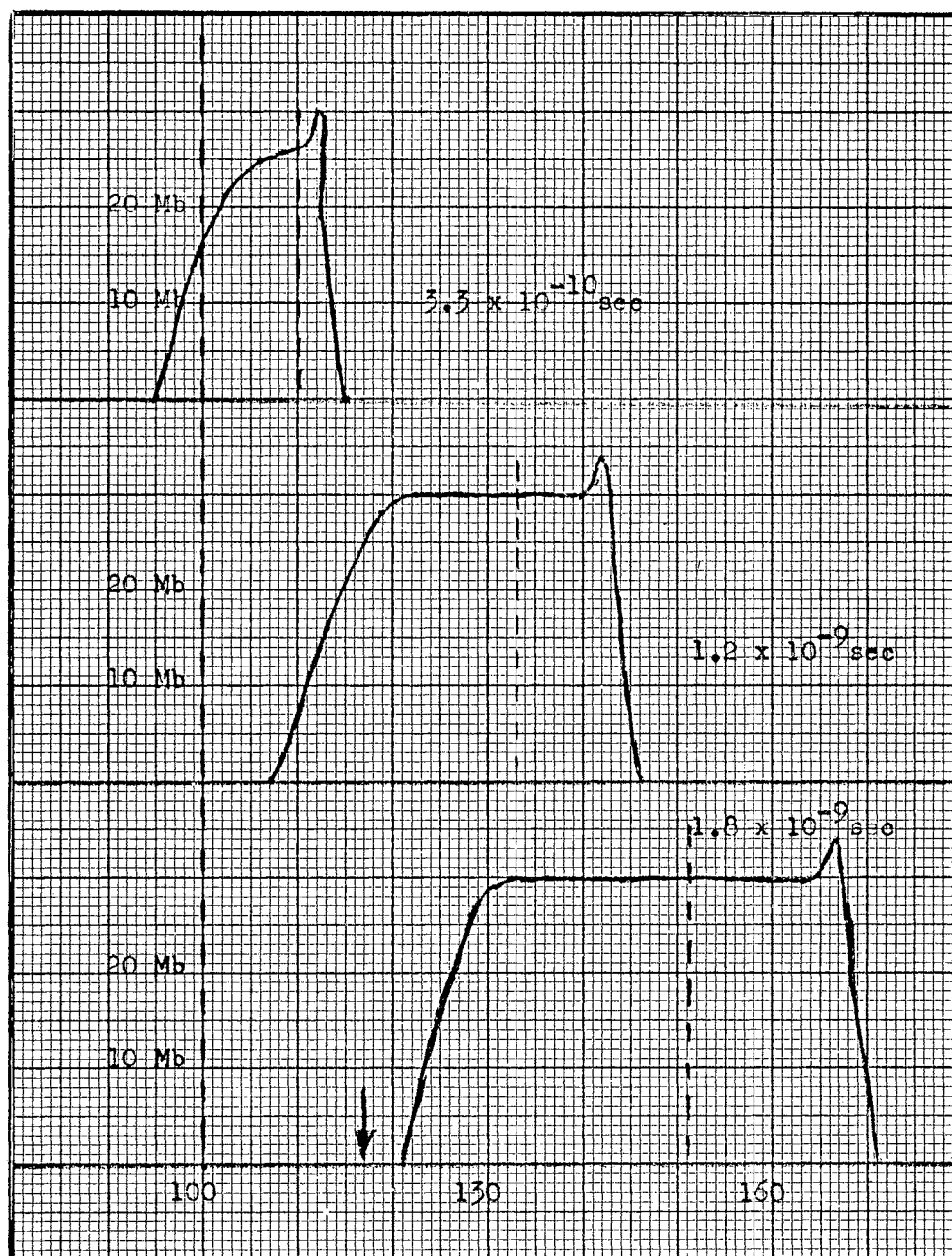
Figure 99. Pressure Profiles Resulting from
Impact of Stone Plate of
Porosity 1 Traveling at 60.6
Km/sec
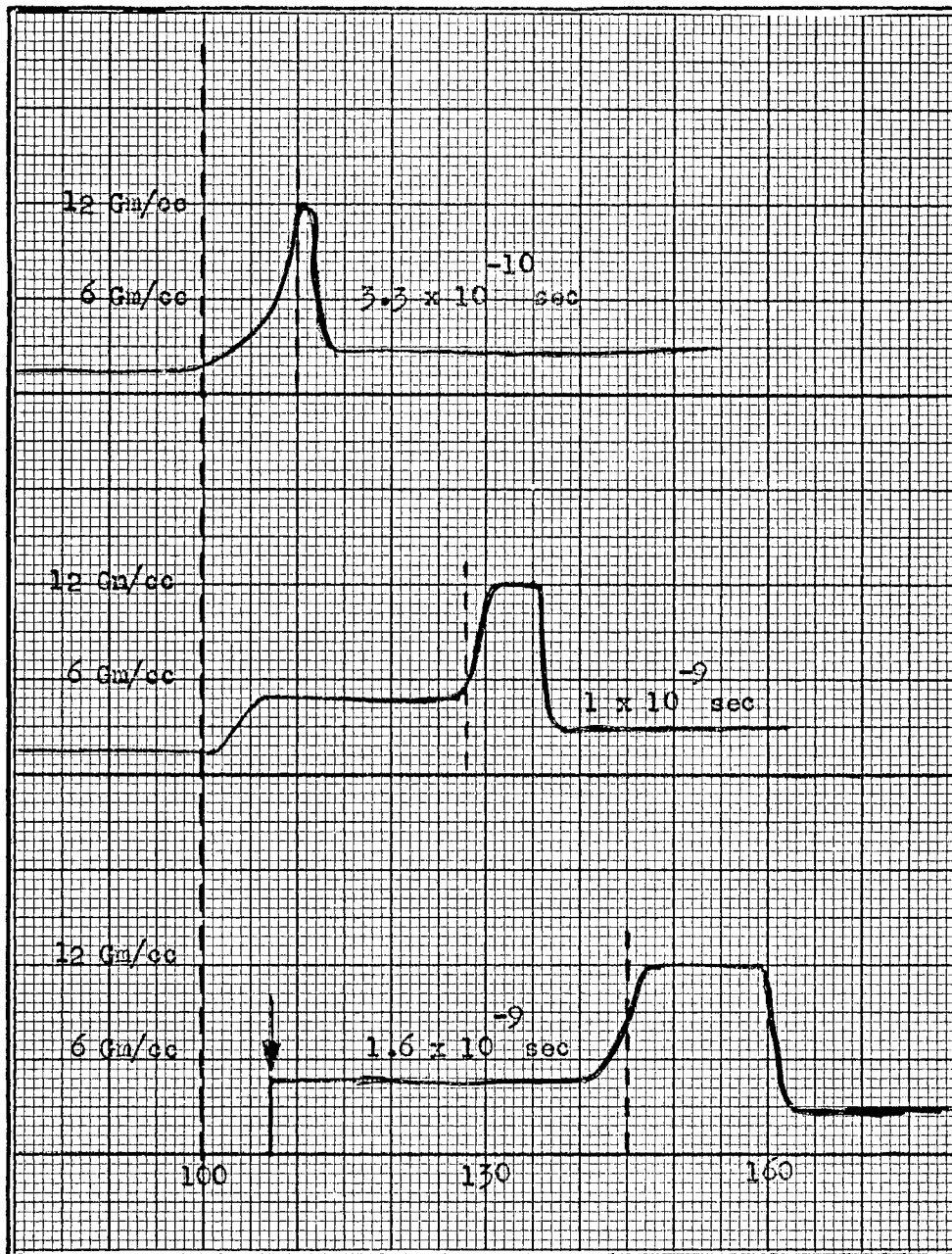
Figure 100. Density Profiles Resulting from
Impact of Stone Plate of
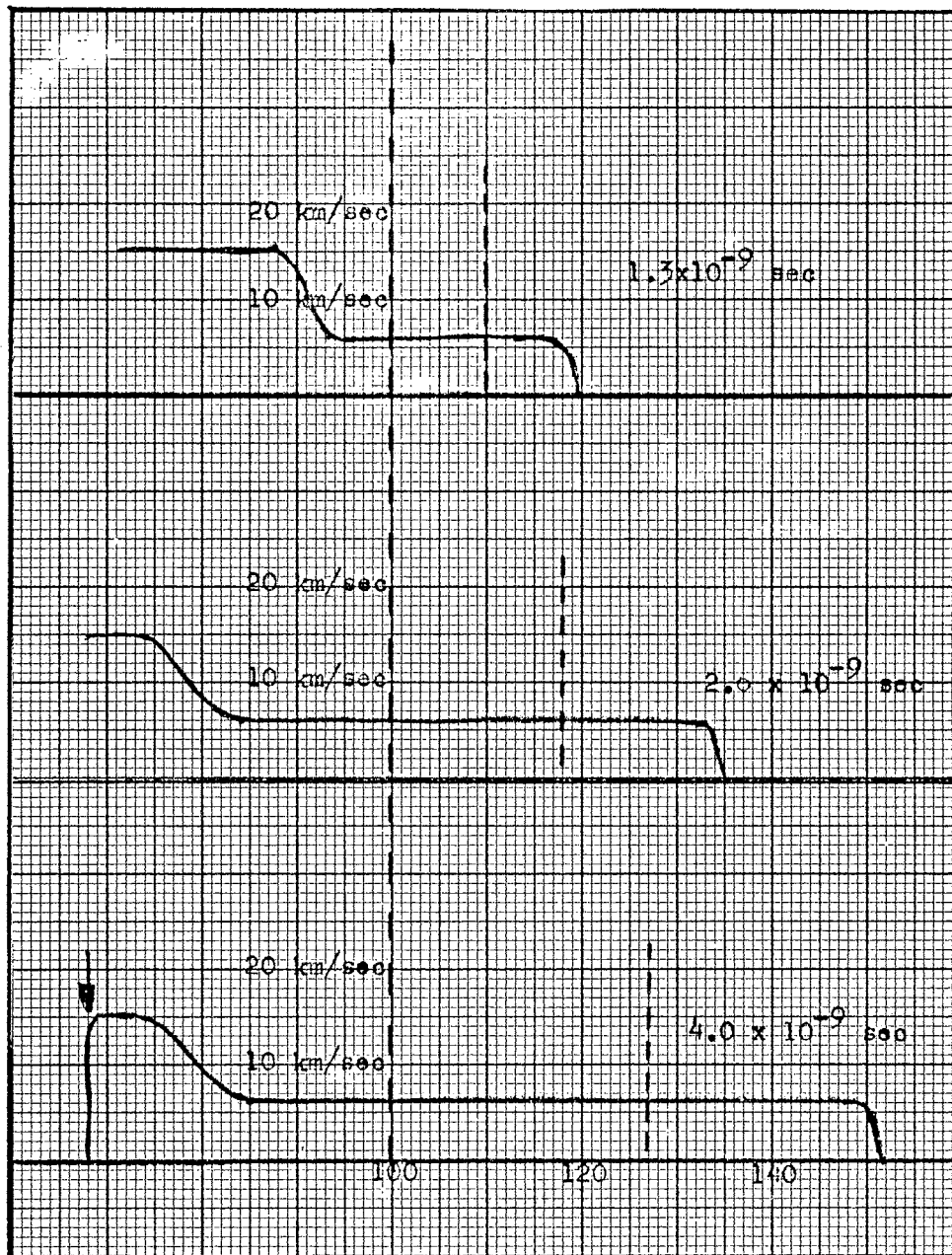Porosity 1.33 Traveling at
60.6 Km/sec
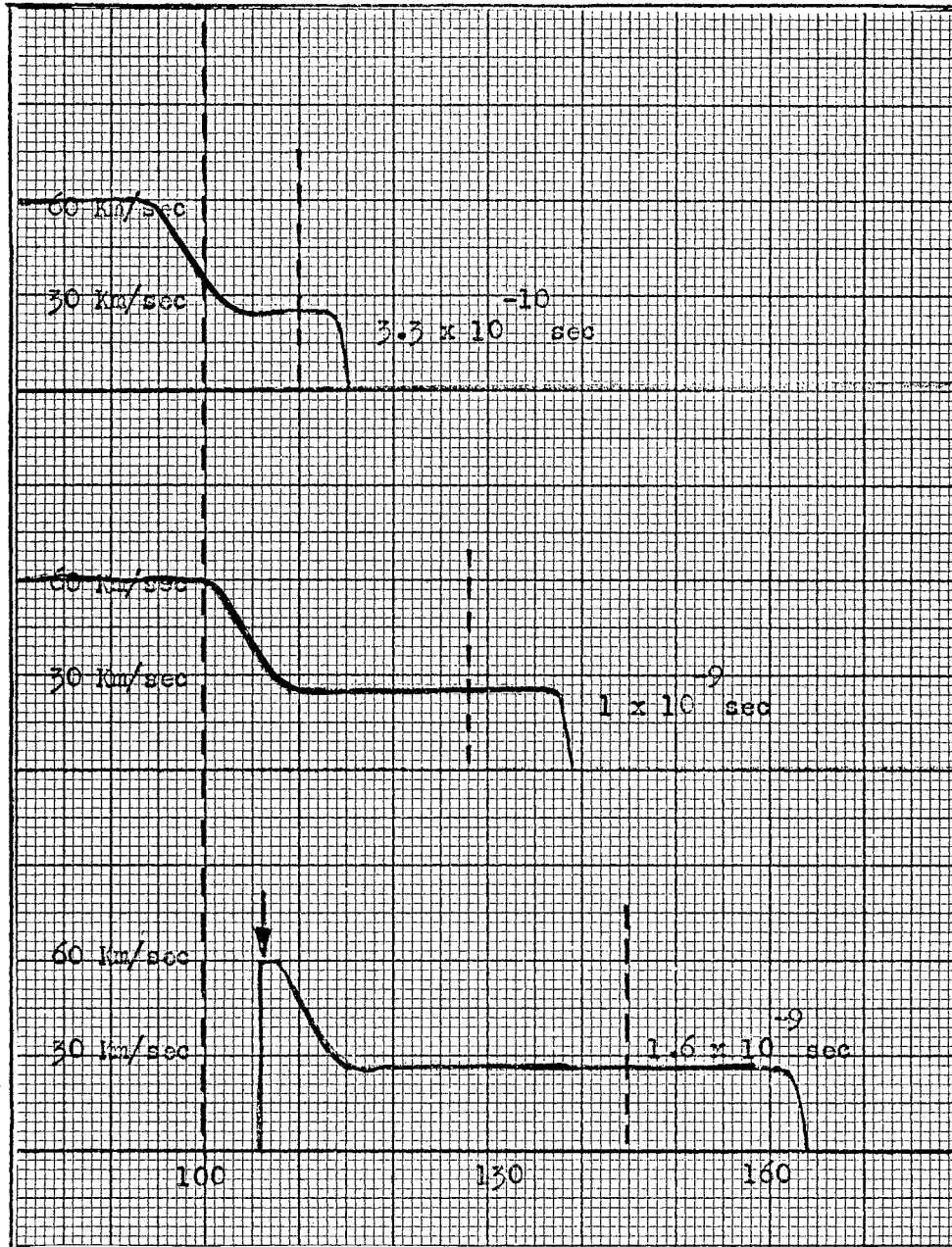
Figure 101.   Velocity Profiles Resulting from
Impact of Stone Plate of
Porosity 1.33 Traveling at
60.6 Km/sec
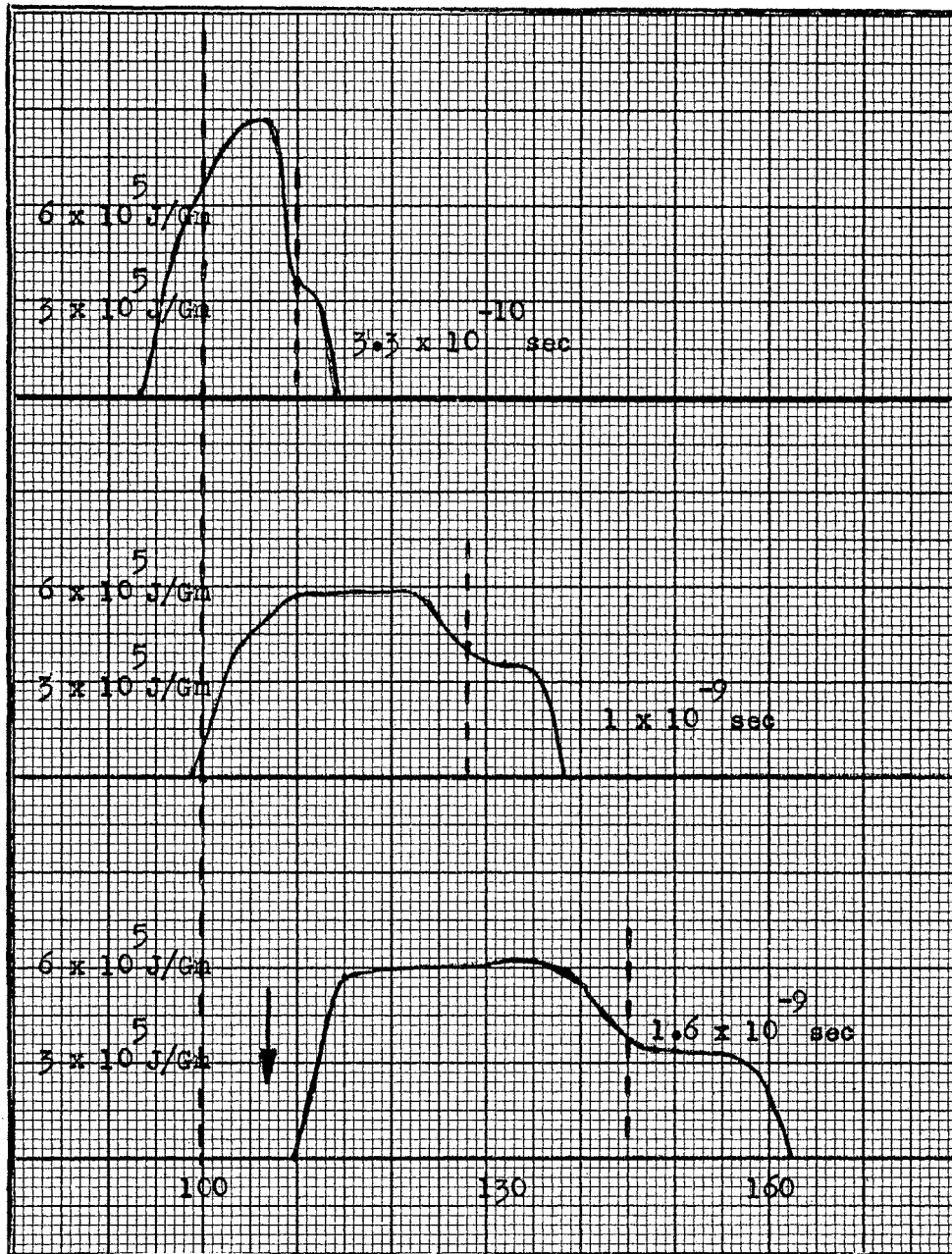
Figure 102. Internal Energy Profiles Resulting
from Impact of Stone Plate of
Porosity 1.33 Traveling at
60.6 Km/sec
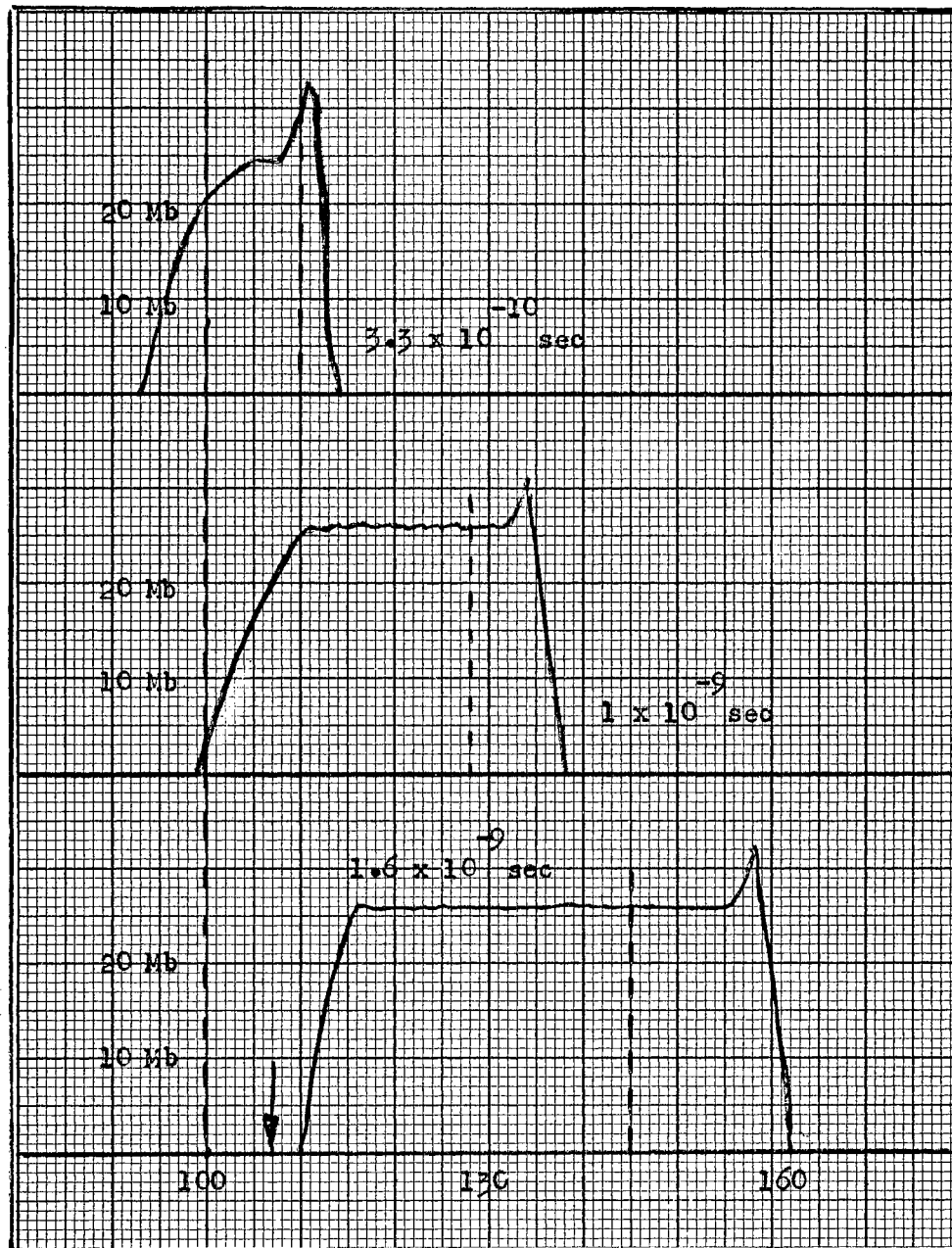
Figure 103. Pressure Profiles Resulting from
Impact of Stone Plate of
Porosity 1.33 Traveling at
60.6 Km/sec
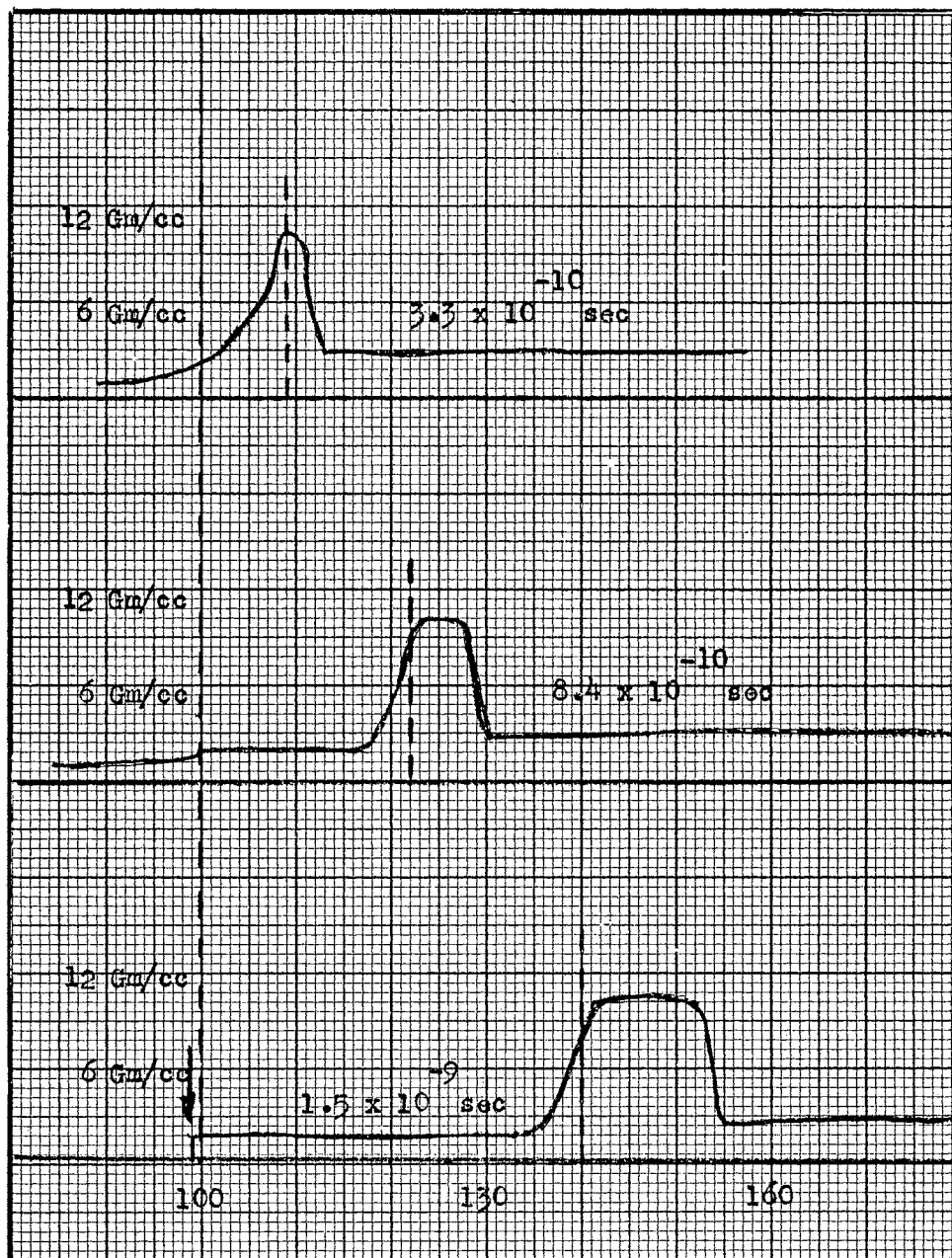
Figure 104.   Density Profiles Resulting from
Impact of Stone Plate of
Porosity 2 Traveling at
60.6 Km/sec
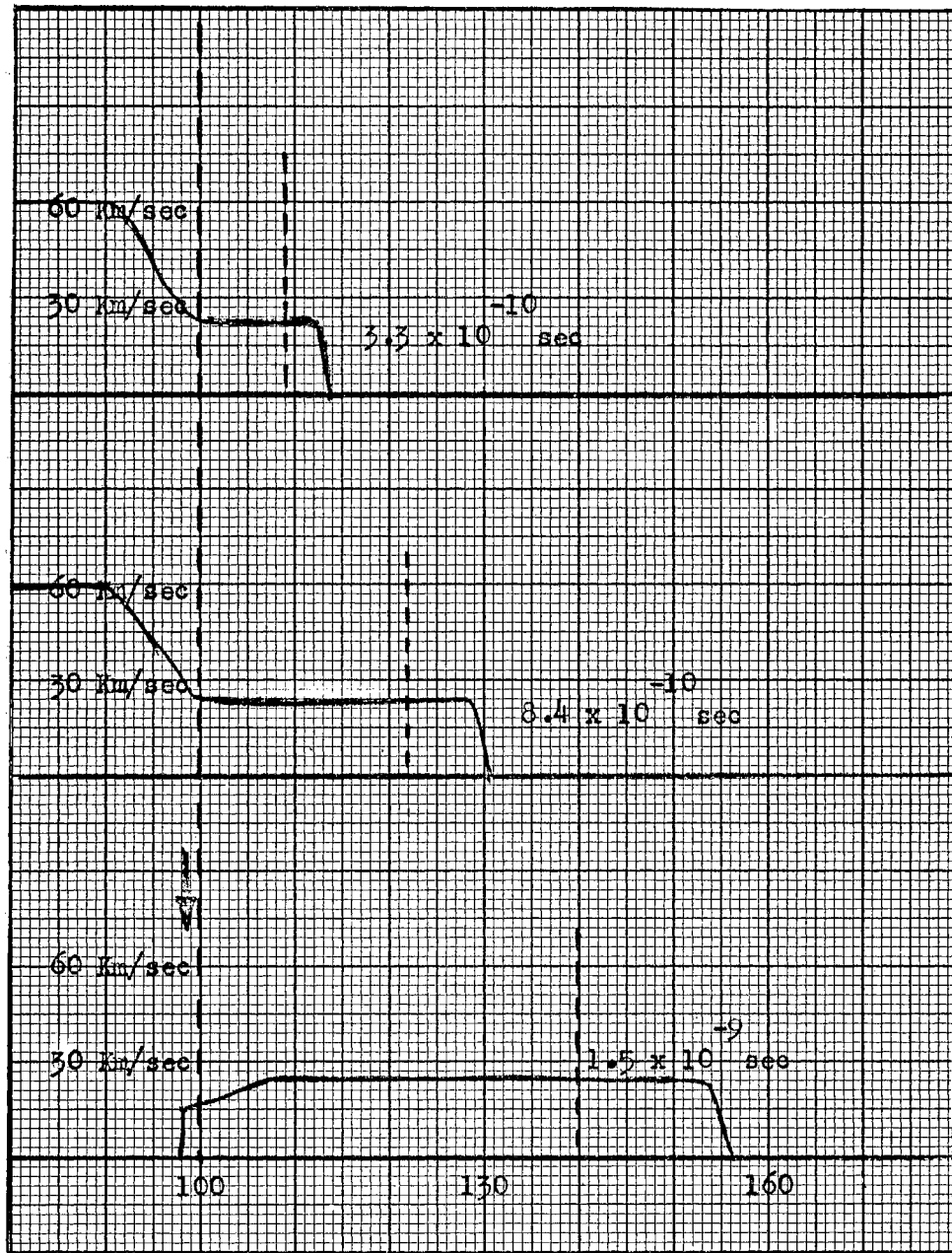
Figure 105. Velocity Profiles Resulting from
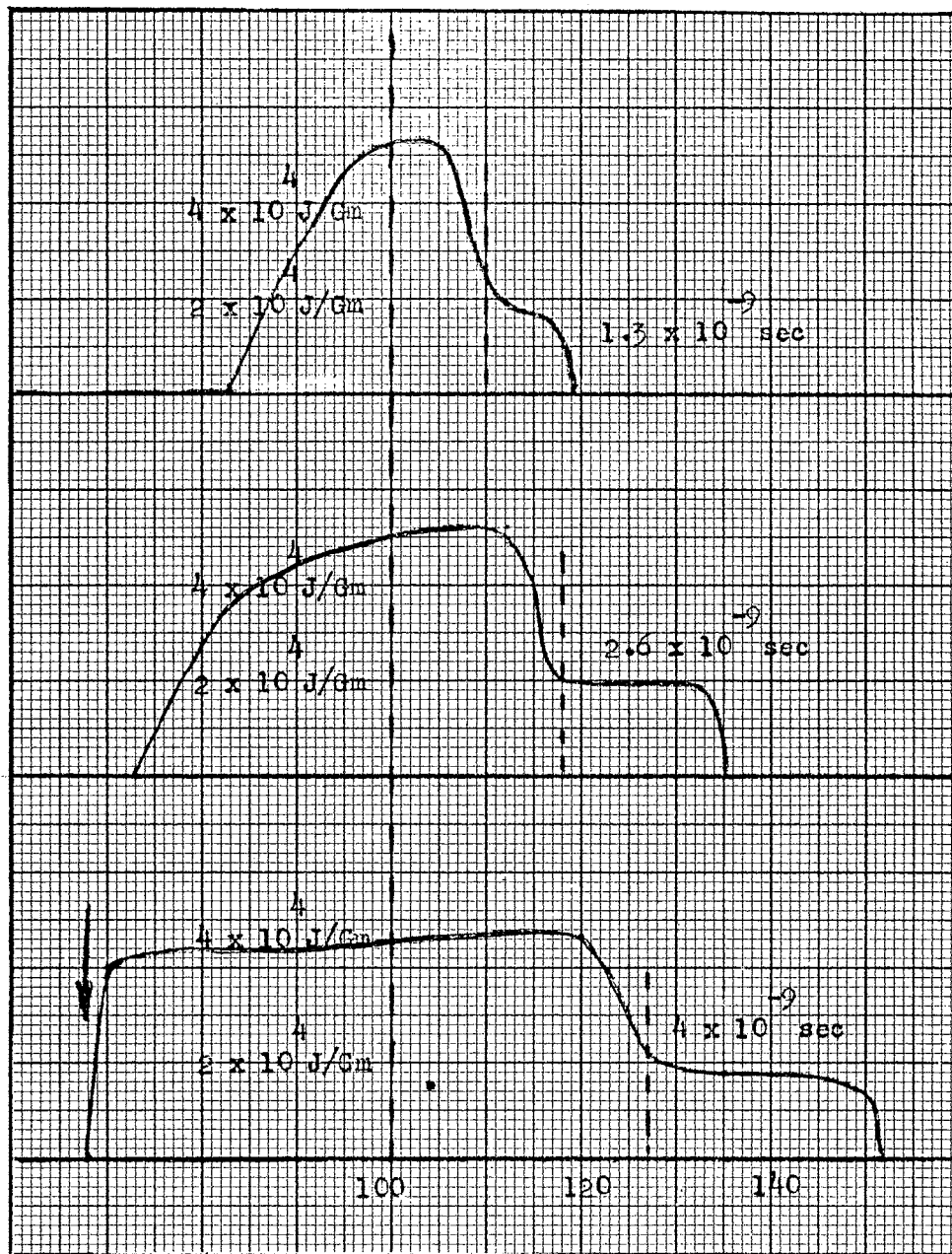Impact of Stone Plate of
Porosity 2 Traveling at
60.6 Km/sec
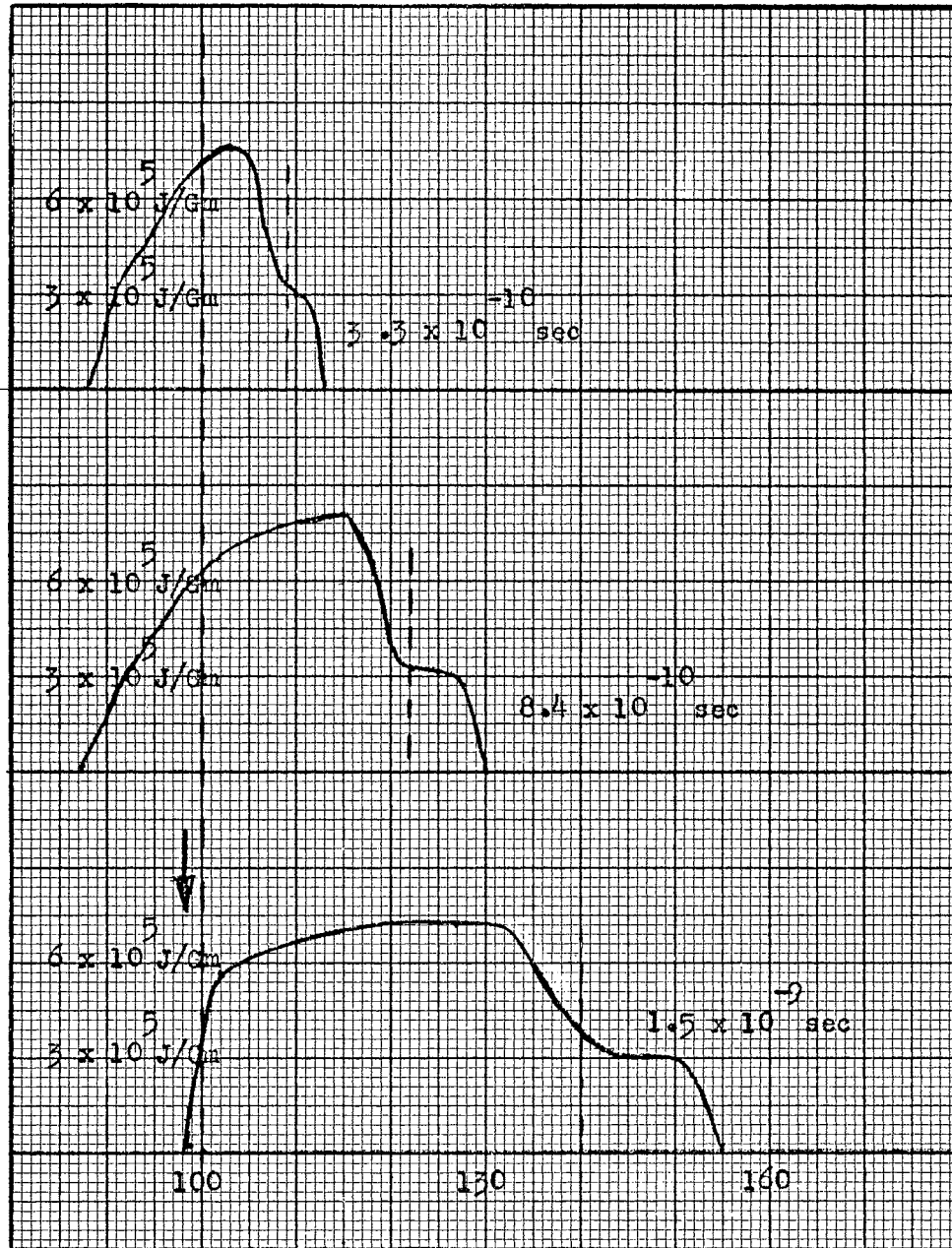
Figure 106.   Internal Energy Profiles Resulting
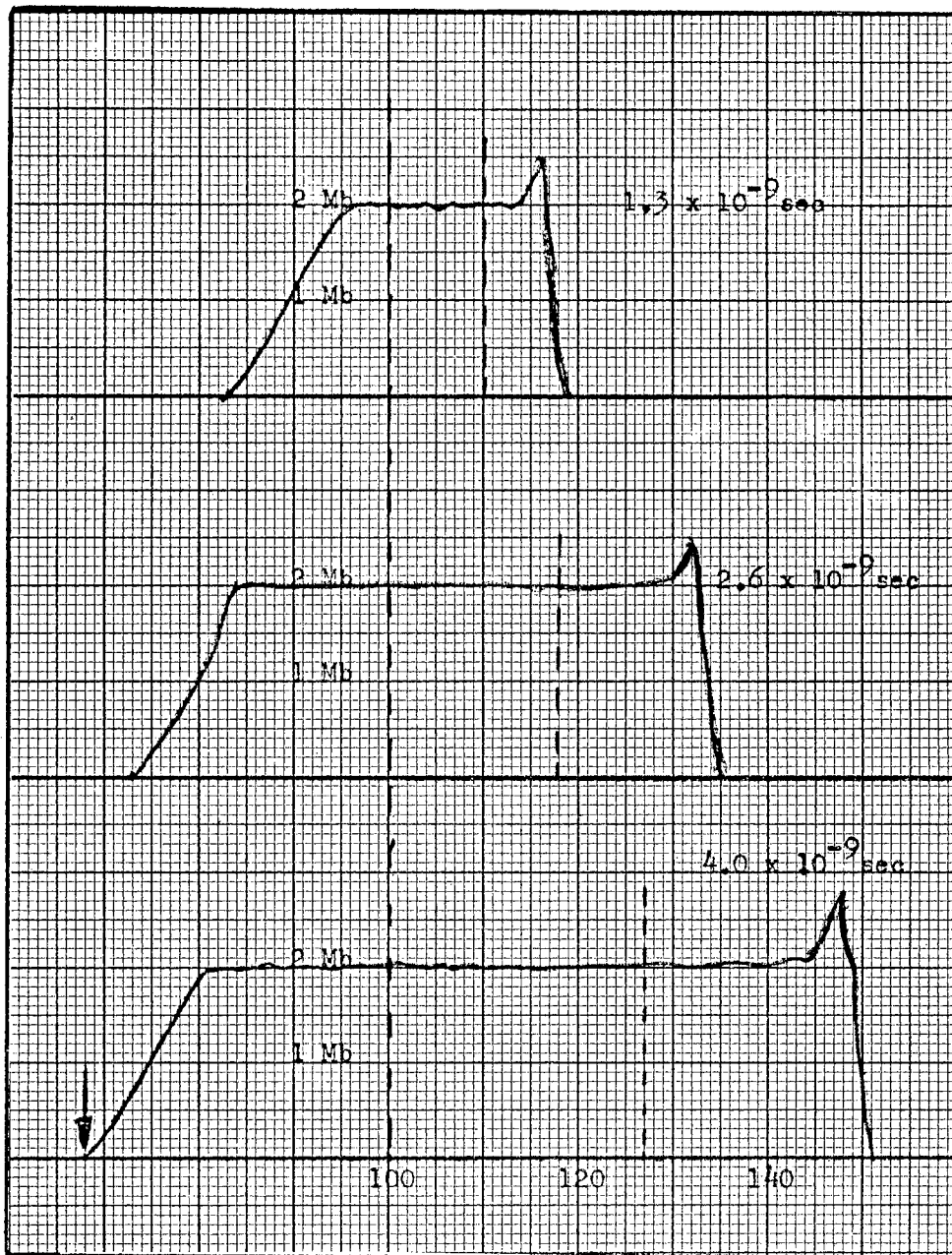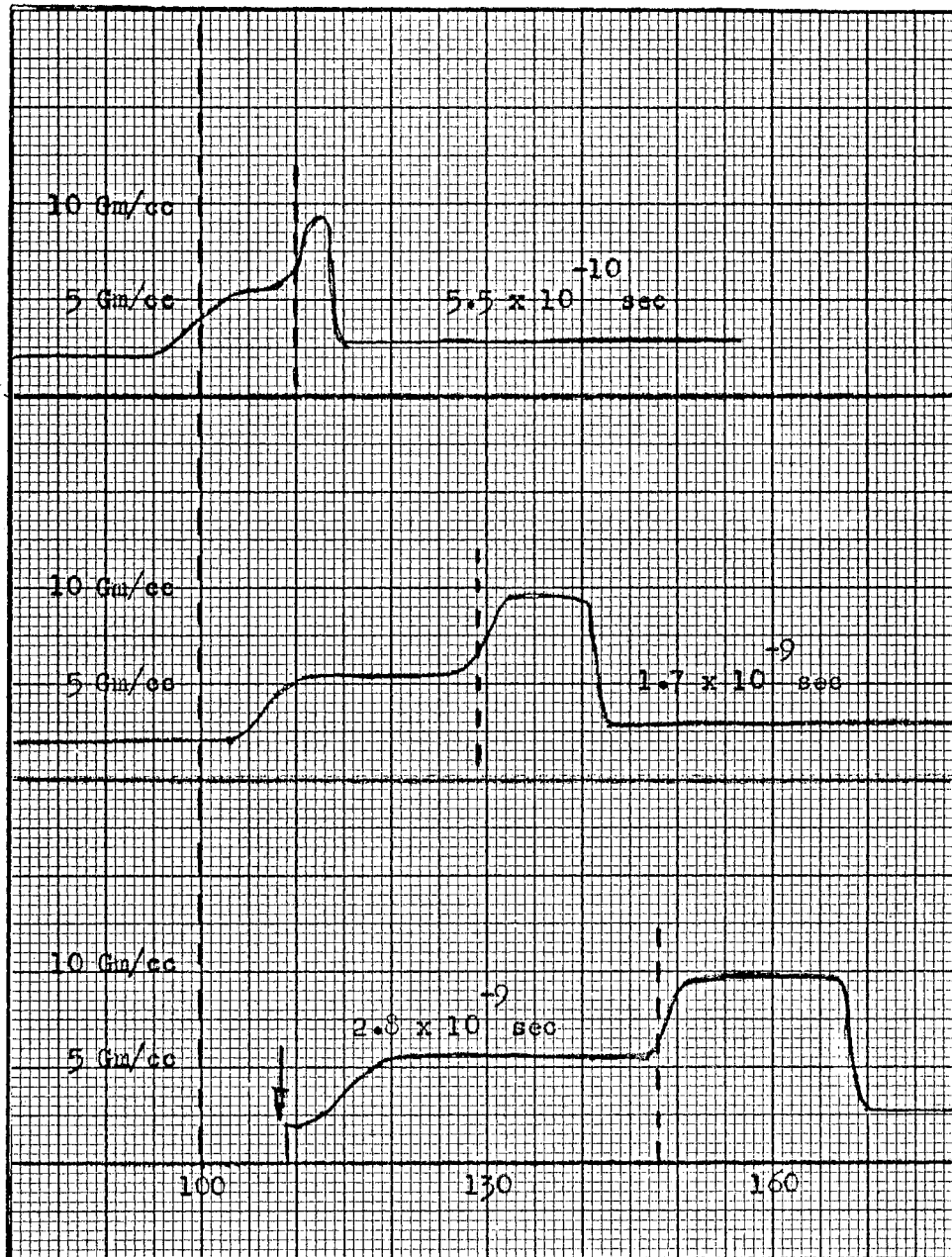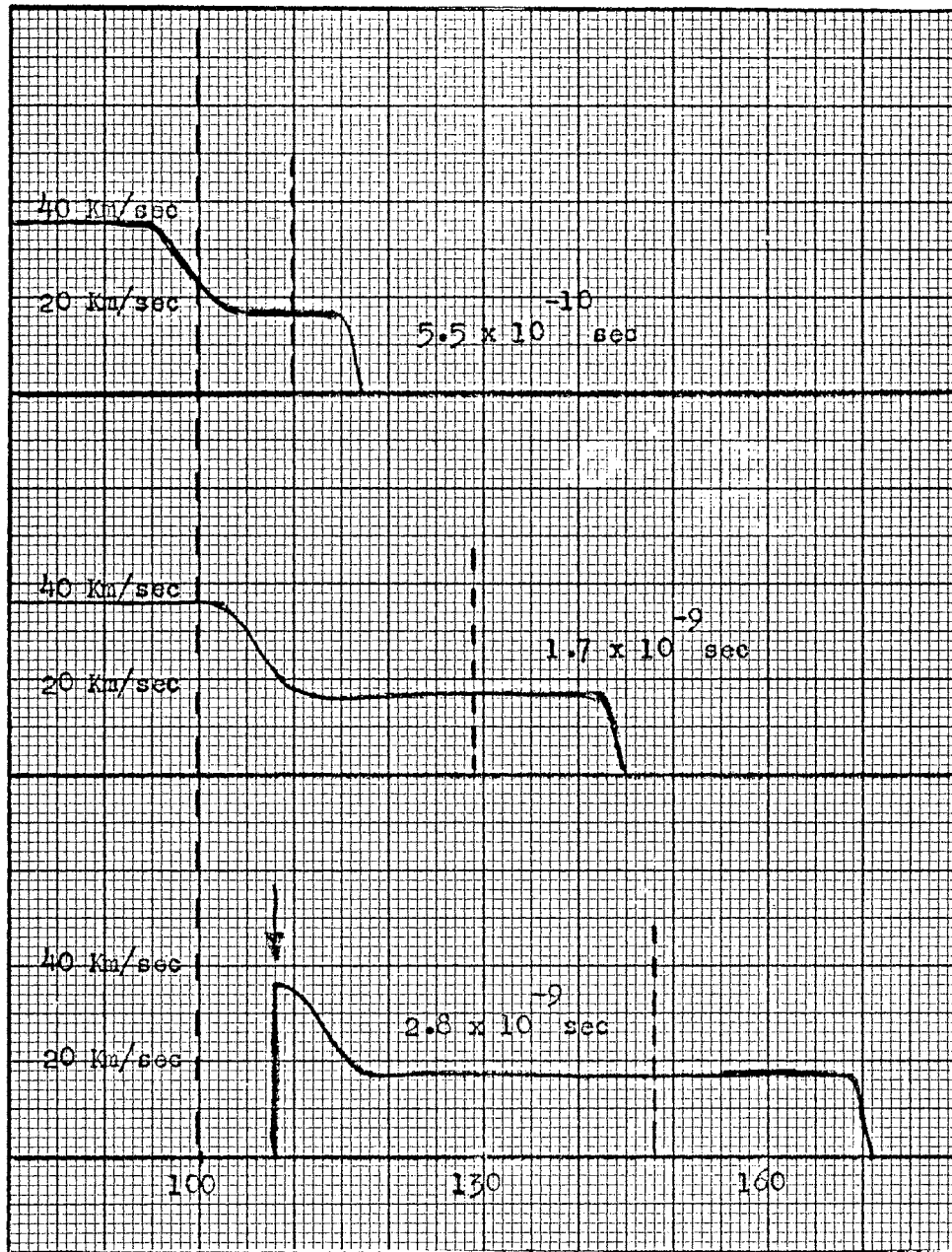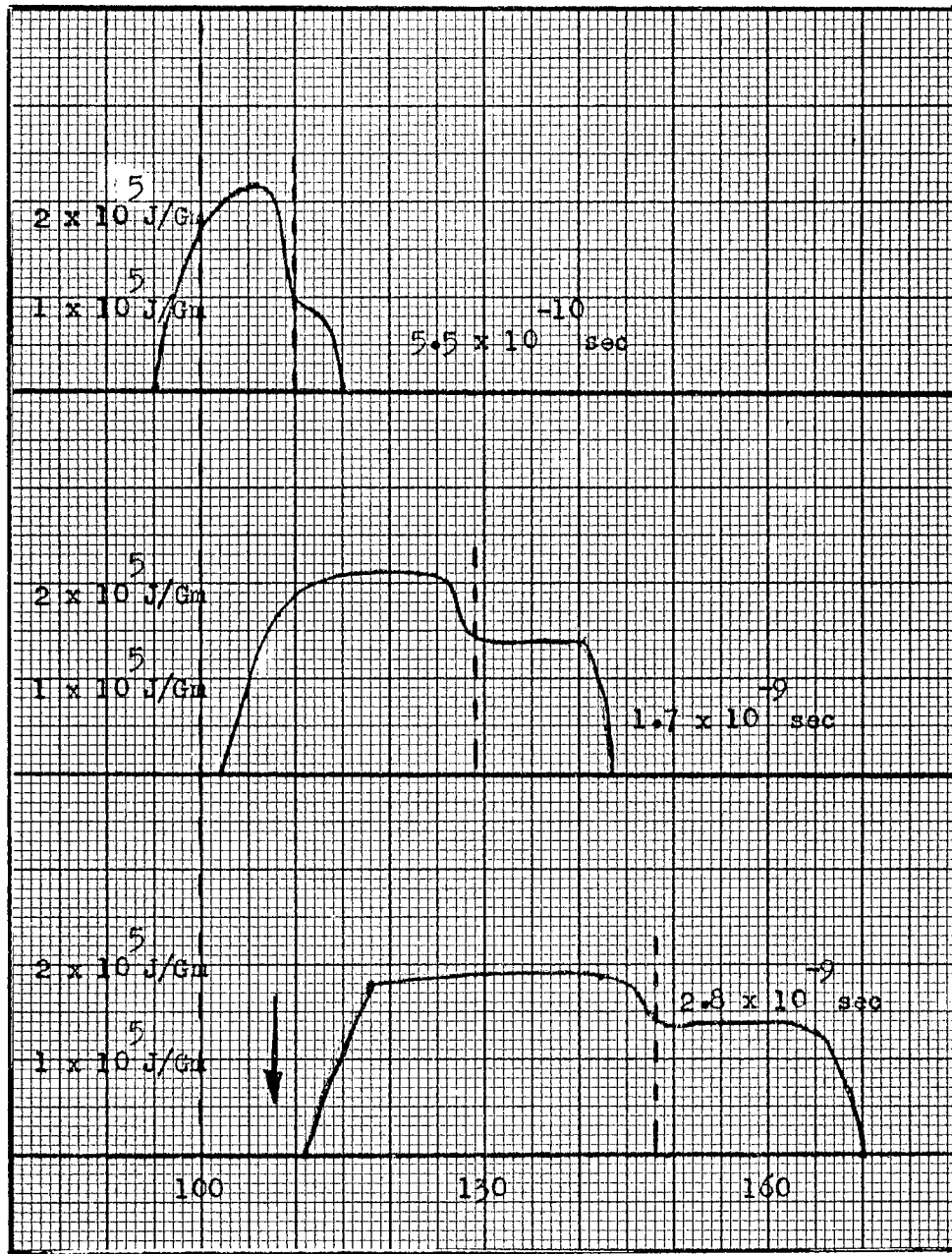from Impact of Stone Plate of
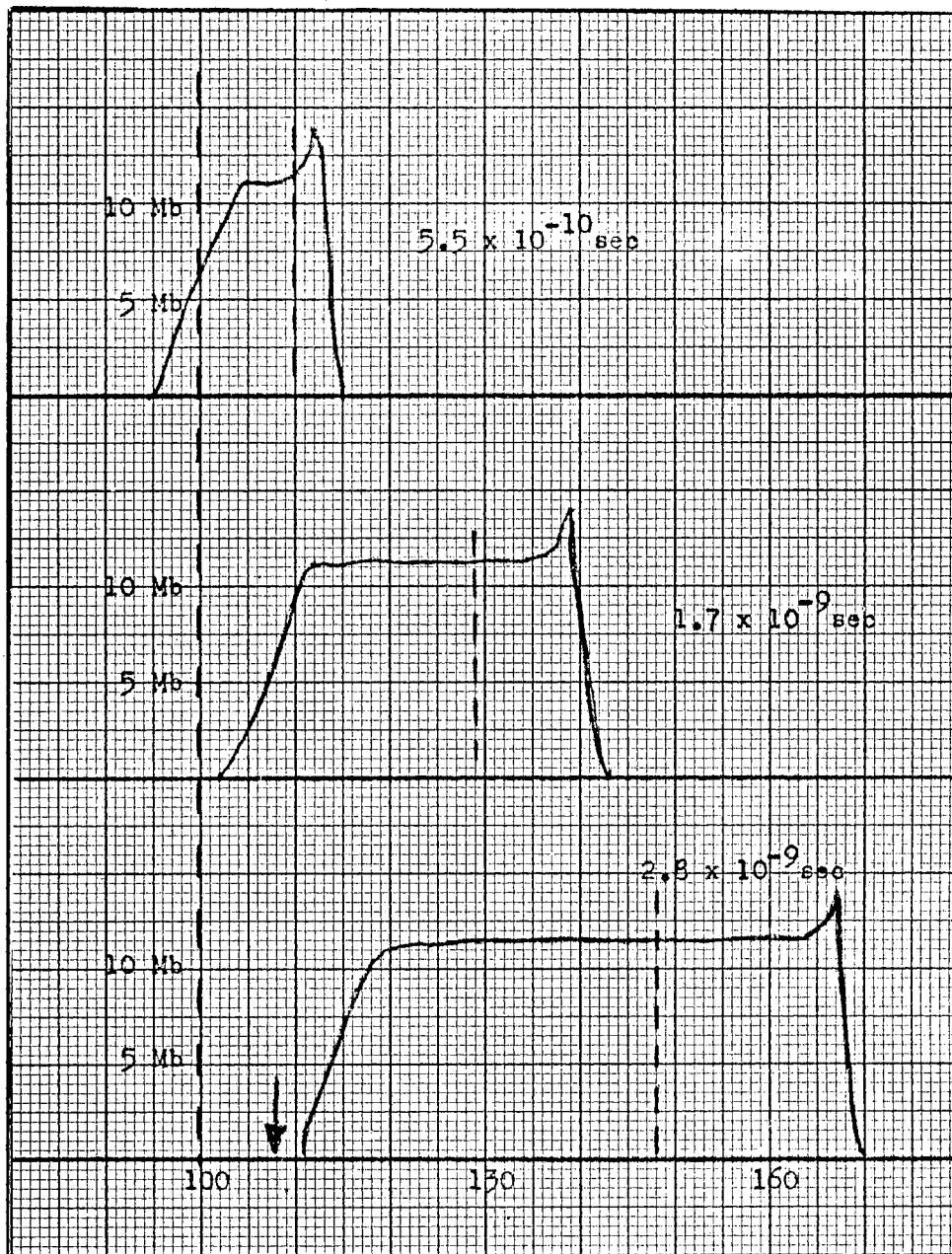Porosity 2 Traveling at
60.6 Km/sec
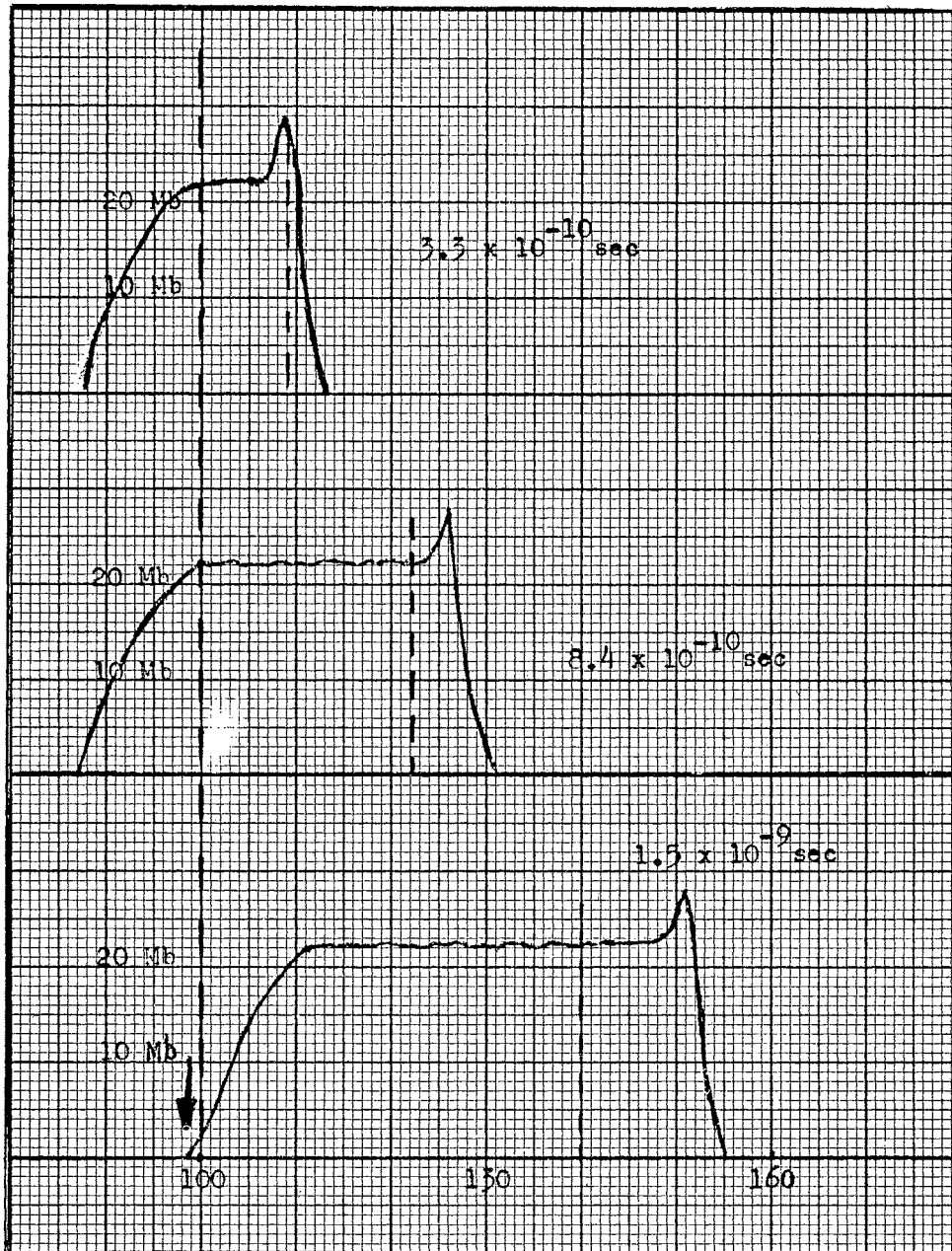
Figure 107. Pressure Profiles Resulting from
Impact of Stone Plate of
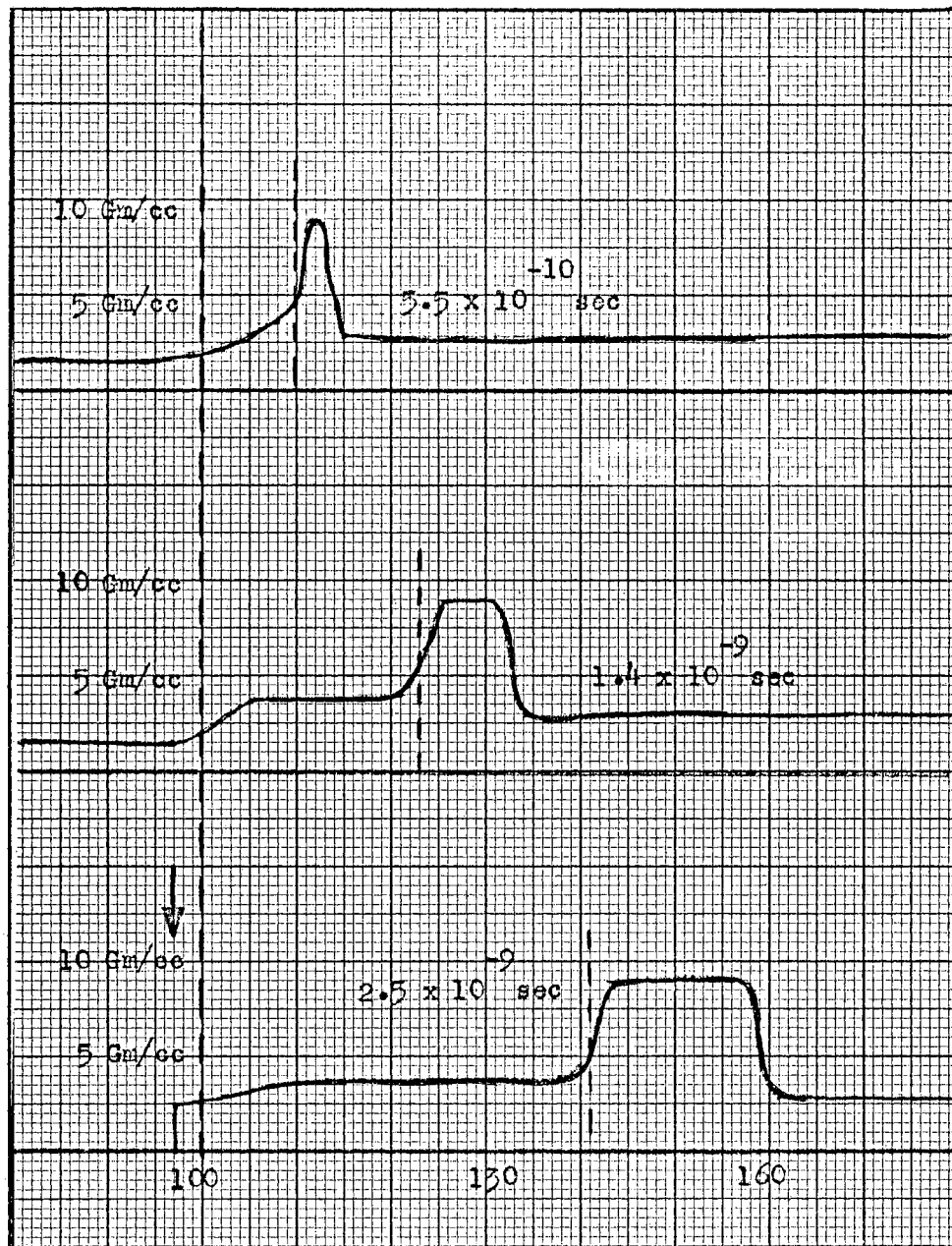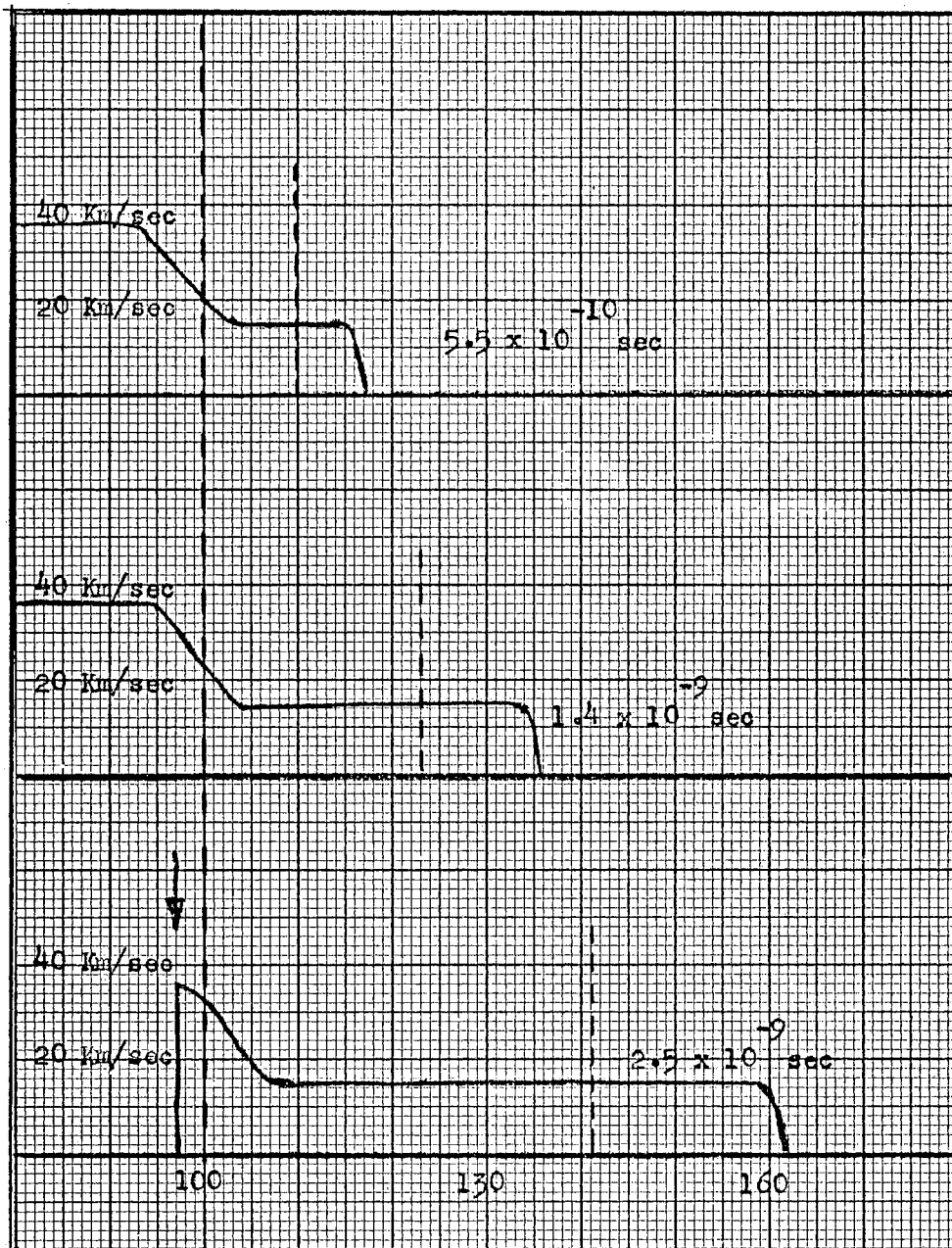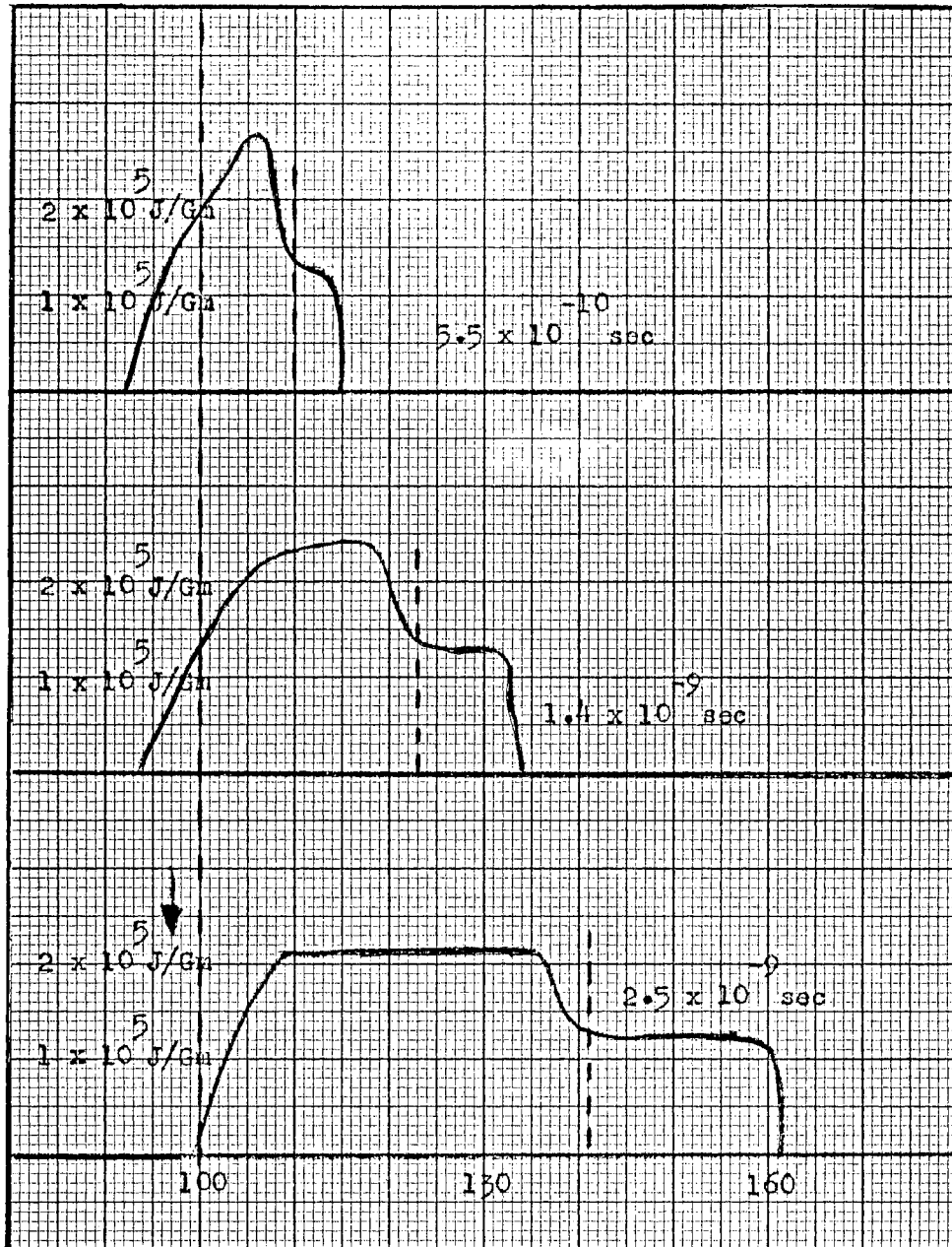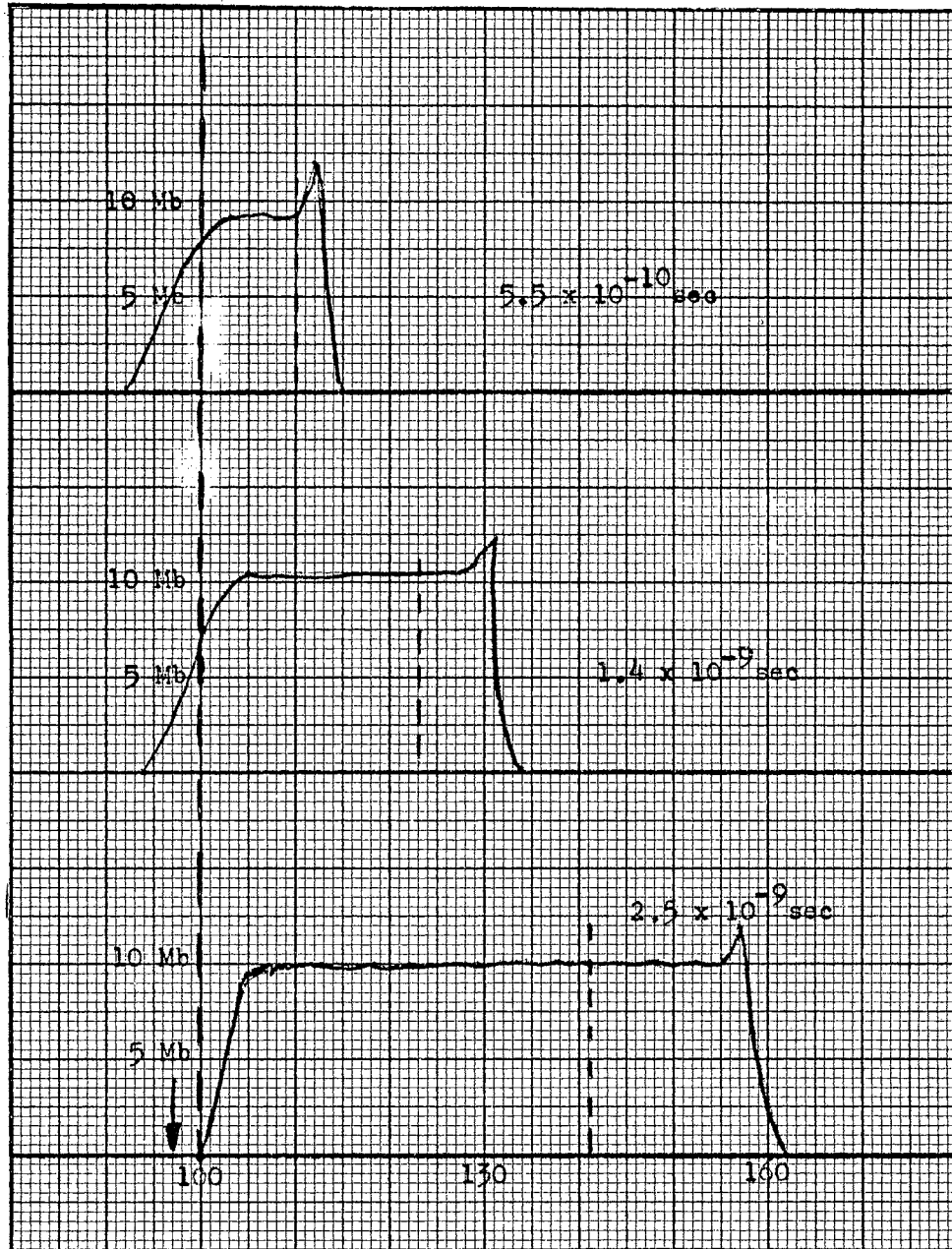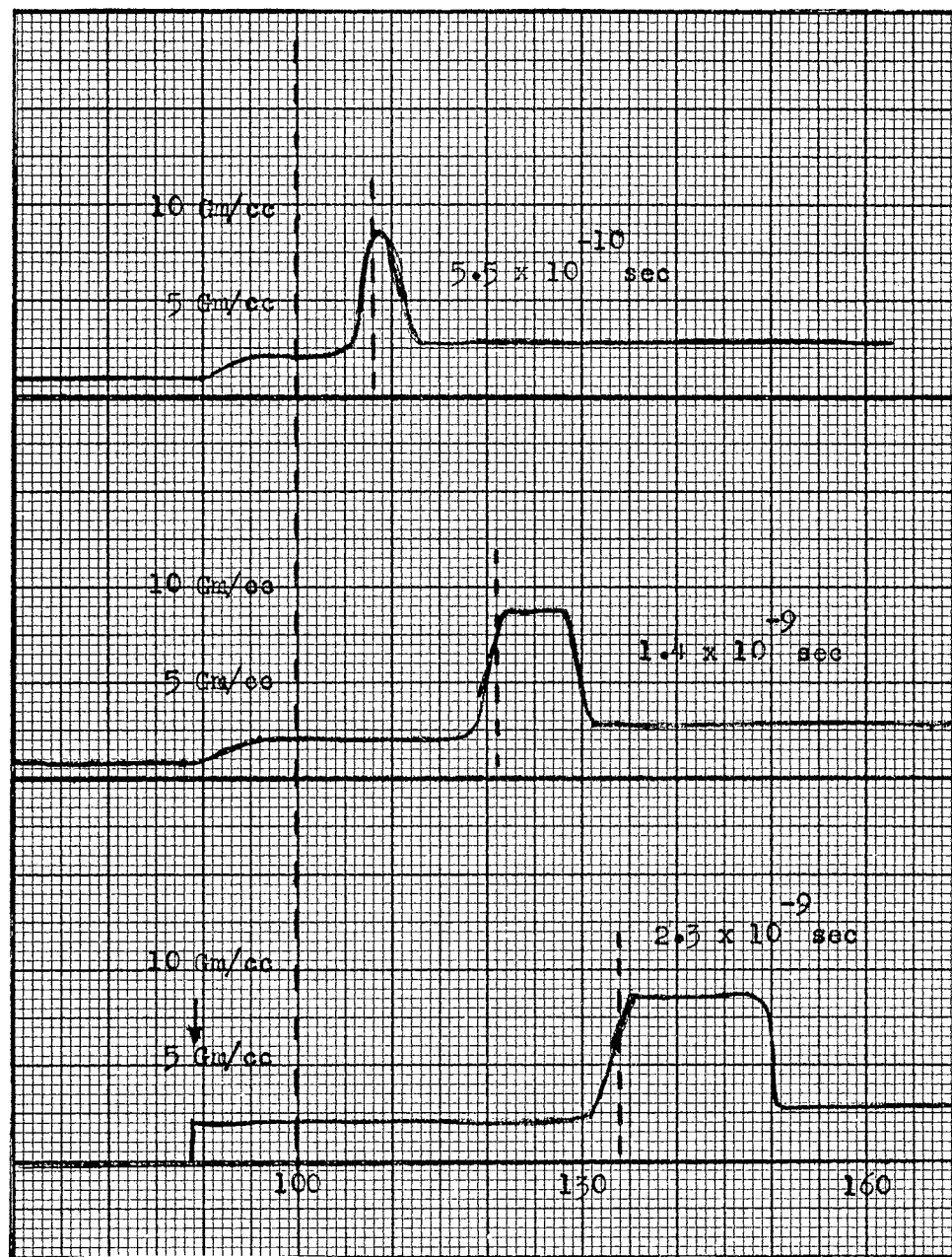Porosity 2 Traveling at
60.6 Km/sec

Discussion of Numerical Solutions

Every profile illustrates the formation of two shock waves. These two shocks are initiated at the contact interface between the plate and the target. One shock wave travels into the target, and its propagation velocity is larger than the propagation velocity of the interface. The other shock wave travels back into the impacting plate. This shock does not propagate with the same velocity as the shock in the target, and is usually carried to the right by the on-rushing plate.

All of the shock pressures are in the megabar range and emphasize the validity of assuming the fluid flow model. These pressures increase as the velocity of the impacting plate increases and decrease if the proosity of the plate decreases. This behavior is illustrated in Figures 108-111.

The material velocity of the impacting plate decreases as a result of the impact, and the loss in kinetic energy appears as internal energy in both the plate and the target. The specific internal energy in the impacting plate increases as the velocity of the impacting plate is increased, and it also increases quite markedly when the porosity of the plate is increased. This behavior is shown in Figures 112 to 115.

The increase of internal energy with the porosity implies that a plate of high porosity will have a hotter temperature than a plate of lower porosity. This temperature effect plays an important role in analyzing the light flash that accompanies hypervelocity impact. The large pressures from the impact convert the target and the impacting body to a plasma. When the pressure is released and the plasma returns
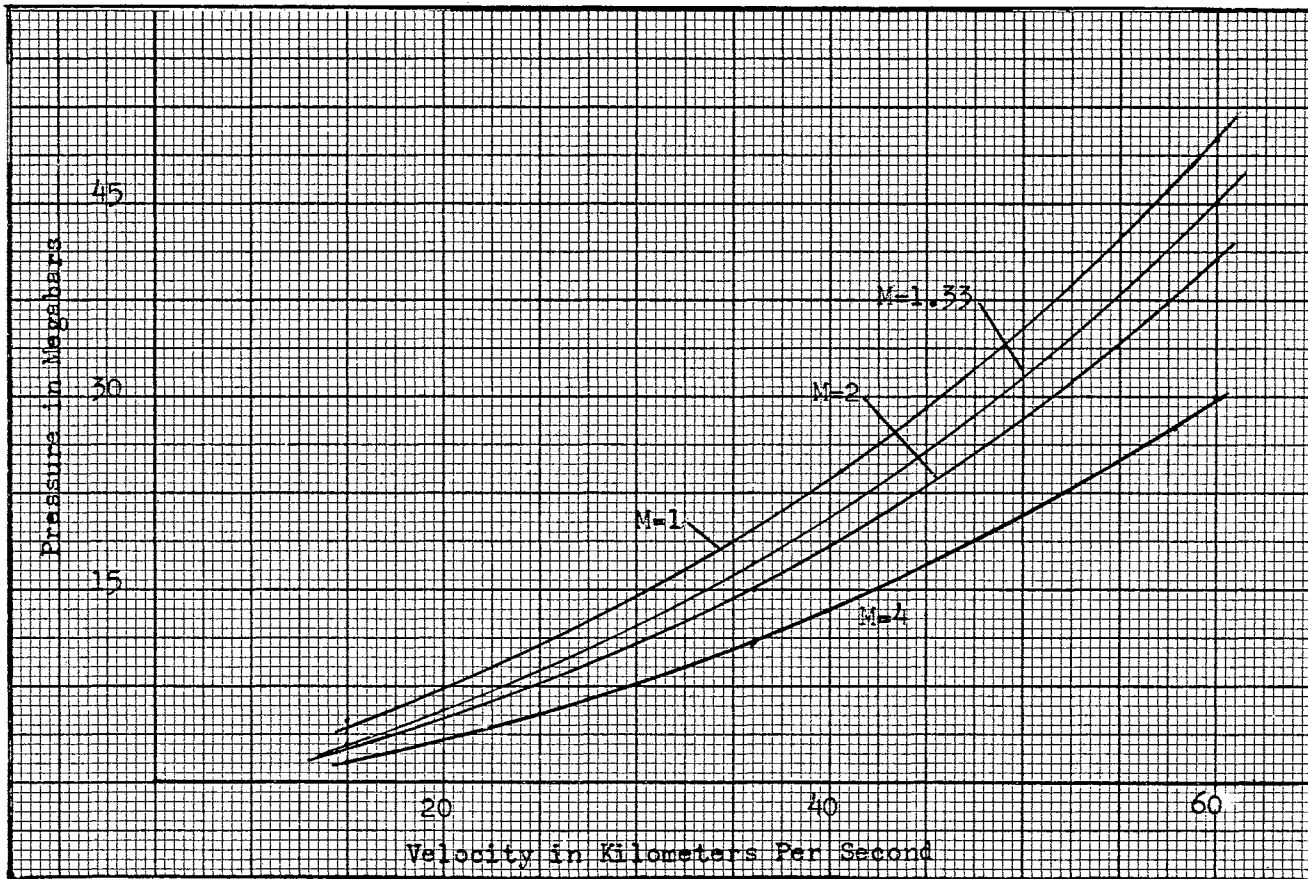
Figure 108. Shock Pressure Created in Iron Plate as a Function of the
Plate Velocity. M is the Porosity of the Plate.
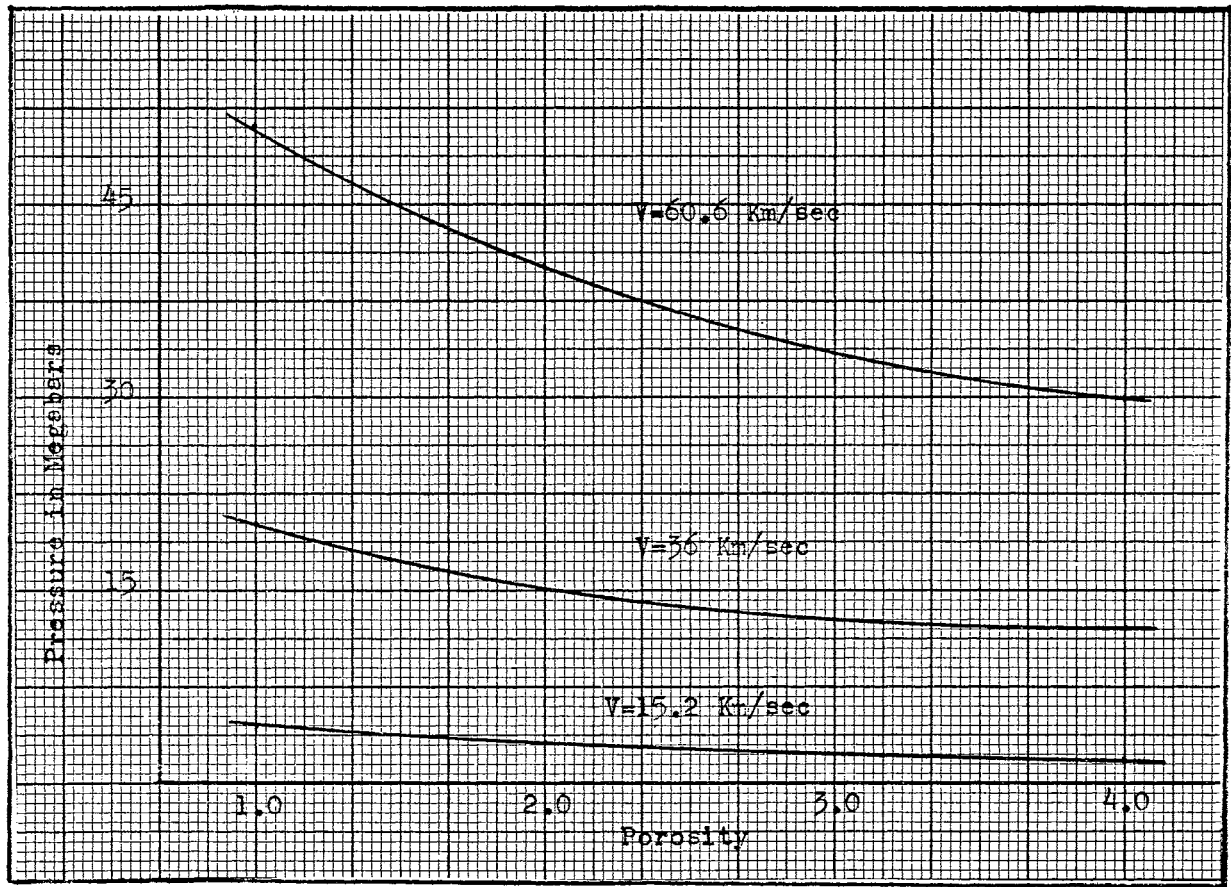
Figure 109. Shock Pressure Created in Iron Plate as a Function of the
Plate Porosity. V is the Impact Velocity of the Plate.
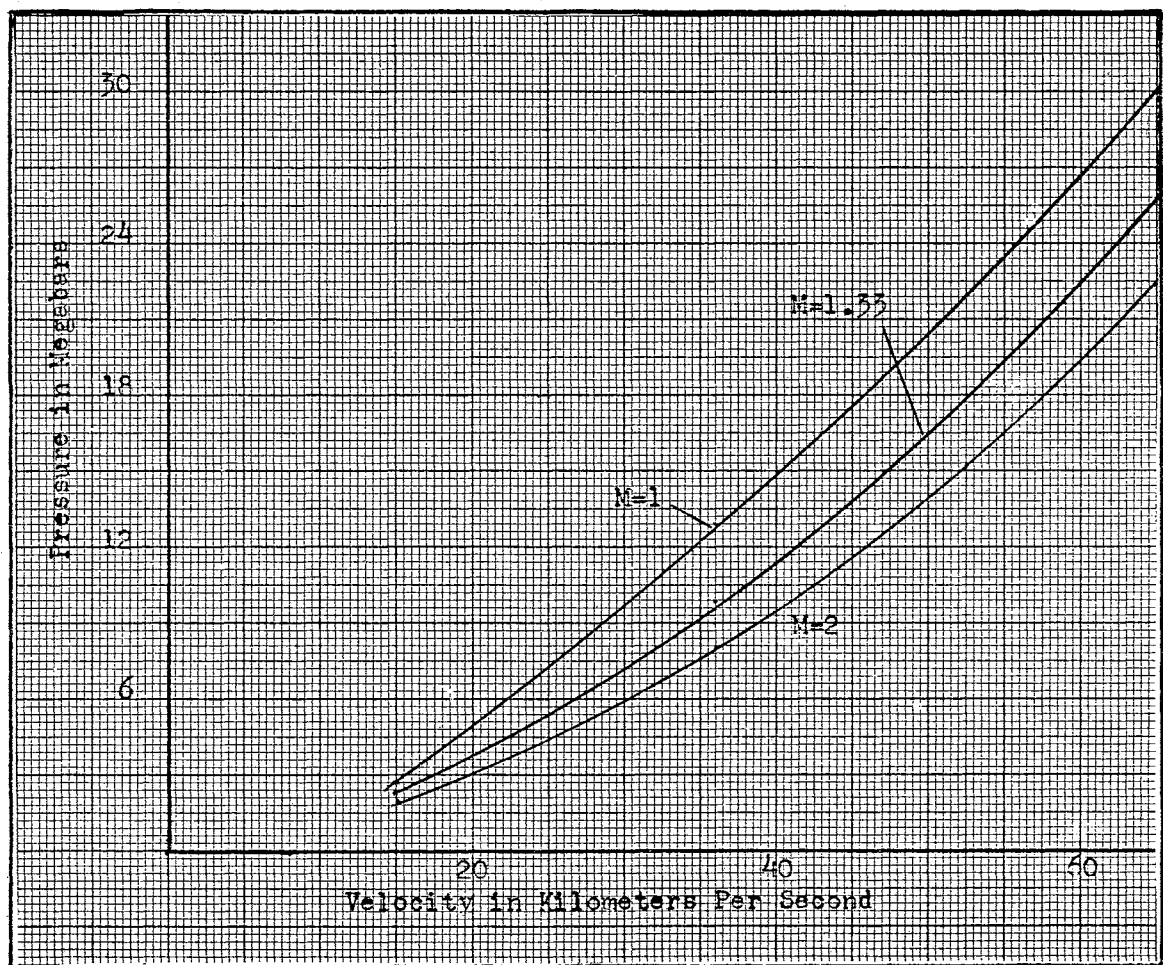
Figure 110. Shock Pressure Created in Stone Plate as a Function of Plate Velocity. M is the Porosity of the Plate.
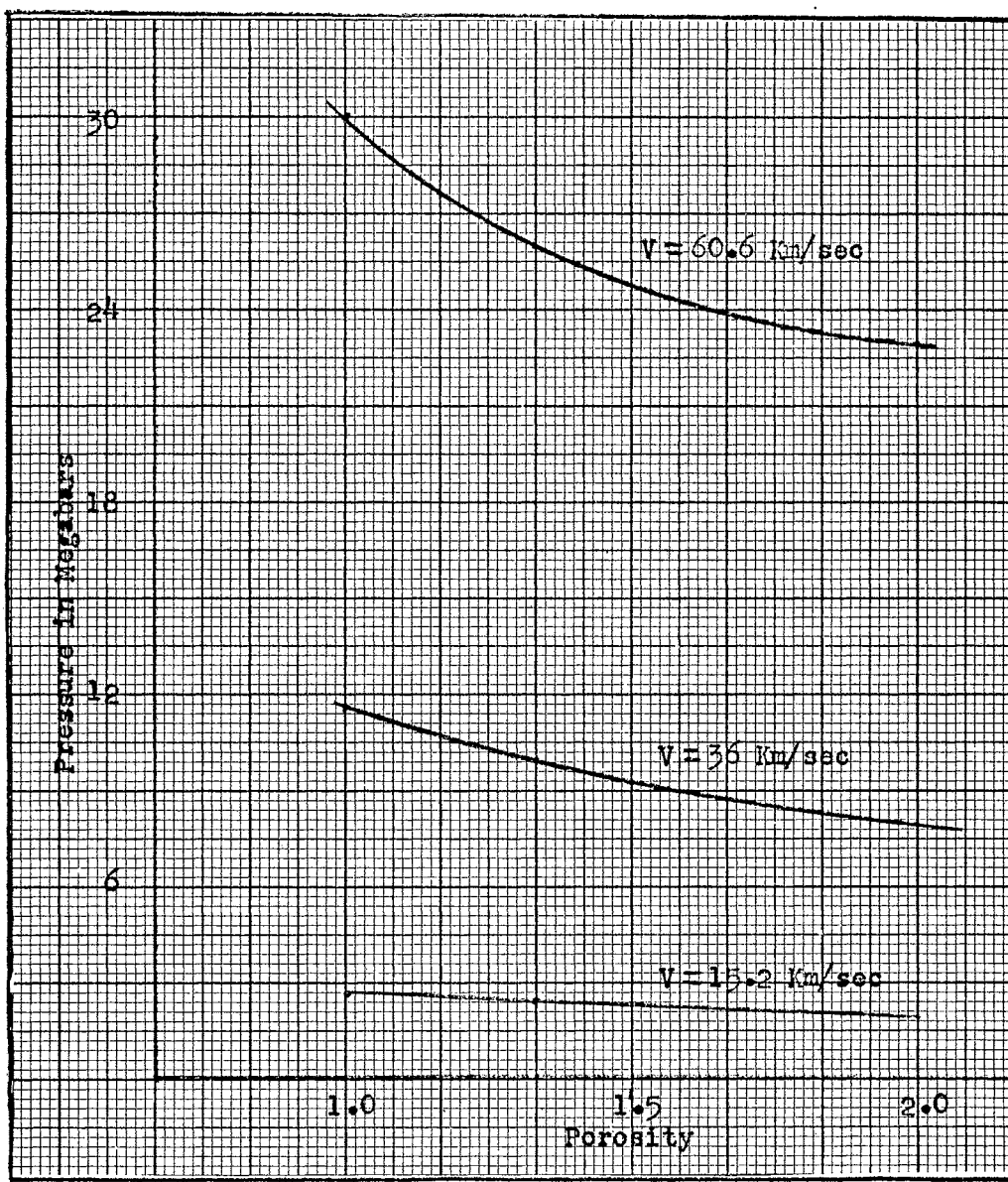
Figure 111.   Shock Pressure Created in Stone Plate as a
Function of the Plate Porosity. V is the
Impact Velocity of the Plate.
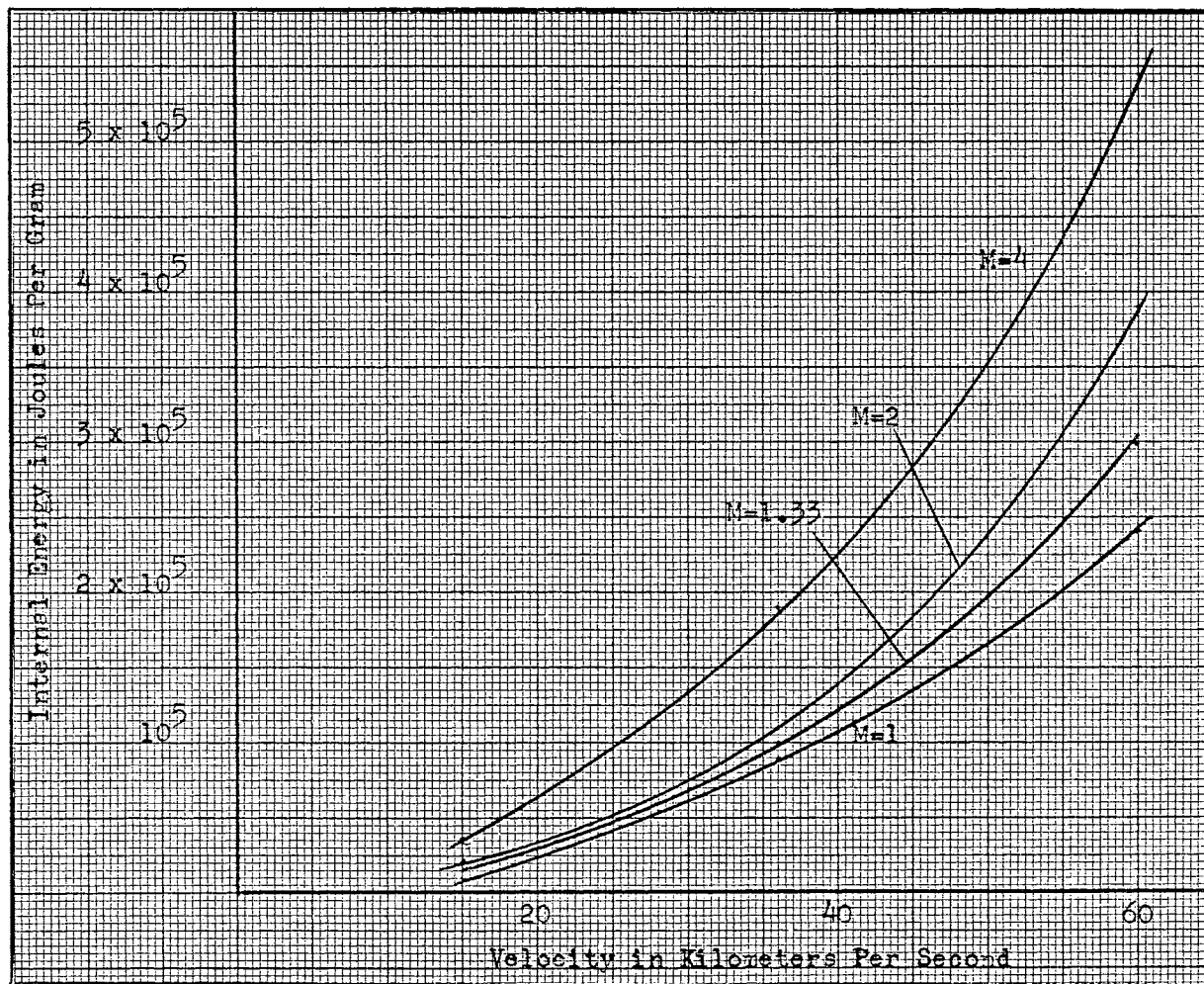
Figure 112. Internal Energy Created in Iron Plate as a Function of the
Plate Velocity. M is the Porosity of the Plate.
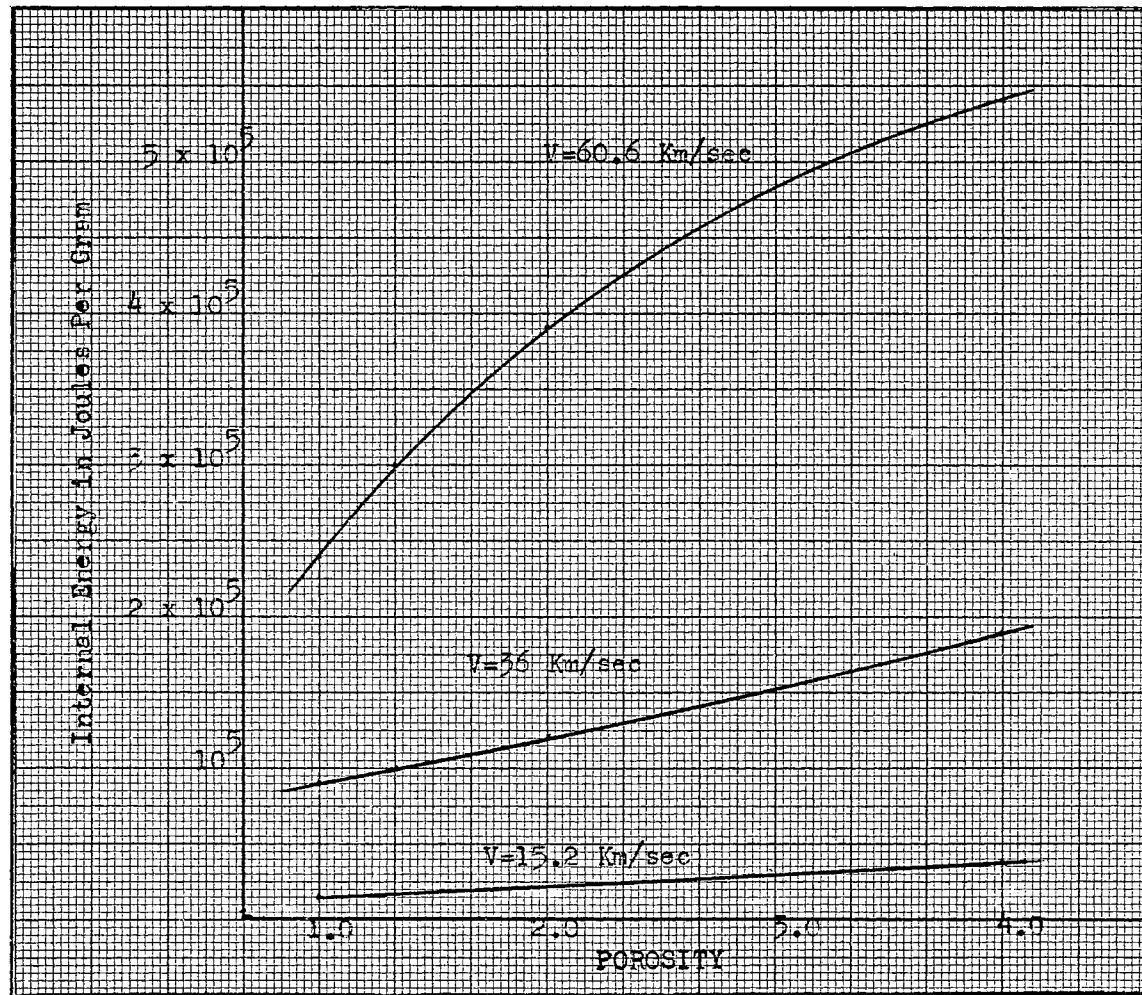
Figure 113. Internal Energy Created in Stone Plate as a Function
of the Plate Porosity. V is the Impact of the
Plate.
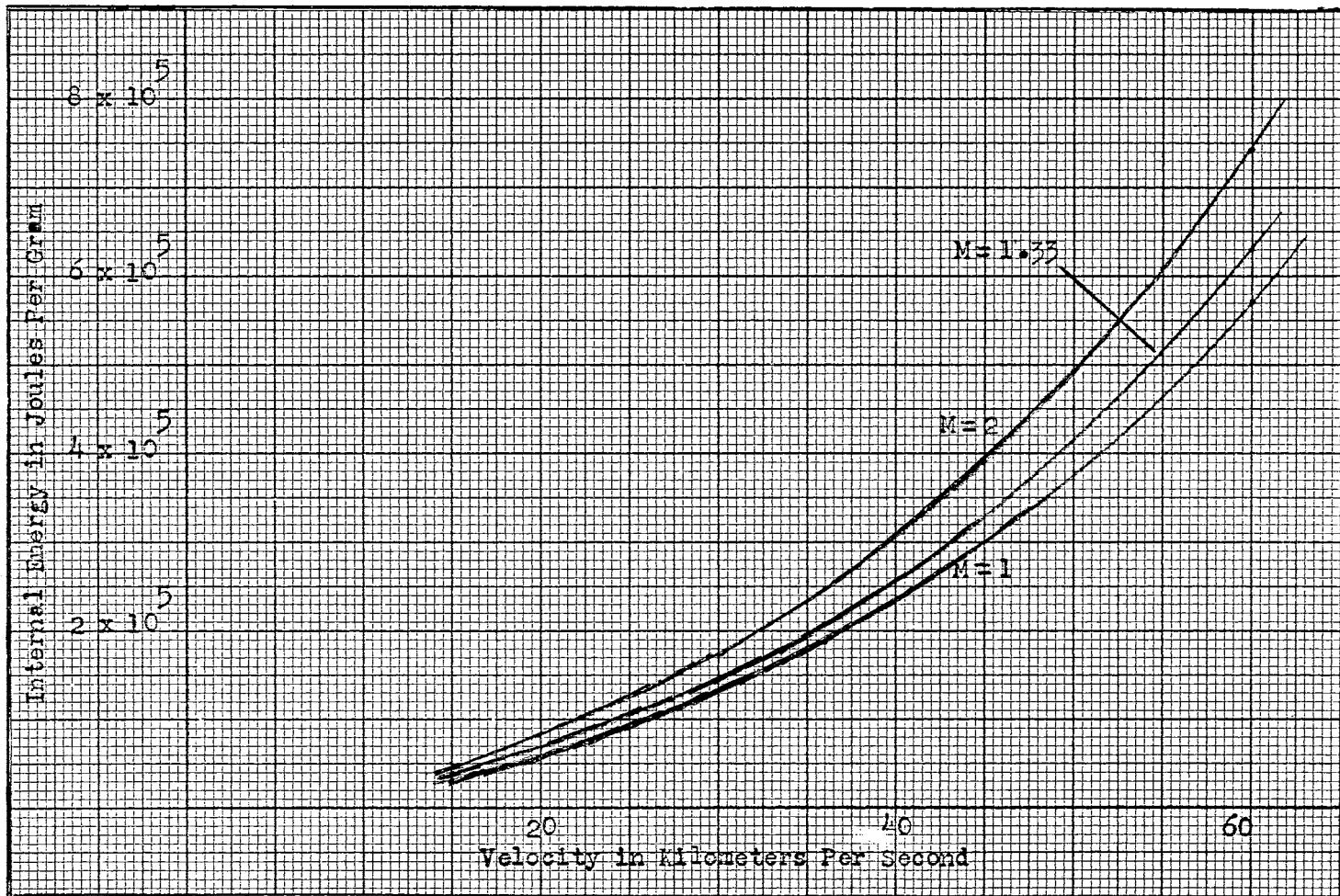
Figure 114. Internal Energy Created in Stone Plate as a Function of the
Plate Velocity, M is the Porosity of the Plate.
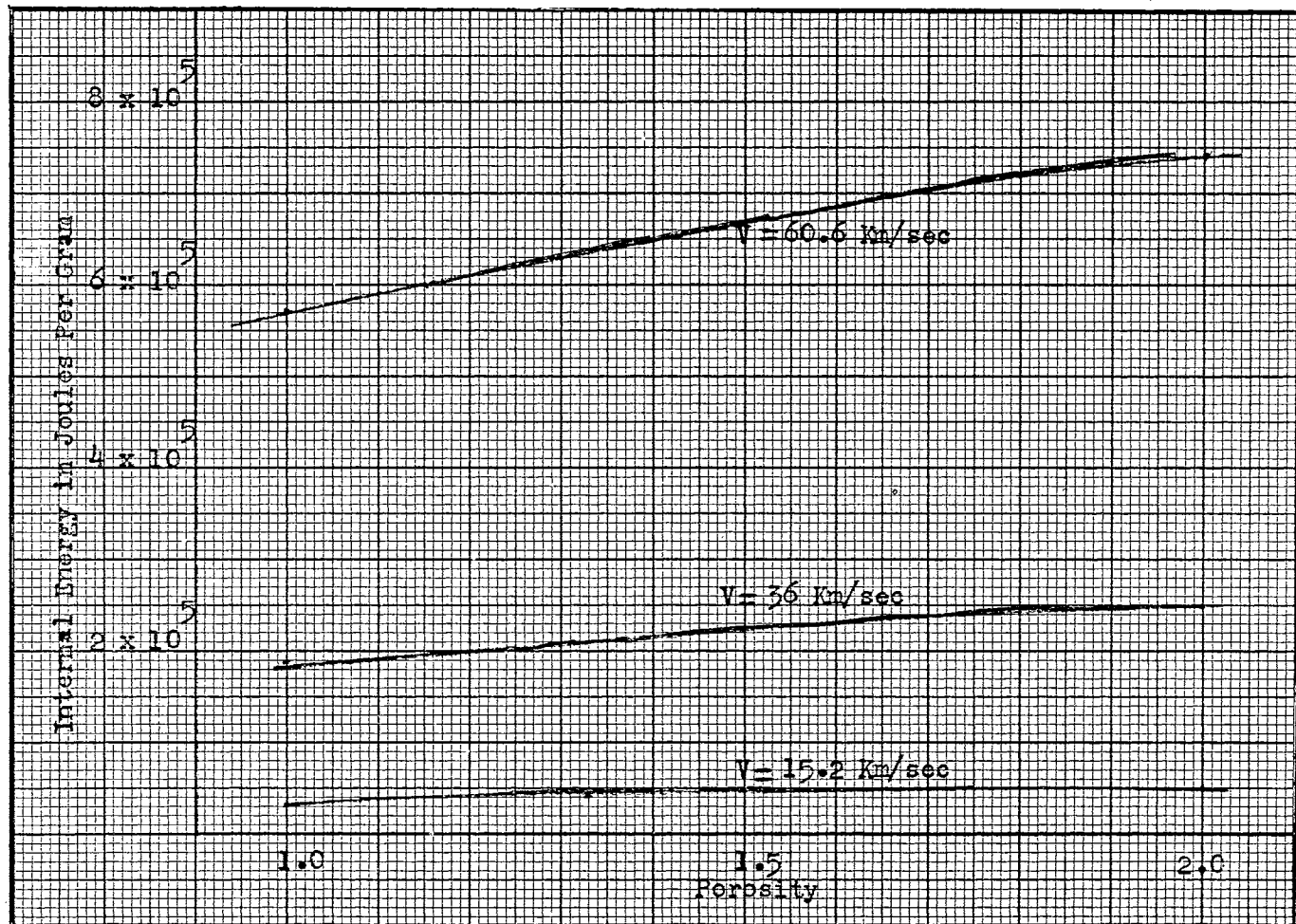
Figure 115. Internal Energy Created in Stone Plate as a Function of the Plate Porosity. V is the Impact Velocity of the Plate.

to the ground state, the released radiation appears as ultraviolet and visible light. An estimate of the temperature of the plasma will assist in the analysis of the emitted radiation. The temperature's in the impacting stone plate are listed in Table V. These are the temperatures from the equations of state, they are very much higher than would be obtained for the same energy density in a plasma.

TABLE V

TEMPERATURES IN IMPACTING PLATE

Plate Porosity	Plate Velocity In KM/Sec	Temperatures in Degrees Kelvin
1	15.2	120,000
1.33	15.2	150,000
2	15.2	190,000
1	36	260,000
1.33	36	340,000
2	36	590,000
1	60.2	760,000
1.33	60.2	1,100,000
2	60.2	1,600,000

CHAPTER IX

SUMMARY AND CONCLUSIONS

Part I

A helium gas gun was designed, constructed and tested for launching small aluminum cylinders at velocities that are greater than 10,000 feet per second. The gun has been fired successfully, is structurally safe, and is considered to be fully operational. The gun was fired at approximately one-half of the rated powder charge and launched an aluminum projectile with a velocity of about 6000 feet per second.

The test firings revealed two design deficiences which were corrected. The framework for supporting the optical-electronic system to measure the projectile's velocity was completely rebuilt since mechanical vibrations of the framework did not permit measurements to be obtained. It was also necessary to redesign the pump tube piston since the first design permitted the gunpowder gases to blow past it into the helium which was in front of the piston. The new piston utilities boretight aluminum rings at the front and rear of the piston, and these have proved to be effective seals in a later test.

It was particularly gratifying to discover that the projectile does not tumble in its flight, but strikes the target head on. This is very important for the impact tests that are proposed. It permits the front end of the projectile to have different geometric shapes. These

173

shapes may be employed to give two, or more successive shocks to the target.

The experimental data from hypervelocity impacts with the light gas gun are to be correlated with an analytical solution for a hyper-velocity impact. An intercomparison of the results should clarify many of the uncertainties that presently exist in this field. There is practically no information in the literature with respect to the propagation of a shock from an inviscid fluid into a plastic medium. The light gas gun was designed and constructed to clarify this uncertainty, in particular. This is the reason that the bullet is designed to give multiple shocks and the displacement of the outside wall of the hemis-pherical target is to be measured with very high resolution. Work subsequent to this thesis has shown that the viscosity of a plastic medium should be predictable from measurements with this gun. Provided the viscosity of the plastic is a linear function of the pressure, the viscosity is expected to be measured to 140 kilobars, approximately.

PART II

The light gas gun requires auxiliary equipment in order to conduct a meaningful experiment. Rather than complete the equipment for the measurement of surface displacement at high speed for the gun, the author of this thesis decided to initiate a new phase of the correlat-ing analytical study for hypervelocity impact. As an introduction to the much more involved phases of the analytical problem, a one-dimensional solution was sought for the hypervelocity impact of a thin, porous plate on a very thick slab. Particular attention was directed toward following the compacting of the porous plate and toward following

the position and motion of the interface. Preliminary studies were also made on the effect of the reflection of the shock from the rear face of the thin plate.

Although all phases of the impact were considered and followed, the primary purpose of the simplified problem is to investigate the effect that the porosity of the incident body has on the impact process. This solution is the initial step in obtaining the numerical solution of the impact of a small, porous-stone sphere on an aluminum target, and it has provided much valuable information. The solution shows that two shock waves originate at the contact interface between the target and the plate and travel away from the interface in opposite directions. The flow velocity and pressure are continuous across the interface, and the magnitude of these variables depends upon the velocity and porosity of the impacting plate. The internal energy in the target and in the plate also has a functional dependence upon the impact velocity and the porosity of the plate. The internal energy in the plate increases considerably when the porosity of the plate increases. The temperature of a highly porous plate is then much greater than the temperature of a slightly porous plate when both plates are compressed by the same ratio.

SELECTED BIBLIOGRAPHY

(1)   "Aircraft Damage Studies," Progress Reports, New Mexico School of
            Mines (1948-1952) (Confidential)

(2)   Al'tshuler, L. V., A. A. Bakanova, and R. F. Trunin, "Shock
            Adiabats and Zero Isotherms of Seven Metals at High
            Pressures," Soviet Phys.-JETP, 11, 1, (1962) 65-74

(3)   Al'tshuler, L. V., L. V. Kuleshova, and M. N. Pavlovskii, "The
            Dynamic Compressibility, Equation of State, and Electrical
            Conductivity of Sodium Chloride at High Pressures," Soviet
            Phys.-JETP, 12, 1, (1961), 10-15

(4)   Bengson, M. H., T. K. Slawecki, and F. J. Willig, "A Multi-Stage
            Hypervelocity Projector," Hypervelocity Impact Fourth
            Symposium, Eglin Air Force Base, Florida, (1960)

(5)   Bioletti, C. and B. E. Cunningham, "A High-Velocity Gun Employing
            a Shock-Compressed Light Gas," NASA TN D-307

(6)   Birkoff, G., D. P. McDougall, E. M. Pugh, and G. Taylor, J. Appl.
            Phy., 19, 563 (1948)

(7)   Bruce, R. E., "A Model and Calculations for the Properties of an
            Exploding Plasma Sphere," Ph.D. Thesis, Oklahoma State
            University, (1966)

(8)   Charters, A. C., B. P. Denardo, and V. J. Rossow, "Development
            of a Piston-Compressor Type Light-Gas Gun for the Launching
            of Free-Flight Models at High Velocity," NACA TN 4143,
            (1957)

(9)   Charters, A. D., Scientific American, Vol. 203 (Oct. 1960) 128

(10)   Cook, M. A., "Mechanics of Cratering in Ultra High Velocity
            Impact," J. Appl. Phys., 30 (1959) 725-735

(11)   Corner, J., Theory of the Interior Ballistics of Guns, John Wiley
            and Sons, Inc., (1950) 361-364

(12)   Curtis, J. S., "An Accelerated Reservoir Light-Gas Gun," NASA
            TN D-1144 (1962)

(13)   Donn, B., "The Origin and Nature of the Solid Particles in Space,"
            Annals New York Acad. of Sci., 119, Article 1, (1964)

(14) Fogg, W. E. and C. W. Fleischer, "Acceleration of Projectiles
     with the Sequenced High Explosive Impulse Launcher," Hyper-
     velocity Impact Fourth Symposium (1960)

(15) Friichtenicht, J. F. and B. Hamermesh, "Ballistic Impacts by
     Microscopic Projectiles," Hypervelocity Impact Fourth
     Symposium (1960)

(16) Kinard, W. H. and R. D. Collins, "An Investigation of High-
     Velocity Impact Cratering into Nonmetallic Targets and
     Correlation of Penetration Data for Metallic and Non-metallic
     Targets," NASA TN D-726 (1961)

(17) Kineke, J. H., "An Experimental Study of Crater Formation in
     Metallic Targets," Hypervelocity Impact Symposium (1960)

(18) Kolsky, H. G., "A Method for the Numerical Solution of Transient
     Hydrodynamic Shock Problems in Two Space Dimensions,"
     Los Alamos Report LA-1867 (1955)

(19) Kormer, S. B., A. I. Funtikov and V. D. Urlin, "Dynamic Compres-
     sion of Porous Metals and the Equation of State with
     Variable Specific Heat," Soviet Phys.-JETP, 15, 3 (1962)
     477-488

(20) Lake, H. R., "Digital Computer Solution for Propagation of a
     Spherical Shock Wave in Aluminum," Master's Thesis, Oklahoma
     State University (1962)

(21) Landshoff, R., "A Numerical Method for Treating Fluid Flow in the
     Presence of Shocks," Los Alamos Report LAMS-2379 (1959)

(22) McClosky, D. J., "An Analytical Formulation of Equations of State,"
     Rand Memorandum RM-3905-PR (1964)

(23) Pugh, E. M., R. J. Eichelberger, and N. Rostocker, J. Appl. Phys.,
     23, 532 (1952)

(24) Scully, C. N. and D. L. Cowan, "Hypervelocity Gun for Micro-
     meterite Impact Simulation Employing Capacitor Discharge
     in a Condensed Phase," Hypervelocity Impact Fourth Symposium
     (1960)

(25) Scherrer, V. E. and P. I. Richards, "An Exploding Wire Hyperveloc-
     ity Projector," Hypervelocity Impact Fourth Symposium (1960)

(26) Sodek, B. A., "The Penetration of an Aluminum-Glass Interface by
     an Originally Radial Shock Wave," Master's Thesis, Oklahoma
     State University (1965)

(27) Sodek, B. A., "A Hydrodynamic Model of Micrometeroid Impact,"
     Ph.D. Thesis, Oklahoma State University (1966)

(28) Swift, H. F., "Electroballistic Techniques," Hypervelocity Impact
        Fourth Symposium (1960)

(29) Tillotson, J. H., "Metallic Equations of State for Hypervelocity
        Impact," General Atomic Report, GA-3216 (1962)

(30) Volpe, V. F., "A Sequential Electrical Discharge Light Gas Gun,"
        Hypervelocity Impact Fourth Symposium (1960)

(31) von Neumann, J. and R. D. Richtmeyer, "A Method for the Numerical
        Calculations of Hydrodynamic Shocks," J. Appl. Phys., 232-
        237 (1950)

APPENDIX A

DEVELOPMENT OF THE EQUATIONS FOR P_1 AND P_2, THE PRESSURES

OF THE GUN POWDER GASES

The pumping cycle starts immediately after the ignition of the gunpowder. It is assumed that all of the gunpowder burns instantaneously, and that the gunpowder chamber is immediately filled with a gas at a pressure P_1, having a ratio of specific heats, Γ. This gas expands isentropically and drives the piston down the pump tube. The motion of the piston is opposed by the helium pressure, p. The equation of motion for the piston is (again refer to Table I and Table II for a complete description of the symbols and subscripts):

$$A1) \qquad W_p \frac{du_p}{dt} = A_p(P - p)$$

or, if the variables are changed

$$A2) \qquad \frac{du_p}{dt} = \frac{dx}{dt}\frac{du_p}{dx} = -u_p\frac{du_p}{dx}$$

A1) may be written as

$$A3) \qquad W_p u_p \frac{du_p}{dx} = -A_p(P - p)$$

The helium pressure, p, is known from the condition

$$A4) \qquad p = p_1\left(\frac{x_1}{x}\right)^\gamma$$

and the gunpowder gas pressure is given by

$$A5) \qquad P = P_1\left(\frac{\mathcal{U}}{\mathcal{V}}\right)^\Gamma$$

179

where V is the volume of the gunpowder gas at the time that the pressure P exists.

The volume, V, consists of the volume of the gunpowder chamber, the volume which exists between the gunpowder chamber and the rear face of the piston, and the volume of gunpowder gas which has escaped out of the blowout hole in the breech plug; that is

$$A6) \quad V = U + A_p(x_1 - x) + v$$

where v is the volume of the gunpowder gas which has escaped out the blowout hole. This volume, v, is given by

$$A7) \quad v = \mu t A$$

where μ is the flow velocity of the gunpowder gas out of the blowout hole, t is the length of time the flow occurs, and A is the cross-sectional area of the blowout hole.

The flow velocity can be found from the following equation

$$A8) \quad \mu = \sqrt{\frac{2\Gamma}{\Gamma-1} R(T_0 - T)}$$

where T is the temperature in degrees Rankine of the environment into which the gas is flowing, and T_0 is the stagnation temperature, or the temperature which exists inside the gunpowder chamber.

T_0 can be calculated from RT, which is the force constant

$$A9) \quad RT_0 = 70 \frac{long\ tons}{in^2} \frac{cm^3}{gram}$$

Converting R and the right side of A9) to the same units gives

$$A10) \quad T_0 = 6553\ °Rankine$$

The value of R used in A9) is the value for air because the combustion products of gunpowder have approximately the same molecular weight as air.

Letting $T = 530^{o}R$ and using the calculated value of T_o together with the value of R for air in equation A8) gives

$$A11) \quad \mu = 9450 \ ft/sec$$

Charters, et al., quote the length of the pumping cycle of their gun as 15 milliseconds (8). Since the geometry of their gun does not differ too greatly from the gun that is described in this paper, it will be assumed that this is also the length of the pumping cycle for this gun.

The cross-sectional area of the blowout hole is $8.53 \times 10^{-5} \ ft^{2}$; therefore, the volume of gunpowder gas which flows out of the blowout hole during the time required for the pumping cycle is

$$v = (9450 \ ft/sec) \ (15 \times 10^{-3} sec) \ (8.53 \times 10^{-5} ft^{2})$$

or

$$A12) \quad v = 20.8 \ in^{3}$$

At any instant between the time when the piston first begins its motion at $x = x_1$ and the time that it comes to rest at $x = x_2$, it will be assumed that the volume of gas which has flowed from the blowout hole is given by

$$A13) \quad v = \frac{20.8}{(x_1 - x_2)} \ (x_1 - x)$$

Thus at time $t = 0$ (i.e., $x = x_1$), $v = 0$, and at time $t = 15$ milliseconds (i.e., $x = x_2$), $v = 20.8$ in.

The appropriate form of V from A6) is then

$$A14) \quad V = U + A_p(x_1 - x) + \frac{20.8}{(x_1 - x_2)}(x_1 - x)$$

From A5),

$$A15) \quad P = P_1 \left(\frac{1}{1 + \frac{A_p}{U}(x_1 - x) + \frac{20.8}{U(x_1 - x_2)}(x_1 - x)} \right)^{\Gamma}$$

and so from A3) and A4),

$$A16) \quad \int_0^{u_{p_2}} w_p u_p \, du = -A_p P_1 \int_{x_1}^{x_2} \left[1 + \left(\frac{A_p}{U} + \frac{20.8}{U(x_1 - x_2)} \right)(x_1 - x_2) \right]^{-\Gamma} dx + A_p p_1 x_1^{\delta} \int_{x_1}^{x_2} x^{-\delta} dx$$

or

$$A17) \quad \frac{1}{2} w_p u_p^2 = \frac{U A_p P_1}{\left(A_p + \frac{20.8}{x_1 - x_2} \right)(1 - \Gamma)} \left(1 + \frac{A_p}{U}(x_1 - x_2) + \frac{20.8}{U} \right)^{1 - \Gamma} - 1 + \frac{A_p p_1 x_1^{\delta}}{1 - \delta} \left(x_2^{1 - \delta} - x_1^{1 - \delta} \right)$$

Solve this equation for P_1 and

$$A18) \quad P_1 = \frac{(\Gamma - 1)\left(A_p + \frac{20.8}{x_1 - x_2} \right)}{U A_p \left[1 - \left(1 + \frac{A_p}{U}(x_1 - x_2) + \frac{20.8}{U} \right)^{1 - \Gamma} \right]} \left[\frac{1}{2} w_p u_p^2 + \frac{A_p p_1 x_1^{\delta}}{\delta - 1} \left(x_2^{1 - \delta} - x_1^{1 - \delta} \right) \right]$$

To find the expression for P_2, substitute $x = x_2$ into A15) and

$$A19) \quad P_2 = \frac{P_1}{\left(1 + \frac{A_p}{U}(x_1 - x_2) + \frac{20.8}{U} \right)^{\Gamma}}$$

APPENDIX B

CONVERSION OF THE HYDRODYNAMIC FLOW EQUATIONS

TO FINITE DIFFERENCE EQUATIONS

For one dimension, inviscid fluid flow, the conservation of mass is given by

$$B1) \quad \frac{\partial \rho}{\partial t} = -\frac{d}{dx}(\rho u)$$

and the conservation of momentum is given by

$$B2) \quad \rho \frac{du}{dt} = -\frac{dp}{dx}$$

Since $u = u(x,t)$, then

$$\frac{du}{dt} = \frac{\partial u}{\partial t} + \frac{\partial u}{\partial x}\frac{\partial x}{\partial t} = \frac{\partial u}{\partial t} + u\frac{\partial u}{\partial x}$$

Thus B2 becomes

$$B3) \quad \rho \frac{\partial u}{\partial t} = -\frac{\partial p}{\partial x} - \rho u \frac{\partial u}{\partial x}$$

add $u\frac{\partial \rho}{\partial t}$ to both sides of B3 and

$$B4) \quad \rho \frac{\partial u}{\partial t} + u\frac{\partial \rho}{\partial t} = -\frac{\partial p}{\partial x} - \rho u \frac{\partial u}{\partial x} + u\frac{\partial \rho}{\partial t}$$

Substitute B1 for $\frac{\partial \rho}{\partial t}$ on the right side of B4 and

$$\rho \frac{\partial u}{\partial t} + u\frac{\partial \rho}{\partial t} = -\frac{\partial p}{\partial x} - \rho u \frac{\partial u}{\partial x} - u\frac{d}{dx}(\rho u)$$

183

or

$$B5) \quad \frac{d}{dt}(\rho u) = -\frac{\partial p}{\partial x} - \frac{d}{dx}(\rho u^2)$$

This equation is equivalent to B2 except that all derivatives are now partial derivatives instead of total derivatives so that the equation is in a form to apply finite difference approximations.

The conservation of energy for one dimensional flow is

$$\rho \frac{dE}{dt} = -\frac{d}{dx}(\rho u)$$

Since $E = E(x,t)$, where E is the total energy, then

$$\rho \left(\frac{\partial E}{\partial t} + u \frac{\partial E}{\partial x} \right) = -\frac{d}{dx}(\rho u)$$

add $E \frac{\partial \rho}{\partial t}$ to each side and

$$B6) \quad \rho \frac{\partial E}{\partial t} + E \frac{\partial \rho}{\partial t} = -\frac{d}{dx}(\rho u) - \rho u \frac{\partial E}{\partial x} + E \frac{\partial \rho}{\partial t}$$

Substitute B1 for $\frac{\partial \rho}{\partial t}$ on the right side of B6 and

$$\rho \frac{\partial E}{\partial t} + E \frac{\partial \rho}{\partial t} = -\frac{d}{dx}(\rho u) - \rho u \frac{\partial E}{\partial x} - E \frac{d}{dx}(\rho u)$$

or

$$B7) \quad \frac{d}{dt}(\rho E) = -\frac{d}{dx}(\rho u) - \frac{d}{dx}(\rho u E)$$

This equation; likewise, is now in a form so that finite difference approximations may be used to evaluate it.

A partial differential equation of the form $\frac{\partial f}{\partial t} = g(x,t)$, where $f = f(x,t)$, may be approximated by

$$B8) \quad \frac{\partial f}{\partial t} = \frac{f(x, t+\Delta t) - f(x,t)}{\Delta t}$$

and $\frac{\partial f}{\partial x}$ may be approximated by

$$B9) \quad \frac{\partial f}{\partial x} = \frac{f\left(x+\frac{1}{2}\Delta x, t\right) - f\left(x-\frac{1}{2}\Delta x, t\right)}{\Delta x}$$

The smaller values of Δx and Δt give the best approximations.

If these approximations are applied to equation B1, that equation may be written as

$$B10) \quad \frac{\rho(x, t+\Delta t) - \rho(x, t)}{\Delta t} = -\frac{\rho\left(x+\frac{1}{2}\Delta x, t\right) u\left(x+\frac{1}{2}\Delta x, t\right) - \rho\left(x-\frac{1}{2}\Delta x, t\right) u\left(x-\frac{1}{2}\Delta x, t\right)}{\Delta x}$$

This is the finite difference form of the conservation of mass.

Apply the approximations to equations B5 and B7, and the finite difference forms or the conservation of momentum and conservation of energy are:

$$B11) \quad \frac{\rho(x, t+\Delta t) u(x, t+\Delta t) - \rho(x, t) u(x, t)}{\Delta t} = -\frac{p\left(x+\frac{1}{2}\Delta x, t\right) - p\left(x-\frac{1}{2}\Delta x, t\right)}{\Delta x}$$

$$-\frac{\rho\left(x+\frac{1}{2}\Delta x, t\right) u\left(x+\frac{1}{2}\Delta x, t\right) u\left(x+\frac{1}{2}\Delta x, t\right) - \rho\left(x-\frac{1}{2}\Delta x, t\right) u\left(x-\frac{1}{2}\Delta x, t\right) u\left(x-\frac{1}{2}\Delta x, t\right)}{\Delta x}$$

and

$$B12) \quad \frac{\rho(x, t+\Delta t) E(x, t+\Delta t) - \rho(x, t) E(x, t)}{\Delta t} = -\frac{p\left(x+\frac{1}{2}\Delta x, t\right) u\left(x+\frac{1}{2}\Delta x, t\right) - p\left(x-\frac{1}{2}\Delta x, t\right) u\left(x-\frac{1}{2}\Delta x, t\right)}{\Delta x}$$

$$-\frac{\rho\left(x+\frac{1}{2}\Delta x, t\right) u\left(x+\frac{1}{2}\Delta x, t\right) E\left(x+\frac{1}{2}\Delta x, t\right) - \rho\left(x-\frac{1}{2}\Delta x, t\right) u\left(x-\frac{1}{2}\Delta x, t\right) E\left(x-\frac{1}{2}\Delta x, t\right)}{\Delta x}$$

In the simplified problem for this thesis, the impacting plate is assumed to have a finite thickness, but to have infinite lateral dimensions. The finite difference mesh which represents the target and the impacting plate contains cells which have only two sides, as shown in Figure 22. A particular cell, L, will have a side L-½ and a side L+½ which are separated by a distance Δx . The flow variables are to be evaluated at the center of each cell. Let D(L), U(L), E(L), P(L), and Q(L) represent the values of the flow variables at the center of cell L at time t, and CD(L), CU(L), and CE(L) represent the value of the density, flow velocity, and total energy at the center of cell L at time t $+\Delta t$. Let D1, U1, E1, P1, and Q1 represent the values of the variables at side L-½ of cell L at time t, and D2, U2, E2, P2, and Q2 represent the values at side L+½ at time t.

In equations B10, B11, and B12, the following changes may be made:

$$\rho(x, t+\Delta t) = CD(L)$$
$$\rho(x, t) = D(L)$$
$$\rho(x+\tfrac{1}{2}\Delta x, t) = D2$$
$$\rho(x-\tfrac{1}{2}\Delta x, t) = D1$$
$$u(x+\tfrac{1}{2}\Delta x, t) = U2$$
$$u(x-\tfrac{1}{2}\Delta x, t) = U1$$

B13)

$$p(x+\tfrac{1}{2}\Delta x, t) = P2$$
$$p(x-\tfrac{1}{2}\Delta x, t) = P1$$
$$E(x+\tfrac{1}{2}\Delta x, t) = E2$$
$$E(x-\tfrac{1}{2}\Delta x, t) = E1$$
$$u(x, t+\Delta t) = CU(L)$$
$$u(x, t) = U(L)$$
$$E(x, t+\Delta t) = CE(L)$$
$$E(x, t) = E(L)$$

Thus B10 becomes

$$B14) \quad CD(L) = D(L) + \frac{\Delta t}{\Delta x}\left(D1 * U1 - D2 * U2\right)$$

This is the final form of the finite difference equation expressing conservation of mass.

Introducing the variable changes listed in B13 into B11 and B12 gives the forms of the conservation of momentum and conservation of energy which were used in the computer code. These equations are

$$B15) \quad CD(L) * CU(L) = D(L) * U(L) + \frac{\Delta t}{\Delta x}\left(D1 * U1 * U1 - D2 * U2 * U2\right)$$

and

$$B16) \quad CD(L) * CE(L) = D(L) * E(L) + \frac{\Delta t}{\Delta x}\left(P1 * U1 - P2 * U2 + D1 * U1 * E1 - D2 * U2 * E2\right)$$

The expression for the artificial dissipation term may be found in a manner that is similar to the proceeding. The differential equation

$$B17) \quad q = -A_1^2 \frac{\partial u}{\partial x}\left(\left|\frac{\partial u}{\partial x}\right| + A_2\right)$$

may be approximated by the difference equation

$$B18) \quad q = -A_1^2 \frac{u(x+\frac{1}{2}\Delta x, t) - u(x-\frac{1}{2}\Delta x, t)}{\Delta x}\left(\left|\frac{u(x+\frac{1}{2}\Delta x, t) - u(x-\frac{1}{2}\Delta x, t)}{\Delta x}\right| + A_2\right)$$

Using the terms defined in B13, the finite difference equation for q at the center of cell L is

$$B19) \quad q(L) = -A_1^2\left(\frac{U2 - U1}{\Delta x}\right) * \left(\left|\frac{U2 - U1}{\Delta x}\right| + A_2\right)$$

VITA

Bob Adrain Hardage

Candidate for the Degree of

Master of Science

Thesis: THE DESIGN AND CONSTRUCTION OF A HELIUM GAS GUN AND A NUMERICAL SOLUTION OF THE HYPERVELOCITY IMPACT OF A THIN PLATE

Major Field: Physics

Biographical:

Personal Data: Born at Checotah, Oklahoma, April 5, 1939, the son of Charles M. and Edna Hardage.

Education: Attended grade school at Onapa School; graduated from Onapa High School in 1957; received the Bachelor of Science degree from the Oklahoma State University, with a degree in Physics, in May, 1961; completed the requirements for the Master of Science degree in May, 1967.

Professional Experience: Named the outstanding freshman in Physics, 1958; a member of the Arts and Sciences Honor Society; Pi Mu Epsilon, honorary mathematics society; and Sigma Pi Sigma, honorary physics society; president of the Oklahoma State University chapter of Sigma Pi Sigma, 1962-1963; delegate to national Sigma Pi Sigma meeting, 1962; named the outstanding senior in Physics, 1961; and NDEA Fellow, 1961-1964, member of Oklahoma Academy of Science.